The chronology of prehistoric high-energy wave events (tropical cyclones, tsunamis) in the southern Caribbean and their impact on coastal geo-ecosystems – a case study from Bonaire (Leeward Antilles)

Inaugural-Dissertation

zur

Erlangung des Doktorgrades

der Mathematisch-Naturwissenschaftlichen Fakultät

der Universität zu Köln

vorgelegt von

Max Engel

aus Groß-Umstadt

Köln 2012

Berichterstatter: Prof. Dr. Helmut Brückner

Prof. Dr. Frank Schäbitz

Prof. Dr. Christophe Morhange

Tag der mündlichen Prüfung: 16.05.2012

„A peine ont-ils mis le pied dans la ville, en pleurant la mort de leur bienfaiteur, qu'ils sentent la terre trembler sous leurs pas; la mer s'élève en bouillonnant dans le port, et brise les vaisseaux qui sont à l'ancre.“

(Voltaire – Candide ou l’optimisme, 1759)

Abstract

By using sediment archives along the coast of Bonaire (Leeward Antilles; political status: special municipality of the Netherlands), such as bokas (enclosed lagoons), narrow floodplains and mangrove swamps, and by investigating supralittoral blocks and boulders, the goal of this thesis is (i) to identify prehistoric high-energy wave events, (ii) to differentiate between extraordinary storms and tsunamis, and (iii) to date these events. Furthermore, the spatio-temporal impact of high-energy wave events on coastal geo-ecosystems is evaluated. A total of 45 vibracores (max. depth 11 m) and push cores (max. depth 1.62 m) was taken from all around the island (Lagun, Boka Washikemba, Lac Baai, Saliña Tam, Klein Bonaire, Boka Funchi, Wayaka, Boka Bartol, Playa Grandi). Cores from the most promising locations were investigated in terms of sedimentology, geochemistry, mineralogy and faunal remains.

The coasts of the Caribbean Sea are prone to tsunami hazard, proven by numerous observed events of the last 500 years. Bonaire was chosen as the site of interest for this study due to the antagonism of a total lack of historical accounts on tsunami occurrence and its massive record of coarse-clast coastal landforms and single blocks and boulders, which are attributed to deposition by extreme wave events (tsunamis, hurricanes).

The largest coastal blocks were studied as evidence for the occurrence of more powerful waves than those of strong tropical cyclones (locally known as hurricanes). By comparing calculated minimum storm wave heights required to quarry and move the largest blocks of Spelonk and Boka Olivia on northeastern Bonaire, with maximum wave heights observed during recent high-category hurricanes and the buoy record, little doubt remains that one or more major tsunamis occurred in Mid- to Late Holocene times. This confirmation of the previously established (and in the meantime challenged) tsunami hypothesis provides a very important framework condition for the interpretation of the subsurface overwash deposits in the coastal stratigraphical archives.

A tentative chronology of tsunami occurrence was established, based on a comparison of subsurface overwash deposits identified in the sediment cores from the stratigraphical geoarchives with characteristic signature types of modern tsunamis and calibrated ^{14}C data. Uncertainties in sediment interpretation, associated with the fact that most of these signature types may also occur in storm deposits, were reduced according to (i) the results from the numerical boulder study, (ii) the high tsunami potential of the southern Caribbean (abundant potential tsunami trigger mechanisms), (iii) the identification of sediment source areas which are out of reach for storm waves, and (iv) the lack of littoral and marine sand/mud input during recent high-category hurricanes.

Several sites reflect long-lasting environmental change subsequent to palaeotsunami impact. At the open embayment of Lagun, this is confirmed by palynological investigations. Pollen spectra prior to the wave impact are dominated by mangrove types (*Rhizophora*), whereas significantly lower percentage of *Rhizophora* pollen was detected in the post-tsunami samples. Mangroves seem to have only gradually recovered from the impact, probably on centennial scales. In contrast to Lagun, the bokas and saliñas of Bonaire are cut off from the sea by a quasi-impermeable barrier of beachrock and coral rubble. The candidate tsunami deposit of Boka Bartol is vertically confined by mangrove peat (below) and evaporite-rich mud (above). This pattern is interpreted as the transformation of an open mangrove-fringed embayment (pre-tsunami) into a poly- to hypersaline lagoon (post-tsunami)

due to the establishment or closure of the barrier of coral material during the event. The high amount of gypsum and halite crystals and thin layers of inorganic carbonate are the result of limited water input and high evapotranspiration rates during the dry season. The absence of marine faunal remains also indicates very limited exchange with the ocean.

The chronology of potential tsunamis based on data from the sediment cores starts with extreme wave event I (EWE I), around 3600 BP, represented by a carbonate sand deposit bracketedby mangrove peat, which was found on Klein Bonaire. A well-preserved candidate tsunami deposit from Boka Bartol with a maximum age of 3300 BP (EWE II) has counterparts on the leeward coast (Klein Bonaire, Saliña Tam, possibly between Saliña Tam and Punt'i Wekua) and the windward coast (Playa Grandi, possibly Boka Washikemba). EWE II can be identified as the best-documented candidate palaeotsunami on Bonaire. EWE XII, with a maximum age of 2000 BP, left massive shell-dominated deposits at Lagun (windward side) and carbonate sands at Saliña Tam, both of which were interpreted as tsunamigenic. Deposits of another younger, unspecified EWE XVI (pre-500 BP) were found between Saliña Tam and Punt'i Wekua, and Boka Washikemba. Based on these results, a preliminary estimation of the recurrence interval of high-energy wave events on Bonaire, which reveal magnitudes significantly exceeding those of recent high-category hurricanes and which are therefore likely to be major tsunamis, is in the order of roughly 1000 years or less.

This study corroborates conclusions of predecessor studies that the hazard of tsunami does exist on Bonaire, although historical accounts on tsunami ocurrence are lacking. It is strongly suggested to the authorities of Bonaire, to conduct a local analysis of tsunami risk, similar to the one recently established for the neighbour island of Curaçao. A study of modelling tsunami inundation based on the spectrum of tsunami triggering mechanisms and past inundation inferred from the overwash deposits identified in this research may be useful to determine high-risk areas, which are prone to potential future tsunami damage.

Kurzzusammenfassung

Feinsedimentarchive entlang der Küste von Bonaire („Inseln unter dem Winde“; politischer Status: Besondere Gemeinde der Niederlanden), wie etwa Bokas (vom Meer abgetrennte Lagunen), schmale Küsteneben oder Mangrovensümpfe, sowie supralitorale Blöcke liefern die Basis dieser Arbeit und dienen der (i) Identifikation prähistorischer Extremwellenereignisse, (ii) der Unterscheidung zwischen Tsunamis und tropischen Zyklonen (Lokalname: Hurricanes) und (iii) der Datierung dieser Ereignisse. Weiterhin unterstützen sie die Analyse des Einflusses dieser Ereignisse auf die küstennahen Geo-Ökosysteme sowohl auf zeitlicher als auch auf räumlicher Ebene. Eine Serie von 45 Rammkernsondierungen mit einer maximalen Tiefe von 11 m und „push cores“ mit einer maximalen Tiefe von 1,62 m von Lokalitäten aller Küstenabschnitte der Insel (Lagun, Boka Washikemba, Lac Baai, Saliña Tam, Klein Bonaire, Boka Funchi, Wayaka, Boka Bartol, Playa Grandi) bildet das Rückgrat dieser Dissertation. Die wichtigsten Bohrkerne wurden mit Hilfe sedimentologischer, geochemischer, mineralogischer und paläontologischer Methoden untersucht.

Die karibischen Küsten sind tsunamigefährdet. Dies ist belegt durch zahlreiche Ereignisse der vergangenen 500 Jahre. Die Wahl Bonaires als Untersuchungsgebiet basiert auf dem Widerspuch zwischen gänzlich fehlenden historischen Belege für das lokale Auftreten von Tsunamis und dem enormen Ausmaß grobklastischer Ablagerungen entlang der Küste, die mit Transport durch extreme Wellenereignisse (Tsunamis, Hurricanes) assoziiert werden.

Die größten Blöcke wurden untersucht auf Grund ihres Zeigerwertes für das Auftreten höher energetischer Wellen als jene, die während eines starken Hurricanes generiert werden. Der Vergleich an Hand numerischer Modelle kalkulierter minimaler Wellenhöhen, die zur Dislokation der größten Blöcke bei Spelonk und Boka Olivia (Nordost-Bonaire) benötigt werden, mit maximalen beobachteten Wellenhöhen während Hurricanes der oberen Kategorien und den Aufzeichnungen von Bojen der südlichen Karibik, lässt wenig Zweifel, dass ein oder mehrere Tsunamis während des Mittel- bis Spätholozäns aufgetreten sind. Diese Bestätigung der bereits zuvor aufgestellten Tsunamihypothese für Bonaire, die unmittelbar im Anschluss in Frage gestellt wurde, stellt eine wichtige Rahmenbedingung für die Interpretation der küstenstratigraphischen Archive dar.

Eine initiale Chronologie von Tsunamiereignissen für Bonaire und seine unmittelbare Umgebung wurde auf Basis des Vergleichs subterraner mariner Überspülsedimente in den küstennahen morphologischen Depressionen der Insel mit sedimentären Charakteristika rezenter, weltweit dokumentierter Tsunamiablagerungen und kalibrierten ^{14}C-Daten erarbeitet. Unsicherheiten in der Interpretation der Sedimente, die mit der Tatsache zusammen hängen, dass viele dieser sedimentären Charakteristika auch in Sturmablagerungen auftreten können, wurden reduziert durch (i) die Resultate der Blockstudie, (ii) das hohe Tsunamipotenzial der südlichen Karibik (zahlreiche mögliche Auslösemechanismen), (iii) die Identifikation von Sedimentliefergebieten, die außerhalb des durch Sturmwellen erfassten Bereichs liegen, sowie (iv) dem überwiegenden Fehlen von Sandablagerungen rezenter Hurricanes der oberen Kategorien.

Mehrere untersuchte Lokalitäten erfuhren nachhaltige ökologische und geomorphologische Modifikationen durch den Einfluss von Paläotsunamis. In der offenen Bucht von Lagun spiegeln sich diese Veränderungen beispielsweise im Pollenbefund wieder. Pollenspektren vor Auftreten des Tsunamis sind dominiert von Mangroventypen (*Rhizophora*), während jene unmittelbar im Hangenden der

potenziellen Tsunamilage einen signifikant geringeren Anteil an Mangrove aufweisen, der erst in den subrezenten Proben wieder graduell ansteigt. Im Gegensatz zur offenen Bucht von Lagun sind die Bokas und Saliñas entlang der Küste von Bonaire durch eine wenig durchlässige Barriere aus Korallenschutt und Beachrock vom Meer getrennt. Die mögliche Paläotsunamiablagerung in der Stratigraphie von Boka Bartol im Nordwesten Bonaires wird von einem reinen Mangroventorf unter- und einem evaporitreichen Feinsediment überlagert. Dieses Muster wird als Transformation einer zum Meer hin offenen, mangrovengesäumten Bucht hin zu einer poly- bis hypersalinen Lagune interpretiert, die auf der Entstehung bzw. dem subaerischen Wachstum der Korallenschuttbarriere durch den Paläotsunami beruht. Der hohe Anteil an Gips- und Halitkristallen sowie die anorganisch gefällten Karbonatlaminae sind das Resultat des limitierten Wasserdargebots und der hohen Evapotranspirationsraten während der Trockenzeit. Das Fehlen mariner Faunenreste in der evaporitreichen post-Tsunami-Lage stützt diese Interpretation.

Die Chronologie potenzieller Tsunamis auf Basis der Daten der Sedimentbohrkerne beginnt mit Extremwellenereignis I (EWE I) um ca. 3600 BP, das durch eine Karbonatsandlage auf Klein Bonaire repräsentiert wird. Eine sehr gut erhaltene, wahrscheinlich tsunamigene Sedimentschicht aus Boka Bartol mit einem Maximalalter von 3300 Jahren (EWE II) lässt sich mit entsprechenden Ablagerungen der leeseitigen Küste (Klein Bonaire, Saliña Tam, möglicherweise zwischen Saliña Tam und Punt'i Wekua) und der windwärtigen Küste (Playa Grandi, möglicherweise Boka Washikemba) korrelieren. EWE II kann als der am besten dokumentierte mögliche Paläotsunami auf Bonaire bezeichnet werden. EWE XII, ca. 2000 Jahre oder jünger, hinterließ massive Mollusken-dominierte Sedimente bei Lagun (windwärtige Küste) und Karbonatsande bei Saliña Tam (leeseitige Küste), die sich jeweils als tsunamigen interpretieren ließen. Sedimente eines weiteren jüngeren, unspezifizierten EWE XVI (prä-500 BP) wurden zwischen Saliña Tam und Punt'i Wekua sowie in Boka Washikemba identifiziert. Auf Grundlage dieser Ergebnisse liegt die Wiederkehrfrequenz hochenergetischer Wellenereignisse, deren Magnitude jene rezenter starker Hurricanes deutlich überschreitet und bei denen es sich wahrscheinlich um Tsunamis handelt, im Bereich von 1000 Jahren oder weniger.

Aus dieser Studie lässt sich schlussfolgern, dass eine Gefährdung Bonaires durch Tsunamis existiert, wenngleich historische Belege fehlen. Es wird den zuständigen Behörden aus diesem Grund die Durchführung einer entsprechenden lokalen Risikoanalyse empfohlen, ähnlich des seit kurzem existierenden Beispiels der Schwesterinsel Curaçao. Eine Modellierung von Überflutungsszenarien auf Basis des Spektrums möglicher Auslösemechanismen von Tsunamis sowie Überflutungsdistanzen abgeleitet aus den identifizierten Überspülsedimenten dieser Studie würden hier eine zielführende Komponente bei der Ausweisung von Hochrisikoarealen darstellen, die der Schädigung durch zukünftige Tsunamis ausgesetzt wären.

Acknowledgements

This dissertation was prepared in the framework of the research project “Key Processes in the Holocene Evolution of Tropical Coasts – Evaluating the Role of Hurricanes and Tsunamis”, funded by the Deutsche Forschungsgemeinschaft (DFG; Reference code of the subproject: BR 877/26-1).

The completion of this thesis concludes an episode of focused studies and the intense and positive experience of taking a research project from A to Ω. No doubt will I look back on this episode as an episode of professional and, most importantly, personal happiness and satisfaction. Moments of trouble existed, but they were of ephemeral nature and never got out of hand. The reason why working on this dissertation was such an entirely positive experience, are the people who accompanied me during this time and provided invaluable support in many ways.

The person to whom I owe the most is Prof. Dr. Helmut Brückner. His open-minded way of supervising my work and his confidence in the abilities of his students has enabled me to accomplish this research project by following my own ideas and it also taught me a lot about project management. He always took care for me and provided support in every way he could since I joined his research group as a student assistant with the Philipps-Universität Marburg.

Furthermore, I would like to express my sincere thanks to

- A/Prof. Dr. Anja Scheffers for her guidance during the first field campaign and her invaluable support in many ways;
- Prof. Dr. Dieter Kelletat for his enthusiastic introduction to the unique geology and geomorpology of Bonaire. I truly benefited from his countless ideas and critical assessment of my work;
- Dr. Matthias May for his tremendous support during two field campaigns and the analysis of the field data;
- Prof. Dr. Frank Schäbitz for co-supervising this thesis and for his help during the first field season;
- PD Dr. Peter Frenzel and Sascha Fürstenberg for analyzing the microfossil content of sediment samples from Bonaire;
- Timo Willershäuser for his support during the first field season and the enthusiasm while working on the Bonaire project;
- Karoline Meßenzehl, Anna Maria Konopczak, and Ingo Middelhaufe, for bringing this research forward during and after their B.Sc. phase;
- Kirstin Jacobson, for her invaluable contribution to language polishing;
- Dr. Michael Wille for investigating pollen samples from Lagun;
- Dr. Volker Wennrich and Armine Shahnazarian for providing acces to the ITRAX-XRF core scanner of the Institue of Geology and Mineralogy, Universität zu Köln;

- Dr. Gerhard Daut for providing the opportunity to conduct analyses of magnetic susceptibility at the Institute of Geography, Friedrich-Schiller-Universität Jena;
- Andreas Ginau for supporting the semi-quantitative analysis of XRD data;
- Prof. Dr. Andreas Vött for his contribution to the pilot field work in 2006, which represented the basis for the subsequent successful research proposal and for his fruitful remarks on parts of the thesis;
- Prof. Dr. Tibor Dunai, who accepted to chair the commission for defence of the dissertation and Dr. Daniel Kelterbaum who joins the commission as well;
- Dr. Andreas Bolten for supporting post-processing of bathymetric data and calculation of 3D boulder models;
- Dr. Sander Scheffers for administrative support during the first two field seasons and critical reviews of my results;
- Prof. Dr. Michael Amler for supervising the determination of mollusc remains;
- Elsmarie Beukenboom, Fernando Simal and Ramon de Leon, representing the management board of STINAPA (Bonaire National Parks Foundation), who provided essential logistic and admistrative support in the field;
- Frank van Slobbe, representing the Department of Environment and Natural Resources, Bonaire, for supporting this dissertation by providing administrative access to study sites;
- Jan Brouwer, for various support during field work;
- Prof. Dr. Jody Bourgeois, Dr. Michaela Spiske, A/Prof. Dr. Adam Switzer, Prof. Dr. Ronald Martin, Prof. Dr. Guiseppe Mastronuzzi, Prof. Dr. Klaus Reicherter, Dr. Alan Ruffman, as well as several anonymous persons for their critical and very fruitful assessment of particular chapters of this thesis;
- Dr. Walter-Wilhelm Jungmann, Marita Budde and Christine Günther for their support in the sediment laboratory of the Faculty of Geography, Philipps-Universität Marburg;
- Dr. Renaud Joannes-Boyau for providing the relative frequency plots of the coarse-clast datings;
- the entire working group of Prof. Dr. Helmut Brückner who provided backup and valuable discussion, and kept me free of other tasks during the final stage of writing the dissertation;
- the INQUA 1001 "Late Quaternary records of coastal evolution" program and the German Working Group on Geomorphology (AK Geomorphologie) for travel grants, which enabled the presentation of results of this dissertation at international conferences.

I want to use this opportunity to warmly thank my parents Margit and Günter Engel, who never questioned my decisions and were a source of reliability, mental support, and confidence throughout my life.

I dedicate this thesis to my wife Charlotte, who demonstrated tremendous patience within the last years, who is my great motivation and simply the most important person in my life – not to forget her dedication during field work in 2011!

Table of Contents

List of Figures

List of Tables

1 Introduction

1.1 Coastal hazards, vulnerability and risk in the Caribbean

Coasts experience severe demographic increase. Thus, a growing amount of human population is prone to hazards associated with the sea and continental margins (Brückner, 2000). Following the definition of Gornitz (2005: p. 678), *coastal hazards* "are physical phenomena that expose the coastal zone to risk of property damage, loss of life, or environmental degradation". Coastal hazards are separated into "slow-onset hazards" which build up or develop over time scales of centuries to millennia, such as coastal erosion or relative sea level rise, and those typically associated with the term, lasting from minutes to days, such as earthquakes, volcanism, landslides, storm surges, or tsunamis ("rapid-onset hazards") (Gornitz, 2005: p. 678).

The Caribbean region (Fig. 1) is disproportionally vulnerable to coastal hazards (Fitzpatrick, 2012), since a relatively high percentage of the population lives right at the coasts of the Greater and Lesser Antilles, the Bahamas, as well as those of northern South America and eastern Central America (McGregor and Potter, 1997). Tourism, a major economic factor on many islands, has a spatial focus on coastal areas, while, in turn, tourism-related infrastructure represents a man-made hazard to the natural environment (McGregor and Potter, 1997; Schleupner, 2008) and cultural heritage (Fitzpatrick, 2012). *Vulnerability* may in a geographical sense be defined as "the characteristics of a person or group in their situation that influence their capacity to anticipate, cope with, resist and recover from the impact of a natural hazard" (Wisner et al., 2004: p. 11). Cutter (1996: p. 533) adds the "vulnerability as hazard of place" to the concept, which includes the physical environment – the central element of this study.

The traditional triad of hazards in the Caribbean, as perceived some decades ago, is summarized by Tomblin (1981) and consists of earthquakes, volcanism and hurricanes. This focus is justified in the light of the devastating earthquake of Haiti in 2010, which represents a regional maximum in magnitude with a death toll of more than 230,000 (Bilham, 2010). The eruption of Mount Pelée on Martinique, which destroyed the former principal town of the island and killed around 28,000 inhabitants (Tanguy, 1994), and the Great Hurricane of 1780 with a similar number of fatalities along the Antilles island arc (Rappaport and Fernandez-Partagas, 1995) were outstanding disasters in terms of magnitude. Moreover, the frequency during the 500 years of historical documentation, at least regarding earthquakes and hurricanes, is high as well (Tomblin, 1981; Reading, 1990; McAdie et al., 2009; NGDC, 2012).

However, history tells that the Caribbean is also prone to the *risk* – generally defined "as the product of the probability of occurrence of a particular geophysical event and expected losses" (Tobin and Montz, 2009: p. 406) – of tsunamis. This risk is, in turn, related to the high seismic activity and volcanism mentioned above, as well as to coastal and submarine landslides, and teletsunamis generated in the open Atlantic Ocean. O'Loughlin and Lander (2003) compile observations of 127 different tsunamis, of which 53 were finally considered to be real tsunamis (see also Fig. 1). Worldwide devastating events of the last decade, such as the Indian Ocean Tsunami in 2004 (IOT), the Chilean Tsunami in 2010, or the Tohoku-oki Tsunami of Japan in 2011, not only stimulated research in all branches of tsunami science (Scheffers et al., 2009b; Sagar et al., 2010), but also led to an increase in media cov-

erage, public awareness, community preparedness, and early warning technology (e.g Farreras et al., 2007; Lauterjung et al., 2009, 2010; Clark, 2010; Spahn et al., 2010). However, in the Caribbean there is still a lack of information regarding long-term occurrence patterns of high-magnitude tsunamis (Rowe et al., 2009) and an early warning system is only partially established (IOC, 2008a, 2011).

1.2 Aims of the study

This study takes up on the deficit in information on long-term frequency and magnitude of tsunamis over millennial time scales in the Caribbean. Better knowledge on long-term frequency/magnitude patterns of tsunamis through investigations of the geological record aids in the determination of tsunami vulnerability. Initial milestones in reconstructing the Holocene history of extreme wave events (tsunamis, hurricanes)* were established by analyzing and dating onshore coarse clast deposits, such as corals and coral limestone boulders, on several Caribbean islands (e.g. Jones and Hunter, 1992; Kelletat et al., 2004; Scheffers et al., 2005; Scheffers, 2006; Scheffers and Kelletat, 2006; Robinson et al., 2006). The most extensive coarse-clast deposits linked to extreme flooding events were studied on the island of Bonaire (Leeward Antilles) in the southern Caribbean (Fig. 1). The size of the clasts, their areal extent, and a set of more than 90 radiometric datings led to the inference of at least five tsunamis around 4300 BP, 3900 BP, 3300 BP, 1200 BP, and 500 BP (Scheffers, 2005). These events left coarse debris in the form of ridges or ramparts, boulder fields and single blocks. Extreme tsunami magnitudes and a strong impact on both coastal morphology and coral reefs was inferred from the huge amount of debris in a position several meters above present sea level and far from the surf zone (Scheffers, 2002, 2004, 2005; Scheffers et al., 2006; Radtke et al., 2003). According to Scheffers et al. (2009a), the severity of these *palaeotsunamis* – defined as "tsunamis occurring prior to the historical record or for which there are no written observations" (IOC, 2008b) – might even have induced demographic changes and migration of prehistoric human populations.

However, in the following time, diverging conclusions on the origin of the boulder record emerged, some of which attributed the subaerial deposits to coastal flooding by tropical cyclones (Morton et al., 2006; Spiske et al., 2008). This vivid discussion triggered the setting up of the research program "Key Processes in the Holocene Evolution of Tropical Coasts – Evaluating the Role of Hurricanes and Tsunamis", designed by A/Prof. Dr. Anja Scheffers, Prof. Dr. Helmut Brückner, Prof. Dr. Ulrich Radtke, and Prof. Dr. Frank Schäbitz, and funded by the Deutsche Forschungsgemeinschaft (SCHE 676/8-1, BR 877/26-1, RA 383/17-1, SCHA 472/10-1). As outlined in Fig. 2, its main aims were to identify extreme wave events in the sedimentary record and to evaluate their influence on the coastal sedimentary environments and ecosystems of Bonaire.

This dissertation is focused on subproject *Geo-archive 3* (Fig. 2), though it also covers significant aspects of *Geo-archive 1* and *4*, which, however, was designed as a concise pilot study. The investigations that eventually entered this dissertation can be summarized under two main goals:

➔ **Improving the chronology of prehistoric tsunamis for Bonaire and the southern Caribbean**

Telltale deposits of ancient tsunamis provide the opportunity to extend the short historical record of the Caribbean far into the Holocene. On Bonaire, where tsunami occurrence has never been reported, they even expose a previously unknown risk to

* The terms "extreme wave event" and "high-energy wave event" are used interchangeably and include both tsunamis and waves generated by strong tropical cyclones, which are locally known as hurricanes.

lives as well as private and public property. The identification, characterisation – differentiation of tsunami deposits from those related to other processes –, and dating of palaeotsunami sediments in coastal geoarchives provides the scientific basis for

(i) calculating recurrence rates of major tsunami events and, thus, improve future predictions;

(ii) the designation of high-risk areas;

(iii) creating public awareness for the generally underestimated tsunami hazard;

(iv) local risk mitigation.

➔ **Long-term influence of extreme wave events on coastal geo-ecosystems of the tropics**

The geomorphological and ecologic response of low-lying coasts and lagoons to tsunami impact has been paid little attention on in the past, though recently several studies dealt with recovery of mangrove and coral populations as well as beach environments after the IOT (e.g. Kamthonkiat et al., 2010; Liew et al., 2010; Sawall et al., 2011). The identification and interpretation of subsurface extreme wave deposits in coastal sediment traps, such as floodplains, bokas, and saliñas (both landlocked lagoons) in their stratigraphical context may provide evidence whether tsunamis have a long-term influence on coastal landscapes on Holocene time scales. A similar discussion has recently been led by May et al. (2012) for Mediterranean environments.

1.3 The study area

The geographical entity of the Caribbean comprises the Caribbean Plate and adjacent coastal areas (Fig. 1). It includes the Greater Antilles (Cuba, Jamaica, Hispaniola, Puerto Rico) and the more eastern and southern Lesser Antilles, the Bahamas and Turks and Caicos Islands, as well as the eastern and northern coastlines of Yucatán, Belize, Guatemala, Honduras, Nicaragua, Costa Rica, Panama, Colombia, and Venezuela. Situated in the tropics of the northern hemisphere and influenced by the trade winds, most parts of the Caribbean experience pronounced dry and wet seasons and constantly high temperatures (Blume, 1962). High atmospheric temperatures and related high sea surface temperatures east of the Caribbean, as well as decreasing wind shear support the transformation of easterly waves over the north Atlantic Ocean into warm-core tropical cyclones, which track westwards. A significant percentage of them cross the Caribbean as high-category hurricanes (Hobgood, 2005).

The Leeward Antilles, represented by the ABC Islands (Aruba, Bonaire, Curaçao) and the Venezuelan archipelago, lie in a peripherical position of the Caribbean hurricane belt and rarely experience severe events (Bries et al., 2004; McAdie et al., 2009). Since 1605, a total number of only 33 tropical cyclones are listed passing within 100 nautical miles of Curaçao (Meteorological Service of the Netherlands Antilles and Aruba, 2010c). However, Hurricane Lenny in 1999, Hurricane Ivan in 2004, and Hurricane Omar in 2008 caused considerable shoreline modifications (Scheffers, 2005; Scheffers and Scheffers, 2006) and damage on the coral reefs (Bries et al., 2004; Sommer et al., 2011). Bonaire, as the island of interest for this dissertation, has a semi-arid climate characterized by high evaporation rates, low average annual precipitation of 463 mm (1971-2000) (Meteorological Department Curaçao, n.d.), and significant interannual variability (Martis et al., 2002). As a consequence, surface water discharge is generally bound to arroyos and periodic sheetwash (Zonneveld et al., 1977).

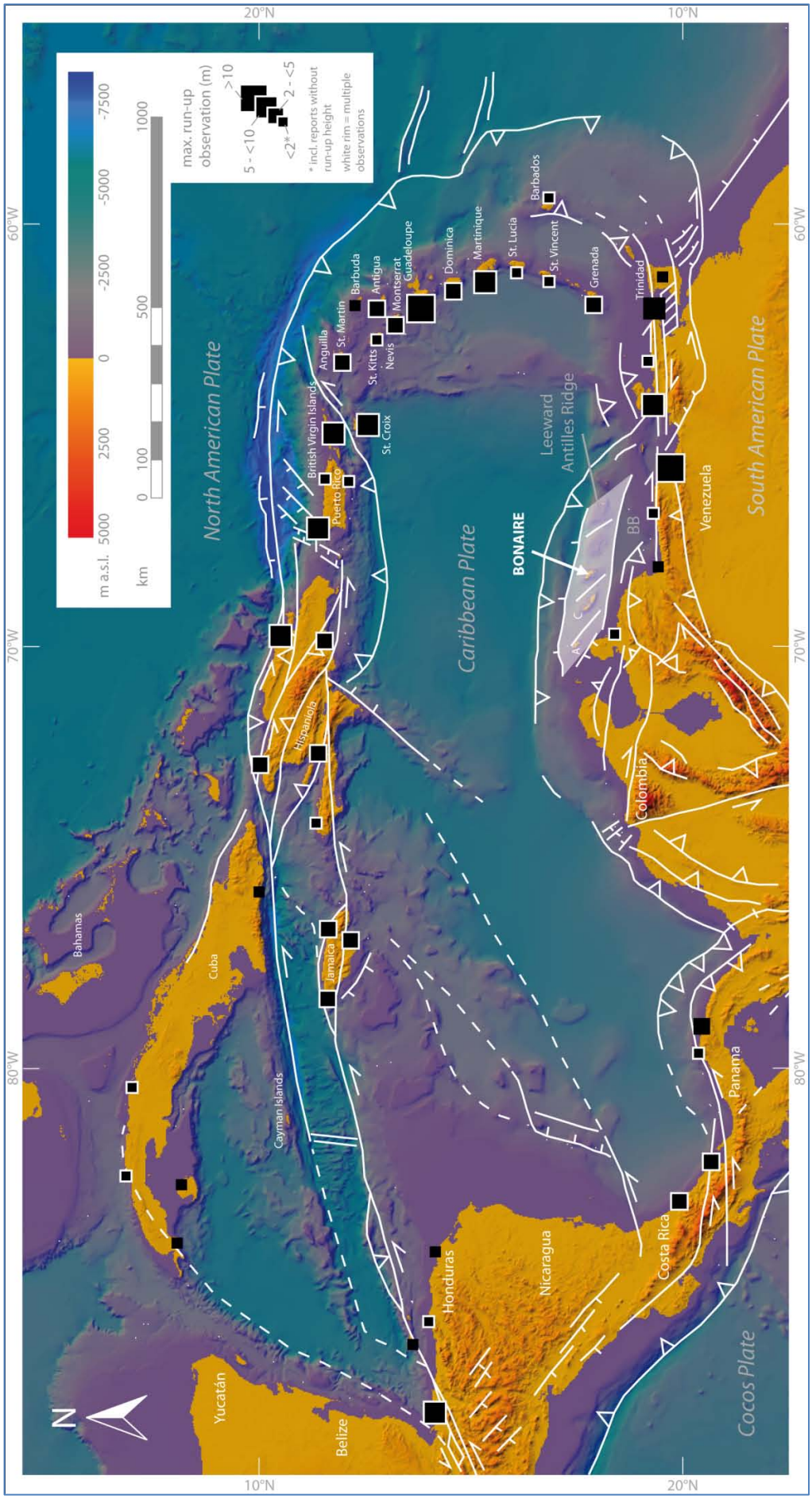
20°N
10°N
60°W
70°W
80°W
m a.s.l. 5000 2500 0 -2500 -5000 -7500
km 0 100 500 1000
max. run-up observation (m)
>10
5 - <10
2 - <5
<2*
* incl. reports without run-up height
white rim = multiple observations
North American Plate
Caribbean Plate
South American Plate
Cocos Plate
Leeward Antilles Ridge
BONAIRE
BB
Barbados
St. Lucia
St. Vincent
Grenada
Trinidad
Venezuela
Colombia
Panama
Costa Rica
Nicaragua
Honduras
Belize
Yucatán
Cayman Islands
Jamaica
Cuba
Bahamas
Hispaniola
Puerto Rico
British Virgin Islands
Anguilla
St. Martin
St. Kitts
Nevis
Antigua
Barbuda
Montserrat
Guadeloupe
Dominica
Martinique
N

Fig. 1: Overview map of the Caribbean region based on the GEBCO One Minute Grid, version 2.0 (http://www.gebco.net). The tectonic pattern was adapted from Pindell and Kennan (2009). Black squares show observations of tsunami run-up since 1498, whereas the white rims indicate that multiple historical tsunamis were recorded at one site (data based on the Natural Hazards Interactive Map of NOAA, http://ngdc.noaa.gov/hazard/hazards.shtml). BB = Bonaire Basin.

The controversial discussions on the tectonic evolution of the Caribbean Sea involve the "Pacific models", suggesting Late Cretaceous formation of the oceanic crust in the eastern Pacific, and "Alternative models" implying crustal formation west of its recent location, though still between North and South America (Meschede and Frisch, 1998: p. 269-270). Currently, the model of "single-arc Pacific origin", which is outlined in detail by Pindell and Kennan (2009), experiences the broadest acceptance. Eastward migration of the Caribbean Plate (CP) relative to the North (Cenozoic offset c. 1000 km) and South American Plates (NAP, SAP) resulted in a major subduction zone in the east and complex patterns of strike-slip processes in the north and south (Fig. 1) (Meschede and Frisch, 1998). Though being part of the Caribbean geographical region, the ABC Islands are located on the Bonaire microplate, which is a component of the Late Cretaceous-Early Cenozoic Leeward Antilles Ridge (LAR), in the active transpressional boundary zone between the CP and the SAP (Audemard et al., 2005). The LAR involves northeast-southwest extension, creating a roughly northwest-southeast-striking normal fault pattern (Hippolyte and Mann, 2011).

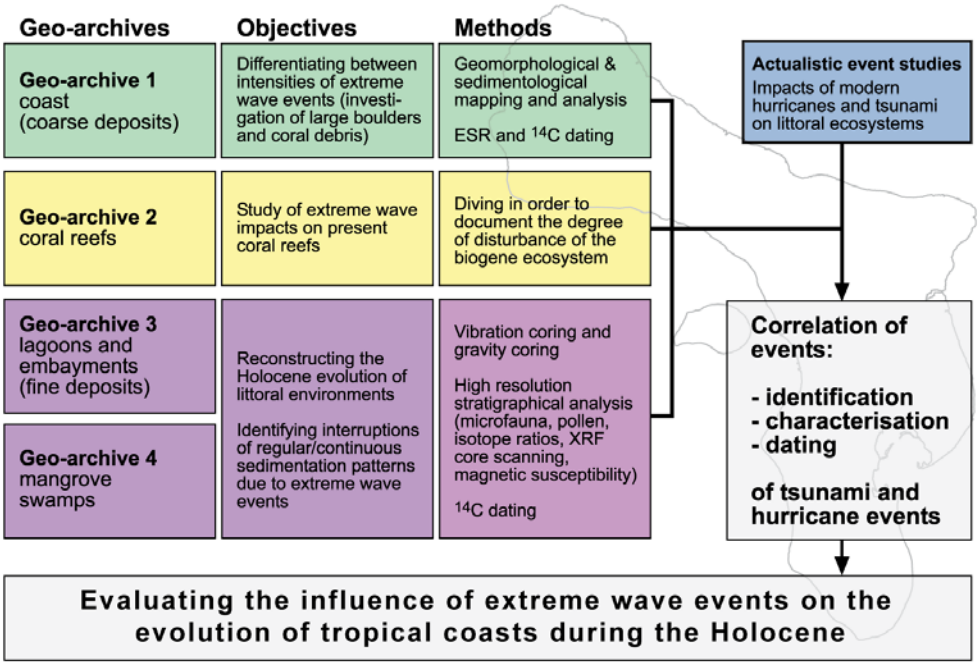

Fig. 2: Organisational chart of the research program "Key Processes in the Holocene Evolution of Tropical Coasts – Evaluating the Role of Hurricanes and Tsunamis", which provides the conceptual framework of this dissertation (modified after Engel et al., 2009a).

The geology of Bonaire is depicted in the following chapters. The oldest geological unit of Bonaire (Washikemba Formation) comprises the Late Cretaceous volcanic core of basalt, andesite, and dacite, as well as pelagic cherts, limestones, volcanoclastic boulder beds, conglomerates, and sandstones (Beets et al., 1977). It represents an intra-oceanic arc sequence slightly older than the bulk of the Caribbean plateau itself (Thompson et al., 2004). A sequence of Quaternary marine limestone terraces connects and fringes the Washikemba Formation. The limestone terraces were formed by *in-situ* deposition of coral reefs during periods of sea level highstand and subsequent tectonic uplift (De Buisonjé, 1974; Herweijer and Focke, 1978). The youngest terrace (Lower Terrace) dates back to MIS

5e (Bandoian and Murray, 1974; Jackson and Robinson, 1994). It has a width of up to 600 m at the windward coast and is dissected by narrow cuts perpendicular to the shoreline. These features, named bokas or saliñas, represent drainage systems formed during periods of sea level lowstands (Zonneveld et al., 1977). Today, these former river valleys are inundated and characterised by high salinity and lacustrine sedimentation. Most of them are separated from the sea by a barrier of coral debris.

1.4 Study outline

The key topic of this dissertation is the analysis of Holocene stratigraphical archives along the coast of Bonaire. The idea, however, that tsunamigenic overwash deposits can be expected in these archives, is based on predecessor studies of the coarse-clast record on Bonaire, which eventually raised the tsunami hypothesis (Scheffers, 2002). This hypothesis was challenged later on (see Chapter 1.2). Thus, *Chapter 2*, following this introduction (*Chapter 1*), deals with a re-evaluation of the boulder- and block-sized deposits using new high-accuracy field measurements and improved state-of-the-art models of coarse-clast transport by waves. Based on the calculation of minimum wave heights required to quarry and transport the largest boulders, storm waves were ruled out for being capable to move the largest blocks, thus corroborating the tsunami hypothesis. *Chapter 3* is dedicated to sedimentary criteria common in tsunami and storm deposit. It also provides a short introduction and references to physical properties of tsunamis and potential triggering mechanisms. The thorough literature review exposes the difficulties in distinguishing between storm and tsunami deposits in Holocene stratigraphical archives and points out possible strategies to minimize these problems.

The first case study on subsurface overwash deposits of extreme wave events and their influence on coastal geo-ecosystems covers the windward (east) coast of Bonaire (*Chapter 4*). A detailed facies model for the sediment archive is established supporting the identification and interpretation of tsunamigenic strata. *Chapter 5* refers to the first pollen study of the ABC Islands from the same location and, thus, is tightly connected to *Chapter 4*. Samples from sediment cores of *Chapter 4* were used to investigate the impact of extreme wave events on vegetation and to evaluate pollen as a proxy for the detection of possible disturbances by tsunamis in the light of similar applications in international literature. Research on the sedimentary archives of the leeward (west) coast of Bonaire is depicted in *Chapter 6*, again focusing on the identification, characterisation (storm or tsunami) and dating of sand-sized overwash deposits. *Chapter 7* contains sedimentary evidence for an outstanding prehistoric wave event and its long-term impact on bokas from the Washington-Slagbaai National Park, northwestern Bonaire. Furthermore, it summarises findings from other parts of the island and, for the first time, potential sedimentary evidence from further fine-grained sediment archives of the Caribbean coasts.

Sedimentary data elaborated in *Chapters 4, 6* and *7* were used to construct and discuss the first local relative sea level curve for Bonaire in *Chapter 8*. *Chapter 7* already contains substantial concluding elements, thus, the actual summary and synopsis (*Chapter 9*) is kept concise. It incorporates selective ESR and ^{14}C ages of onshore coral samples taken from sites covered by this dissertation, which belong to an entirely new and unpublished dataset.

2 Bonaire's boulder fields revisited: evidence for Holocene tsunami impact on the Leeward Antilles*

Abstract: Supralittoral boulders and blocks are prominent sedimentary features along rocky shorelines worldwide. In many cases, their deposition is attributed to high-energy wave events (tsunamis, severe storms). Even though tsunami waves are expected to have higher transport capacities compared to storm waves, clasts of up to 100 t were observed to have been moved laterally by the latter waveform. The deduction of certain extreme wave events (tsunamis, severe storms) from the boulder record thus remains a major challenge in palaeo-event research; the debate on their differentiation is ongoing. At the eastern coast of Bonaire (Leeward Antilles) in the southern Caribbean, numerous limestone blocks and boulders (up to c. 130 t) are distributed on top of a 3-6 m a.s.l. (above mean sea level) palaeo-reef platform. Disagreement exists among a number of authors concerning the transport processes involved in the formation of the boulder fields. In this paper, state-of-the-art modelling approaches of coastal boulder entrainment and transport were applied in order to provide new and more reliable data to support/challenge the working hypothesis of tsunami deposition. To improve the reliability of the boulder transport model, more realistic input parameters were provided by new DGPS measurements of the boulder dimensions and the calculation of bulk densities by taking into account the heterogeneity of the reef-rock boulders. Existing hydrodynamic equations were modified to allow for the irregular shape and real dimensions of the boulders. The results indicate that (i) boulder weight and dimension, and thus (ii) calculated wave energy and wave heights were overestimated in most of the previous studies, where calculations of boulder volume were based on multiplication of the main axes. The results of this study and wave heights observed during recent severe tropical cyclones seem to rule out storm-generated waves for the dislocation of the largest blocks. However, the majority of coarse-clast deposits may have been generated by periodic hurricane swells. The results underline the significance of more realistic field data in modelling boulder transports by waves.

Keywords: *Boulder transport, Tsunami, Volume calculation, Bulk density, Coral limestone, Caribbean, Coastal hazard*

2.1 Introduction

Supralittoral boulders are prominent sedimentary features along rocky shorelines worldwide (Moore and Moore, 1984; Mastronuzzi and Sansò, 2000; Rubin et al., 2000; Kelletat and Schellmann, 2002; Scheffers and Kelletat, 2003; Noormets et al., 2004; Matsukura et al., 2007; Scicchitano et al., 2007; Hansom et al., 2008; Frohlich et al., 2009; Goto et al., 2009, 2010; Bourgeois and MacInnes, 2010; May et al., 2010; Regnauld et al., 2010; Switzer and Burston, 2010; Etienne et al., 2011). In the Caribbean, they have been studied in terms of their transport processes on Grand Cayman (Jones and Hunter, 1992), Jamaica (Robinson et al., 2006, 2008; Khan et al., 2010), the Bahamas (Hearty, 1997;

* This chapter is based on: Engel, M., May, S.M., 2012. Bonaire's boulder fields revisited: evidence for Holocene tsunami impact on the Leeward Antilles. Quaternary Science Reviews, doi: 10.1016/j.quascirev.2011.12.011.

Kelletat et al., 2004), Puerto Rico (Moya and Mercado, 2006), Anegada (Buckley et al., 2011), Barbados, Anguilla, St. Martin, Guadeloupe, Grenada (Scheffers et al., 2005; Scheffers and Kelletat, 2006), Venezuela (Schubert,1994), as well as Aruba, Curaçao and Bonaire (Scheffers, 2002, 2005; Morton et al., 2006, 2008; Spiske et al., 2008; Pignatelli et al., 2010; Watt et al., 2010). Supralittoral boulder accumulations have been attributed to "exceptional disturbances of sea level" (Bird, 2008: p. 32) due to storm surges, tropical cyclones (known locally as hurricanes), or tsunamis. Thus, they have the potential to provide a historical context of past inundation and represent a basis for the definition of possible future inundation zones – provided that their transport mechanisms are inferred correctly.

Although the extraordinarily long period of a tsunami (in the order of 5-60 min) implies a higher transport capacity compared to shorter waves induced by storms or tropical cyclones (in the order of 10-20 s) (Noormets et al., 2004), clasts of up to 96 t were observed to have been moved laterally for short distances by the latter waveform (e.g. Noormets et al., 2004; Goto et al., 2009; Khan et al., 2010). Even cliff-top deposits in high elevations may be generated by large swell waves (Hansom et al., 2008). This hampers the deduction of certain extreme wave events, extraordinary storms or tsunamis, from the boulder record; hence, the debate on their differentiation is ongoing (e.g. Nott, 2003; Goff et al., 2004; Scicchitano et al., 2007; Barbano et al., 2010; Benner et al., 2010; Goto et al., 2010; Regnauld et al., 2010; Switzer and Burston, 2010; Nandasena et al., 2011), which is particularly true for Bonaire (Leeward Antilles).

During the past decade, the supralittoral boulder up to medium block (longest axis >8.2 m, cf. Blair and McPherson, 1999) deposits on Bonaire were the focus of several studies. Scheffers (2002) was the first to establish a link between episodic extreme wave events and the supralittoral coarse-clast ridges (elongated formations of coral rubble with steep flanks and sharp crests, up to 5-6 m a.s.l. [above mean sea level]), ramparts (poorly sorted coral debris with a planar, gently inland sloping profile, mostly 6-10 m a.s.l.) and single boulders (longest axis up to 10 m) on top of the Lower Terrace (LT) of Bonaire (Fig. 3). Based on the distribution of coastal landforms, altitude, shape and size of the clasts, their distance to the coastline, as well as observations on sediment transport during strong hurricane swells, it was suggested that tsunamis were responsible for some of the deposits (Scheffers, 2002; Scheffers et al., 2006). Previous workers attributed these accumulations solely to storm wave action (e.g. De Buisonjé, 1974; Zonneveld et al., 1977). Based on relative chronological contexts and radiocarbon data of infralittoral organisms attached to the boulders, Scheffers (2002) inferred dislocation and deposition of the boulders during the Mid- to Late Holocene. To date, precise chronological estimates of particular events were not possible (see *Chapters 2.5.4* and *9.3.2*).

Studies by the United States Geological Survey (USGS) challenged the interpretation on the tsunami origin of the deposits by Scheffers (2002, 2005) and concluded that the landforms described as ridges and ramparts were the product of "long-term coastal deposition" (Morton et al., 2008: p. 636), i.e. periodic storm waves, and that some of the boulders may have derived from the receding older terrace (Middle Terrace I [MT I]). Their high elevation was explained by post-depositional tectonic uplift (Morton et al., 2006). However, a second, more detailed study by the USGS stated "that the deposits were probably formed by a series of storm/hurricane events superimposed by at least one tsunami over 10s' to 1000s' of years" during the Holocene. The "large solitary boulders" were considered to be "consistent with tsunami deposits" (Watt et al., 2010: pp. 63, 60).

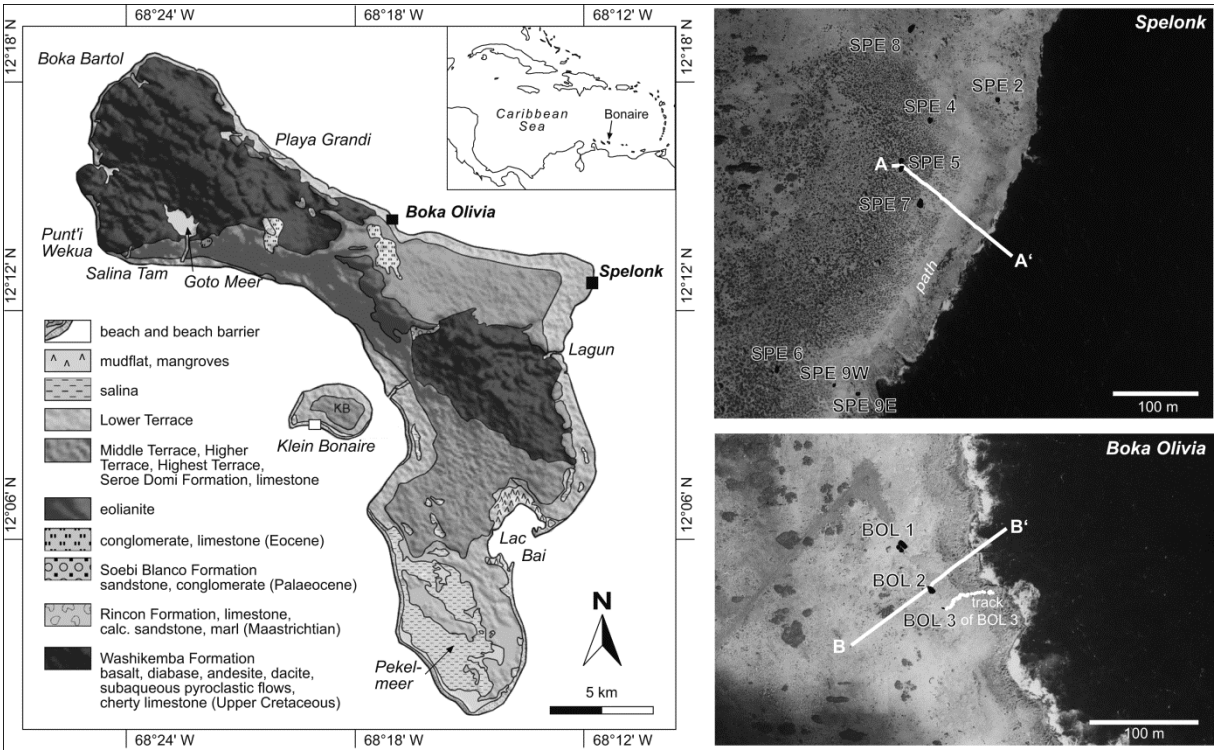

Fig. 3: Basic geological map of Bonaire based on Pijpers (1933), Westermann and Zonneveld (1956), and De Buisonjé (1974) as well as SRTM data (http://dds.cr.usgs.gov/srtm). Aerial views (1996; property of DROB) of the study sites at Spelonk and Boka Olivia are provided including the location of studied boulders, topographic/bathymetric transects (Figs. 4 and 6) and the exact track of clast BOL 3 (Fig. 7) which was recently quarried and transported during a storm event. The geographical positions of the boulders are given in Table 1.

Based on a re-evaluation of the bulk densities of the supralittoral boulders involving detailed Archimedean and optical 3D-profilometric investigations, Spiske et al. (2008) concluded that hurricane waves may also be capable of transporting the clasts by applying the hydrodynamic equations of Nott (2003). The authors considered a submerged scenario, an averaged empirical bulk density, and boulders of V (volume) = 5.3 m^3 and 7.0 m^3. Calculated minimum storm wave heights are consistent with observations during past tropical cyclones, whereas inferred minimum tsunami heights are lower than the elevation of the LT.

A second study on the hydrodynamic transport mechanisms based on Nott's (2003) model of boulder transport was conducted by Pignatelli et al. (2010), corroborating the conclusions of Scheffers (2002, 2005). The authors considered

(i) the largest boulders from Spelonk and Washikemba, assuming that V = a-axis · b-axis · c-axis,

(ii) bulk densities of 1.8 g cm^{-3} (Spiske et al., 2008) and 2.5 g cm^{-3} (Scheffers, 2005), and

(iii) a joint-bounded pre-transport scenario (JBBS) (Nott, 2003).

Pignatelli et al. (2010) inferred that the interplay of exceptionally strong storms and several tsunamis created the nearshore coarse-clast deposits of Bonaire.

For this study, new field data from the boulder fields of Bonaire were collected in order to provide more realistic input parameters for the reconstruction of minimum wave heights required to quarry and transport the boulders inland. We emphasize that V ≠ a-axis · b-axis · c-axis in the case of irregular boulders, even though most of the recent studies on nearshore boulder transport modes rely on this relationship (e.g. Nott, 2003; Noormets et al., 2004; Spiske et al., 2008; Pignatelli et al., 2009;

2010; Barbano et al., 2010; Benner et al., 2010; Regnauld et al., 2010; Switzer and Burston, 2010; Nandasena et al., 2011). Thus, we used DGPS volume measurements, a cost- and time-effective method, to establish more realistic values for V.

The blocks and boulders represent heterogeneous reef-rock and consist of varying percentages of several different lithofacies. Instead of using averaged (Spiske et al., 2008) or theoretical (Scheffers, 2005; Pignatelli et al., 2010) values, individual bulk densities (r_{bi}) for each boulder were identified by using the Archimedean principle, by conducting field mapping of the percentages of the various lithofacies units of a boulder, and by considering previous studies on local coralline lithofacies distribution (De Buisonjé, 1974; Kim and Lee, 1999). Enhanced values for V and r_{bi} lead to more realistic boulder weight (w_b) data. DGPS-based elevation data of the LT were generated in order to augment the calculations of maximum flooding (X_{max}) of extreme waves by Pignatelli et al. (2009).

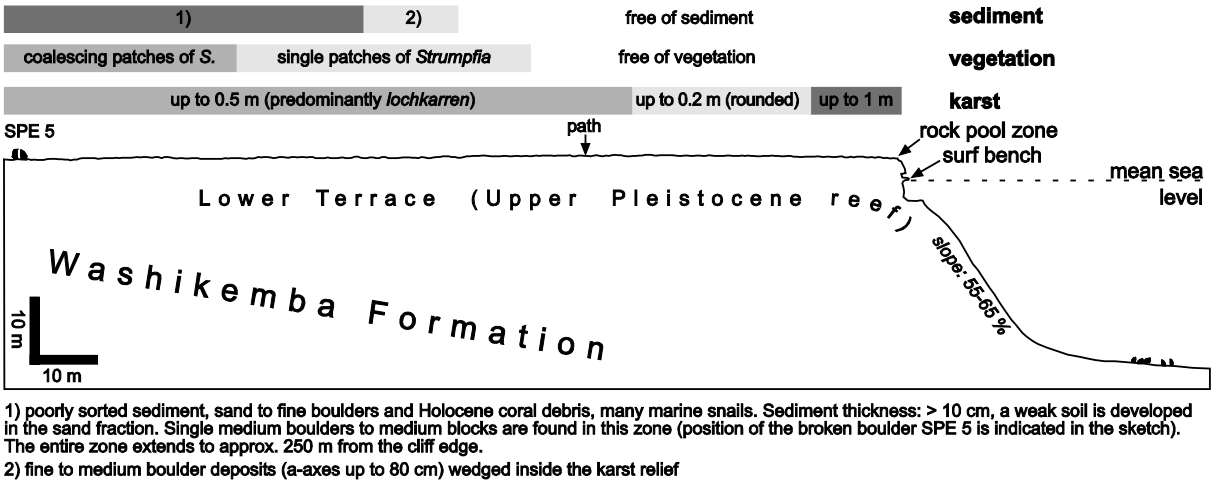

Fig. 4: Elevation transect A-A' (Fig. 3) of the Lower Terrace (LT) at Spelonk showing the distribution of sediment, vegetation and karst features. Elevation data is based on DGPS. Bathymetry is taken from Scheffers et al. (2006).

Based on the improved field data, minimum wave heights of storm waves and tsunamis required for quarrying and transporting megaclasts to their present position were calculated using hydrodynamic equations presented by Nandasena et al. (2011) based on Nott (2003). By using the calculated wave heights, which roughly represent the energy (dynamic pressure) of a wave (Noormets et al., 2004), the transport by (cyclone-generated) swell waves may or may not be ruled out, either supporting or challenging the tsunami hypothesis initially established by Scheffers (2002). Additionally, wave decay curves on top of the supralittoral platform are calculated according to Noormets et al. (2004) and Barbano et al. (2010), respectively, in order to provide a cross check for the results derived from the modified Nandasena et al. (2011) model. An approach of Pignatelli et al. (2009, 2010), developed from a formula of Hills and Mader (1997), is used to evaluate the maximum local flooding of a tsunami based on the landward distance of the largest megaclast.

2.2 Study area

2.2.1 Bonaire

The island of Bonaire, a special municipality of the Netherlands, is located in the southern Caribbean Sea, off the coast of Venezuela. Together with its western neighbours Curaçao and Aruba it represents the former Leeward Dutch Antilles or ABC Islands.

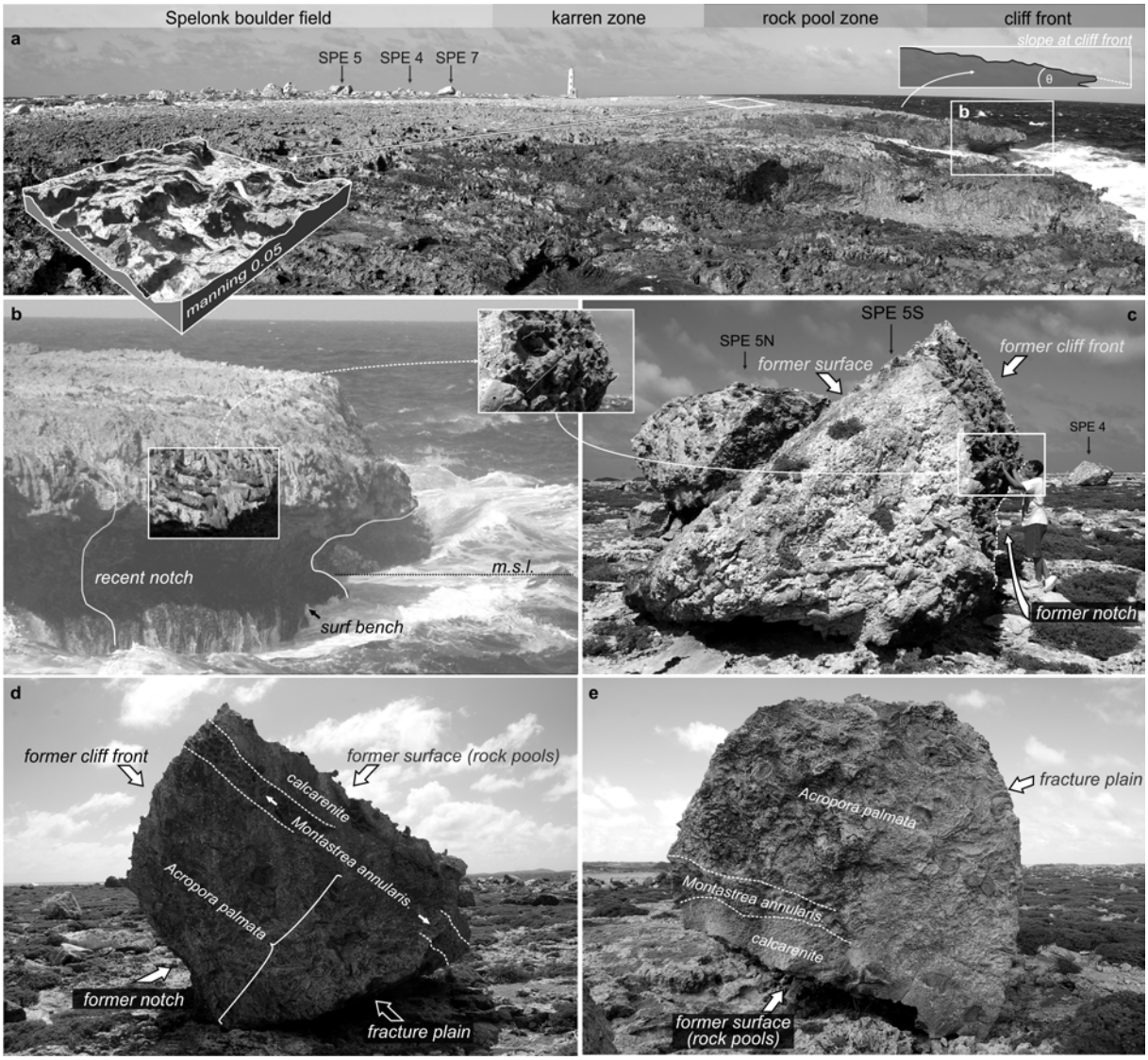

Fig. 5: Lower Terrace platform and boulders in the Spelonk area (photographs: S.M. May, M. Engel). a) Overview of the Spelonk setting with karstified platform and location of the Spelonk boulder field; inlay shows degree of karstification relating to a Manning coefficient n ≈ 0.05 (cf. Pignatelli et al., 2009); b) detail of cliff front showing recent notch and intense weathering at the terrace edge. Highlighted: horizontally bedded slabs of *Acropora palmata*, sculptured from the reef body by intense weathering; c) Boulder SPE 5S showing former notch and the same sculptured *A. palmata* remains as illustrated in b), giving clear evidence of the former position of the boulder; d-e) Boulder SPE 5S seen from the north (d) and SPE 5N seen from the south (e). SPE 5 was cracked at the end of transport and gives insight into the typical "*Acropora palamata* rudstone" (Kim and Lee, 1999) or "Barrier reef zone" (De Buisonjé, 1974) facies.

2.2.1.1 Tectonic setting

The island lies on the Bonaire microplate within the transpressional boundary zone between the Caribbean Plate (CP) and the South America Plate (SAP). The general vector motion of the CP relative to the SAP is towards the east implying right-oblique convergence inside the boundary zone, where microplate interaction involves strike-slip motion, compression, as well as extension (Audemard et al., 2005). NE-SW extension along the Leeward Antilles ridge including the Bonaire microplate determines the roughly NW-SE-striking normal fault pattern (Hippolyte and Mann, 2011). Tectonic uplift of 5 cm/1000 years and tilting is linked with active folding or faulting (Herweijer and Focke, 1978), and the southward shallow subduction of the CP under the SAP west of the right-oblique convergence zone (Hippolyte and Mann, 2011).

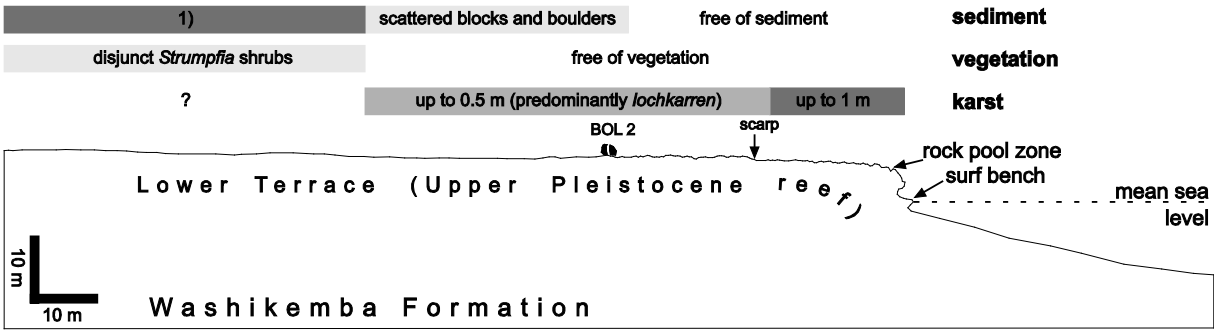

Fig. 6: Elevation transect B-B' (Fig. 3) of the Lower Terrace (LT) at Boka Olivia showing the distribution of sediment, vegetation and karst features. Elevation data is based on DGPS. Bathymetry is taken from Watt et al. (2010).

2.2.1.2 Geology

Mid- to Late Cretaceous submarine volcanism initiated the genesis of Bonaire (Fig. 3). Today, the c. 5 km thick succession of basalt, andesite, dacite, pelagic cherts and cherty limestones (Washikemba Formation) is exposed in the northwest and the east of the island. The Washikemba Formation is unconformably overlain by small and disjunct units of Late Cretaceous limestones and sandy marls (Rincon Formation), Paleocene fluvial conglomerates and sandstones (Soebi Blanco Formation), as well as Eocene conglomerates limestones and marls (Pijpers, 1933; De Buisonjé, 1974; Beets et al., 1977). The two volcanic units of the island are surrounded and linked by a sequence of depositional limestone terraces representing reef bodies of former sea level highstands. Five main levels have been identified between 150 and 10 m a.s.l., which can be traced on Aruba and Curaçao as well (De Buisonjé, 1974). The youngest fossil carbonate platform (Lower Terrace [LT]) is of MIS 5e age, the subsequent stage (Middle Terrace I [MT I]) formed approx. 500,000 years ago (Herweijer and Focke, 1978; Schellmann et al., 2004). The LT has a height of up to 15 m a.s.l. in the northwest, 3-6 m a.s.l. in the central part and descends to sea level in the south, where it has its widest extension. Along the eastern and northern coast, the LT is 600 m wide on average (De Buisonjé, 1974).

2.2.1.3 Wave climate

The east coast of Bonaire, including the study sites of Spelonk and Boka Olivia, is exposed to easterly trade winds and experiences wave heights of 2.0-3.5 m throughout the year (Van Duyl, 1985). During regular wave action, an average wave period (T) of 6 s was measured near Boka Olivia (Jan. 4th 2011). Extreme waves induced by E-W-tracking tropical cyclones and their influence on the coastal morphology of Bonaire are best documented for Hurricane Ivan (Scheffers and Scheffers, 2006), which was a typical Cape Verde hurricane developing from a tropical wave off West Africa (Stewart, 2004). Between the 8th and 9th of Sep. 2004, the eye of Ivan passed at a distance of 130 km north of the ABC Islands generating wind speeds of up to 230 km/h (Meteorological Service of the Netherlands Antilles and Aruba, 2010c). It passed Bonaire as a major hurricane and reached category 5 just northwest of Aruba. Waves rose up to 12 m (face) on Sep. 15th (Scheffers and Scheffers, 2006), which is in accordance with other reports of maximum swell wave heights in the Caribbean (e.g. Cambers, 2008). The waves originated from a wide, easterly swell. The flow depth on top of the LT at the north coast was up to 1.5 m, flow velocity amounted to approximately 5-7 m s^{-1} and landward inundation was up to several hundred meters (Scheffers, 2005; Scheffers and Scheffers, 2006). A wave period of 13 s at the northwestern coast was deduced from videos taken by A. Scheffers and S. Scheffers (pers. comm.). This is in line with maximum wave periods of hurricane swells measured by buoys in the central Car-

ibbean Sea (e.g. T = 16 s during the passage of Hurricane Emily, Jul. 15th 2005, 15.093N 75.064W, http://www.ndbc.noaa.gov/historical_data.shtml).

For Hurricane Joan (Jul. 16th 1988), Kobluk and Lysenko (1992) report waves of up to 3 m at the BOPEC oil storage on the leeward side of Bonaire near Saliña Tam. Hurricane Lenny (Nov. 16th, 1999) approached Bonaire from the west and generated waves of at least 3-6 m at the leeward side (Bries et al., 2004), which created several fresh beach ridges (Scheffers, 2005; Spiske and Jaffe, 2009). Accompanied storm surge, i.e. a rise in sea level induced by wind shear, is supposed to be relatively small on Bonaire due to the steep submarine slope and narrow reef (Spiske and Jaffe, 2009; pers. comm. D. Kelletat). For Hurricane Lenny it was reported to be in the range of up to 0.6 m (Richter and Richter, 1999). Tsunamis, however, have never been directly observed on Bonaire during the past 500 years, even though they repeatedly impacted the vicinal Venezuelan coast (Schubert, 1994; O'Loughlin and Lander, 2003).

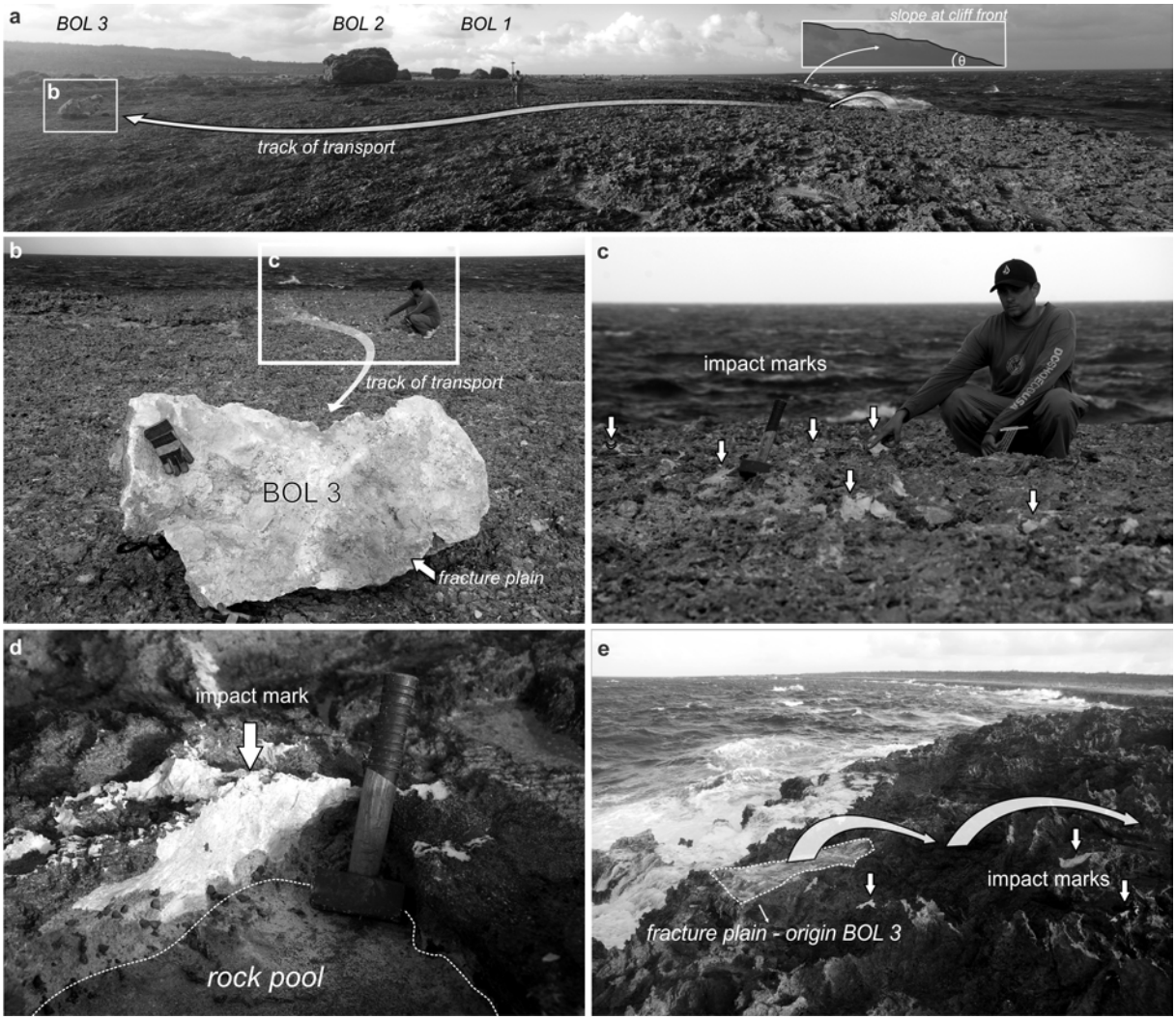

Fig. 7: Boulder BOL 3 at Boka Olivia, moved and transported during a recent storm event (photographs: S.M. May, M. Engel). a) Overview of boulder setting; b) track of transport along the reef top platform (cf. Fig. 3); c-d) impact marks along the track, generated by rolling and saltation during boulder transport; e) origin of boulder BOL 3 at the cliff front. Fracture plane shown in b) is marked by dotted area.

2.2.2 Spelonk (SPE) and its coarse-clast record

The area south of Spelonk Lighthouse at the eastern windward coast occupies the LT platform and exhibits the most extensive supralittoral coarse-clast record of Bonaire (Scheffers et al., 2006; Pignatelli et al., 2010). The seaward platform has a height of c. 3.5 m and the inland slope angle (α) is c. 0°. Only at shoreline reentrants (small indentations generated by sea-directed surface runoff, cf. Watt et al., 2010) close to the terrace edge, is α between 2.3 and 5.5°. A rock pool zone at the terrace edge with high bioabrasive activity merges into a moderately karstified surface on top of the platform (Figs. 4 and 5a).

The nearshore sediment-free zone, influenced by periodic storm wave overwash, extends up to 65 m inland. Up to 80 m, fine to medium boulders are wedged into the *lochkarren* (solution cavities) topography. From c. 80-250 m, blocks and boulders are distributed over the LT, which is covered by a very poorly sorted sheet of sand to fine boulders and coral debris (thickness >10 cm) containing many marine gastropod shells. The sand fraction hosts an initial soil horizon.

The sublittoral zone of Spelonk consists of a narrow platform (5-9 m below mean sea level) descending with a slope angle of 55-65% to a level of c. 20 m where the inclination significantly decreases (Fig. 4). According to the huge amount of coral rubble transported onshore, a fringing Holocene reef must have existed along large parts of the southern and northeastern windward coast (Sommer et al., 2011). At Spelonk, however, onshore coral rubble is almost absent since the water depth did not support Mid- to Late Holocene reef growth. It is suggested that the windward reef has been irreversibly destroyed by a tsunami around 3100 years BP (Scheffers et al., 2006). At Spelonk, eight blocks and boulders were studied in detail, including the largest ones (Figs. 3 and 5; Table 1).

2.2.3 Boka Olivia (BOL) and its coarse-clast record

Boka Olivia forms an indentation along the ENE-oriented coast (Fig. 3). The height of the terrace is c. 5 m and the slope angle in the area of the studied boulders ($\alpha \approx 8.7°$) is significantly larger compared to Spelonk, because they cluster inside the shoreline reentrants (cf. Watt et al., 2010). The seaward belt is intensely weathered, comprising large flat-bottom rock pools. *Lochkarren* dominate the platform surface further inland (Fig. 6). Twenty-five metres from the terrace edge, a scarp c. 0.5 m in height occurs. Block BOL 2 is located c. 45 m away from the terrace edge (6.8 m a.s.l.). Several other large boulders are scattered landward of BOL 2, while smaller ones are wedged into the karst relief. At c. 70-175 m inland, Watt et al. (2010) investigated a flat ridge of sand, cobbles, pebbles and boulder material with two crests at 78 and 110 m inland. Its thickness is up to 0.65 m.

At Boka Olivia, the bathymetry is not as steep as at Spelonk (Fig. 6). Instead, the sea floor descends gently to a depth of 20 m about 120 m offshore. 725 m from the terrace edge, the shelf drops stepwise to a depth of 140 m (Watt et al., 2010). A cluster of three boulders representing one former megaclast which broke during deposition was studied (BOL 1). BOL 2 is the largest block and BOL 3 was quarried and transported during a recent storm event, leaving impact marks on top of the karstified platform during rolling/saltation (Figs. 3 and 7; Table 1).

2.3 Field and laboratory measurements

In a first step, the blocks and boulders of the Spelonk and Boka Olivia boulder fields were chosen according to their size, shape, distance to other boulders and distance to the terrace edge. The can-

didate clasts include the largest observed blocks, slab-like, roughly cubic and rectangular boulders, as well as assembled and isolated ones. In addition, two smaller boulders moved during Hurricane Ivan in 2004 (Scheffers and Scheffers, 2006) and a later storm, respectively, were selected.

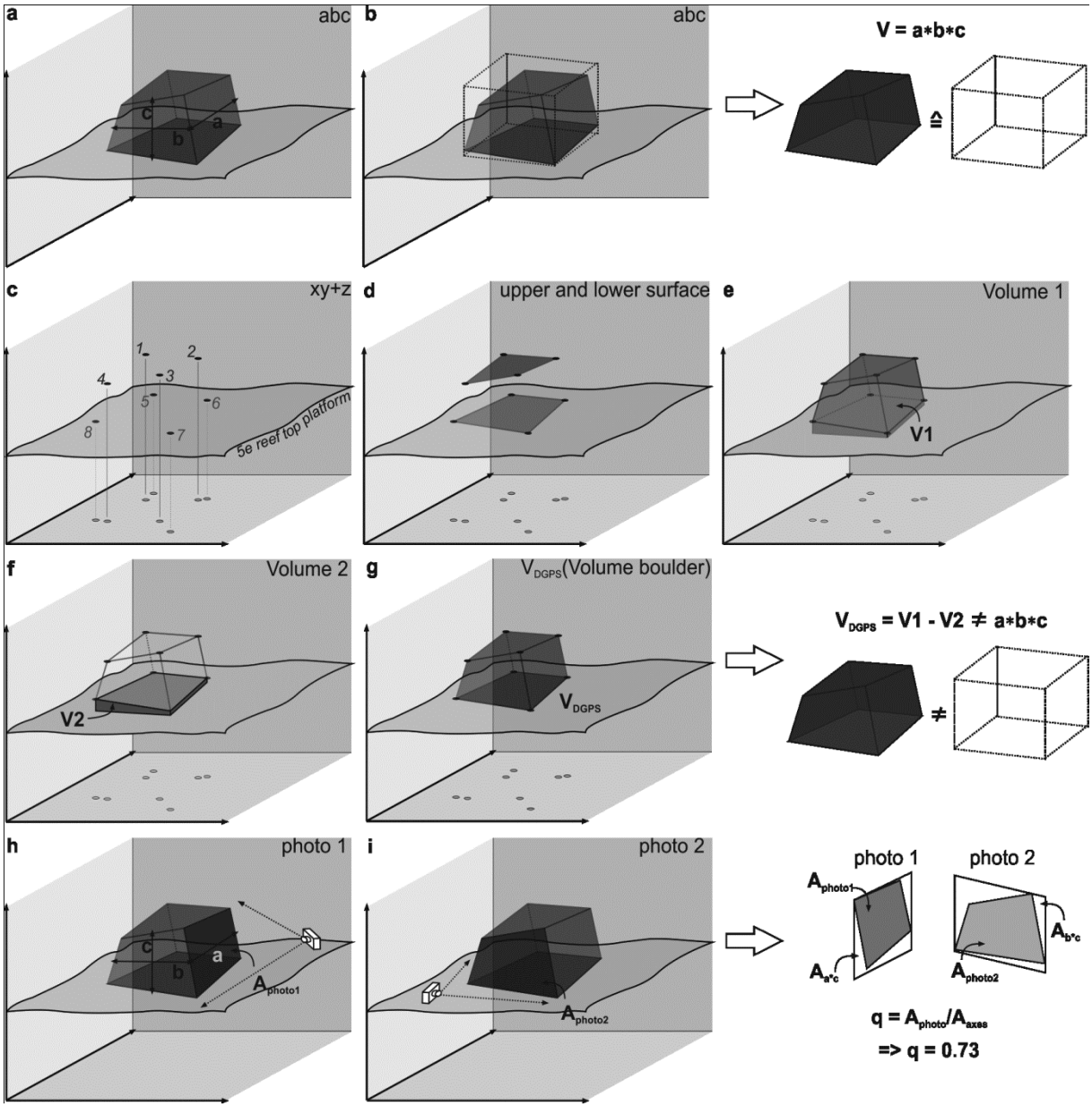

Fig. 8: a-b) Volume calculation by multiplication of a- (length), b- (width) and c- (height) axes of a boulder in case V = a · b · c is assumed; c-d) volume calculation using high-resolution DGPS (vertical/horizontal error: ±2 cm); c) position of upper and lower vertices and edges of the boulder were measured and imported into a GIS (ESRI ArcGIS; x/y = latitude/longitude; z = elevation); d) upper and lower boulder edges were used to translate point clouds into 3D surfaces of the upper and lower side of the boulder; e) calculation of volume between a boulder's upper surface, additional selected lateral points of the boulder (boulder surface envelope) and the ground surface/reef platform (V1); f) calculation of volume between a boulder's lower surface and the ground surface/reef platform (V2); g) calculation of boulder volume (V_{DGPS}) by subtraction of V2 from V1. Prominences were subtracted the same way. V_{DGPS} in one case is only 38% of V_{abc}, whereas the average value is 49% (Table 2); h-i) calculation of area coefficient q after Robinson et al. (2008). Lateral areas of each boulder were photographically documented and measured using a graphics programme. The coefficient q is the average value of all measured lateral areas with respect to a uniform rectangle put around the area (average value of A_{photo}/A_{axes} in Table 2) (design: S.M. May).

For calculating the boulders' dimensions, three general approaches were applied (Fig. 8):

(i) a- (length), b- (width) and c- (height) axes of the selected boulders were measured for conventional calculations of $V_{abc} = a \cdot b \cdot c$ using a measuring tape (Fig. 8a-b).

(ii) Upper and lower vertices and edges were measured using a Leica SR 530 and a Topcon HiPer Pro differential global positioning system (DGPS) in order to calculate their volume with high accuracy. Lateral and vertical deviations of the DGPS lie in the range of ±2 cm. The DGPS-measured point cloud was imported into a GIS (ESRI ArcGIS) and translated into 3D surfaces by computing triangulated areas between the GPS points. The boulder volume (V_{DGPS}) was calculated by subtraction of the volume between the boulder's lower surface and the ground surface/reef platform (V2) from the volume between the boulder's upper surface and the ground surface/reef platform (V1) (Figs. 8c-g and 9).

(iii) Additionally, lateral areas of each boulder were photographically documented and measured using a graphics software, following the procedure described by Robinson et al. (2008) to compensate for the overestimation of area calculations if simply two axes are multiplied (Fig. 8h-i). An average aspect coefficient q = 0.73 was calculated.

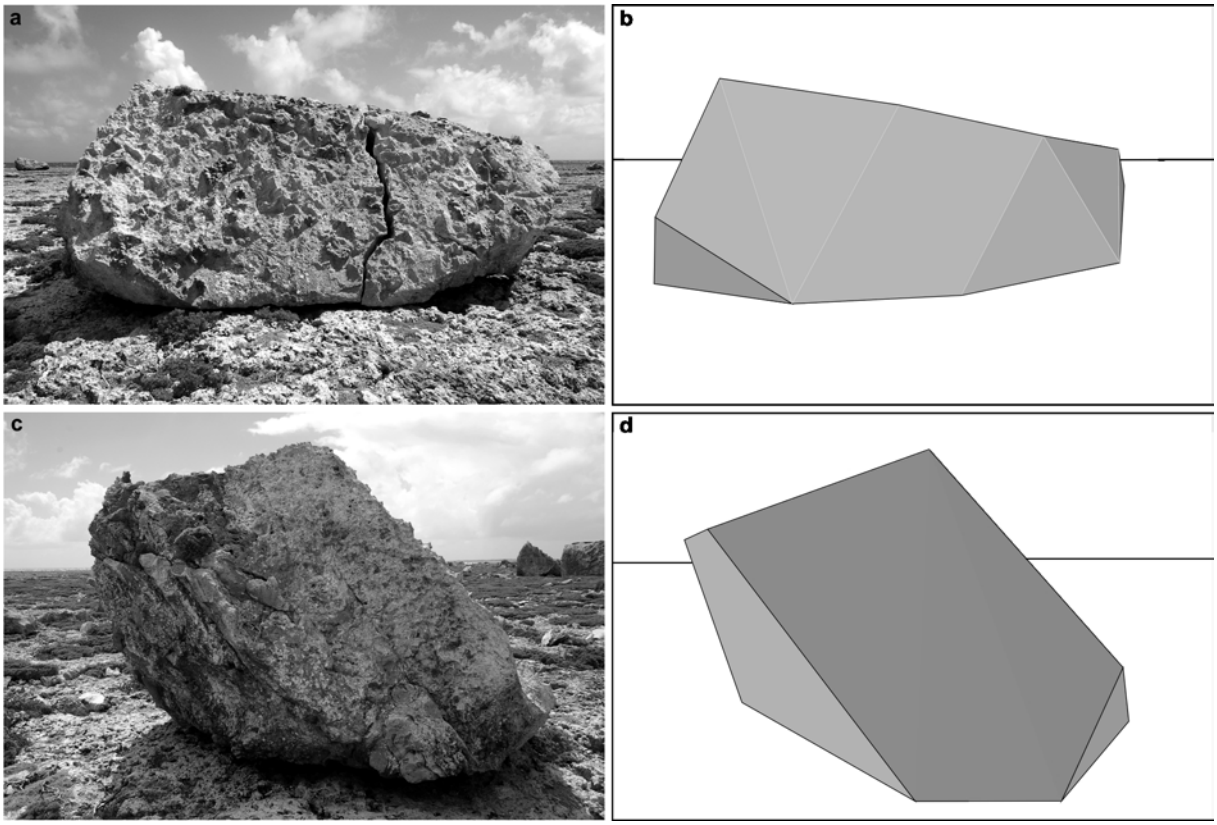

Fig. 9: Boulder SPE 4 viewed from two different perspectives as photo (a and c) and DGPS-based 3D model for volume calculation (b and d) (design, photographs: S.M. May, M. Engel).

In order to determine boulder weights (w_b), individual bulk densities of each boulder (ρ_b) were calculated. Realistic bulk densities are decisive for inferring minimum storm and tsunami wave heights from the boulder record (Spiske et al., 2008). Thus, the estimated percentage of different coralline lithotypes (ρ_i) and the calcarenite matrix was multiplied with their correlating densities (ρ_{bi}).

The presence of coralline lithotypes was estimated in the field by considering the clear zonation of coral assemblages in the boulders (Fig. 5d-e) and by taking into consideration the quantitative de-

scriptions of Kim and Lee (1999). Densities of each coralline lithotype (ρ_{bi}) were calculated using the Archimedean principle (buoyancy in sea water) as described by Hughes (1987), Bucher et al. (1998) and Spiske et al. (2008):

(1) $$\rho_{bi} = \rho_{sw} \cdot \frac{w_a}{(w_a - w_f)}$$

where ρ_{sw} = 1.02 g cm^3 = density of sea water, w_a = weight of the sample in air, and w_f = weight of the sample in sea water (constant temperature). Bulk densities are calculated through

(2) $$\rho_b = \sum \rho_{bi} \cdot r_i.$$

Digital hanging scales were used to determine w_a and w_f. All data are available in Table 1. The largest boulder at Spelonk weighs 135 t (SPE 5, Fig. 5c-e). At Boka Olivia, the maximum weight is 149 t (BOL 2, Fig. 7a). Boulders quarried and moved during Hurricane Ivan and a later storm, respectively, are 9 (SPE 9) and 1 t (BOL 3).

2.4 Extreme waves on Bonaire

2.4.1 Entrainment, transport and emplacement of boulders by tsunamis and storm-induced waves

When swell waves, e.g. generated by tropical cyclones, approach the coast, they increase in height (H_b) due to a decrease in water depth (h_w). Waves break if H_b/h_b ($h_b = h_w$ at the breaking point) reaches values of 0.71-0.78 in the case of a low subaquatic slope angle and 0.78-1.03 in the case of a steeper slope as on Bonaire (Noormets et al., 2004).

In the open ocean, tsunamis have amplitudes in the order of decimeters but they grow in amplitude when reaching shallow waters (Switzer and Jones, 2008a). Per definition, tsunamis are long waves ($L_0/h_w > 20$ in the open ocean) with wavelengths (L_0) in the order of hundreds of kilometers compared to hundreds of meters regarding swell waves. Approaching the shelf region, a tsunami reduces its speed while increasing its height. Coastal inundation occurs in the form of a temporary sea level rise by the shoreward moving of a broad sheet of water or by a wall of water similar to a tidal bore (Sugawara et al., 2008).

At a vertical cliff, breaking swell waves initially induce a short but very intense pressure impulse, before applying a longer persisting wave pressure – both forms adding to dynamic pressure which positively correlates with wave height. In contrast, tsunamis with periods (T) of minutes up to an hour or more generate turbulent unidirectional flows along the entire vertical profile of the bore and stress the seaward platform for several minutes (Noormets et al., 2004). Regarding the Caribbean, T = 10 min was documented for the 1867 Virgin Island Tsunami on St. Thomas, NE Caribbean (O'Loughlin and Lander, 2003). A small tsunami generated by the Caracas Earthquake in 1967 (M_w = 6.1) had a period of 10.8 min at the Venezuelan coast (Robson and Canales, 1968).

Concerning the pre-dislodgement setting of the boulders at Spelonk and Boka Olivia, the joint-bounded boulder scenario (JBBS), a concept which was introduced by Nott (2003), is the most likely one (see also Pignatelli et al., 2010), similar to the geomorphological conditions described by Noormets et al. (2004). Previously, all of the large boulders investigated in this study must have been part of the terrace edge, since they comprise the upper part of the notch as well as rock pools from the most seaward surface of the LT (Fig. 5b-c). Furthermore, according to eyewitness accounts, sev-

eral boulders recently emplaced by swell waves were unambiguously dislodged from the seaward end of the platform and transported landward during the same process (see Figs. 20, 22 in Scheffers and Scheffers, 2006). Additional proof is provided by the tracks of freshly damaged karst surface, generated by rolling/saltating boulder transport, which lead directly from the fresh scarp at the terrace edge to the boulder's current position (BOL 3, Fig. 7). Quarrying the boulders requires the presence of initial cracks. Based on a case study from Oahu, Hawai'i, Noormets et al. (2004) estimate that fracturing has to amount to 60% of the later failure plain in case of swell waves and even c. 70% in case of a tsunami until a boulder becomes dislodged from the terrace edge. Quarrying occurs during a balance of moments, when

$$F_C \cdot l_C + F_L \cdot l_L = F_W \cdot l_W + F_G \cdot l_G + F_T \cdot l_T \quad (3)$$

where F_C = force applied by the wave in the cracks; F_L = lift force of the wave; F_W = wave force applied on the terrace edge (including inertia force); F_G = submerged weight of the boulder; F_T = tensile force of the attached part of the boulder (Noormets et al., 2004). Parameter l indicates the lever arm of each force (Fig. 10).

Table 1: Compilation of investigated boulders including their geographical position, lithofacies (each represented by at least one sample), estimated percentages of lithofacies subtypes within the boulder (ρ_i), weight of the samples in air (w_a) and seawater (w_f), densities of lithofacies subtypes (ρ_{bi}) and bulk densities (ρ_b). For calculation of ρ_{bi} and ρ_b see Eqs. (1) and (2).

Boulder	Samples	Lithofacies subtype	w_a (kg)	w_f (kg)	ρ_{bi} (g cm^{-3})	ρ_i	ρ_b (g cm^{-3})	Remarks
SPE 2 12.20998027N 68.19766319W	SPE 2/1	*A. palmata*	0.86	0.45	2.17	0.15	2.28	Palaeo-surface inclined (45 °); 2 rock pool generations indicate dislocation during one event; former notch at the bottom
	SPE 2/2	rudstone matrix	3.38	1.86	2.26	0.25		
	SPE 2/4	*A. cervicornis*	1.73	0.97	2.31	0.60		
SPE 4 12.20976823N 68.19838404W	SPE 4/1	*A. palmata* + rudstone matrix	4.60	2.52	2.25	0.30	2.15	Former rock pool surface inclined westwards
	SPE 4/2	*Montastrea* sp.	1.04	0.43	1.73	0.20		
	SPE 4/3	rudstone matrix	2.24	1.23	2.26	0.20		
	SPE 4/4	rudstone matrix	2.80	1.53	2.25	0.30		
SPE 5S 12.20928088N 68.19869388W	SPE 5S/1	*A. palmata* + rudstone matrix	1.74	1.00	2.39	0.30	2.24	SPE 5 broke into two main pieces during deposition; emplacement and transport occurred in one piece;
	SPE 5S/2	*A. cervicornis* + rudstone matrix	2.31	1.26	2.26	0.10		
	SPE 5S/3	*A. palmata*	2.15	1.08	2.05	0.20		
	SPE 5S/4	rudstone matrix	0.45	0.25	2.32	0.30		
	SPE 5S/5	*Montastrea* sp. + rudstone matrix	1.11	0.51	1.90	0.10		
SPE 5N 12.20934351N 68.19869805W	SPE 5N/1	rudstone matrix	2.23	1.19	2.19	0.35	2.07	
	SPE 5N/2	rudstone matrix	1.60	0.76	1.95	0.25		
	SPE 5N/3	*Montastrea* sp.	0.97	0.17	1.23	0.05		
	SPE 5N/4	*A. cervicornis* + rudstone matrix	0.85	0.47	2.29	0.05		
	SPE 5N/5	*Montastrea* sp.	0.33	0.10	1.44	0.05		
	SPE 5N/6	*A. palmata* + rudstone matrix	2.27	1.25	2.28	0.25		

SPE 6 12.20712529N 68.20000551W	SPE 6/1	*A. palmata* mix	2.28	1.29	2.37	0.40	2.30	Notch can be identified and is turned landward; b-axis is the longest axis
	SPE 6/2	rudstone matrix	0.88	0.47	2.22	0.20		
	SPE 6/3	rudstone matrix	1.62	0.98	2.57	0.20		
	SPE 6/4	*Montastrea* sp. + rudstone matrix	0.84	0.48	2.37	0.10		
	SPE 6/5	*Diploria* sp.	1.51	0.56	1.62	0.10		
SPE 7 12.20888111N 68.19848703W	SPE 7/1	*A. palmata*	1.82	1.03	2.35	0.25	2.40	Boulder upside down; former cliff edge turned landward
	SPE 7/2	rudstone mix	0.67	0.41	2.59	0.55		
	SPE 7/3	*Diploria* sp.	1.58	0.86	2.22	0.05		
	SPE 7/4	*Montastrea* sp.	0.32	0.13	1.74	0.10		
	SPE 7/5	*A. cervicornis* + rudstone matrix	2.30	1.19	2.12	0.05		
SPE 8 12.21076258N 68.19857905W	SPE 8/1	*A. palmata +* rudstone matrix	2.44	1.40	2.39	0.75	2.37	Flat, long a-axis
	SPE 8/2	*Diploria sp.* + rudstone matrix	1.94	1.12	2.41	0.05		
	SPE 8/3	*A. cervicornis* + rudstone matrix	3.60	2.00	2.30	0.20		
SPE 9E 12.20686109N 68.19914242W		100 % *Montastrea sp.* + rudstone matrix	$\rho_b = 0.5(\rho_{SPE\ 5S/5} + \rho_{SPE\ 6/4})$				2.14	Turned upside down, moved by Hurricane Ivan
SPE 9W 12.20695097N 68.19940350W		100 % *Montastrea sp.* + rudstone matrix	$\rho_b = 0.5(\rho_{SPE\ 5S/5} + \rho_{SPE\ 6/4})$				2.14	
BOL 1N 12.23779692N 68.28267341W	BOL 1N/1	rudstone matrix	4.30	2.50	2.44	0.40	2.27	BOL 1 in the same position as in its pre-transport setting; broke into three main pieces during deposition; emplacement and transport occurred in one piece
	BOL 1/AP	*A. palmata* + rudstone matrix	3.82	2.02	2.16	0.60		
BOL 1E 12.23776232N 68.28269024W		100% *A. palmata* + rudstone matrix	see BOL 1N				2.27	
BOL 1W 12.23778078N 68.28271668W		100% *A. palmata* + rudstone matrix	see BOL 1N				2.27	
BOL 2 12.23744082N 68.28246452W	BOL 2/1	*A. cervicornis* + rudstone matrix	3.34	1.94	2.43	0.1	2.19	Notch can be identified and is turned eastward; b-axis is the longest axis
	BOL 1/AP	*A. palmata* + rudstone matrix	3.82	2.02	2.16	0.9		
BOL 3 12.23727539N 68.28235839W	BOL 3/1	*A. palmata* + rudstone matrix	5.84	3.34	2.38	1.0	2.38	Recent storm boulder, rolling transport mode

2.4.2 Wave heights inferred from the boulder record

Nott (2003) suggests a simplified relationship concerning Eq. (3): if the lift force moment exceeds the restraint force moment ($M_L \geq M_R$), a joint-bounded boulder (JBB) at the terrace edge defined by cracks will be moved. The initial definition of F_L by Nott (2003) was modified since it is determined by the upper surface area of a JBB (e.g. Pignatelli et al., 2009; Benner et al., 2010; Nandasena et al., 2011):

(4) $$M_L = F_L \cdot \frac{b}{2} = 0.5 \cdot \rho_w \cdot C_L \cdot A_p \cdot u^2 \cdot \frac{b}{2}$$

(5) $$M_R = F_R \cdot \frac{b}{2} = (\rho_b - \rho_w) \cdot V \cdot g \cdot \frac{b}{2}.$$

The restraint force F_R is set equal with the vector sum of F_G and F_T in Eq. (3) and Fig. 10. Parameter A_p represents the upper area of the clast, defined by the product of width (a-axis) and depth (b-axis) of a clast in its original position at the terrace edge, multiplied with an empirical aspect coefficient q = 0.73. According to photographic measurements (cf. Robinson et al., 2008) of several aspects of the Spelonk boulders, the real aspect is only 73% on average of the product of the two axes (Fig. 8; Table 2). The remaining parameters are ρ_w = density of sea water = 1.02 g cm^{-3}; ρ_b = density of the boulder; u = speed of the water flow; C_L = coefficient of lift = 0.178 (e.g. Nott, 2003; Pignatelli et al., 2009; Switzer and Burston, 2010; Nandasena et al., 2011); V = V_{DGPS} = DGPS-based boulder volume; g = gravitational constant = 9.81 m s^{-1}.

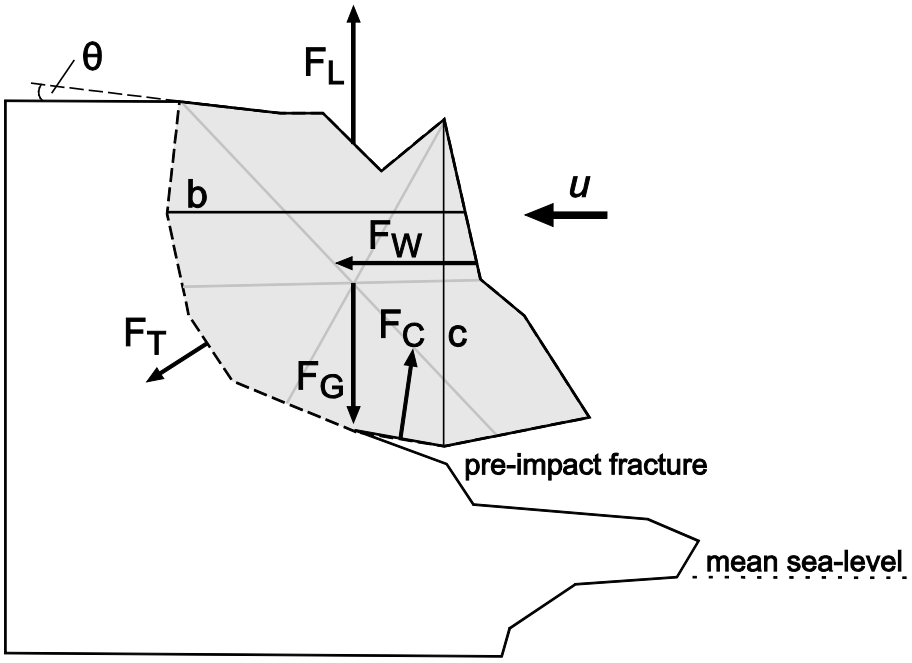

Fig. 10: Forces acting on a joint-bounded boulder (JBB) as described in Eq. (3) (after Noormets et al., 2004). Flow direction is indicated by the arrow of velocity (u). F_C = force applied by the wave in the cracks; F_L = lifting force of the wave; F_W = wave force applied to the terrace edge (including inertia force); F_G = submerged mass of the boulder; F_T = tensile force of the attached part of the boulder; θ = slope angle of the pre-transport setting; b = depth axis; c = height axis.

However, Nandasena et al. (2011) emphasize the necessity to balance the forces in the direction of lift in case of a JBBS and that the coefficient of static friction (μ = 0.65, cf. Benner et al., 2010) and the angle of the bed slope of the pre-transport setting θ (Fig. 10) should be considered. Thus, a boulder is detached from a rock platform when

(6) $$F_L \geq F_R \cdot \cos\theta + \mu \cdot \sin\theta.$$

The transposition of the balanced forces using Eqs. (4)-(6) reads:

(7) $$u^2 = \frac{(\rho_b - \rho_w) \cdot V \cdot g \cdot (\cos\theta + \mu \cdot \sin\theta)}{0.5 \cdot \rho_w \cdot C_L \cdot a \cdot b \cdot q}.$$

Flow velocity determines the transport capability of a wave and positively correlates with wave height H at the coastline after shoaling (Nott, 2003):

(8) $$u^2 = \delta \cdot g \cdot H.$$

Table 2: Boulder axes, volume and weight. Volume was calculated by multiplying the main axes and also by DGPS measurements. Discrepancies between the two methods are shown in column V_{DGPS}/V_{abc}. Column A_{photo}/A_{axes} shows the ratio between the estimation of certain surface areas of a boulder using the photo method of Robinson et al. (2008) and the product of the two main axes of the same boulder surface area. The average value of this ratio is defined as area coefficient q in order to generate more realistic values for the upper surface of a certain boulder (A_p) where the lift force (F_L) applies. θ is the bed slope angle of the pre-dislocation setting and was estimated based on elevation transects A-A' and B-B' (Fig. 3); SD = standard deviation.

Boulder	**ρ_b (g cm^{-3})**	**Θ (°)**	**D_i (m)**	**Dimensions (m)**			**Volume (m³)**		**Weight (kg)**		**V_{DGPS}/V_{abc}**	**A_{photo}/A_{axes}**
				a-axis	b-axis	c-axis	a · b · c	DGPS	a · b · c	DGPS		
SPE 2	2.28	5	48	4.10	3.00	1.95	23.99	13.0	54.61	29.60	0.54	0.74; 0.73
SPE 4	2.15	5	90	6.06	3.50	3.46	74.02	25.5	159.16	54.83	0.34	0.78; 0.67
SPE 5	2.14	5	130	5.80 4.70	2.30 4.00	4.24 3.20	71.81 + 60.16 = 131.97	27.0 + 36.0 = 63.0	160.73 + 134.69 = 295.42	60.44 + 74.62 = 135.06	0.48	0.59; 0.65; 0.67; 0.89; 0.73;
SPE 6	2.30	5	125	2.60	5.40	2.50	35.10	18.5	80.84	42.61	0.53	0.72; 0.81
SPE 7	2.40	5	87	9.90	4.20	2.80	116.42	44.3	279.58	106,38	0.38	0.67
SPE 8	2.37	5	150	9.10	4.20	2.80	76.44	37	181.50	87.86	0.48	0.67
SPE 9	2.14	8	15; 43	2.70 3.00	3.00 1.90	0.50 0.50	4.05 + 2.85 = 6.90	2.5 + 1.9 = 4.4	8.67 + 6.10 = 14.77	5.35 + 4.07 = 9.42	0.64	-
BOL 1	2.27	14	60	7.70	5.20	2.50	100.10	53.83	227.34	122.38	0.54	0.83; 0.76
BOL 2	2.19	14	45	4.80	8.70	3.80	158.69	68.34	347.77	149,77	0.43	0.72; 0.81
BOL 3	2.38	18	52	1.70	0.80	0.70	0.95	0.42	2.27	1.00	0.44	-
Average	2.25										0.49	0.73 (= q)
SD	0.10										0.11	0.07

Table 3: Compilation of inferred minimum wave heights of swell waves (H_S) and tsunamis (H_T) required for quarrying and transporting each of the investigated boulders using the Nott (2003)-based formula given by Nandasena et al. (2011) and the modified approach from this study. X_{max} after Pignatelli et al. (2009) refers to the local maximum inundation of a tsunami.

Boulder	Minimum HT (JBBS)		Minimum HS (JBBS)		Xmax (m) based on inferred HT	
	Modified approach	Nandasena et al. (2011)	Modified approach	Nandasena et al. (2011)	HT after modified approach	HT after Nandasena et al. (2011)
SPE 2	5.3	7.3	21.2	29.1	182	270
SPE 4	5.4	11.6	21.4	46.3	184	515
SPE 5	6.7	14.0	26.7	56.2	241	681
SPE 6	6.7	9.5	26.8	37.9	243	388
SPE 7	5.8	11.4	23.4	45.7	204	507
SPE 8	5.2	8.0	20.8	31.9	178	307
SPE 9	1.2	1.7	4.7	6.8	No flooding	No flooding
BOL 1	7.3	10.1	29.3	40.5	118	254
BOL 2	8.9	15.4	35.6	61.6	190	580
BOL 3	1.8	3.1	7.3	12.3	No flooding	No flooding

The empirical coefficient δ describes the type of wave: $\delta_{tsunami} = 4$; δ_{swell} wave = 1 (Fukui et al., 1963). Thus, the following equation derives the minimum wave height of a tsunami (H_T) or swell wave (H_S) which is required to dislodge a particular JBB:

(9) $$H_T = \frac{(\rho_b - \rho_w) \cdot V \cdot (\cos\theta + \mu \cdot \sin\theta)}{2 \cdot \rho_w \cdot C_L \cdot a \cdot b \cdot q}$$

(10) $$H_S = \frac{(\rho_b - \rho_w) \cdot V \cdot (\cos\theta + \mu \cdot \sin\theta)}{0.5 \cdot \rho_w \cdot C_L \cdot a \cdot b \cdot q}.$$

Table 3 gives an overview of inferred wave heights based on new field data and Eqs. (9) and (10). For boulders which have been dislodged from the terrace edge and the top of the LT and transported during a tropical cyclone (SPE 9, BOL 3), minimum storm wave heights of 4.7 m and 7.3 m have been calculated. The larger clasts (SPE 2-8, BOL 1-2) indicate storm wave heights of more than 35 m. Inferred minimum tsunami heights based on the larger clast are in the range of 5.2-8.9 m, whereas they are lower than the seaward platform in case of the boulders evidently entrained and dislocated by storm waves.

2.4.3 Inundation of the LT and wave dissipation

In order to test the tsunami hypothesis, an approach presented by Noormets et al. (2004) and previously applied to boulder deposits on eastern Sicily by Barbano et al. (2010) is used. It involves the phase of entrainment and emplacement right after dislocation of the boulder and allows for tentatively ruling out swell wave transport if values of size of the clast, landward position and wave period are high enough.

The transport capability of long-period tsunamis is significantly greater compared to storm waves since it correlates with wavelength (Noormets et al., 2004). The transport of detached boulders occurs in turbulent flow conditions (tsunami), mostly by rolling or saltation. The mode changes to sliding when the flow velocity decreases. In most cases, the longest axis of a block or boulder is perpendicular to the wave direction. Otherwise hydraulic force is spent to rotate the axis horizontally resulting in reduced transport capacity (Imamura et al., 2008).

Minimum wave heights required to dislocate the boulders were calculated in *Chapter 2.4.2*. Subsequently, the boulder is entrained in the flow (rolling, saltating) as long as the sum of lift force (F_L) and drag force (F_D) exceeds the resisting force (F_R) (Noormets et al., 2004):

(11) $$F_L + F_D > F_R$$

(12) $$F_D = 0.5 \cdot C_D \cdot (a \cdot c \cdot q) \cdot \rho_w \cdot u^2$$

The coefficient of drag (C_D) is estimated to be 1.95 (Noormets et al., 2004; Paris et al., 2010; Nandasena et al., 2011); a = a-axis, c = c-axis of a megaclast; q = boulder area coefficient = 0.73 (Table 3); ρ_w = density of sea water = 1.02 g cm^{-3}; u = flow velocity. For F_L and F_R see Eqs. (4) and (5).

H_S and H_T at the location where a certain boulder is deposited can be deduced by combining Eqs. (4), (5), (8), (11) and (12):

(13) $$H_T \geq \frac{0.5 \cdot (\rho_b - \rho_w) \cdot V}{\rho_w \cdot a \cdot q} \cdot \frac{1}{(C_D \cdot c + C_L \cdot b)}$$

(14) $$H_S \geq \frac{2 \cdot (\rho_b - \rho_w) \cdot V}{\rho_w \cdot a \cdot q} \cdot \frac{1}{(C_D \cdot c + C_L \cdot b)}.$$

During the final stage of boulder transport the current velocity decreases and transport most likely occurs in a sliding mode (Imamura et al., 2008); thus, F_L is negligible (Noormets et al., 2004). Transport ends when

(15) $$F_D \leq F_\mu.$$

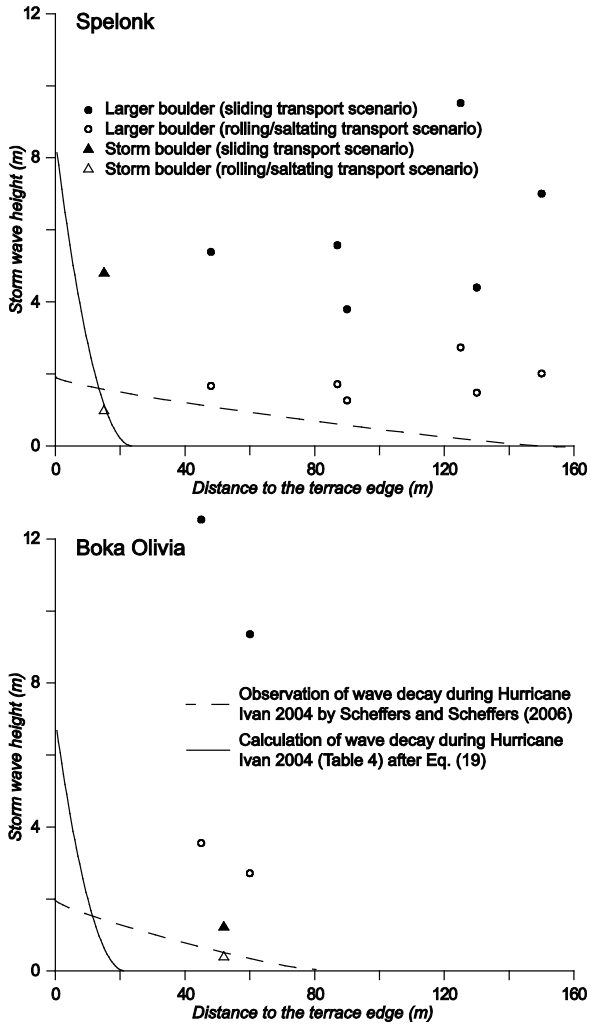

Fig. 11: Graphs showing dissipation of waves during Hurricane Ivan in 2004 as listed in Table 4 at Spelonk and Boka Olivia. Wave dissipation is based on observations made by Scheffers and Scheffers (2006) and calculations using Eq. (19) according to Barbano et al. (2010). Dots and circles represent minimum storm wave heights (H_S) required to move each boulder at its current position on the abscissa. Triangles indicate the boulders displaced by storm waves.

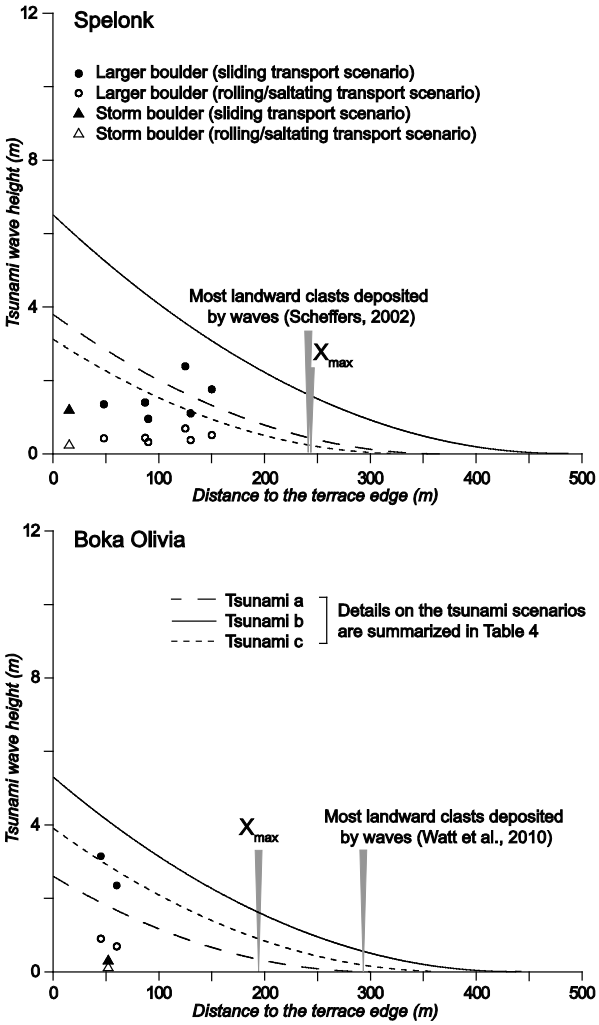

Fig. 12: Graphs showing wave dissipation of possible tsunami scenarios as listed in Table 4 at Spelonk and Boka Olivia after Eq. (19) according to Barbano et al. (2010). Dots and circles represent minimum tsunami wave heights (H_T) required to move each boulder at its current position on the abscissa. Triangles indicate the boulders displaced by stormwaves. Circles and white triangles provide more realistic values since rolling/saltating is the most common transport mode of megaclasts by a tsunami (Imamura et al., 2008). X_{max} shows the maximum flooding after Eq. (20) according to Pignatelli et al. (2009).

F_μ represents the normal friction force and is defined by

$$F_\mu = \mu \cdot V \cdot \rho_b \cdot g \quad (16)$$

where μ = coefficient of friction was estimated to be 0.65 (Benner et al., 2010). The duration of entrainment in the flow either during a tsunami or a series of storm waves as well as the distance of dislocation are determined by critical boundary shear stress which is related to both height and speed of a wave overtopping a coastal platform (Barbano et al., 2010). By using Eqs. (12), (15) and (16) and substituting g with the relation given in Eq. (8), minimum wave heights for storm waves and tsunamis are calculated:

$$H_S = \frac{2 \cdot \mu \cdot V \cdot \rho_b}{c_D \cdot (a \cdot c \cdot q) \cdot \rho_w} \quad (17)$$

(18) $$H_T = \frac{0.5 \cdot \mu \cdot V \cdot \rho_b}{C_D \cdot (a \cdot c \cdot q) \cdot \rho_w}.$$

As demonstrated by Barbano et al. (2010) for eastern Sicily, the values can be compared with the modelled or observed dissipation of storm waves and tsunamis overtopping a shore platform. Therefore, equations presented by Cox and Machemehl (1986) and Noormets et al. (2004) were used to evaluate whether storms are capable to transport the largest boulders at Spelonk and Boka Olivia to their present position. The authors consider the inland decrease in wave height to correlate with distance to the shoreline due to energy dissipation within a turbulent flow regime. The authors establish a correlation strongly dependent on wave period (T):

(19) $$H_i = [\sqrt{(R - E)} - \frac{5 \cdot X_i}{T \cdot \sqrt{g}}]^2$$

where H_i = wave height at a certain distance to the shoreline X_i. R represents the height of the breaking wave (H_T, H_S in Eqs. (9) and (10)) and E is the height of the seaward platform. H_i becomes zero at the point of maximum flooding. Fig. 11 displays the decrease in height of the overtopping swell waves. Input parameters of wave height at breaking point and wave period are based on observations of Scheffers and Scheffers (2006) during Hurricane Ivan (Table 4), which generated the highest waves ever recorded in the Intra-Americas Seas (Wang et al., 2005). However, the modelled wave decay due to energy dissipation after breaking and during inundation of the LT does not match the direct observations of wave overtopping made by Scheffers (2005) and Scheffers and Scheffers (2006) (Fig. 11). Inundation of the LT in the form of a sheet of water, 1-2 m deep near the terrace edge, was found to reach at least 150 m inland at Spelonk according to stranded fish. Observations from Boka Olivia involving the modification of a rampart 70 m inland by Ivan waves (Scheffers and Scheffers, 2006) also provide minimum values for Boka Onima, which exceed the maximum calculated inundation.

The values of flow depth and inundation distance reported by Scheffers and Scheffers (2006) imply sufficient energy to dislocate the boulders known to have been quarried and transported during storm events (SPE 9, BOL 3) to their current position, assuming a rolling/saltating transport mode (Fig. 11). Rolling/saltation has been verified for BOL 3 based on evenly distributed impact marks at all sides of the boulder (see Fig. 7). The flat boulder SPE 9 was most probably transported by stepwise entrainment in the flow. The largest boulders require significantly higher transport energy than provided by Ivan-like waves overtopping the LT. Physical properties typical for major historical Caribbean tsunamis (see Table 4) were used to calculate a wave decay curve. Fig. 12 shows that these parameters generate overland flow conditions capable of transporting all boulders to their current position.

A different numerical approach to estimate the extent of tsunami flooding (X_{max}) depending on the height of a tsunami (H_T) and surface roughness, as described by the Manning coefficient (n), is presented by Hills and Mader (1997). Pignatelli et al. (2009) include the distance of the largest boulder (D) and the slope angle of the platform surface (α):

(20) $$X_{max} = D + (H_T - E)^{4/3} \cdot n^{-2} \cdot k \cdot \cos\alpha$$

where k = 0.06 (Bryant, 2008). The Manning coefficient is about 0.015 for smooth surfaces and may rise to 0.07 at very rough terrain with dense vegetation (Hills and Mader, 1997). At karstified rocky coasts as in the case of Spelonk and Boka Olivia, n ranges between 0.047 and 0.052 (Pignatelli et al., 2009). The height of the terrace edge, c. 3.5 m a.s.l. at Spelonk and c. 5 m a.s.l. at Boka Olivia, is represented by h_c (Fig. 13).

Thus, a palaeo-tsunami of H_T = 8.9 m inferred from the megaclast record would have inundated an area of approx. 243 m inland at Spelonk. At Boka Olivia, maximum inundation would have been 190 m.

Table 4: Framework parameters for the calculation of wave decay on top of the Lower Terrace (LT) and maximum flooding of a hypothetical tsunami including height (R = H_T, H_S), wave period (T), terrace elevation (E), slope angle (α) and reference. The value for T of tsunamis was chosen tentatively and is unconfirmed.

Site	Wave type	Remarks	R (m)	T (s)	E (m)	α (°)
Spelonk	Swell wave	Observations of wave characteristics during Hurricane Ivan 2004 (Scheffers and Scheffers, 2006), representing maximum local values based on literature	12	13	3.5	0
	Tsunami a)	R according to observations at Paria, Venezuela, 01 Sep 1530, triggered by an earthquake (Mw ~ 8.0) near Cumana (NGDC, 2011)	7.3	300	3.5	0
	Tsunami b)	R according to observations at Puerto Tuy, Venezuela, 29 Oct 1900, triggered by an earthquake (Mw ~ 8.4) near Caracas (NGDC, 2011)	10	300	3.5	0
	Tsunami c)	Inferred minimum tsunami height from this study	6.7	300	3.5	0
Boka Olivia	Swell wave	Observations of wave characteristics during Hurricane Ivan 2004 (Scheffers and Scheffers, 2006), representing maximum local values based on literature	12	13	5.0	8.7
	Tsunami a)	R according to observations at Paria, Venezuela, 01 Sep 1530, triggered by an earthquake (Mw ~ 8.0) near Cumana (NGDC, 2011)	7.3	300	5.0	8.7
	Tsunami b)	R according to observations at Puerto Tuy, Venezuela, 29 Oct 1900, triggered by an earthquake (Mw ~ 8.4) near Caracas (NGDC, 2011)	10	300	5.0	8.7
	Tsunami c)	Inferred minimum tsunami height from this study	8.9	300	5.0	8.7

2.5 Discussion

2.5.1 Boulder volume and bulk density

Large discrepancies were documented between boulder volumes based on multiplication of the three main axes (V_{abc}), an approach commonly used for studies on boulder transport, and boulder volumes based on DGPS data (V_{DGPS}). The more realistic V_{DGPS} amounts to 49% of V_{abc} on average, implying strong influence on the output of hydrodynamic models of boulder transport. Hence, it is strongly suggested to use either DGPS measurements of boulders or, if available, 3D laser scanning techniques (cf. Ntageretzis et al., 2011) for this purpose.

Bulk density of the LT reef-rock boulders on Bonaire is not homogeneous due to varying percentages of different coral species and calcarenite, and ranges from 2.07 to 2.40 g cm^{-3}. These values are lower than assumptions made by Scheffers (2005) but higher than empirical values used by Spiske et al. (2008). The latter authors demonstrated that the densities of single components of the LT reef-rock lie between 0.92 (*Diploria* sp.) and 2.65 (calcarenite matrix) g cm^{-3}. They deduced an average bulk density of 1.8 g cm^{-3}. This value is based on thorough density analyses, though it may be too low since the real percentages of the coral species and the calcarenitic matrix material as they occur in each of the dislocated clasts and the LT reef-rock are not explicitly considered. The LT reefrock is divided into several coralline lithofacies corresponding with subzones of the Pleistocene reef ecosystem. Most of the exposed terrace edges along the windward side of Bonaire and thus the megaclasts

of the Spelonk boulder field belong to the "*Acropora palmata* rudstone" (APR) (Kim and Lee, 1999) or "Barrier reef zone (*A. palmata* zone)" (De Buisonjé, 1974). This lithofacies is characterised by roughly imbricated crescent-like slabs of *A. palmata* or colonies in growth position and minor proportions of *Montastrea annularis* and *Diploria* sp. Approximately 20-50% of the lithofacies consists of *A. palmata*, the remaining part is calcarenite matrix (Kim and Lee, 1999), implying high densities. The APR represents the former reef crest with shallow turbulent water conditions protecting a landward lagoonal reef zone ("*M. annularis* zone", "*Siderastrea sidera* zone"). It still exists in a width of up to some tens of metres from the edge of the LT (De Buisonjé, 1974). Low-density corals such as *Diploria* sp. or *M. annularis* were found to make up less than 5-10%, in one case c. 20%, of the larger clasts.

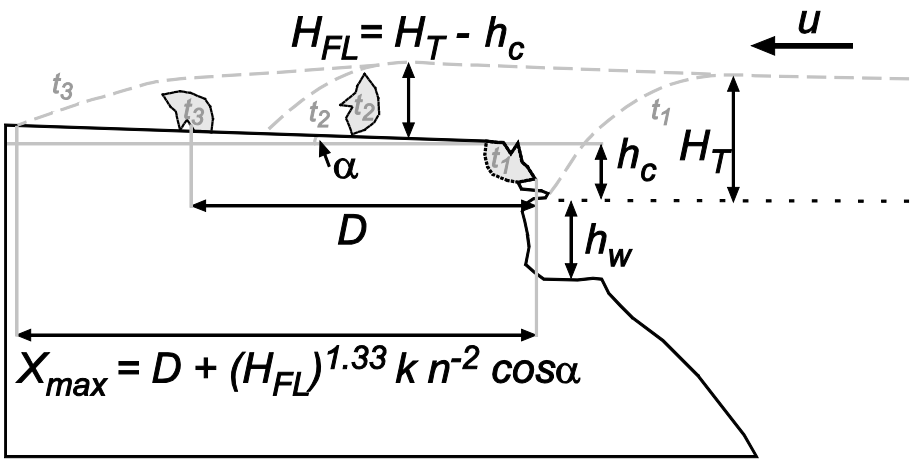

Fig. 13: Three stages of boulder transport at Spelonk and Boka Olivia by a tsunami (after Pignatelli et al., 2009). t1: the bore with a height (H_T) > the height of the terrace edge (h_c) approaches the coast. t2: the tsunami has quarried a boulder from the edge, it inundates the Lower Terrace (LT) and dislocates the boulder in a rolling/saltating mode. t3: the moment of maximum inundation (X_{max}). The final position of the boulder was reached between t2 and t3. Parameter u describes velocity and approaching direction of the bore; h_w = water depth; α = angle of the platform surface; D = landward distance of the largest boulder; n = Manning's coefficient of roughness; k = dimensionless constant (see Eq. (20)).

2.5.2 Minimum wave heights

Minimum swell wave heights of 4.7 m and 7.3 m were calculated for boulders dislodged from the terrace edge and the top of the LT and transported during Hurricane Ivan (SPE 9) and a later storm in 2009 or 2010 (BOL 3). This is in line with waves of 10-12 m in maximum height at their breaking point as observed by Scheffers and Scheffers (2006) during the event. The larger boulders and blocks (SPE 2-8, BOL 1-2) which have not been moved during recent tropical cyclones indicate storm wave heights of up to 35 m. These values are far beyond all eyewitness reports (Kobluk and Lysenko, 1992; Bries et al., 2004; Scheffers and Scheffers, 2006) and even exceed the highest significant wave heights ever reported by the National Data Buoy Center (NDBC) for the Intra-Americas Seas (Wang et al., 2005). Inferred minimum tsunami heights are in the range of 5.2-8.9 m. Since accounts on tsunamis on Bonaire do not exist, local comparison is not possible. Regional tsunamis generated at the southern Caribbean plate boundary are likely to reach 10 m at the coast as reported from Puerto Tuy near Caracas, Venezuela, after a M_W 8.4-earthquake occurred in the area of Isla Orchila, approx. 220 km WSW of Bonaire in 1900. In 1530, the entire northern coast of South America was hit by a tsunami (observed height up to 7.3 m) triggered by an earthquake of M_W = 8.0 off the N coast of Venezuela (O'Loughlin and Lander, 2003; NGDC, 2011). Though tsunamis have never been directly witnessed on the ABC Islands, Parsons and Geist (2009) calculated a local 30-year tsunami probability (run-up >0.5

m [height of onshore flooding above a reference sea-level]) of c. 7% based on data of regional tsunami sources, historical accounts on tsunami effects and a Poissonian probability model. For the 1867 Virgin Islands Tsunami, generated by an earthquake of M_W = 7.5 in the Anegada Passage along the northern Caribbean plate boundary, a height of up to 0.8 m was modelled for Bonaire's coast (Zahibo et al., 2003), while it reached up to 10 m on Guadeloupe (O'Loughlin and Lander, 2003).

Although the larger boulders from this study may point to Mid- to Late Holocene tsunamigenic influence as previously suggested by Scheffers (2002, 2005), Scheffers et al. (2006), Pignatelli et al. (2010) and Watt et al. (2010), other supratidal landforms generated by high-energy waves such as the gently inland sloping ramparts consisting of poorly sorted sand to fine boulders, as well as the ridges of imbricated coral rubble, are more difficult to assign to either periodic storm waves or episodic tsunamis (cf. discussion in Scheffers, 2002, 2005; Scheffers et al., 2006; Morton et al., 2006, 2008; Spiske et al., 2008; Pignatelli et al., 2010). However, recent investigations on the lagoonal archives of leeward and windward Bonaire also tend to support tsunami occurrence (Engel et al., 2010a,b).

Even though the input parameters of the equations of Nott (2003) and Nandasena et al. (2011) have been improved (DGPS-based volume measurements, area coefficient q, boulder-based density estimation) and the inferred storm wave and tsunami heights provide conclusive results and point to the occurrence of major tsunamis on Bonaire during the Holocene, several potential uncertainties have to be considered. The hydrodynamic equations themselves rely on simplified assumptions concerning the acting forces and moments during wave impact and boulder transport. There are several factors influencing the quarrying and transport potential of a wave which are not adequately included in the formulas provided by Nott (2003), such as boulder shape, sublittoral bathymetry, small-scaled onshore topography, onshore flow regime etc. However, validation based on observations after recent tsunamis revealed that inferred wave heights according to this model often even underestimate observed wave heights (e.g. Bourgeois and MacInnes, 2010; Goto et al., 2010).

2.5.3 Wave decay and boulder positions

The decay curves of waves inundating an onshore platform (Cox and Machemehl, 1986; Noormets et al., 2004) were previously used by Barbano et al. (2010) in order to test whether certain clasts of a Sicilian boulder field could have been transported to their current inland position by the largest swell waves of the local buoy record. By applying this approach on Bonaire, significant discrepancies between calculated and observed flooding during Hurricane Ivan conditions were identified (Fig. 11). The observed distance of maximum flooding at Spelonk during Ivan amounts to more than seven times the calculated value, the latter being even smaller than the distance which the clast was moved inland during the event. However, the observed wave decay seems to validate the calculated minimum wave heights required to transport the Ivan boulder at its current location in a rolling/saltation mode. Simulating the wave decay of hypothetical tsunamis by using physical characteristics of major historical Caribbean tsunamis (Fig. 12), all scenarios suggest the capability to transport even the largest boulders to their current position in case of rolling/saltation which is the most common transport mode for boulders by tsunamis (Imamura et al., 2008).

The calculations of onshore dissipation of broken waves should be treated with caution since surface roughness is not considered and considerable underestimation of inundation distance for storm waves was observed. The approach of Cox and Machemehl (1986) and Noormets et al. (2004) strongly depends on the wave period, leading to unrealistic maximum flooding distances for storm waves. Tsunami (long-period wave) inundation, however, seems to be slightly overestimated if compared

with X_{max} (Spelonk: 243 m; Boka Olivia: 190 m) as calculated according to Hills and Mader (1997) and Pignatelli et al. (2009), but matches the observations of scattered wave-transported clasts north of Boka Olivia (up to 285 m inland according to Watt et al., 2010). X_{max} at Spelonk, provided by Pignatelli et al. (2010), lies between 160 and 650 m. The authors use H_T based on the multiplication of boulder axes and hypothetical densities between 1.8 and 2.7 g cm^{-3} which demonstrates that boulder-specific in-field measurements are crucial when inferring inundation limits and wave heights based on Nott-type (2003) hydrodynamic equations.

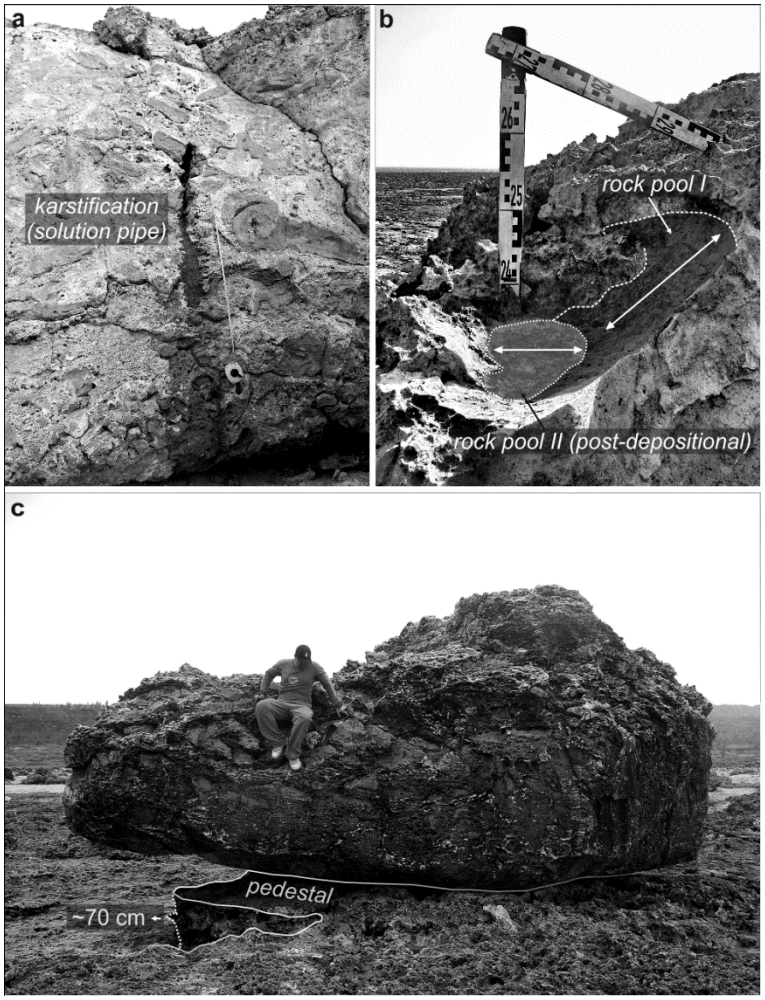

Fig. 14: Karst features indicating deposition of the large boulders in prehistoric times (photographs: S.M. May, M. Engel). a) Solution pipe in BOL 1; b) two rock pool generations on SPE 4: rock pool I developed when the boulder was still a part of the cliff, rock pool II is post-depositional and formed after the boulder was quarried, transported and tilted; c) BOL 2 rests on a pedestal of up to 0.7 m indicating a long period of protection from solution agents in the order of many hundreds or even thousands of years.

2.5.4 Age of the boulders

The boulders and blocks consist of coralline lithofacies of MIS 5e since they were part of the LT which they are currently located on. Their dislocation by waves as discussed above implies a relative sea level position similar to present day levels. During the post-MIS 5e period, these conditions were given only since ca. 7000-6000 years (*Chapter 8*; Lambeck and Chappell, 2001; Milne et al., 2005), narrowing the age of dislocation to the last 7000 years. A published set of 45 ^{14}C (Scheffers, 2002) and 73 electron spin resonance (ESR) (Radtke et al., 2003; Scheffers, 2005) age determinations obtained on corals, shells, and eulittoral organisms (e.g. vermetids) attached to boulders collected from

all around Aruba, Bonaire and Curaçao (including Spelonk and the Boka Olivia–Boka Onima area) shows a quite uniform distribution of ages between 4200 and 2800 years BP and some clustering around 1500 as well as 500 years BP. Thus, a Mid- to Late Holocene age for the transport event(s) can be safely concluded. Nevertheless, its/their exact timing remains unclear since it is uncertain whether the event(s) and the time of death of the dated organisms coincide.

Pedestals of up to 0.7 m have formed at Boka Olivia where the boulders protect the underlying surface from rainfall-driven solution (Fig. 14c). Similar pedestals have been described by Scheffers and Kelletat (2006) for Barbados and Matsukura et al. (2007) for Kikai-jima, SW Japan, implying one-time dislocation many centuries ago. Post-depositional rock pool formation (Fig. 14a) and the formation of solution pipes (Fig. 14b) corroborate this relative chronological interpretation.

^{14}C data of subsurface fine-grained extreme wave deposits from the circumlittoral lagoonal stratigraphies of Bonaire indicate major wave impacts around 3600, 3300-3000, 2000-1700 and pre-500 cal years BP (Engel et al., 2010a,b). In order to deduce distinct tsunami events from the coarse-clast record, further dating efforts are crucial, e.g. by directly dating the transport process. Determining exposure ages of surfaces of overturned boulders using cosmogenic nuclides (^{36}Cl) is currently being applied to resolve the timing of these events.

2.6 Conclusions

This study was motivated by conflicting interpretations during the past decade concerning the hydrodynamic processes which create the sedimentary pattern on top of the Lower Terrace (LT) of eastern and northeastern Bonaire. Several groups thoroughly investigated the boulder fields and come to divergent conclusions. Improvements in the application of the hydrodynamic equations of Nott (2003) and Nandasena et al. (2011) are provided in this paper by including more accurate field data of DGPS-based boulder volume (V_{DGPS}), individual bulk density (ρ_b), and face area ($a \cdot c \cdot q$) upon which the lift force (F_L) acts. Those parameters significantly influence inferred wave heights and are assumed to lead to more realistic wave height estimations.

The use of boulder-specific densities by considering the real lithofacies distribution in heterogeneous reef-rock is important on Bonaire, since average values or those from literature may deviate significantly. We demonstrate that it is even more important to apply accurate DGPS- or, if available, 3D laser scanning-based volume measurements in order to generate more reliable weight data of boulders. Simple multiplication of main boulder axes ($a \cdot b \cdot c$) leads to 100% overestimation on average.

Reconstructed storm wave heights based on the new and improved field data from boulders moved during Hurricane Ivan in 2004 and a subsequent tropical cyclone, and equations in Nandasena et al. (2011) are within the range of real wave heights observed during Ivan. Based on the line of arguments used in this study and regardless of the diverging sedimentological interpretations existing in literature (e.g. Scheffers, 2002; Morton et al., 2006; Spiske et al., 2008), a substantial part of the supralittoral coarse-clast deposits on Bonaire – in particular boulders in the order of BOL 3 or SPE 9 – may have been transported onshore by strong swells of tropical cyclones.

However, storm wave heights calculated for the largest clasts of the boulder and block fields are three times higher and far beyond any observation ever made or data ever recorded in the southern Caribbean. Inferred tsunami heights are in the range of historical tsunami heights reported from Venezuela and other sites in the Caribbean. Even though reports on historical tsunami impact on Bonaire are lacking – may be due to phases of very low population densities on the island in the past

(Hartog, 1978) – and though the equations in Nott (2003) and Nandasena et al. (2011) are based on numerous simplifying assumptions concerning the quarrying and transport processes of boulders by waves, the results from this study support the hypothesis initially raised by Scheffers (2002) and fostered by recent stratigraphical investigations (Engel et al., 2010a,b) that prehistoric tsunamis flooded and modified the coasts of the island. We emphasize that interpretations concerning transport processes based on these boulder-specific data should precede any dating approach since they may support chronological interpretation and the estimation of recurrence intervals of events of different magnitudes. Thus far, the large existing chronological dataset of coarse clasts (Scheffers, 2002, 2005; Radtke et al., 2003) points to prehistoric events of the last 5000 years, whereas it does not enable unequivocal temporal differentiation between particular events.

Thus, we believe that the coastal coarse-clast pattern of Bonaire results from the interplay of deposition (and erosion) during one or more tsunamis (recurrence interval in the order of 1000s of years) and in particular tropical cyclones (recurrence interval in the order of 10s-100s of years) of the last 5000 years. This is similar to the conclusions of Scheffers (e.g. 2002), Pignatelli et al. (2010), and Watt et al. (2010).

3 The identification of palaeotsunami deposits – a major challenge in coastal sedimentary research*

Abstract: Extreme wave conditions associated with severe storms or tsunamis represent major hazards along coasts worldwide. For appropriate hazard assessment, reliable information on the magnitude and frequency of catastrophic events of the past is crucial. Especially in areas where historical accounts are fragmentary or cover only short periods, the onshore sedimentary record provides a promising key to reconstruct impacts of extraordinary waves. However, the differentiation between tsunami and storm surge deposits in onshore stratigraphies is extremely difficult, since most of their characteristics only indicate marine flooding. We discuss the most recent strategies to identify tsunami sand and mud deposits in coastal stratigraphies. In order to pre-evaluate the local hazard, (i) potential tsunami triggering mechanisms (local – regional – far-field), (ii) local and regional historical accounts (including historical documents/tsunami catalogues, interviews with contemporary witnesses, etc.) on the effects of tsunami and severe storms, and (iii) extreme atmospheric conditions have to be analyzed. A holistic study of the sedimentary environments within the area of interest (especially source areas) is essential since it will determine the sedimentary record of any extreme wave event. Local reference deposits from either recent or historically well documented tsunami or severe storm surges guarantee the safest conclusions and should be favoured over a schematic application of global 'tsunami signature types'.

Keywords: *Tsunami deposits, Storm deposits, Sedimentary analysis, Facies, Hazard assessment*

3.1 Introduction

In recent years, dramatic human and economic losses due to extreme wave events have triggered a significant increase in the public perception of coastal geohazards and have also drawn the attention of geoscientists to the sedimentary signature of tsunamis and severe storms (e.g. Nott, 1997; Clague et al., 2000; Dawson and Shi, 2000; Nanayama et al., 2000; Goff et al., 2001, 2004; Felton, 2002; Tuttle et al., 2004; Dominey-Howes et al., 2006; Kortekaas and Dawson, 2007; Morton et al., 2007; Switzer and Jones, 2008a; Scheffers et al., 2009; Goto et al., 2010; Lario et al., 2010; Peters and Jaffe 2010a; Regnauld et al., 2010). Detailed analyses of sediments transported onshore by tsunamis of the past two decades (e.g. Nishimura and Miyaji et al., 1995; Dawson et al., 1996; Dominey-Howes, 1996; Nanayama et al., 2000; Gelfenbaum and Jaffe, 2003; Jaffe et al., 2003; Richmond et al., 2006; Szczuciński et al., 2006; Babu et al., 2007; Bahlburg and Weiss, 2007; Dawson, 2007; Kelletat et al., 2007; Paris et al., 2007; Dahanayake and Kulasena, 2008; Martin et al., 2008; Matsumoto et al., 2008; Sawai et al., 2009; Srinivasalu et al., 2009; Okal et al., 2010; Srisutam and Wagner, 2010) contributed to an initial concept of a tsunami facies model. This facies model supported the differentiation of tsunami deposits from sedimentary deposits laid down by storm waves.

* This chapter is based on: Engel, M., Brückner, H., 2011. The identification of palaeo-tsunami deposits – a major challenge in coastal sedimentary research. In: Karius, V., Hadler, H., Deicke, M., von Eynatten, H., Brückner, H., Vött, A. (eds.), Dynamische Küsten - Grundlagen, Zusammenhänge und Auswirkungen im Spiegel angewandter Küstenforschung. Coastline Reports 17, 65-80.

Where palaeotsunami deposits are found, they expose needs for countermeasures which will reduce the damages of possible future impacts. These include early warning systems (Lauterjung et al., 2009, 2010), education programs, and capacity building on a local level (Spahn et al., 2010) in order to increase public awareness for the hazard of tsunamis. The estimation of recurrence rates of major tsunami events based up on predecessor deposits is essential for risk assessment and coastal management along heavily populated coastlines, especially where historical documentation is short and/or fragmentary (e.g. Africa, the Americas, SE Asia, Australia).

In this paper, we discuss interdisciplinary strategies which have recently been developed and applied to identify fine-grained deposits transported onshore by tsunamis. Suggestions concerning the interpretation of the field record are based on a thorough review of the latest case studies in tsunami geosciences as well as on our own analytical experiences in the field and laboratory, gained in the context of palaeotsunami research on the Netherlands Antilles (Engel et al., 2009, 2010a,b), Thailand (Brückner et al., 2010; Brill et al., 2011) and Greece (May et al., 2007; Vött et al., 2007, 2008, 2010, 2011; Floth et al. 2009). Taking the 'Tsunami deposits and sedimentology matrix of knowledge' in Bourgeois (2009) as a basis, the focus of this paper solely lies on *Tsunami Deposits* (sand/mud) and their *Differentiation* from *Other Deposits*. For a more comprehensive overview covering further aspects of tsunami sedimentology, the reader is referred to Sugawara et al. (2008) and Bourgeois (2009).

3.2 Tsunami deposits

3.2.1 The era of overlooking and misinterpretation

Until the late 1980's, accounts on tsunami deposits were mostly restricted to isolated post-disaster reports (e.g. Shepard et al., 1949; Wright and Mella, 1963; Reimnitz and Marshall, 1965). In this era, scholars did not take into consideration that tsunamis could be significant agents in coastal geomorphology and sedimentology, as indicated, for instance, by the chronological distribution of tsunami-related publications (Fig. 15). The left-skewed distribution of the literature (dataset A) indicates that tsunami geosciences as a discipline is young. Its immaturity in this context is demonstrated by the following regional examples:

Prior to the late 1980s, the widely occurring subsurface layer of sand and gravel on the eastern coast of Scotland (>7000 years BP) was interpreted as a deposit of the Flandrian Transgression (Morrison et al., 1981; Smith et al., 1983) or a storm surge of extraordinary magnitude (Smith et al., 1985). Today, this unit can be clearly associated with the early Holocene Storegga slides off the mid-Norwegian coast, which caused a large tsunami affecting all coasts of the North Sea region and those of Norway and various offshore islands such as the Faroe Islands. Sediments transported onshore during this event were later found in the eastern UK (Dawson et al., 1988; Long et al., 1989; Smith et al., 2004), Norway (Bondevik et al., 1997), the Faroe Islands (Grauert et al., 2001), the Shetland Islands (Bondevik et al., 2005) and possibly east Greenland (Wagner et al., 2007).

The Caribbean region provides another example for the increased perception of tsunamis among coastal geoscientists in recent times. Previously, on the island of Bonaire, southern Caribbean, only a Mid-Holocene sea level highstand was taken into consideration for the deposition of intertidal and sublittoral sand in nearshore morphological depressions (Lucia, 1968; De Buisonjé, 1974). More re-

cent studies pointed to the likely contribution of tsunamis to the coastal stratigraphical pattern and landforms (Scheffers, 2002, 2004; Engel et al., 2009, 2010b; Watt et al., 2010).

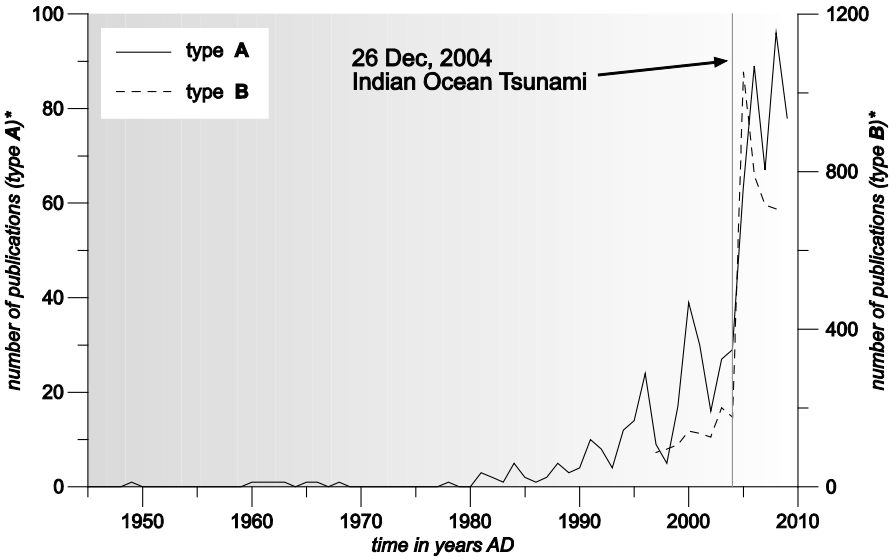

Fig. 15: Tsunami-related publications. A: papers in peer-reviewed international publications covering field-based studies on Quaternary tsunami deposits and post-tsunami surveys; n_A = 674 (own bibliographical compilation). Non-English publications – especially those in Japanese – are certainly underrepresented. B: any tsunami-related scientific publications 1997-2008 as appeared in the Scopus™ database; n_B = 4338 (Sagar et al., 2010).

3.2.2 The paradigm shift

A fundamental shift in paradigm was mainly initiated by the contributions of Atwater (1987) and Dawson et al. (1988). For the first time ever, their high-impact case studies established a link between coastal stratigraphies and seismic or landslide-induced tsunamis of the recent geological past. From this time on, systematic concepts and principles of tsunami-laid sediments or tsunami deposits started to develop. In several cases, they triggered a reassessment of coastal sedimentary sequences, Holocene shoreline evolution and destruction layers at coastal archaeological sites (Smith et al., 2004; Pareschi et al., 2007; Pantosti et al., 2008; Vött et al., 2011).

Table 5: Sedimentary signatures of tsunami deposits found in literature and their occurrence within onshore deposits of modern tsunamis. Descriptions/hypotheses were adapted from (1) Dominey-Howes et al. (2006: p. 1097), Mamo et al. (2009: p. 264), (2) Tuttle et al. (2004: p. 129), (3) Switzer and Jones (2008a: p. 789), (4) Donato et al. (2008: p. 202) and (5) Goff et al. (2001: p. 4). The idea behind this compilation of what is commonly referred to as tsunami deposit characteristics is to show that most of the sedimentary features may also be found in onshore storm deposits. Thus, their occurrence in the field record does not necessarily provide evidence for a palaeotsunami event. References in square brackets only partially refute the general applicability of the signature type.

	Tsunami signature type	Description/hypothesis	Reference, event and site locations supporting the signature type	Reference, event and site locations which may refute the general applicability of the signature type
a)	Erosional basal contact	"Lower contact between base of tsunami-deposit unit and underlying sediment may be unconformable or erosional" (1)	Srinivasalu et al. (2009), IOT 2004, India; Srisutam and Wagner (2010), IOT 2004, Thailand	Horton et al. (2009) Hurricanes Rita and Katrina 2005, US Gulf Coast; Wang and Horwitz (2007), Hurricane Ivan 2004, Florida Gulf Coast
b)	Basal load structures	"Lower/basal tsunami unit contains loading structures" (1)	Matsumoto et al. (2008), IOT 2004, S Thailand	Not reported

c)	Fining upward sequence	"Tsunami sediment horizons fine upwards" (1)	Gelfenbaum and Jaffe (2003), Papua New Guinea Tsunami 1998; Srisutam and Wagner (2010), IOT 2004, Thailand	Morton et al. (2007), Hurricane Isabel 2003, North Carolina
d)	Landward fining sequence	"Particle sizes of tsunami sediments fine landward from the shore" (1)	Srinivasalu et al. (2009), IOT 2004, India; Srisutam and Wagner (2010), IOT 2004, Thailand	Williams (2009), Hurricane Rita 2005, Louisiana; Deicke et al. (2007), storms since 1914 on Hallig Hooge
e)	Greater landward extent	"Tsunami deposits occur in landscape positions, including landward of tidal ponds, that are not expected for storm deposits" (2)	Tuttle et al. (2004), Grand Banks Tsunami 1929; Goff et al. (2004), 15th-century Okoropunga tsunami, New Zealand	Bahlburg (2008), Cyclone Nargis 2008, Irrawaddy Delta, Myanmar; Nott (2006), Cyclone Vance 1999, Australia
f)	Cross bedding	"Landward and seaward currents shown by imbrications of shells and/or low-angle wedged shaped lamination and/or cross-bedding" (1)	Bahlburg and Weiss (2007), IOT 2004, SE India	Williams (2009), Hurricane Rita 2005, Louisiana
g)	Grain size distribution	"Tsunami deposits […] are often bi-modal" while "storm deposits have unimodal particle size distributions" (3)	Babu et al. (2007), IOT 2004, SW India; Paris et al. (2007), IOT 2004, Indonesia	Williams (2009), Hurricane Rita 2005, Louisiana
h)	Rip-up clasts	"Lower/basal tsunami unit may contain 'rip-up' or intraclasts or reworked or underlying material" (1)	Srisutam and Wagner (2010), IOT 2004, Thailand; Szczuciński et al. (2006), IOT 2004, Thailand	Wang and Horwitz (2007), Hurricane Ivan 2004, Florida Gulf Coast
i)	Heavy minerals	"Heavy minerals from offshore […] usually found below storm wave base are […] more likely attributed to tsunami than large storm" (3)	Babu et al. (2007), IOT 2004, SW India; Bahlburg & Weiss (2007), IOT 2004, Kenya	Dahanayake and Kulasena (2008), IOT 2004, Sri Lanka
j)	Microfossil content	"May be pelagic and/or benthic species in shallow water environments. Tests/frustules may be crushed and broken in significant percentages" (1)	Kortekaas and Dawson (2007), Lisbon Tsunami 1755	Kortekaas and Dawson (2007), post-1755 storm, Portugal
k)	Macrofossil content	"The following collective taphonomic characteristics are useful indicators of tsunamigenic shell deposits: large vertical and lateral extent, allochthonous mixing of articulated bivalve species (e.g., lagoonal and offshore) out of life position, and high amount of fragmented valves, with angular breaks and stress fractures" (4)	Donato et al. (2008), Makran Tsunami 1945, Oman	[Boyajian and Thayer (1995), winter storm 1992, New Jersey]
l)	Diatoms	"Both tsunami and storm deposits contain mixtures of diatoms indicative of an offshore or bayward source, but tsunami deposits are more likely to contain broken valves and benthic marine diatoms" (2)	Sawai et al. (2009), IOT 2004, S Thailand; Dawson (2007), Papua New Guinea Tsunami 1998	[Parsons (1998), Hurricane Andrew 1994, Louisiana]
m)	Distinctive layering	"Separate waves in the tsunami wave train may deposit individual layers that contain distinctive subunits" (1)	Richmond et al. (2006), IOT 2004, Indonesia; Szczuciński et al. (2006), IOT 2004, Thailand	[Morton et al. (2007), Hurricane Isabel 2003, North Carolina; Williams (2009), Hurricane Rita 2005, Louisiana]
n)	Geochemical pattern	"Increases in concentrations of Na, S, Cl, Ca and Mg occur in tsunami deposits relative to under- and overlying sediments" (5)	Szczuciński et al. (2006), IOT 2004, Thailand	Engel et al. (2010), hurricanes of the decade 1998-2008, Bonaire
o)	Sorting	"Generally tsunami deposits tend to be much more poorly sorted than storm deposits" (3)	Babu et al. (2007), IOT 2004, SW India; Paris et al. (2007), IOT 2004, Aceh	Morton et al. (2007) Hurricane Carla 1961, Texas → proximal part of the deposit

3.2.3 Towards a tsunami facies model…

A tsunami may be triggered by, a sudden tectonic movement rupturing the ocean floor (e.g. 2004 IOT: Tanioka et al., 2006), a submarine slump (e.g. 1998 Papua New Guinea [near-field]: Tappin et al., 2008), a coastal landslide into the sea (e.g. 1958 Lituya Bay: Miller, 1960), explosive volcanism (e.g. 1883 Krakatau: Nomanbhoy and Satake, 1995), pyroclastic flows (e.g. 2003 Montserrat: Mattioli et al., 2007), volcanic flank collapse (2002 Stromboli: Tinti et al., 2005), atmospheric high-frequency disturbances (e.g. Black Sea meteotsunami 2007 [?]: Vilibić et al., 2010), calving or edge wasting of icebergs ('micro-tsunamis' in the Ross Sea, Antarctica: MacAyeal et al., 2009) or a meteorite impact. Among these triggering mechanisms, the sudden impulse on the water column directly induced by plate uplift at a subduction zone is the most common one, while impact-generated tsunamis have never been observed directly and are still a matter of scientific debate (Kelletat, 2003).

Tsunamis have wave lengths of up to hundreds of kilometers and heights of just a few centimeters to meters in the open ocean. Approaching the shelf region, a tsunami reduces its speed while increasing its height. Coastal inundation occurs in the form of a temporary sea level rise by the shoreward moving of a broad sheet of water or by a landward moving wall of water similar to a tidal bore (Sugawara et al., 2008). Even though storm surges induced by wind stress and falling atmospheric pressure may produce wavelengths and amplitudes similar to those of tsunamis, mainly depending on the spatial extent of the low-pressure system, they have a lower velocity, grow slower and smaller in amplitude, and build up lower shear stress and erosion potential when approaching shallow waters. Storm surges result in a large number of inundation pulses releasing less energy (Switzer and Jones, 2008a). Thus, tsunami sediments are dislocated and deposited under a turbulent and/or laminar flow regime within minutes and hours, while storm deposits are associated with primarily laminar flow conditions and a depositional process which takes place within hours and days (Tuttle et al., 2004).

Assuming that these hydrodynamic differences should create characteristic onshore sedimentary patterns and bedforms, initial facies models were established in order to support the differentiation between tsunami-laid sediments and storm wave deposits (e.g. Dominey-Howes et al., 2006; Morton et al., 2007; Switzer and Jones, 2008a; Mamo et al., 2009). The models are mainly based on the results of post-tsunami field surveys and palaeo-tsunami studies from different coastal environments worldwide.

3.2.4 ...and straight into the dilemma!

Compilations of sedimentary features found in tsunami deposits are useful. However, they may provide a misleading basis for inductive theory building by suggesting that a layer within a coastal stratigraphical sequence comprising one or more of these features will automatically be representative of a palaeotsunami event. Table 5 in combination with the following text section shows that most of the common 'tsunami signature types' appearing in the literature may also be found in storm wave deposits.

a) A *sharp lower contact* is a common feature found in high-energy wave deposits regardless of the exact hydrodynamic process.

b) In modern examples *basal load casts* or *flame wisps* have been described by Matsumoto et al. (2008). Several accounts exist for fossil high-energy wave deposits which are likely tsunamigenic (Minoura and Nakata, 1994; Delaney and Devoy, 1995; Vött et al., 2010).

c) *Normally graded sequences* are typical for tsunami deposits, but layers of inverse grading and massive sand units without any structure do also occur (e.g. Richmond et al., 2006). In overwash deposits associated with storm events or tropical cyclones normal and inverse grading has been observed (e.g. Williams, 2009).

d) A *fining trend in the distal part* of overwash deposits may also result from both hydrodynamic processes discussed here**.**

e) *Landward extent* is primarily a question of coastal morphology and surface gradient which has been demonstrated in a dramatic way in the Irawaddy Delta, Burma (Myanmar), by Cyclone Nargis in 2008 (Bahlburg, 2008). The extent of inundation reached up to 50 km inland (Fritz et al., 2009). Nevertheless, where a tsunami and an exceptionally large storm hit a certain coast, the tsunami deposit will probably have a greater areal extent (cf. Nanayama et al., 2000; Goff et al., 2004).

f) *Cross stratification* does not exclusively result from tsunami overland flow and backwash currents. It also occurs within the basal part of storm surge deposits...

g) …where it may be associated with bimodal *grain size distribution* (Williams, 2009).

h) *Ripped-up clasts* of underlying strata are very common in tsunami sediments (Fig. 16B). Where suitable subsoil conditions exist, cyclone waves are also capable to produce them (Bridge, 2008; Wang and Horwitz, 2007). However, this seems to be rare (Jaffe, et al. 2008).

i) Concentrations of major *heavy minerals* such as tourmaline or zircon are entirely site dependent. While at some sites heavy mineral concentrations of the IOT deposit were elevated compared to the pre-tsunami sediment (e.g. southwest India: Babu et al., 2007; southern Thailand: Jagodziński et al., 2009), others observed reduced heavy mineral content (Sri Lanka: Dahanayake and Kulasena, 2008).

j) *Heavy metal* concentrations within the acid-leachable fraction of tsunami sediments, which in general are increased in the IOT deposits (Kozak and Siepak, 2009), are also solely a matter of source availability.

k) In theory, *microfaunal assemblages* (benthic foraminifera, ostracods) within tsunami deposits tend to contain many broken tests from a wide range of marine, brackish and even freshwater habitats. However, in field records where tsunami- and storm-generated sediments occur at the same site, the differences in terms of assemblage and preservation of the tests may be rather marginal (Kortekaas and Dawson, 2007). For a better comparison of data from site to site, the application of multivariate statistics on taxa composition, palaeoecological significance of a thanatocoenosis or preservation of foraminiferal tests or ostracod carapaces is recommended (cf. Mamo et al., 2009).

l) In a promising study, Donato et al. (2008) compared *taphonomic characteristics of bivalve shells* from known storm and tsunami layers at one particular site (Sur lagoon, Oman) and found that only the tsunami deposit comprised several articulated specimen – besides a high percentage of disjointed valves with primarily angular breaks. Nevertheless, in other coastal environments articulated bivalves may also occur in large numbers within a storm surge sediment, e.g. at the Jersey Shore (Boyajian and Thayer, 1995).

m) Assemblages of benthic *diatoms* (siliceous algae) with abundant valve fractures have been found to be indicative for marine flooding and high-energy flow conditions resulting from tsunamis (Tuttle et al., 2004). However, Parsons (1998) also found chaotic assemblages including marine forms in hurricane deposits; hence, it is hardly possible to distinguish between tsunami and storm deposits relying only on diatoms (Hemphill-Haley, 1995). Sawai et al. (2009) make an effort to enhance this

signature type by linking distinctive units within an IOT layer with characteristic diatom assemblages to successive onshore flow regimes of tsunami inundation.

n) *Laminasets* of hurricane deposits may not necessarily differ from graded sequences resulting from a tsunami. However, tsunami deposits sometimes tend to form distinct sand layers with mud drapes or distinct subunits representing in- and outflow processes of one single wave (Fig. 16C) which has rarely been observed in storm deposits (Komatsubara and Fujiwara, 2007). This also applies for backflow incision patterns (Fig. 16B). In general, the number of laminasets is higher in storm deposits (Morton et al., 2007).

o) The *geochemical pattern* of an overwash sediment body solely proves marine flooding but does not represent a criterion to distinguish between tsunami or storm origin. Chagué-Goff (2010) speculates that the marine geochemical signature in a storm deposit might be diluted due to associated heavy rainfall. This has to be verified by further research.

Further attempts to characterize and identify palaeotsunami deposits include scanning electron microscope-based analysis of quartz grain microtextures (Costa et al., 2009) or stratigraphical analyses at the thin section level (Kilfeather et al., 2007) as well as measurements of magnetic susceptibility (Font et al., 2010). However, it is clear, given the vagaries of sediments and sediment deposition that there will never be a single proxy, or definitive signature, which unequivocally discriminates between storm and tsunami deposits (and solves the dilemma). Researchers will always have to consider a broad variety of factors to come to a balanced conclusion on the origin of a possible palaeotsunami deposit.

Potential post-depositional changes within event deposits additionally hamper their interpretation, especially in humid tropical environments. After monitoring the IOT deposit in southern Thailand for the period of five years, Szczuciński (2010) found that

(i) the deposit was preserved at only 50% of the investigated sites (30% loss due to human impact, 20% loss due to pedogenesis),

(ii) modification is primarily due to bioturbation, and

(iii) thickness of the deposit mostly determines the preservation potential.

Another obstacle in finding palaeotsunami deposits by means of geological sampling is the discontinuous pattern of tsunami sand sheets (Fig. 16A) which is often controlled by the pre-impact coastal morphology. While the IOT deposit had an original thickness of up to 150 cm in morphologic depressions, it is absent in topographic highs (Paris et al., 2007, Srinivasalu et al., 2009).

3.2.5 Strategies for interpreting coastal event stratigraphies

Since universally applicable criteria in sand/mud deposits to unambiguously distinguish between tsunami and storm wave overwash processes are not available (Switzer, 2010), data on regional physical preconditions for either one of these processes are required. These include potential tsunami triggering mechanisms (local – regional – far-field), local and regional historical accounts on the effects of tsunamis and severe storms (including historical documents and tsunami catalogues, interviews with eyewitnesses, etc.), and regional extreme atmospheric conditions (maximum storm/cyclone intensities, storm/cyclone tracks, etc.) in order to pre-evaluate the overall tsunami/storm surge risk. This evaluation may be supported by numerical models of tsunami and storm surge hydrodynamic behaviour, coastal flooding and sediment transport involving data on local ba-

thymetry, topography, triggering source mechanisms and sediment sources (e.g. Martin et al., 2008; Floth et al., 2009). Coarse-clast deposits and landforms in the littoral zone may represent another criterion assisting in the differentiation between storms and tsunamis. In certain cases, the tsunami hypothesis can be validated by discarding storm wave transport due to the weight and altitude of single boulder deposits (*Chapter 2*; Nott, 1997; Frohlich et al., 2009; Benner et al., 2010).

By thoroughly interpreting high-energy wave deposits, ideas or theories as "a set of propositions which purport to explain the structure of some *system* and/or how the *system* develops" (Wilson, 1972: p. 32) in the basic sense of theoretical geography (cf. Wirth, 1979) are crucial. The *system* here is defined as the coastal area of interest including the entire range of its morphodynamic processes. Thus, the theory is based on the unique configuration and development of the local foreshore, long-term wave energy, sediment sources, fluxes and availability, onshore topography, active tectonics and even the ecosystem. If, for instance, different source regions for the sediment load transported onshore by tsunami and storm waves can be identified, the application of certain 'tsunami signature types' (e.g. heavy mineral or microfauna) is far more promising. A good example in generating conclusive evidence for palaeotsunami deposits by thoroughly analyzing the local *system* is provided by Switzer et al. (2005) who found unambiguous similarities between heavy mineral assemblages of a candidate tsunami sand sheet and shelf sediments from below the local storm wave base. In this case, tsunamigenic sedimentation is a reliable inference. At Puget Sound, one of the geographical nuclei of palaeotsunami research, growth-position rhizomes of high intertidal marsh vegetation within a matrix of grey mud are vertically confined by a sand layer containing marine fossils. The overlying well-bedded and rhizome-free sand and mud indicates high sedimentation rates and a lowered position within the intertidal zone. Atwater and Moore (1992) linked the sand layer with a tsunami triggered by a local earthquake and co-seismic subsidence of the intertidal marshes, providing the only possible explanation for this particular stratigraphical pattern.

However, (sub-)recent deposits of well documented storm and/or tsunami events provide the most reliable reference to locally calibrate sedimentary criteria for a differentiation between tsunami- and storm-laid sediments. Recent sedimentary input of storm and hurricane events or tsunamis substantially supported evidence for a palaeo-tsunami occurrence in case studies for instance from Thailand (Jankaew et al., 2008; Brückner et al., 2010; Brill et al., 2011), the Netherlands Antilles (Engel et al., 2010b), and Chile (Cisternas et al., 2005). One's ability to separate palaeo-tsunami and palaeo-storm deposits is enhanced, if there are local recent examples of both types of deposit in the same area to allow for a comparison and contrasting of the two (e.g. Nanayama et al., 2000; Tuttle et al., 2004).

Ground penetrating radar (GPR) is increasingly being used in order to evaluate the extent and sedimentary structures of fossil tsunami deposits. Studies by Switzer et al. (2006) or Nair et al. (2010) show that erosional unconformities confining palaeotsunami deposits are well reflected in the GPR profiles which thus are a useful complement of data from sediment cores or trenches.

Where a tsunami deposit is identified, the stratigraphy may be used to reconstruct characteristics of the tsunami itself. Tsunami flow speed or inundation depth may be determined by inverse modeling (Jaffe and Gelfenbaum, 2007; Soulsby et al., 2007; Spiske et al., 2010).

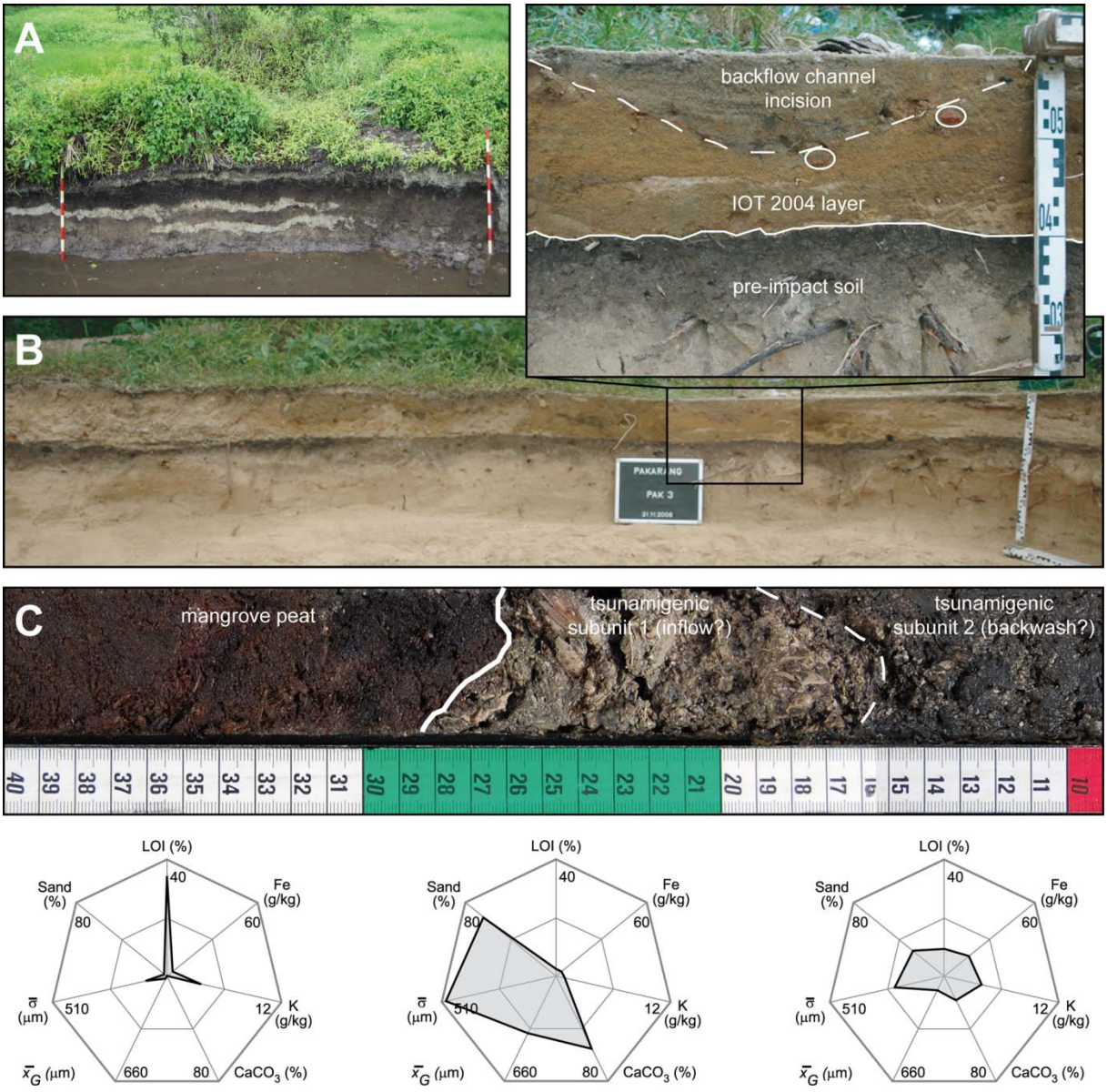

Fig. 16: Examples of tsunamigenic sedimentary patterns. A: discontinuous sheets of palaeotsunami deposits at Koh Phra Thong, southern Thailand. The uppermost grey sand layer is related to the IOT 2004 (photograph: K. Jankaew). B: IOT 2004 layer (uppermost sediment unit) at Cape Pakarang, southern Thailand (photographs: H. Brückner, A. Vött). The trench exposes bedforms and other sedimentary features associated with tsunami overland flow and subsequent sedimentation, e.g. incised backflow channels or roof tile intraclasts (detail photo). C: sediment core (3.40-3.09 m below surface) from Lagun, Bonaire (Netherlands Antilles) (photograph: G. Daut, M. Engel). The erosional contact between the underlying mangrove peat and the shell-rich candidate tsunami deposit comprising two subunits is associated with bidirectional flow behaviour of a palaeotsunami. The mollusc thanatocoenosis indicates that most of the sediment stems from a local shallow embayment. The tripartition of the core section is supported by sedimentary characteristics (web diagrams: x_G = mean grain size; σ = sorting; LOI = loss-on-ignition). See Engel et al. (2010b) for details on geographical contexts, analytical approach and complete line of argument concerning the origin of the deposit. Further bedform structures are difficult if not impossible to detect in a sediment core.

3.3 Summary

To date, distinguishing between tsunami- and storm wave-generated onshore deposits is still challenging and an extremely difficult task. Tsunami geoscience, and in particular palaeotsunami research, most certainly requires more interdisciplinary field studies including detailed sedimentological and geomorphological documentation to adjust tsunami and storm wave facies

models as well as to enhance coastal hazard assessment on a local and regional basis. Nowadays, post-tsunami field surveys are often conducted following field manuals developed by the Intergovernmental Oceanographic Commission (IOC, 1998) or the research group around Synolakis and Okal (2005) in order to create homogenous databases (cf. Okal et al., 2010, concerning the recent incident on Samoa 2009). Databases of tsunami deposits already exist and are continuously updated and expanded (Keating et al., 2008; Peters and Jaffe, 2010b). Only recently, Peters and Jaffe (2010a) made a valuable contribution by publishing a list of identification criteria for fossil tsunami deposits as a guideline for interdisciplinary palaeotsunami research and stratigraphical documentation. In this regard, we also propose to carefully analyse the sedimentary and geomorphological environment within the area of interest (especially the potential source region) since it will determine the sedimentary record of any extreme wave event. It will always be most valuable to have local reference deposits from either recent or historically well documented tsunamis or severe storms, to ensure the best deduction as to a deposit's origin. Basing one's choice of the origin of a high-energy wave deposit on existing modern analogies should be favoured over a schematic application of global ‘tsunami signature types’. However, the presence of several ‘tsunami signatures types’ listed in Table 5 in a trench or in a suite of sediment cores may be a substantial support of the tsunami hypothesis.

4 Coastal stratigraphies of eastern Bonaire (Netherlands Antilles): new insights into the palaeotsunami history of the southern Caribbean*

Abstract: A sediment record of three alluvial sites along the east- and northeast-oriented shore of Bonaire (Netherlands Antilles) provides evidence for the recurrence of several extraordinary wave impacts during the Holocene. The interpretation of onshore high-energy wave deposits is controversially discussed in recent sedimentary research. However, it represents a powerful tool to evaluate the hazard of tsunamis and severe storms where historical documentation is short and/or fragmentary. A facies model was established based on sedimentary and geochemical characteristics as well as the assemblage and state of preservation of shells and shell fragments. Radiocarbon data and the comparison of the facies model with both recent local hurricane deposits and global "tsunami signature types" point to the occurrence of three major wave events around 3300, 2000-1700 and shortly before 500 BP. Since (i) the stratigraphically correlated sand layers fulfill several sedimentary characteristics commonly associated with tsunamis and (ii) modern strong hurricanes left only little or even no sediment in the study areas, they were interpreted as tsunamigenic. However, surges largely exceeding the energy of those accompanying modern hurricanes in the southern Caribbean cannot entirely be ruled out. The results are partially consistent with existing chronologies for Holocene extreme wave events deduced from supralittoral coarse-clast deposits on Aruba, Bonaire and Curaçao as well as overwash sediments from Cayo Sal, Venezuela.

Keywords: *Washover deposits, Tropical cyclones (hurricanes), Tsunami, Holocene stratigraphy, Facies model, Coastal hazard*

4.1 Introduction

The steady morphodynamic processes shaping the coastlines worldwide are well understood; long-term wave action and littoral drift, for example, contribute to cliff erosion and significantly modify paralic sedimentary environs on short geological time scales (Kraft, 1978; Stanley and Warne, 1994). In the past, overwash deposits or supralittoral coarse-clast accumulations were often solely attributed to exceptionally large storms or a temporary sea level highstand (e.g. Lucia, 1968; De Buisonjé, 1974, regarding the case of Bonaire). But, especially since the works of Atwater (1987) and Dawson et al. (1988), tsunamis have been increasingly taken into consideration as potential agents in littoral geosystems (Kelletat et al., 2005; Ruiz et al., 2005; May et al., 2007; Switzer and Jones, 2008a; Vött et al., 2009; Goff et al., 2010).

A growing number of detailed studies on sedimentation patterns of modern tsunamis testify to the increasing perception of tsunamis in coastal sedimentology and geomorphology. Among other

* This chapter is based on: Engel, M., Brückner, H., Wennrich, V., Scheffers, A., Kelletat, D., Vött, A., Schäbitz, F., Daut, G., Willershäuser, T., May, S.M., 2010. Coastal stratigraphies of eastern Bonaire (Netherlands Antilles): new insights into the palaeo-tsunami history of the southern Caribbean. Sedimentary Geology 231, 14-30.

coastal areas, sedimentary investigations on recent and sub-recent tsunami events were carried out in Oman (Donato et al., 2008), Chile (Cisternas et al., 2000), the Aegean (Dominey-Howes, 1996), at Kamtchatka (Martin et al., 2008), and after the incidents on Flores 1992 (Shi et al., 1995), Hokkaido 1993 (Sato et al., 1995; Nanayama et al., 2000), Java 1994 (Dawson et al., 1996) and 2006 (Lavigne et al., 2007), Papua New Guinea 1998 (Gelfenbaum and Jaffe, 2003), at the Peruvian coast 2001 (Jaffe et al., 2003) and 2007 (Fritz et al., 2008), the Kuril Islands 2006 (MacInnes et al., 2009b), Samoa 2009 (Richmond et al., 2010), and most of all on the Indian Ocean circumlittoral zone after 2004 (e.g. Richmond et al., 2006; Kelletat et al., 2007; Paris et al., 2007, 2009; Srinivasalu et al., 2007; Szczuciński et al., 2007).

Research on both modern storm and tsunami deposits (e.g. Nanayama et al., 2000; Switzer and Jones, 2008b) helps to improve the interpretation of onshore sedimentary archives and the reconstruction of large wave impacts in the past. Identifying, dating, and, if possible, classifying extreme wave deposits is an essential strategy to estimate recurrence rates and potential magnitudes of future catastrophic events.

In the Caribbean, strong hurricane activity is triggered by atmospheric easterly waves crossing the North Atlantic between 10 and 20° (Goldenberg and Shapiro, 1996). Since the mid-1990s, an increasing trend in their destructive potential along the Antillean islands and the intra-American coasts has been observed which may be attributed to ongoing (anthropogenic?) climatic change (Emanuel, 2005). The analysis of the decadal frequencies of hurricanes in ten Caribbean subregions based on climate data starting in 1870 identified Venezuela and the southern Dutch Antilles, including Bonaire (area of interest for this study; Fig. 17), as the region least affected by storm events (Reading, 1990). Nevertheless, several recent hurricanes have caused heavy surf damage to Bonaire's coastal infrastructure (Table 6).

Table 6: Severe hurricanes of the last decade affecting the coastline of Bonaire. Data is adapted from annual climatological summaries of the Meteorological Service of the Netherlands Antilles and Aruba (http://www.weather.an/reports/index.asp) and McAdie et al. (2009).

Name	Date	Max. category (SSH[1])	Distance[2]	Hurricane track
Lenny	15 Nov 1999	4	375 km N	W-E
Ivan	08 Sep 2004	5	130 km N	E-WNW
Emily	15 Jul 2005	5	185 km NE	E-WNW
Felix	02 Sep 2007	5	60 km N	E-WNW
Omar	15 Oct 2008	4	145 km N	SW-NE[3]

[1]Saffir-Simpson Hurricane Scale (cf. Meteorological Service of the Netherlands Antilles and Aruba, 2010).
[2]The minimum distance of the hurricane's center to the ABC Islands (12.5N, 69.0W).
[3]After a counter-clockwise rotation in the central Caribbean (Beven and Landsea, 2009).

A broad range of triggering factors underlines the high tsunami risk of the Caribbean, such as strike-slip motion along the North American-Caribbean plate boundary (Grindlay et al., 2005), the subduction zone of the Lesser Antilles arc (O'Loughlin and Lander, 2003), various regional volcanic sources (Heinrich et al., 1999; Pararas-Carayannis, 2004), landslides (Teeuw et al., 2009) or even teletsunamis originating off the Portuguese coast or the Canary Islands (Ward and Day, 2001; Barkan et al., 2009).

Not only the sources but also the effects are well documented. The 500-year history of Caribbean tsunamis includes 127 incidents with highly varying degrees of destructiveness (O'Loughlin and Lander, 2003). Beyond historical evidence, several sedimentary studies at calm back-barrier environments report on intercalations of high-energy wave facies and thus have the potential to extend the record until the Mid-Holocene. While throughout the Caribbean most of these sand and carbonate-

rich sediments are interpreted as hurricane-borne (e.g. Bertran et al., 2004; Donnelly and Woodruff, 2007; McCloskey and Keller, 2009; Urquhart, 2009), Weiss (1979) is one of the few scholars who has considered tsunami impact, in this case on the island of Cayo Sal, Venezuela.

Beside sediment layers in back-barrier stratigraphical sequences, geological imprints of extreme wave events also include boulder-sized deposits (Kelletat et al., 2005; Morton et al., 2008). Bonaire as part of the ABC Islands (Leeward Antilles) in the southern Caribbean exhibits the most extensive and best preserved record of high-energy wave debris of the entire intra-American seas, consisting of broad ramparts of imbricated coral rubble and large cliff-top boulders from the littoral zone (Scheffers, 2002, 2004, 2005; Scheffers et al., 2009a).

A facies model for the Holocene stratigraphy of three nearshore floodplains along the windward coast of Bonaire is presented, focusing on the identification of marine overwash deposits. The sites were chosen due to exposure to regular hurricane tracks and potential local tsunamis or teletsunamis approaching from the Atlantic Ocean. All sites of this study are close to previously studied boulder deposits which evidence impacts of high-energy waves (cf. Scheffers 2002, 2004; Morton et al., 2008). New age estimates for these sedimentary deposits as well as a discussion on their origin in the context of regional and global research on extreme wave deposits are provided. For the first time, strong indication for tsunami deposits in fine-grained stratigraphies as well as an attempt of correlating them with supralittoral coarse-clast accumulations is presented for the southern Caribbean. This study contributes to local coastal hazard assessment and also to the recent controversial discussion on the interpretation of high-energy wave deposits in geoarchives worldwide.

4.2 Sedimentary signatures of extreme wave events

Although facies patterns of onshore tsunami deposits are gradually finding their way into textbooks of geomorphology and sedimentology (e.g. Bridge and Demicco, 2008), there is still a considerable lack of certainty concerning the interpretation of the field record. The accurate differentiation between storm and tsunami deposits is a major topic in recent publications (e.g. Morton et al., 2008; Engel et al., 2009a; Switzer and Burston, 2010).

In theory, different onshore accumulation patterns of the two varieties of high-energy wave impacts are associated with a higher potential wave run-up, increased inundation depth, accelerated overland flow velocity and, thus, higher transport capabilities of a tsunami. Sediments accumulated onshore by a tsunami either derive from the beach and adjacent land (Sato et al., 1995) where coastal erosion locally may result in shoreline retreat of more than 200 m or to a major extent (>75%) from the sublittoral zone (Kelletat et al., 2007; Paris et al., 2009). The material is suggested to be primarily transported as suspension load, while the contribution of bedload to the sedimentary record is expected to be relatively small (Jaffe and Gelfenbaum, 2007). Onshore deposition occurs during flow attenuation. Subsequent backflow dynamics depend on the nearshore topography and may be weakly developed or even absent in low coastal settings such as lagoons. More details on hydrodynamic characteristics of tsunamis and hurricane-generated waves are provided by Morton et al. (2007) and Scheffers et al. (2009a).

Based on investigations of recent fine-grained tsunami and storm deposits as well as reviews of palaeotsunami studies, several authors have attempted to compile definite signature types (e.g. Tuttle et al., 2004; Kortekaas and Dawson, 2007; Morton et al., 2007; Switzer and Jones, 2008a). However, it is apparent that as more observations on event deposits appear, the more conflicts concerning the

indicator values of the signature types become exposed. For instance, while studying the sedimentological effects of Cyclone Nargis in Burma 2008, Bahlburg (2008) demonstrated that landward extent is not automatically indicative of a tsunami deposit as previously suggested e.g. by Tuttle et al. (2004). Sediments accumulated by a tsunami are also supposed to show distinct basal unconformities where marine sand sheets truncate soils or lagoonal mud of the back-barrier environment. Tsunami sands often contain intraclasts of reworked underlying material and consist of one or several fining-upward sequences. Especially in the upper part of the sequence, terrestrial sediment may be incorporated due to backflow dynamics. Several case studies also emphasized the bimodal grain size distribution, significantly poorer sorting and landward thinning of tsunamiites (Switzer and Jones, 2008a). However, these sedimentary features may form in storm deposits as well. Increased concentrations of geochemical indicators such as Ca, Sr or Na as well as marine faunal remains (molluscs, diatoms, foraminifera, etc.) may relate to flooding by seawater but thus far do not provide clear evidence for either tsunami or heavy storm wave impact (Kortekaas and Dawson, 2007; Szczuciński et al., 2007; Switzer and Jones, 2008a). The presence of heavy minerals is considered to be source dependent and therefore is also not a universally applicable indicator (Morton et al., 2007). While Babu et al. (2007) and Jagodziński et al. (2009) found increased percentages of heavy minerals in 2004-tsunami deposits at Kerala, India, and Kho Khao, Thailand, heavy mineral concentrations were significantly lower at the southwest coast of Sri Lanka compared to palaeo-storm deposits and the active beach (Dahanayake and Kulasena, 2008). However, Switzer et al. (2005) noted that the presence of platy (immature) heavy minerals indicative of low-energy conditions found to co-exist with mature sediments from the nearshore may be indicative of tsunamis from below the storm wave base, if carefully considered within the context of site specific hydrodynamics.

In summary, universally applicable tsunami criteria do not exist for fine-grained stratigraphies and differentiation between tsunami and storm deposits “remains a serious challenge” (Bridge, 2008: p. 94). Thus, by interpreting the sedimentary record of extreme wave events, it is important to consider local modern analogues, i.e. sedimentary traces of either recent tsunami or hurricanes occurring at the same site. Reliable conclusions in terms of distinguishing between tsunami and storm deposits require a detailed analysis of the local coastal settings and the geomorphological characteristics of the land-sea contact zone as well as the fulfilment of as many empirical sedimentary signatures as possible.

4.3 Physical setting

The geology of Bonaire (Fig. 17) comprises volcanic deposits of diabase and porphyrite with intercalated cherts and limestones of Late Cretaceaous age (Pijpers, 1933; Beets et al., 1977). They are exposed in the northwestern and central sections of the island and are separated from the sea by a sequence of Quaternary limestone terraces. The youngest of these palaeo-reef platforms (Lower Terrace) dates back to MIS 5 (Bandoian and Murray, 1974). Its surface is located slightly below sea level in the south and between 8 and 12.5 m a.s.l. (above mean sea level) in the northwestern part of the island (Alexander, 1961) due to slow tectonic uplift (0.05 mm/a) and tilting (Herweijer and Focke, 1978). At the wave-dominated eastern shore, the Lower Terrace locally has a width of more than 600 m (Herweijer et al., 1977). Accordingly, except for the southern part, the coastline consists of steep limestone cliffs characterized by sea level related notches and benches, mainly produced by bioerosion (e.g. by limpets, littorinids, chitons) and bioconstruction (by coralline algae, vermetid gastropods) (Scheffers, 2005).

In contrast to the western leeward coast, which is fringed by a flourishing reef body, living coral communities are lacking at the windward side due to heavy disturbances during extreme wave events. Large amounts of Holocene coral debris aggregated in ramparts on the windward Lower Terrace indicate destruction within the recent geological past (Scheffers, 2002; Scheffers et al., 2009a).

The semi-arid to arid climate and limited catchment sizes cause an episodic discharge regime as well as sheetwash and splash erosion (Zonneveld et al., 1977). Where the arroyos (locally: "rooien") approach the sea, accumulation zones such as floodplains, saliñas and bokas form. The latter two landforms represent shallow inland bays, in most cases cut off from the sea and used for salt production in the past. At these coastal sections the small watercourse systems dissected the limestone terraces during Pleistocene periods of base level fall and build up nearshore sedimentary archives for the Mid- and Late Holocene (Scheffers, 2002). Floodplains at Lagun, Boka Washikemba and Playa Grandi on the wave-exposed windward coast of Bonaire were investigated with the aim of detecting and interpreting sedimentary traces of extreme wave events.

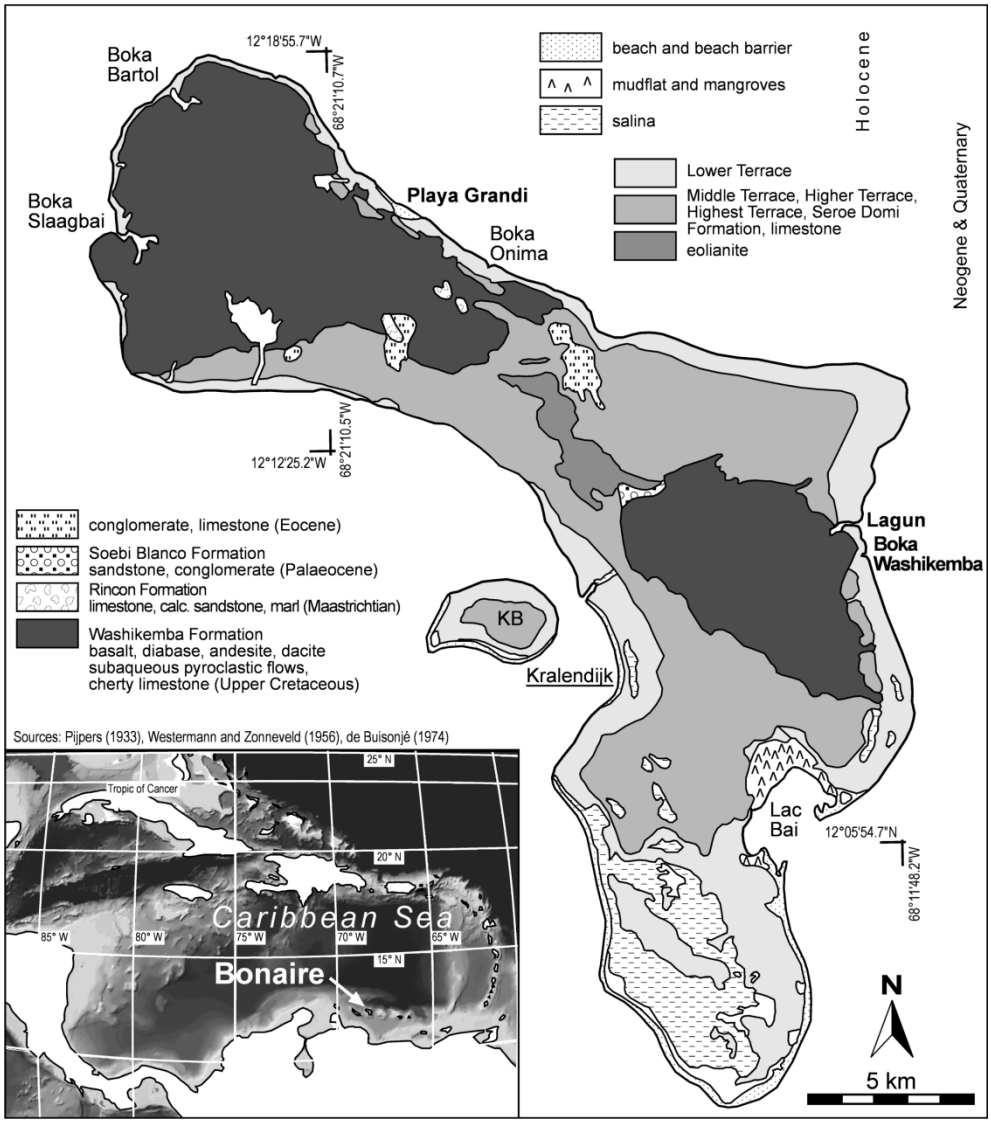

Fig. 17: Geological overview of Bonaire (modified after Anonymous, 1977; NASA World Wind) based on previous mapping of Pijpers (1933), Westermann and Zonneveld (1956), and De Buisonjé (1974).

4.4 Methods

In a first step, suitable geoarchives along the windward coast were determined by means of satellite images and field surveys. A total of twelve open and one closed vibracores of up to 8 m depth were taken for sedimentary analyses and facies determination. Positions and elevations of coring sites as well as the modern beach ridge of Playa Grandi were measured using a high-resolution DGPS (Leica SR 530).

After documentation of the vibracores in thefield (colour according to the Munsell Soil Color Chart , grain size and rounding, texture and carbonate content as recommended by Ad-hoc-Arbeitsgruppe Boden, 2005, macrofaunal remains), samples were taken for multi-proxy analysis with the aim of identifying facies changes and episodic marine sediment input. For a sufficient amount of sediment material each sample represented sections of 5-10 cm from significant stratigraphical units resulting in a maximum of 21 samples per core. Samples for geochemistry were air-dried and pestled by hand. Ca, Fe, Na, and K concentrations of the sand/mud fraction (<2 mm) of all open vibracores were determined using atomic absorption spectrometry (Perkin Elmer A-Analyst 300). Samples were digested with concentrated HCl (37%). $CaCO_3$ was gas-volumetrically measured after the Scheibler method. Loss-on-ignition (LOI) was determined by oven-drying at 105°C for 12 h and ignition in a muffle furnace at 550°C for 4 h (Beck et al., 1993). Grain size distribution was analysed selectively. We applied the wet sieve-pipette technique (Köhn, 1928) after pre-treatment of the aliquots with H_2O_2 (30%) and 0.5 n $Na_4P_2O_7$ (55.7 g/l) to remove organic carbon and for aggregate dispersion. The results were processed with GRADISTAT software (Blott and Pye, 2001). These stratigraphical proxies represent the main basis of facies differentiation at the three sites of interest.

Sediment core BON 9 was preserved in PVC tubes which were split in the laboratory. XRF analysis and magnetic susceptibility measurements (Bartington MS2B sensor) with 1 mm resolution were carried out on the half cores. The inorganic element composition was determined using an ITRAX X-ray fluorescence (XRF) core scanner (Cox Analytical Systems). The ITRAX was equipped with a 3 kW Mo X-ray tube set to 30 kV and 30 mA to analyse semi-quantitative variations of elements from Al to U. Scanning was performed at 1 mm resolution and an exposure time of 20 s. Element amounts were presented as count rates as estimates of the relative concentrations in the sediment. Detection limits range between 2.2% for Al and 5 ppm for heavier elements like Sr or Rb (Croudace et al., 2006).

Macrofaunal remains and coarse sand grains were quantitatively analysed in terms of taphonomic and morphoscopic characteristics similar to Donato et al. (2008). Certain features (articulation, angular/subangular breaks, encrustations, borings, dissolution or abrasion) and species composition relate to (i) transport processes and/or (ii) palaeoenvironmental conditions and thus support the identification and classification of extreme wave events.

A chronostratigraphical framework was established by means of AMS and conventional ^{14}C analyses carried out at the radiocarbon laboratories of the universities of Georgia at Athens (USA), Erlangen and Cologne (Germany). Radiocarbon dates of marine shells were corrected for a regional marine reservoir effect of $\Delta R = -49$ according to Radtke et al. (2003). Since ^{14}C dates of land snails in limestone habitats imply considerable age exaggeration due to the assimilation of ancient carbonate, we considered an age anomaly of 1020±430 years for the sample of *Cerion uva* (terrestrial snail) as calculated by Goodfriend and Gould (1996) after dating several specimen of this genus from the Bahamas. We adopted their value since differences in age anomalies of land snails depend on ecologic conditions and thus the variability within species or genera is rather low (Goodfriend, 1987). All dates were

converted to sidereal years using CALIB 5.0.1 software and the datasets of Reimer et al. (2004) or Hughen et al. (2004). All ages are presented as 2σ sidereal years.

4.5 Holocene stratigraphy of nearshore geoarchives

4.5.1 Lagun

Lagun, located at the windward coast of Bonaire, is an embayment with open access to the sea (Fig. 18). Wave energy inside the embayment is significantly reduced due to the narrow inlet cutting the highly resistant Lower Terrace. Bathymetric data revealed a submarine sill where the Middle Terrace divides Lagun into two subbasins. To the north and south, Scheffers (2002: p. 132) mapped the "most spectacular rampart formations and boulder assemblages" of the entire island distributed over the platform of the Lower Terrace (see also *Chapter 2*). The closed sediment core BON 9 (Fig. 19) and the open core LGU 7 (Fig. 20) from the center of the landward floodplain (Fig. 18) provide detailed information on variable energy levels during Holocene sediment accumulation processes. Since both cores show a very similar stratigraphical pattern they are described together.

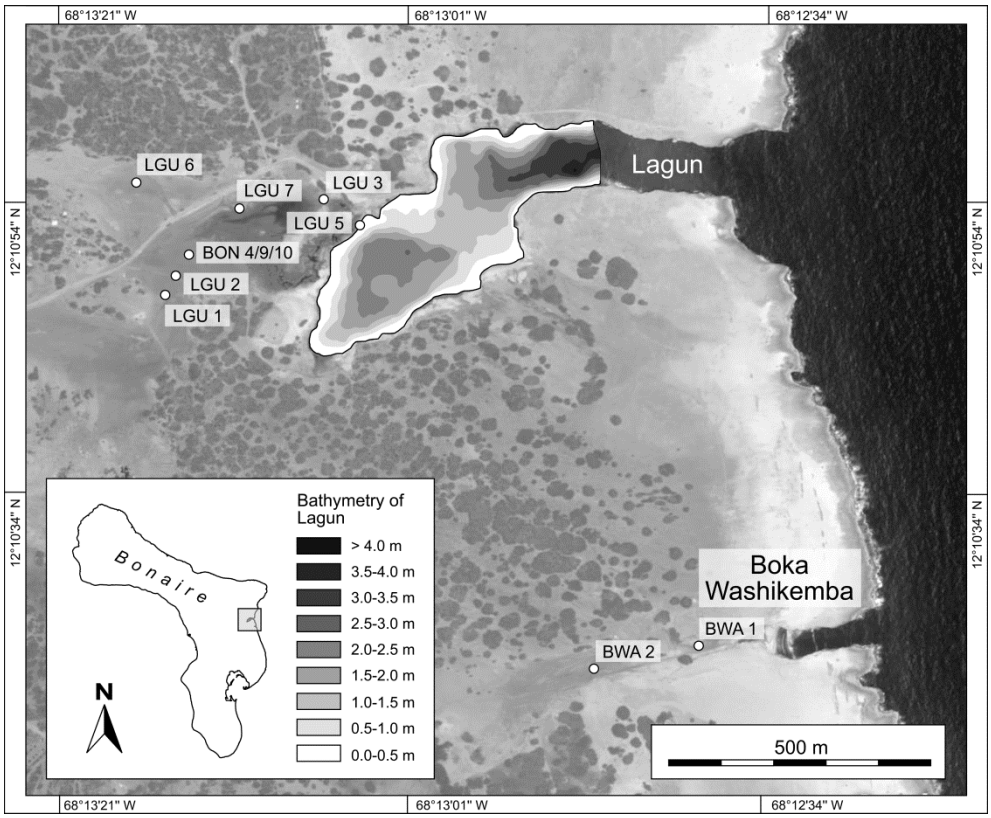

Fig. 18: Overview of the Washikemba area, eastern Bonaire (Fig. 17), providing information on coring sites on the floodplains of Lagun and Boka Washikemba as well as bathymetric data of the Lagun inlet (Google Earth; post-processing of bathymetric data by A. Bolten). Sediment cores not mentioned in the text are discussed by Willershäuser (2008).

The basal unit consists of grey, poorly sorted residual loam which is overlain by well-sorted clayey silt and dark brown peat with several shells of *Crassostrea rhizophora* and *Cerithium* sp. incorporated into the densely packed remains of *Rhizophora* sp. At 3.47 m b.s., values of bulk Ti content and magnetic susceptibility reflect an abrupt facies change. ^{14}C analyses yielded ages of 6283-5999 cal BP and 6406-6029 cal BP (Fig. 19, Table 7). A distinct erosional unconformity separates the mangrove peat

from an overlying unit of shell debris in a carbonate-rich matrix. The thanatocoenosis is dominated by robust shells of *Bulla striata* and *Chione cancellata* and fragments of *Cerithium* sp., *Brachiodontes exustus*, *Trachycardium muricatum*, *Tellina* cf. *tampaensis*, *Arca* sp., *Conus* sp. as well as undetermined marine bivalves and gastropod remains (LGU 7/14 and LGU 9/2 in Table 4). Many shells show angular breaks; however, two articulated specimens of *C. cancellata* were also found (LGU 7/14 and LGU 9/2 in Table 3). Bulk Sr and Ca contents are significantly increased. Shells of *Cerithium* sp. revealed ages of 2333-2168 and 2100-1921 cal BP (Fig. 19).

Well-sorted clayey silt with several plant remains covers the allochthonous shell-rich facies passing into dark brown mangrove peat with valves of *C. rhizophora*. Plant remnants from 1.44 m b.s. were radiocarbon-dated to 503-314 cal BP while a piece of wood from 1.16 m b.s. revealed an age of 275 cal BP to modern. The top sediments of BON 9 are coarse and characterized by high magnetic susceptibility.

Analyses conducted with core LGU 7 revealed a normally graded pattern and a gradual upward increase in LOI and K and Fe concentrations in the shell-rich unit. ^{14}C dating of plant remains (roots?) from the uppermost part of this unit resulted in ages of 1705-1566 and 455-299 cal BP (Fig. 20).

4.5.2 Boka Washikemba

Boka Washikemba is another creek-like drainage feature dissecting the Lower Terrace approx. 900 m south of the entrance of Lagun (Fig. 18). Since its catchment area is smaller, the floodplain has a much lesser extent and mangroves are absent.

BWA 1 (Fig. 21), drilled at a distance of 150 m from the pocket beach, reveals poorly sorted loamy sediments overlying the weathered bedrock. A land snail (*Cerion uva*) at the bottom of this unit revealed an age of 7455-5528 cal BP. At 4.10-3.82 m b.s. the sediment consists of coarse calcarenitic sand, *Halimeda* grainstone and mollusc shell remains. Subangular and rounded components are dominating (BWA 1/19 in Table 8). A thin layer of peat, dated to 3870-3707 cal BP, separates the sand from an olive grey organic-rich silt unit with fragile and well-preserved bivalves and fresh-appearing shells of *Cerithium* sp. The peat is vertically confined by a unit of sandy loam with a plant remnant (root?) and several shells of *Cerithium* sp. showing a moderate degree of abrasion. Above the peat lies a core loss section which is overlain by poorly sorted loamy sand. An abrupt change in environmental conditions is indicated by the overlying well-sorted silt (2.90-2.00 mb.s.) containing well-preserved shells of *Cerithium* sp. The silt unit is interrupted by a thin intercalation of moderately to well-rounded carbonate sand. At 1.55-0.63 m b.s., the sediment coarsens again revealing a high percentage of $CaCO_3$, poor sorting and shells of *Cerithium* sp. as well as a large fragment of an elkhorn coral (*Acropora cervicornis*). The top sediment layer consists of silty clay with several gravel components (Fig. 21).

4.5.3 Playa Grandi

From a geomorphological point of view, the floodplain of Playa Grandi (Fig. 22) can be described as a weakly developed boka with rudimentary features of a ria-type coast (Scheffers, 2004). Two cores were taken from behind the beach ridge (PGR 3) and further landward near the road (PGR 1) (Figs. 22 and 23).

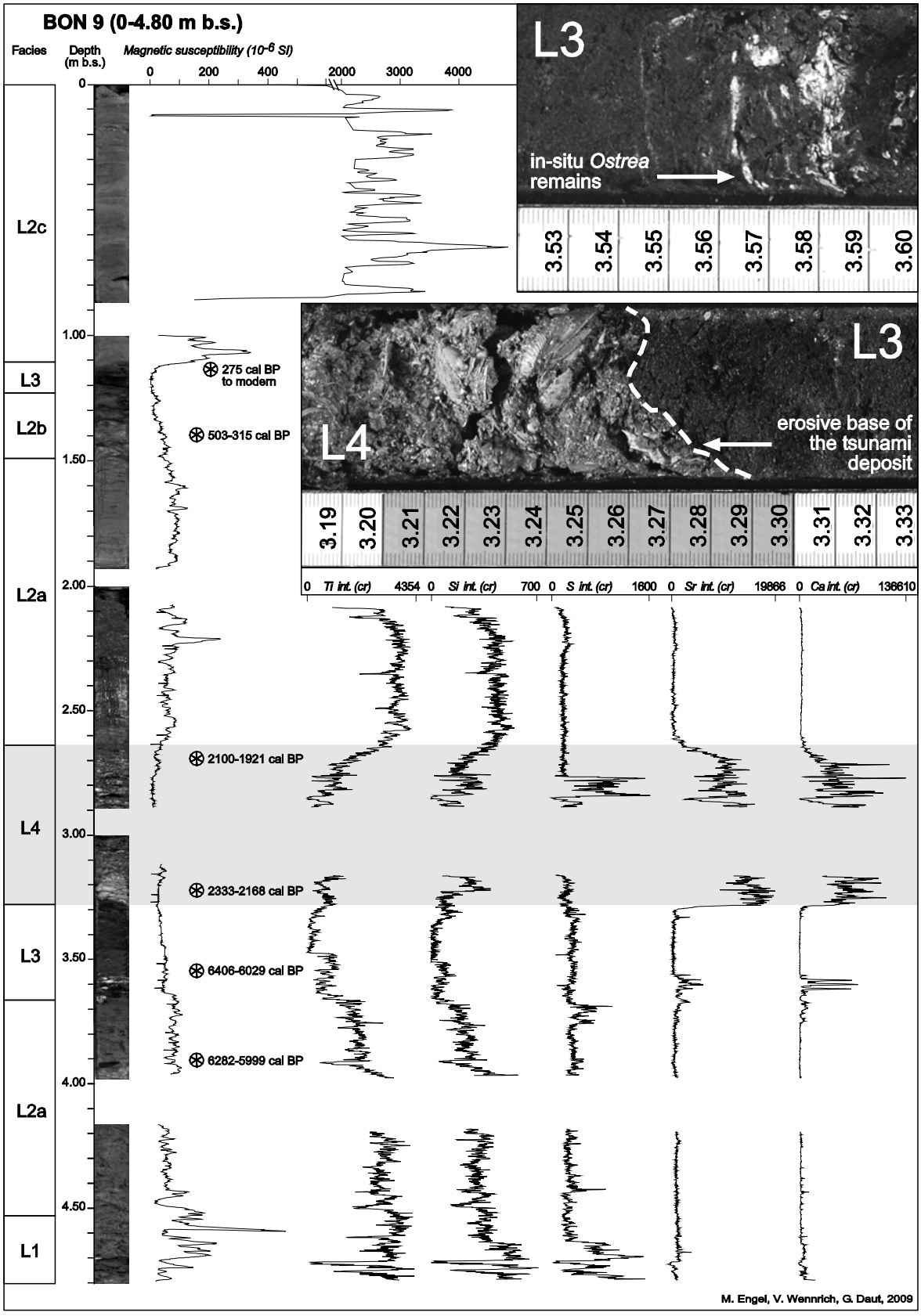

Fig. 19: Sediment core BON 9 and high-resolution proxies of magnetic susceptibility (Engel et al., 2009a), Ti, Si, S, Sr and Ca which were analysed semi-quantitatively using ITRAX XRF (cr = count rate). The upper photo shows autochthonous valves of *Crassostrea rhizophorae* within the mangrove peat unit (L3). The photo below indicates the basal unconformity of the allochthonous high-energy wave deposit (L4). For site location see Fig. 18. Facies characteristics are summarized in Fig. 24. Details concerning radiocarbon dates are provided in Table 7. Chronological data from facies unit L4 is adapted from core LGU 2 (Willershäuser, 2008) based on correlation of strata.

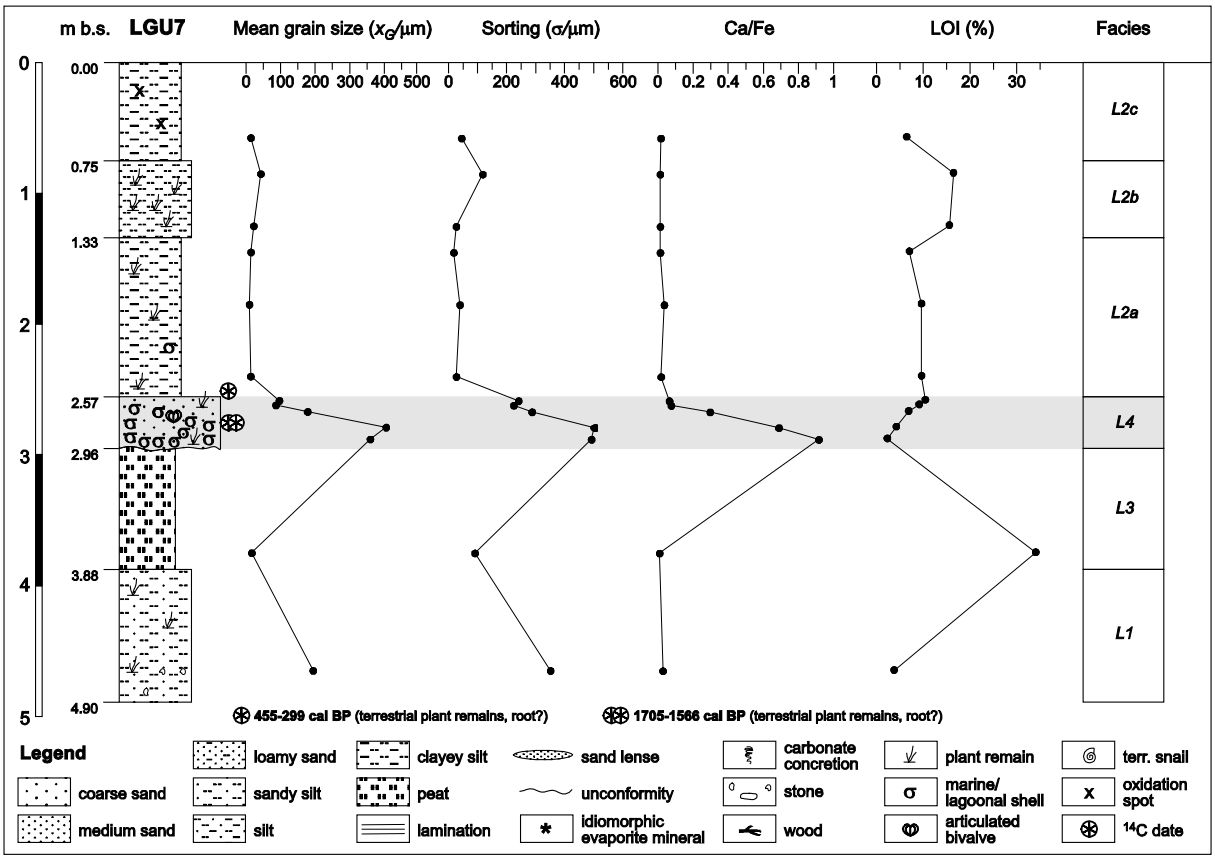

Fig. 20: Sediment core LGU 7 with projected data of mean grain size (x_G), grain sorting (σ), Ca/Fe ratio and LOI. For site location see Fig. 18. Facies characteristics are summarized in Fig. 24. Details concerning radiocarbon dates are provided in Table 7. The legend also applies for Figs. 21 and 23.

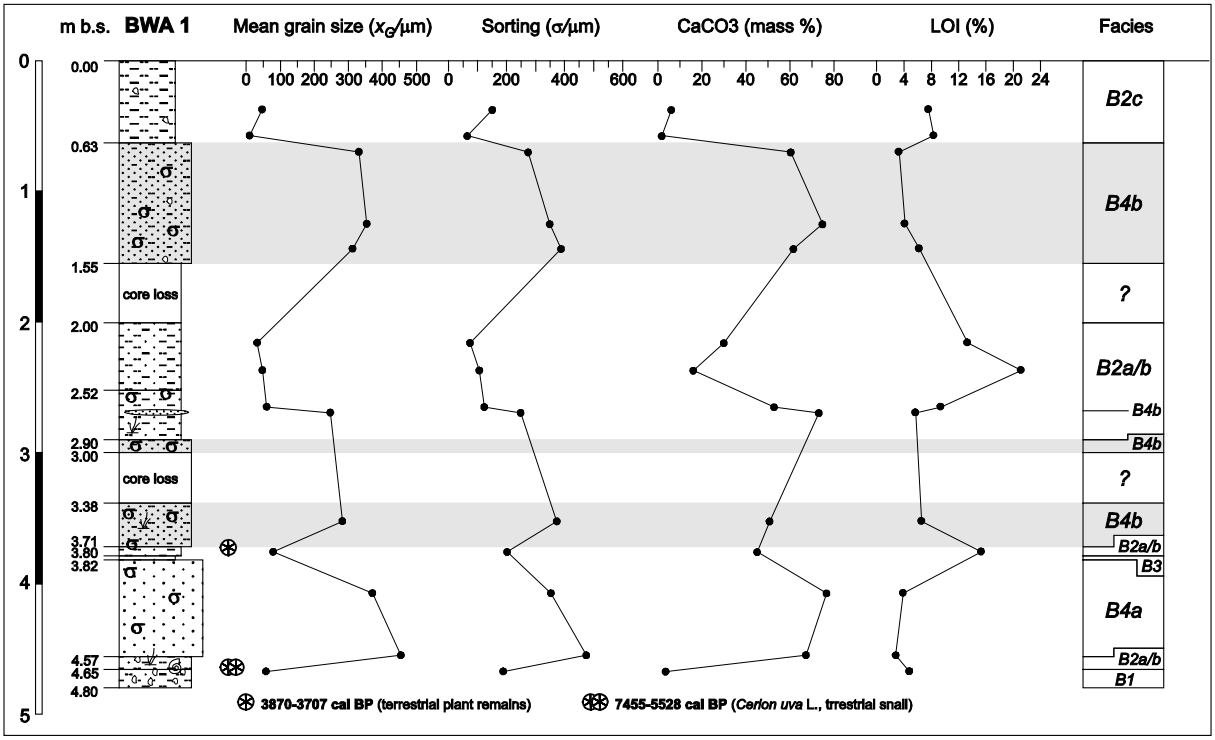

Fig. 21: Sediment core BWA 1 with projected data of mean grain size (x_G), grain sorting (σ), Ca/Fe ratio and LOI. For site location see Fig. 18. Facies characteristics are summarized in Fig. 24. Details concerning radiocarbon data are provided in Table 7. A legend is available in Fig. 20.

4.5.3.1 PGR 3

From 9.00-2.88 m b.s., PGR 3 consists of a massive unit of coarse sand (*Halimeda* grainstone and mostly subangular and rounded coral and mollusc shell fragments). The age of plant remains from its uppermost part is 4066-3843 cal BP. This basal section is vertically confined by silty clay with plant remains that shows significantly increased K values and numerous well-preserved fragile bivalves as well as ostracod valves and shells of *Cerithium* sp. A layer of coarse carbonate sand (2.72-2.58 m b.s.) interrupts the silty clay unit revealing features such as a basal unconformity, an articulated bivalve (*Tellina* cf. *tampaensis*, PGR 3/10 in Table 9), terrestrial plant fragments and a fining-up sedimentary pattern. It was dated to 3384-3247 cal BP. The sand components predominantly consist of *Halimeda* and fragments of worm tubes with more angular breaks and less dissolution and abrasion features compared to the sediment of the massive lowermost sand unit (PGR 3/10 in Table 8).

The overlying fine-grained sediment unit is characterized by low Ca as well as increased Fe and K values. At 2.20 m b.s., abundant shells of *Cerithium* sp. and fragile valves of *Tellina* cf. *tampaensis* (comprising two articulated specimens in living position), juvenile *Bulla striata* and *Brachiodontes exustus* occur (PGR 3/8 F in Table 9). Two thin layers enriched with carbonate sand components are found in the upper sequence. In the surface layer coarsening is associated with poorer sorting and increased Ca values.

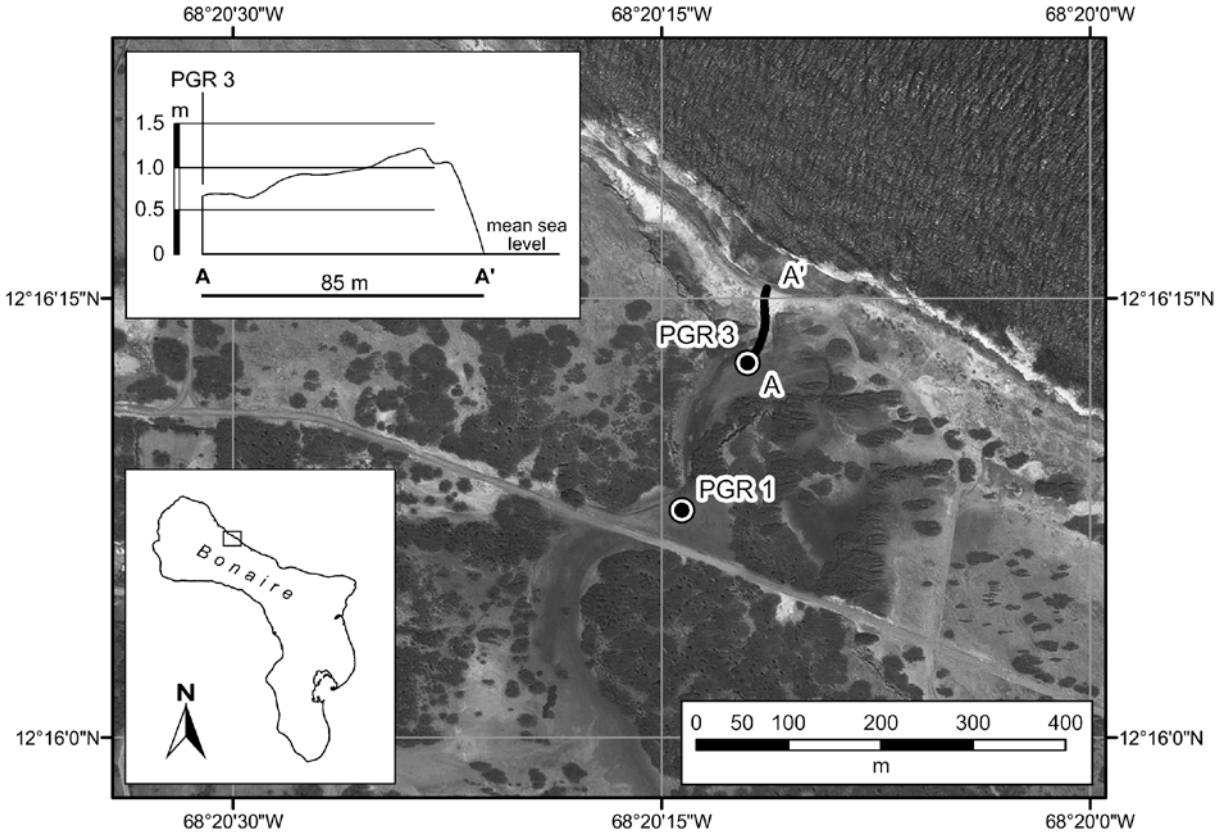

Fig. 22: Overview of Playa Grandi displaying coring sites PGR 1 and 3 on the floodplain (Google Earth). A-A' indicates the altitudinal transect of the boulder beach.

4.5.3.2 PGR 1

Core PGR 1 (0-4.35 m b.s.) was taken 150 m landward of PGR 3. The lowermost section is stratified and contains several entire shells and valves of *Cerithium* sp. and *Brachiodontes exustus* as well as undeterminable mollusc fragments (PGR 1/17 in Table 9). Plant remains were dated to 4518-4299 cal

BP. At 4.12.-4.10 m b.s., a shell pavement was identified. It is incorporated into the lagoonal silt and contains an articulated specimen of *Tellina* cf. *tampaensis* and a juvenile *Bulla striata* among other (fragmented) shells (PGR 1/15 in Tables 8 and 9). The age of plant remains from this layer is 3885-3720 cal BP. *Cerithium* sp. and an articulated specimen of *Tellina* cf. *tampaensis* were also found at 3.63 and 3.25 m b.s. A slight increase in mean grain size at 1.53-1.43 m b.s. is coincident with a lowered Ca/K ratio.

Table 7: Radiocarbon dates for samples from Lagun, Boka Washikemba and Playa Grandi.

Sample	Depth b.s. (cm)	Material	Lab ID[1]	$\delta^{13}C$ (‰)	^{14}C age (BP)	Age in sidereal years (2σ cal BP)
BON 10/1-12	111-116	wood[3]	KN-5851	-26.95	130±30	245-modern
BON 4/18 PF	353-360	peat[3]	Erl10609	-22.7	5469±61	6404-6029
BON 10/1-4	144-145	wood[3]	Erl10610	-27.4	366±46	503-314
BON 10/4-1	385-396	peat[3]	Erl10611	-26.8	5369±60	6282-5999
BWA 1/18	380-382	wood[3]	UGAMS3204	-26.00	3520±25	3870-3707
BWA 1/21 M	466	*Cerion uva* (terr. gastropod)[3,5]	UGAMS3205	-6.47	8480±25	7455-5528
LGU 2/10 G	270-280	*Cerithium* sp. (marine gastropod)[4]	UGAMS3206	-26.60	2330±25	2100-1921
LGU 2/11 G	315-325	*Cerithium* sp. (marine gastropod)[4]	UGAMS3207	-2.09	2540±25	2333-2168
LGU 7/8 14C	256-257	plant remains[3]	UGAMS4199	-26.2	300±25	455-299
LGU 7/12 14C	271-274	plant remains[3]	UGAMS4200	-26.85	1730±25	1705-1566
PGR 1/15 H	411	plant remains[3]	UGAMS4202	-24.58	3530±25	3885-3720
PGR 1/17 H	431-435	plant remains[3]	UGAMS4203	-23.03	3960±25	4518-4299
PGR 3/10 PR	258	plant remains[3]	UGAMS4204	-25.50	3100±30	3384-3247
PGR 3/13 14C	288	plant remains[3]	UGAMS4205	-25.79	3620±30	4066-3843

[1]KN = Radiocarbon Lab Cologne, Institut für Ur- und Frühgeschichte, Universität zu Köln; Erl = AMS-Labor Erlangen, Physikalisches Institut, Friedrich-Alexander-Universität Erlangen-Nürnberg; UGAMS = Center for Applied Isotope Studies, University of Georgia, Athens.
[2]Conventional radiocarbon dating; for all other datings the AMS technique was applied.
[3]Calibration according to Reimer et al. (2004).
[4]Calibration according to Hughen et al. (2004); ΔR = -49 was adapted from Radtke et al. (2003).
[5]1020±430 a were subtracted from the ^{14}C age according to Goodfriend and Gould (1996).

4.6 Discussion

The main results and interpretation of sedimentary and geochemical analyses are compiled in Fig. 24. In combination with taphonomic findings (Tables 3 and 4) as well as sediment thickness and stratigraphical position (Playa Grandi), they relate to the differentiation of local facies units. The distribution of facies units within the backbarrier stratigraphies is shown in Figs. 19-21 and 23. Fig. 25 provides a summary of findings of high-energy wave deposits with their chronological interpretation.

4.6.1 The distribution of high-energy wave facies along the east coast

4.6.1.1 Lagun

At Lagun (BON 9: 3.25-2.65 m b.s.; LGU 7: 2.96-2.57 m b.s.), a sedimentary unit of shell debris (facies unit L4 in Fig. 24) was encountered which is also present in adjacent sediment cores (Willershäuser, 2008). It is vertically confined by compressed mangrove tree material (below, L3) and lagoonal mud

(above, L2a). The macrofaunal remains mainly consist of *Chione cancellata* (endobenthonic), *Crassostrea rhizophora* (sessile), *Bulla striata*, *Cerithium* sp. and *Brachiodontes exustus* and indicate a habitat of shallow soft-bottom areas covered by turtle grass (*Thalassia testudinum*) and fringed by flourishing populations of *Rhizophora mangle* (Mattox, 1949; Moore and Lopez, 1969; Vélez, 1991; Abbott and Dance, 2000). Even though some of the species occasionally occur at greater depths of reefal environments (Buitrago et al., 2006), a dense population of the bivalve *C. cancellata* in particular indicates that the entire deposit stems from the inlet of Lagun and its narrow beach. Communities of *C. cancellata* may reach a density of up to 162 per m^2 in intertidal muds while it declines down to <1 per m^2 in deeper sublittoral environments (Moore and Lopez, 1969). Two articulated bivalves were also identified which is a prominent feature of tsunami deposits, as described in the case studies of Cesarea, Israel (113 AD) and Sur Lagoon, Oman (1945 AD) (Donato et al., 2008). Valves and shells are well-preserved with predominantly angular breaks (LGU 7/14 and LGU 9/2 in Table 3) indicating proximal dislocation from their habitat inside the open embayment (calm environment) into the former landward lagoon during a high-magnitude/low-frequency wave event. The erosional contact between the allochthonous shell layer and the truncated peat (Fig. 19) represents a stratigraphical feature typically associated with palaeotsunami deposits (e.g. Dawson et al., 1988; May et al., 2007; Jankaew et al., 2008; Vött et al., 2007, 2009) but has also been observed in sediments transported onshore by severe storms and hurricanes (e.g. Morton et al., 2007; Wang and Horwitz, 2007). Peaks in Ca, Sr and S (Fig. 19) concentrations as well as low values of K, Ti, Si and Rb resemble the geochemical pattern of tsunami-laid sands from 1755 AD inside the Tagus Estuary, Portugal (Andrade et al., 2003). However, a similar pattern of elemental concentrations may also be produced by hurricane activity (Jessen et al., 2008) or even a gradual marine transgression (Engel et al., 2009b).

Sedimentary analyses from LGU 7 provide supplementary information on the transport process of the shell debris layer (L4). Normal grading as well as a continuous upward increase in LOI (Fig. 20) in combination with the distinct erosional unconformity indicate accumulation by a single major impulse and the mixing with terrestrial material during flow attenuation. By comparing bedform structures of both tsunami and typhoon deposits generated during modern events on SW Hokkaido, Nanayama et al. (2000) concluded that tsunamigenic sediments consist of normally graded sedimentary sequences each representing a single wave. The authors suggest that tsunami deposits often consist of basal sands deposited by inflow and a mixture of marine and non-marine sediment and plant remains due to backflow deposition.

The shell debris layer L4 (Figs. 19 and 20) identified at Lagun meets a broad range of empirical tsunami signatures (cf. Dominey-Howes et al., 2006; Switzer and Jones, 2008a). The fact that waves of recent severe hurricanes approaching Bonaire from the east (Table 6) flooded the nearshore floodplains but left no significant sedimentary imprint at Lagun and Boka Washikemba may also indicate its deposition during a more powerful hydrodynamic process. According to ^{14}C dates (Figs. 19 and 20; Table 7), the event occurred after 2000 and most probably before 1700 BP (Fig. 25) based on molluscs from the deposit representing maximum ages (2333-2168 and 2100-1921 cal BP), and roots which penetrate the deposit and thus provide minimum ages (1705-1566 and 455-299 cal BP). The large hiatus between L4 and the underlying unit L3 (Fig. 19) may indicate the high erosional potential of the overland flow. Thus, the deposit is assumed to be tsunamigenic, even though a powerful hurricane that made landfall on Bonaire, which never occurred in history, cannot be ruled out completely.

The wave impact seems to have entirely transformed the nearshore ecosystem and destroyed a major part of the lush mangrove population based on preliminary results of pollen counts of core BON 9. After the impact, *Rhizophora* pollen declines drastically in favour of grasses accompanied by an in-

crease in charcoal particles which indicates the presence of high amounts of dead wood (*Chapter 5*; Engel et al., 2009a).

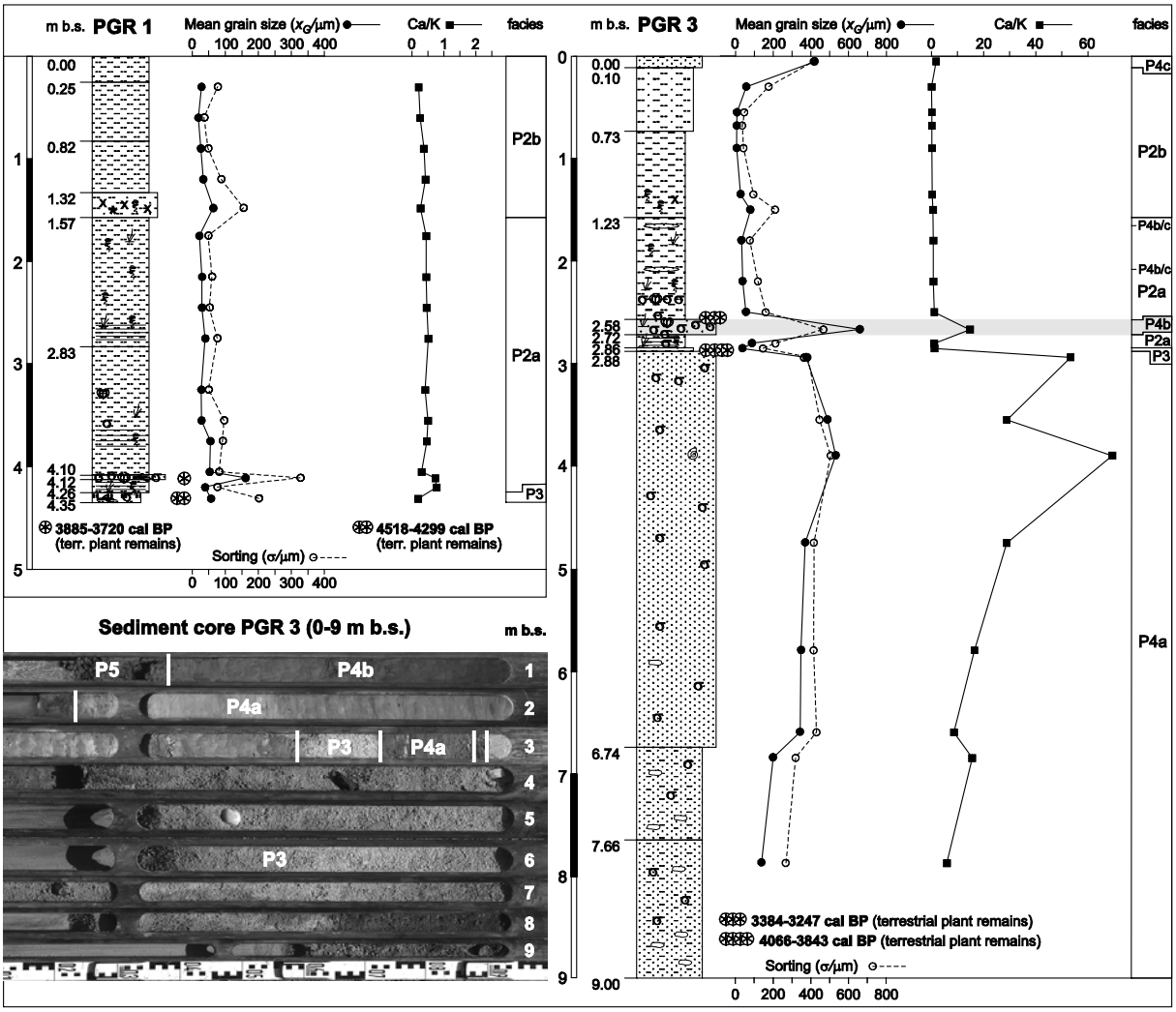

Fig. 23: Stratigraphy of PGR 1 and PGR 3 with projected data of mean grain size (x_G), grain sorting (σ), Ca/Fe ratio and LOI. For site location see Fig. 22. Facies characteristics are summarized in Fig. 24. Details concerning radiocarbon dates are provided in Table 7. A legend is available in Fig. 20.

4.6.1.2 Boka Washikemba

The vertical distribution of marine facies (B4a, B4b in Figs. 21 and 24) at the Boka Washikemba floodplain reveals discrepancies compared to Lagun – although both sites are proximal to one another and have the same orientation. The lowermost marine intrusion (B4a) above the weathered bedrock (B1) and a thin layer of terrestrial facies (7455-5528 cal BP; B2a/b) is interpreted as beach sands of the Holocene marine transgression based on observations on regional sea level history. Relative sea level curves from Curaçao and Venezuela based on ^{14}C data of peat deposits (*Chapter 8*; Rull et al., 1999; Klosowska, 2003) and model predictions (Milne et al., 2005) as well as approximations inferred from reef growth (Focke, 1978a) indicate that relative sea level during the Holocene has never been higher than today. The high postglacial rate of eustatic sea level rise decreased significantly during the Mid- and Late Holocene. This break usually occurs around 6000-5000 BP and marks the maximum flooding surface at many coastal sedimentary environs worldwide (cf. Stanley and Warne, 1994; Engel et al., 2009b) including the narrow inlet of Boka Washikemba.

Table 8: Taphonomy of shells and *Halimeda* particles from the sediment cores of Lagun, Boka Washikemba and Playa Grandi. The parameters were selected according to Donato et al. (2008), values are displayed in %. Comparative data of tsunami and storm sediment layers from Oman and Caesarea (Israel) by Donato et al. (2008) are also provided. Their results suggest that in addition to littoral sediments tsunamis also mobilise shells in living position and shell material from below the storm wave base with less rounded breaks or abrasion/dissolution features.

Sample	Depth m b.s.	Facies	n	Articulated bivalves	Whole shell/valve	Shell fragment	No break	Angular break	Subangular/ rounded break	Boring	Encrustation	Dissolution/ abrasion
LGU 7/14 Ref[3]	2.93-2.83	L4 (tsunami)	243	0.00	18.11	81.89	9.05	82.72	8.23	11.11	0.00	20.16
LGU 9/2[4]	2.95-2.85	L4 (tsunami)	247	0.00	31.58	68.42	16.19	68.83	14.98	15.79	0.40	22.67
BWA 1/6[3]	1.30-1.20	B4b (tsunami)	64	0.00	3.13	96.88	0.00	28.13	81.25	0.00	0.00	87.50
BWA 1/13[1]	2.71-2.68	B4b (sand lense)	147	0.00	0.00	100.00	0.00	17.01	82.99	0.00	0.00	86.39
BWA 1/19[1]	4.10-4.05	B4b, sand lense (tsunami?)	159	0.00	1.26	98.74	0.00	8.18	91.82	1.89	0.63	93.71
PGR 1/15[3]	4.12-4.10	P2a (shallow lagoon)	383	0.26	2.87	97.13	1.31	95.30	3.39	0.00	0.26	2.35
PGR 1/17 Sand[3]	4.35-4.26	P3 (coastal marsh)	17	0.00	11.76	88.24	0.00	29.41	70.59	47.06	0.00	76.47
PGR 3/Surf[2]	0.08-0.00	P4c (hurricane)	236	0.00	0.85	99.15	0.42	8.47	91.10	5.51	0.00	81.78
PGR 3/8 F[3]	2.25-2.15	P2a (shallow lagoon)	169	0.81	43.20	55.62	40.24	57.99	1.78	0.59	0.00	12.43
PGR 3/10[1]	2.72-2.62	P4b (tsunami)	296	0.34	3.72	95.95	4.05	27.03	69.26	5.07	0.00	38.85
PGR 3/11 F[1]	2.84-2.82	P2a (shallow lagoon)	352	0.00	89.77	10.23	82.67	12.50	4.83	0.57	0.00	6.25
PGR 3/12 Sand[3]	2.86-2.85	P3 (coastal marsh)	220	0.00	42.27	57.73	37.27	61.82	0.91	0.00	4.09	1.36
PGR 3/17[1]	4.80-4.70	P4a (beach)	240	0.00	5.00	95.00	2.50	11.67	85.83	14.58	0.00	82.50
Tsunami layer Oman mean[5]			459	6.80	35.60	57.70	-	53.80	9.00	2.30	4.80	1.60
Tsunami layer Oman standard deviation[5]			459	8.40	14.90	11.10	-	11.50	5.80	2.40	3.80	1.90
Tsunami layer Caesarea mean[5]			818	0.50	40.90	59.60	-	51.40	13.20	0.70	5.30	4.90
Tsunami layer Caesarea standard deviation[5]			818	0.10	2.30	4.70	-	4.30	8.60	0.50	0.20	0.70

[1] grain/shell fragment size >0.63 mm
[2] grain/shell fragment size >1 mm
[3] grain/shell fragment size >2 mm
[4] grain/shell fragment size >6.3 mm
[5] Data adapted from Donato et al. (2008), data repository item – Table DR1

Accordingly, facies unit B4a is likely to represent the Holocene maximum landward displacement of the shoreline at Boka Washikemba while the overlying peat stratum (3867-3705 cal BP) of B2a/b belongs to a Mid- to Late Holocene regressive sequence produced by sediment input from the hinterland and moderate tectonic uplift outpacing the slow eustatic sea level rise (Fig. 21). According to this interpretation, the recurrence of marine facies in the upper strata of BWA 1 remains enigmatic. A B4b unit (3.71-2.90 m b.s.) confines the thin terrestrial layer (B2a/b) representative of a lagoonal ecosystem. The loamy sand of B4b most likely interrupts the Mid- to Late Holocene sequence as the imprint of a high-energy wave event. Marine provenance is inferred from the presence of coral rub-

ble, a high portion of subangular and rounded *Halimeda* grainstone and abraded *Cerithium* shell fragments. Compared to facies B4a (beach), the geochemical pattern in B4b reveals more terrestrial influence and a smaller percentage of eulittoral *Halimeda* sand due to the incorporation of terrestrial material and/or post-depositional alteration (Fig. 24). Chronological evidence from the underlying unit indicates post-3800 BP deposition. The layer may even correlate with the post-2000 BP candidate tsunami deposit at Lagun according to its stratigraphical position.

Another high-energy wave event left its thin sedimentary imprint at 2.70 m b.s. (B4b in Fig. 21). Whether it corresponds to a hurricane or a tsunami remains uncertain since thickness of sand-sized deposits is not indicative for either tsunami or storm surge impact. Deposits related to both hydrodynamic processes reach from several millimeters (tsunami: e.g. Gelfenbaum and Jaffe, 2003; tropical cyclone: e.g. Donnelly and Woodruff, 2007) to more than 80 cm (tsunami: e.g. Paris et al., 2007; tropical cyclone: e.g. Morton et al., 2007), depending on the availability of source material, the hurricane center's distance and intensity or tsunami run-up and approaching angle, distance to the shoreline as well as the pre-impact coastal topography.

Between 1.55 and 0.63 m b.s. (Fig. 21), the regressive Holocene sequence (B2a/b, B2c) is once again interrupted by a marine layer (B4b) representing a possible extreme wave impact. Higher concentrations of terrestrial indicators (Fig. 24), a higher percentage of angular particle shapes (Table 8) and a slightly smaller mean grain size (Fig. 21) compared to B4a (beach) as well as the stratigraphical context argue against the long-term deposition as a beach ridge. Unfortunately, the basal contact was not available due to core loss and no chronological data are available for this deposit. However, extrapolating from sedimentation rates of the uppermost meter at Lagun the age of the corresponding high-energy wave event may be around 500 years while it should not exceed 1000 years. At Lagun no stratigraphical counterpart was detectable. Sato et al. (1995) emphasize on the importance of source supply for the creation of the sedimentary record and the minor significance of local run-up heights after conducting post-tsunami surveys at Hokkaido in 1993. Accordingly, extensive sand accumulations on top of the Lower Terrace of Bonaire which are linked to older extreme wave events (Scheffers and Scheffers, 2006) may have served as sediment sources for BWA 1 rather than for LGU 7/BON 9 further landward causing discrepancies in the sedimentary record. The essential role of available source material is also substantiated by a coral rubble sequence of up to 1.5 m at Playa Funchi, NW Bonaire (Spiske and Jaffe, 2009). According to post-hurricane surveys and the interpretation of multitemporal aerial photographs, the deposit is exclusively associated with Hurricane Lenny in 1999 and has hardly been modified by subsequent hurricanes of comparable magnitude (e.g. Hurricane Felix in 2007, Hurricane Omar in 2008, cf. Table 6). A vivid framework of *Acropora cervicornis* inhabiting the sublittoral of Playa Funchi collapsed due to the spread of the white-band disease in the early 1980s (Bries et al., 2004) providing large quantities of coral rubble to be mobilized by the waves induced by Lenny in 1999.

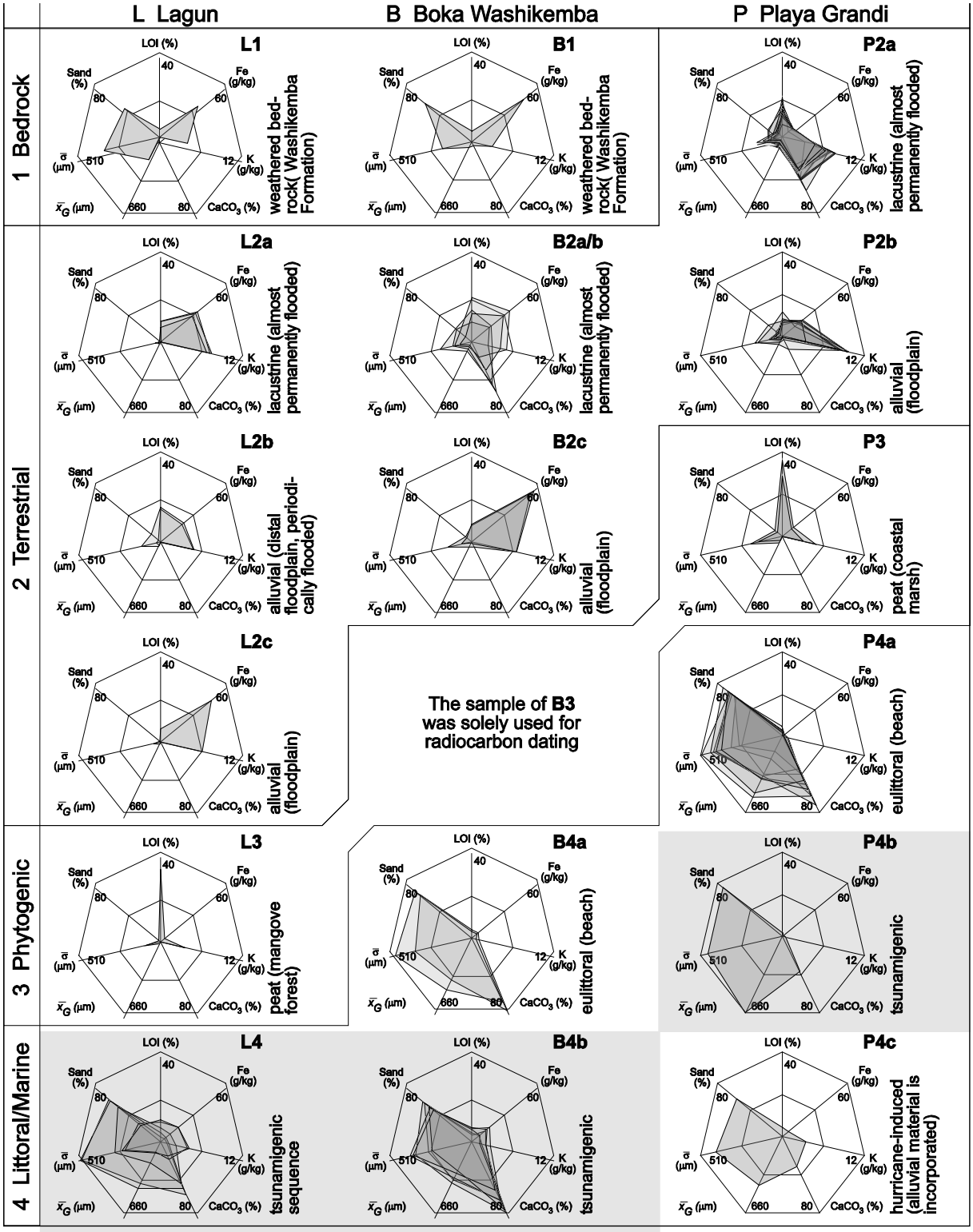

Fig. 24: Facies model for the Holocene stratigraphy of Lagun (left column), Boka Washikemba (centre) and Playa Grandi (right) based on sedimentary (percentage of sand, mean grain size, sorting) and geochemical (LOI, K, Fe, $CaCO_3$) parameters. Rows indicate specific depositional environments. Each spider chart shows heptagons similar in shape representing a certain local lithofacies unit. Each heptagon represents one sediment sample. Facies abbreviations are valid for the text and the sediment cores (Figs. 19-21 and 23). The geochemical and sedimentary fingerprint of possibly tsunamigenic facies is highlighted (grey). Discrimination between different marine subunits (e.g. P4a, P4b, P4c) is not solely based on results compiled in this figure but also on taphonomic analyses (Table 8), as well as sediment thickness (P4a) and stratigraphical position (B4a, P4c).

Table 9: The distribution of mollusc remains in the sediment cores of Lagun, Boka Washikemba and Playa Grandi (ws = whole shell; f = fragment). At Lagun (LGU) the high abundance of thick-walled shells of *Bulla striata* and *Chione cancellata* indicates that elevated wave energy disturbed a geo-ecosystem which is well prepared against regular, long-term wave action. LGU 7 and LGU 9 represent the same site. At Boka Washikemba (BWA) and Playa Grandi (PGR) intertidal or sublittoral species are rare since the habitat in the foreshore zone is small compared to Lagun. Especially at Playa Grandi, the slope dips with a high angle. More details on facies characteristics are provided in Fig. 24. The depth of the samples can be inferred from Table 8. Cores are presented in Figs. 20, 21 and 23.

Sample	Facies (environment or morphodynamic process)	*Cerithium* sp.		*Bulla striata*		marine gastropod undet.		*Chione cancellata*		*Brachiodontes exustus*		*Tellina cf. tampaensis*		*Crassostrea rhizophora*		bivalve undet.		Other taxa/macrofaunal remains (n < 5)
		ws	f	ws	f	ws	f	ws	f	ws	f	ws	f	ws	f	ws	f	
LGU 7/14 Ref	L4 (tsunami)	3	1	9	22	-	16	11	111	-	9	20	-	-	16	-	31	*Trachycardium muricatum (ws)*, *Conus* sp. (ws), Muricidae (f), *Thais* sp. (f)
LGU 9/2	L4 (tsunami)	5	4	8	11	-	18	18	58	-	3	45	4	-	19	-	51	*Trachycardium muricatum* (ws), *Arca* sp. (ws, f)
BWA 1/6	B4b (tsunami)	2	3	-	-	-	7	-	-	-	-	-	-	-	-	-	1	Ostracoda (ws), Decapoda (f), *Acropora cervi-cornis* (coral, f)
BWA 1/13	B4b, sand lense (tsunami?)	-	-	-	-	-	4	-	-	-	-	-	-	-	-	-	5	-
BWA 1/19	B4a (beach)	-	-	-	-	2	7	-	-	-	-	-	-	-	-	-	9	-
PGR 1/15	P2a (shallow lagoon)	4	22	1	-	2	7	-	-	-	2	2	305		-	3	21	-
PGR 1/17 Sand	P3 (coastal marsh)	2	2	-	-	-	2	-	-	-	1	-	-	-	-	-	10	Terrestrial gas-tropod (f)
PGR 3/Surf	P4c (hurricane)	2	1	-	-	-	11	-	-	-	1	-	-	-	-	-	11	-
PGR 3/8 F	P2a (shallow lagoon)	48	3	-	-	-	-	-	-	8	23	19	66	-	-	-	-	-
PGR 3/10	P4b (tsunami)	5	14	-	-	4	16	-	-	-	-	-	-	-	-	1	13	Fissurellidae (ws), *Nerita* sp. (f)
PGR 3/11 F	P2a (shallow lagoon)	13	5	-	-	1	16	-	-	-	-	-	-	-	-	297	14	Ostracoda (ws) Decapoda (f)
PGR 3/12 Sand	P3 (coastal marsh)	78	18	2	-	-	1	-	-	-	6	10	98	-	-	-	4	Terrestrial gas-tropod (f)
PGR 3/17	P4a (beach)	7	4	1	-	-	8	1	-	-	-	-	-	-	-	-	23	*Arca* sp. (ws)

4.6.2 The distribution of high-energy wave facies along the northeastern coast

No evidence for marine sediment input was found at PGR 1 (Fig. 23), located at a distance of c. 250 m from the shore. In contrast, just behind the beach ridge of coral rubble a sequence was cored (PGR 3)

comprising the uppermost part of the Early to Mid-Holocene transgressive sequence (P4a in Fig. 23) and the Mid- to Late Holocene highstand sequence (upper part of P4a to ground surface in Fig. 23). More than 6 m of the lower sediment core reveal a massive ancient beach ridge testifying to Mid-Holocene shoreline retreat. Regression set in well before 4046-3843 cal BP when the site was already invaded by prograding backswamps (P3) and a lagoon (P2a) characterised by dense, thin-walled bivalve populations (PGR 3/12 and PGR 3/11 F in Table 9).

A lens of marine sand (P4b, Fig. 23) indicates the occurrence of a high-energy wave event. Articulated bivalves as well as an increased percentage of angular breaks on mollusc shells and significantly fewer abrasion or dissolution features and borings (sample PGR 3/10, Table 8) allow the discrimination of this unit (P4b) from the beach facies (sample PGR 3/17, Table 8). A promising approach in deducing a certain hydrodynamic process from facies unit P4b is a comparison with the surface unit P4c which represents the sedimentary contribution of recent hurricanes (Fig. 23). There, single events contributed only low amounts of carbonate sands which are mixed with autochthonous fine-grained alluvial matrix.

The interpretation that the sand section of P4b represents a tsunami event is based on the following observations: a sharp erosional contact at the base of P4b (tsunami layer) which is absent in P4c (hurricane layer). There is also a significantly higher percentage of angular shapes and less abrasion or dissolution features on grains and shell material of layer P4b (Table 8). Based on the mollusc shell assemblage both deposits have similar source supply which is the contemporary active beach and sublittoral environment.

The taphonomic results of this study (Table 8) show that the approach presented by Donato et al. (2008) may provide a useful tool in discriminating between palaeo-storm and palaeotsunami deposits. The fact that percentage values of certain morphometric parameters of the Oman tsunami layer and the P4b layer differ is due to local pre-impact sedimentary, ecological and mineralogical settings. Nevertheless, in all cases common tendencies were observed.

A plant remnant from the upper part of the tsunami sand sequence, where terrestrial material is incorporated due to backflow dynamics, revealed an age of 3384-3247 cal BP representing a maximum age for the corresponding event.

Two thin sand layers (2.08 and 1.65 m b.s.) provide evidence for additional extraordinary wave impacts during the late Holocene (Fig. 23). The lower layer may correlate with the major wave event after 2000 BP deduced from deposits from Lagun (Figs. 19 and 20). The upper sand lens represents an unknown event of short-term marine inundation.

4.6.3 Correlation with the coarse-clast record of Bonaire

Dislocated boulders and extended ridges of coral rubble on top of the MIS 5 Lower Terrace of Bonaire are attributed to strong tsunami events that occurred before the arrival of the Europeans and after sea level rise started to decelerate in the Mid-Holocene (Scheffers, 2002, 2004, 2005). Based on geomorphological interpretation of these deposits and a data set of more than 80 radiocarbon dates from Bonaire and the wider Caribbean as well as 120 ESR (Electron-Spin-Resonance) dates from Bonaire – all representing maximum ages for certain extreme wave events – a chronology of strong tsunami impacts around 500 BP, 1200 BP, 3300 BP, 3900 BP and 4300 BP was proposed by Scheffers (2005). Due to the wide span of radiometric ages and the underestimation of long-term coastal processes and minor wave events in the discussion of the genesis of the circumlittoral sedimentary re-

cord, this chronology has recently been challenged (Morton et al., 2006, 2008; Spiske et al., 2008). By reviewing studies on coastal sediment transport, Morton et al. (2006) concluded that the ridges and ramparts may have been generated by periodically occurring storm waves.

However, the tsunami chronology deduced from coarse deposits is only partially supported by the present study. The post-2000 BP major wave impact – possibly a tsunami – reflected by the floodplain stratigraphy of the east coast (Figs. 19 and 20) does not match the chronology of Scheffers (2002, 2004, 2005). A major incident around 500 BP inferred by Scheffers (2005) based on investigations on Bonaire and Weiss (1979) based on a sedimentary sequence from Cayo Sal, c. 150 km ESE of Bonaire, may correspond to the findings at BWA 1, while at Lagun we observed no evidence for such an event. The main reasons for these particular discrepancies may be

(i) errors in sampling for dating purposes,

(ii) fluctuations in sediment availability in the eulittoral and sublittoral zones during certain events, and/or

(iii) incompleteness of the stratigraphical record due to erosion.

At Playa Grandi, a major wave event was indicated by a sand deposit from c. 3300 BP or younger (Fig. 23) which is coeval with the interpretation of the coarse-clast tsunami record by Scheffers (2005).

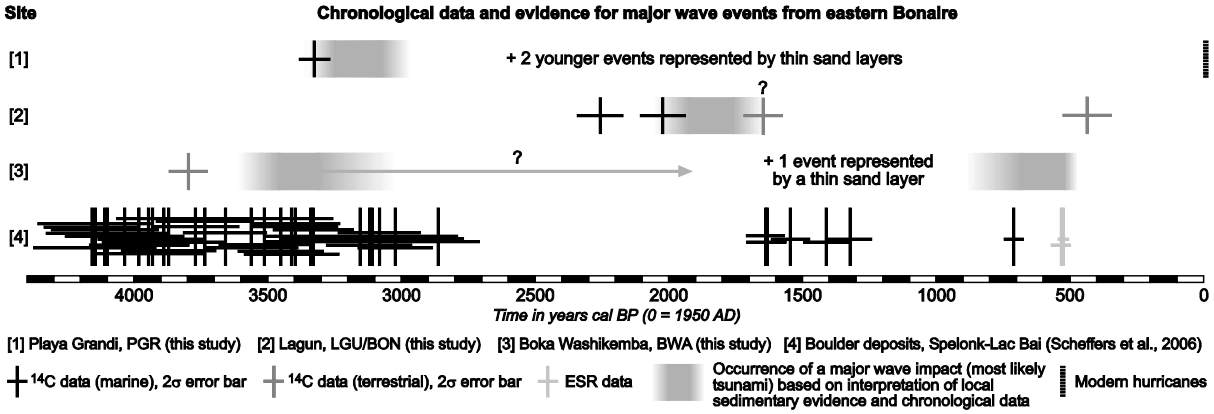

Fig. 25: Sedimentary evidence for and chronological interpretation of major wave events from geoarchives along the E and NE coast of Bonaire. Chronological data of Scheffers et al. (2006) from supralittoral boulder deposits of the coastal area between Spelonk Lighthouse and Lac Baai (Fig. 17) is added. The results of the present study indicate the occurrence of three major wave events during the last 4500 years that significantly exceeded the energy of strong modern hurricanes (Table 6). Their sedimentary traces vary significantly from site to site.

The conclusion of Morton et al. (2008: p. 636) that, according to the wide span of ^{14}C dates available along the shoreline of Bonaire, coarse-clast accumulations are the result of "long-term coastal deposition by many extreme wave events" must be slightly modified. Severe episodic influence on the nearshore environments was unambiguously identified; findings from this study imply large-scale erosion and sedimentation as well as long-lasting alteration of the boka ecosystems by major wave events at a very low frequency. These extraordinary events presumably had significant effects along the coasts of the entire southern Caribbean region. However, we fully agree with Morton et al. (2008) that the resulting landforms and sedimentary imprints were subsequently modified in many cases by long-term wave action and periodically recurring wave events.

4.7 Conclusions

Tsunami and hurricane-generated waves represent a real threat to the southern Caribbean. In this paper, stratigraphical evidence for three major wave impacts along the windward coast of Bonaire is presented (Fig. 25).

The Holocene stratigraphy of the northeasterly exposed shore (Playa Grandi) indicates a major wave event – possibly a tsunami – around 3300 BP as well as two subsequent undated high-energy wave events. Sublittoral sediments interrupting onshore sedimentary sequences on the east coast (Lagun, Boka Washikemba) provide evidence for a major wave impact after 2000 BP which most likely corresponds to a tsunami. Another comparable event may have occurred shortly before 500 BP (Fig. 25).

We found that the application of tsunami signatures, which are based on investigations on sedimentary characteristics of recent onshore tsunami deposits worldwide, reveals certain difficulties, since they strongly depend on local topographic settings as well as sedimentary environments, and thus vary considerably. Even if a large number of tsunami signatures are identified, the interpretation of the field record still remains a serious challenge. Hence, considering local analogues, i.e. comparing a candidate deposit with the sedimentary imprint of recent local events, provides a more promising key to understanding event stratigraphies. In this study, the marginal sedimentary input of severe hurricane swells of the last decade (see surface sediment composition of Lagun, Boka Washikemba and Playa Grandi; Figs. 20, 21, and 23) in particular points to tsunami as the hydrodynamic process responsible for the accumulation of the subsurface sand and shell layers.

Deducing magnitudes of extreme wave events from the thickness of corresponding onshore deposits is subject to large uncertainties. The sublittoral environment of Lagun stores significantly more sediment compared to Playa Grandi, where the slope descends steeply offshore. Thus, vertical extent of event layers onshore will likely be greater. The irregular occurrence of subterraneous high-energy wave deposits between Playa Grandi and the Washikemba area may also indicate the importance of the pre-impact topography, the approaching angle of wave trains and post-depositional erosion or modification.

The results of the present study provide only partial coherence with previous palaeotsunami chronologies of the southern Caribbean based on investigations on supralittoral coarse-clast deposits on the ABC Islands (Aruba, Bonaire, Curaçao). Further studies on onshore stratigraphies – especially in the well-preserved and undisturbed geoarchives of northwestern Bonaire (*Chapter 7*) – are necessary to increase the accuracy of information on the frequency and magnitude of Holocene extreme wave events in the southern Caribbean.

5 Extreme wave events as reflected by the pollen record of Lagun, Bonaire (Leeward Antilles)*

Abstract: Palynological studies are a promising, though often neglected tool to identify palaeotsunami deposits and to evaluate the geomorphological and ecological impact of tsunamis. In a pilot study at Lagun, a mangrove-fringed embayment of eastern Bonaire, nine samples from a vibracore, spanning more than 6000 years, were investigated for their pollen content. The aim was to evaluate the suitability of local pollen spectra for palaeoecological interpretation and to infer ecological and geomorphological effects of extreme wave events. Pollen preservation was good in all samples. The investigated sediment core contains one prominent shell debris layer related to a tsunami. Pre-tsunami pollen spectra reveal high percentages of *Rhizophora*, indicating a well established mangrove community at Lagun. A significantly lower percentage of *Rhizophora* pollen in the samples overlying the tsunami deposit and a subsequent gradual upward increase indicate that the tsunami induced a long-lasting decline in mangrove stands and severe modification of the geomorphology and ecology of Lagun. It seems that the mangroves only gradually recovered from the impact. However, these interpretatiosn have to be verified by further in-depth investigations

Keywords: *Palynology, Pollen analysis, Tsunami, Caribbean, Palaeoecology, Mangroves*

5.1 Introduction

The research program on the influence of Holocene extreme wave events on coastal geo-ecosystems of Bonaire, on which this thesis is based on, comprises a pilot study on the value and general applicability of palynological data in the interpretation of event stratigraphies and the detection of palaeotsunami deposits (see Fig. 2 in *Chapter 1*). A large number of sedimentological, geomorphological, biological, geochemical, and archaeological methods or proxies have successfully been applied to identify tsunamigenic deposits and landforms (see *Chapter 3*; Engel and Brückner, 2011; and the "proxy toolkit" compiled by Goff et al., 2012). However, only a limited number of studies based on sedimentary archives have incorporated the pollen record into their multi-proxy approach.

Minoura et al. (1996) found an increase in arboreal pollen at a coastal site of Kamtchatka after a strong earthquake-induced tsunami in April 1923. This observation is explained by the long duration of flooding of the coastal lowlands by seawater and limited infiltration due to frozen grounds, which in particular harmed non-arboreal vegetation. Further south on Hokkaido, a site also facing the Kuril-Kamtchatka Trench, samples located above a palaeotsunami deposit contained a significantly smaller amount of pollen compared to those further up in the peat sequence, indicating that vegetation severely suffered from tsunami impact and only gradually recovered (Nanayama et al., 2007). In British Columbia (North American Pacific coast), pollen spectra reflect recurring earthquakes and related

* This chapter is based on Chapter 5 in: Engel, M., Bolten, A., Brückner, H., Daut, G., Kelletat, D., Schäbitz, F., Scheffers, A., Scheffers, S.R., Vött, A., Wille, M., Willershäuser, T., 2009. Reading the chapter of extreme wave events in nearshore geo-bio-archives of Bonaire (Netherlands Antilles) – initial results from Lagun and Boka Bartol. Marburger Geographische Schriften 145, 157-178.

tsunamis as well as co-seismic subsidence and gradual interseismic uplift based on precise classification of vegetation assemblages and their narrow elevation ranges (e.g. Hughes et al., 2002). Goff et al. (2010) note increased abrasion and corrosion of spores and pollen and a higher percentage of pollen types of salt tolerant plants in a deposit created by a high-energy wave event on northern North Island, New Zealand. Nichol et al. (2010) demonstrate the use of the pollen record in dating a tsunami deposit. The identification of European pollen types within tsunami sands of a wetland on Chatham Island, southwest Pacific Ocean, links it with the most severe historically known tsunami of the area in 1868. Very low concentrations of pollen grains within high-energy wave deposits were observed by Vött et al. (2009) in sediment sequences from the Lefkada Sound, northwestern Greece. The low numbers are interpreted to derive from "high sedimentation rates and the input of oxygen during extreme events" (Vött et al. 2009: p. 118).

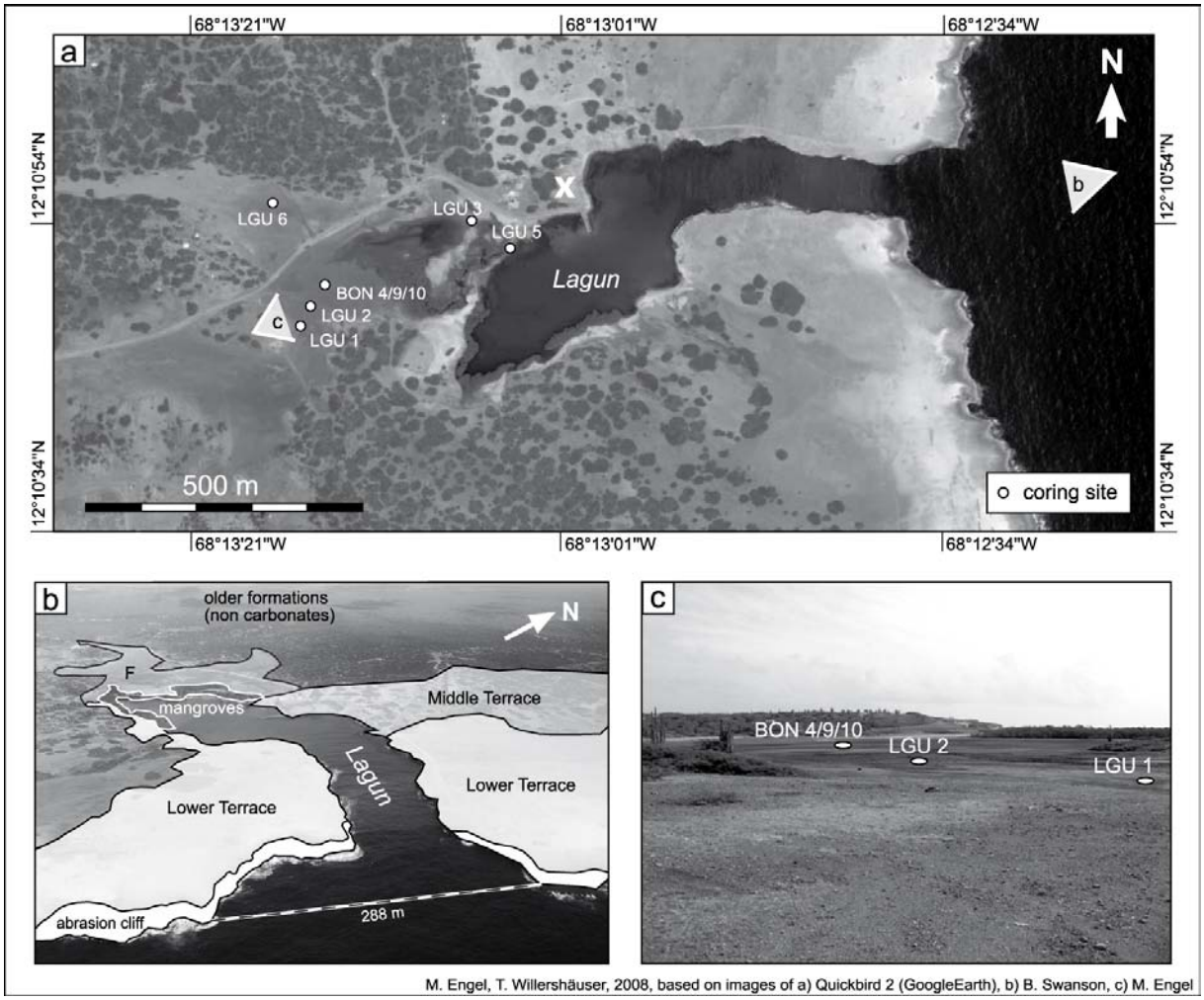

Fig. 26: a) Overview of Lagun and the adjacent floodplain (Google Earth) comprising coring sites. Fig. 17 in *Chapter 4* indicates the exact location of Lagun on Bonaire. The white cross marks the photographer's position in Fig. 27; b) oblique aerial photograph indicating geological-geomorphological units (photography by B. Swanson, 2007, modification by T. Willershäuser and M. Engel); c) floodplain of Lagun, the direction of view is indicated in a) (modified from Engel et al., 2009a).

This chapter presents the pollen record of sediment core BON 9 from Lagun (Figs. 26 and 27) and aims at (i) evaluating the suitability of local pollen archives for palaeoecological interpretation and (ii) providing preliminary evidence of ecological and geomorphological effects of extreme wave events

and their duration. Details on geomorphological processes and the stratigraphy of the study site are depicted in *Chapter 4* and Engel et al. (2010b).

5.2 Present vegetation of Lagun

The dry vegetation of Bonaire is very heterogeneous and is influenced by adjacent floristic provinces, such as the tropical deciduous forest or dry evergreen woodland, though cosmopolitan species can also be found. Human impact on the vegetation is severe since the arrival of the Europeans in the early 16th century. Charcoal production, grazing, and, since the 20th century, land clearance for industry and tourism development are the main reasons for the high degree of degradation (De Freitas et al., 2005).

Lagun is a shallow embayment open to the ocean and fringed by a mangrove population representing the *Rhizophora mangle-Batis maritima* vegetation type (Fig. 27). Mangroves are dominated by *Rizophora mangle*, which prefers shallow water habitats, and are complemented by *Avicennia germinans* and *Laguncularia racemosa*. The latter species prefer higher grounds, flooded only during highest tides (De Freitas et al., 2005).

Fig. 27: Innermost part of the Lagun embayment fringed by a mangrove population. On the hill in the background, the cactus-shrub vegetation is visible, dominated by *Subpilocerus repandus*. Core BON 9 was taken behind the mangrove belt on the right (photograph: F. Schäbitz, 2008).

The adjacent limestone terraces of Lagun only have a rudimentary cover of low herb vegetation. Characteristic species are *Sesuvium portulacastrum* and *Lithophila muscoides* (*Sesuvium portulacastrum-Lithophila muscoides* type) or *L. muscoides* in combination with *Euphorbia* sp. and *Sporobolus pyramidatus* (*Lithophila muscoides-Euphorbia* sp. type) (De Freitas et al., 2005).

The floodplain of Lagun, where the investigated sediment core was taken, is practically free of vegetation. Its surroundings further landward are covered by cactus-shrub vegetation typical for large parts of Bonaire's interior. *Subpilocerus repandus* is the most common cactus in this area.

5.3 Methods

Nine samples of vibracore BON 9 were selected for pollen analysis, which was carried out by Michael Wille (Universität zu Köln). Preparation of the pollen samples, production of pollen slides, counting of charcoal, calculation and presentation of pollen percentages was conducted following the standard procedure of the pollen laboratory of the Seminar of Geography and Education, Universität zu Köln. After adding *Lycopodium* spore markers in order to support the calculation of pollen percentages,

the sample material was wet-sieved (mesh size 112 µm), acetolysed, and sieved again using ultrasonic treatment. Samples were kept in glycerol and later applied on slides using paraffin (Wille et al., 2007). The samples were counted under a light microscope to a sum of 300 pollen grains excluding fern spores. In samples 263 cm b.s. (below surface), 223 cm b.s., 141 cm b.s. and 113 cm b.s., a lower pollen sum was reached due to low pollen concentration. In total, 39 pollen taxa, four fern spore types and four non-pollen-palynomorphs were found.

5.4 Results and discussion

Pollen preservation was good in all samples. No signs of reworking were identified. The most indicative taxa are summarized in Fig. 28.

The lowermost three pollen spectra (431 cm b.s., 411 cm b.s. and 385 cm b.s.) are dominated by *Bursera simaruba* and different Leguminosae types in association with Euphorbiaceae, Arecaceae and Melastomataceae. *Rhizophora* – most likely *R. mangle* – is present only in low abundances. It is likely that during this time the area surrounding the study site was covered with forest. The low abundance of *Rhizophora* indicates only scattered stands of mangrove, which might be related to a significantly lower relative sea level prior to 6000 BP (*Chapter 8*; Rull et al., 1999; Klosowska, 2003) and a lack of suitable habitats. The two overlying pollen spectra (350 cm b.s. and 330 cm b.s.) are strongly dominated by *Rhizophora*. All other taxa show low values. It is likely that in this time interval the shores of the area was densely covered with mangrove due to the development of the calm and shallow embayment of Lagun after 6000 BP and. The significant decrease of *Bursera simaruba* may also be related to habitat shifting due to ongoing, decelerated sea level rise. The overlying section consists of a candidate tsunami deposit of poorly sorted, but well-preserved mollusc shells and angular shell fragments in a carbonate matrix which creates an erosional unconformity. This potential tsunami is dated to 2000-1700 BP indicating that a significant part of the sediment record is lost to erosion during the impact (*Chapter 4*; Engel et al., 2010b).

Mid- to Late Holocene climate fluctuations must also be taken into account as drivers of vegetation change and, thus, composition of pollen samples. Haug et al. (2003) identified several pronounced dry events in the 1st millennium AD and increased aridity during the Little Ice Age based on cores from the Cariaco Basin, southeast of Bonaire. Tedesco and Thunell (2003) found six periods of increased aridity over the last 6000 years using the foraminiferal oxygen isotope record of the Cariaco Basin. However, the low resolution of the current pollen profile hampers safe correlation with these palaeoclimatic data.

The two pollen samples following the high-energy wave impact (263 m b.s. and 223 cm b.s.) are dominated by Cyperaceae and Poaceae. *Rhizophora* is present but in low amounts comparable to the lowermost spectra. Charcoal, Cactaceae, Asteraceae and Chenopodiaceae have a higher abundance. Poor coverage of trees can be inferred from these results. Influx of pollen from plants of the dry and open hinterland is relatively high. A catastrophic wave event probably destroyed most of the mangroves and other trees and the dead wood got burned indicated by increased charcoal values. However, the high percentages of charcoal particles and decline of phanerophytes may also be related to the Archaic population of Bonaire, which made its initial appearance on Bonaire around 3300 BP. At this time, people arrived from Curaçao by boat in search of new food sources and inhabited the area of Lagun (Haviser, 1991). Regarding the mangroves, it can be inferred that the high-energy wave event destroyed significant parts of the mangrove vegetation and had a long-duration impact on the

geo-ecosystem of Lagun. The slightly increased percentage of *Rhizophora* in 223 cm b.s. might indicate that the mangroves started to recover. This interpretation is similar to the observations made by Nanayama et al. (2007) from Hokkaido, where tsunamis induce strong disturbances of the ecological equilibrium and peak vegetation recovers only gradually.

The uppermost two pollen spectra (141 cm b.s. and 113 cm b.s.), representing time slices of the last 500 years, are again dominated by *Rhizophora* reflecting a re-established subrecent mangrove population fringing the shore of the Lagun embayment until the present (Fig. 27).

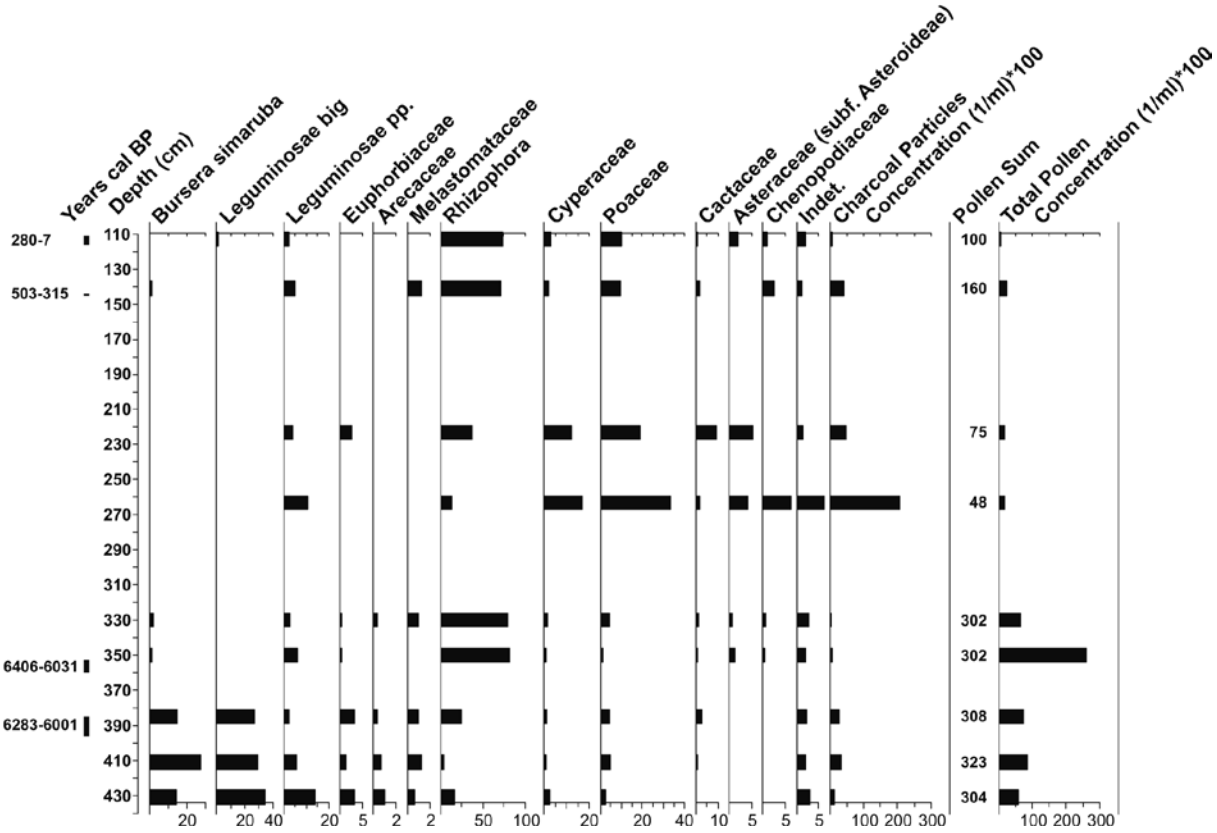

Fig. 28: Pollen diagram of sediment core BON 9 (Fig. 26) depicting selected pollen taxa and their percentages, total pollen sums and charcoal particles (Engel et al., 2009a). Calibrated ^{14}C ages are shown on the left. Details on the stratigraphy and ^{14}C ages are presented in *Chapter 4*. Pollen analysis was conducted by Michael Wille, Universität zu Köln.

5.5 Conclusions and outlook

The pilot study on pollen spectra of the sediment archive of Lagun revealed promising results in terms of pollen preservation and general applicability of the method. Considering the scarcity of pollen records from the southern Caribbean, the results presented here not only justify, they even demand further research.

The investigated sediment core contains one prominent shell debris layer, which was previously linked to a tsunami between 2000-1700 BP (*Chapter 4*; Engel et al., 2010b). Pollen spectra prior to the wave impact are dominated by *Rhizophora*, indicating a well established mangrove community at Lagun. A significantly lower percentage of *Rhizophora* pollen in the post-tsunami samples and a subsequent gradual increase indicate that

(i) the tsunami induced long-lasting modification of the geomorphology and ecology of Lagun, and

(ii) mangroves only gradually recovered from the impact.

The increase of charcoal particles in post-tsunami sediments either points to high amounts of dead wood and natural fires or anthropogenic fires.

These results are preliminary and have to be verified by further in-depth palynological research also incorporating other sediment archives. A higher density of samples in a core would allow for more precise conclusions. Saliña Tam (Chapter 6) and, in particular Boka Bartol (*Chapter 7*) are considered to be suitable for pollen-based studies on the impact of extreme wave events on Holocene coastal geo-ecosystems and the pollen signature of extreme wave deposits. Moreover, sampling of lagoonal sediments from the sheltered part of Lac Baai (e.g. 12°06’23”N, 68°13’06”W) or Goto Mer (e.g. 12°14’11”N, 68°22’29”W) for undisturbed stratigraphical records and the study of Holocene climatic fluctuations is suggested.

6 Shoreline changes and high-energy wave impacts at the leeward coast of Bonaire (Netherlands Antilles)*

Abstract: Supralittoral coarse-clast deposits along the shoreline of Bonaire (Netherlands Antilles) as well as increased hurricane/storm surge frequency during the past decade testify to the major hazard of high-energy wave impacts in the southern Caribbean. Since deducing certain events from the subaerial coarse-clast record involves major uncertainties and because historical reports are restricted to the past 500 years, we use a new set of vibracore and push-core data (i) to contribute to a more reliable Holocene history of regional extreme wave events and (ii) to evaluate their impact on shoreline evolution. Multi-proxy palaeoenvironmental analyses (XRF, XRD, grain size distribution, carbonate, LOI, microfossils) were carried out using nearshore sedimentary archives from the sheltered western (leeward) side of Bonaire and its small neighbor Klein Bonaire. In combination with ^{14}C-AMS data the stratigraphy reflects a long-term coastal evolution controlled by relative sea level rise, longshore sediment transport, and short-term morphodynamic impulses by extreme wave action, all three of which may have significantly influenced the development of polyhaline lagoons and the demise of mangrove populations. Extreme wave events may be categorized into major episodic incidents (c. 3.6 ka [?] BP; 3.2-3.0 ka BP; 2.0-1.8 ka BP; post-1.3 ka [?] BP), which may correspond to tsunamis and periodic events recurring on the order of decades to centuries, which we interpret as severe tropical cyclones. Extreme wave events seem to control to a certain extent the formation of coastal ridges on Bonaire and, thus, to cause abrupt shifts in the long-term morphodynamic and ecological boundary conditions of the circumlittoral inland bays.

Keywords: *Washover deposits, Tropical cyclones (hurricanes), Tsunamis, Holocene stratigraphy, Natural hazards, Coastal environments*

6.1 Introduction

A broad spectrum of potential triggering mechanisms for tsunamis exist throughout the Caribbean region. These include

(i) earthquake-triggering tectonic movement (strike-slip motion, oblique convergence) along the boundary of the Caribbean and North American plates (Grindlay et al., 2005) or the Venezuelan coast (Audemard et al., 2005);

(ii) the Lesser Antilles subduction zone with earthquakes and various sources of explosive and effusive volcanism (e.g. Zahibo and Pelinovsky, 2001; Mattioli et al., 2007);

* This chapter is based on: Engel, M., Brückner, H., Messenzehl, K., Frenzel, P., May, S.M., Scheffers, A., Scheffers, S., Wennrich, V., Kelletat, D., in press. Shoreline changes and high-energy wave impacts at the leeward coast of Bonaire (Netherlands Antilles). Earth, Planets and Space.

(iii) morphological signatures of large-scale submarine mass failure, e.g. north of Puerto Rico (Grindlay et al., 2005; ten Brink et al., 2006) or on Curaçao (Hornbach et al., 2010);

(iv) submarine debris avalanches along the Lesser Antilles arc (Deplus et al., 2001);

(v) teletsunamis from the open Atlantic Ocean as triggered by the 1755 Lisbon earthquake (O'Loughlin and Lander, 2003) or by a future volcanic edifice collapse on the Canary Islands (Ward and Day, 2001).

In some places possible geological evidence for tsunamis has been found such as marine sand sheets deposited inland, barrier breaches or supralittoral boulder deposits in elevated positions significantly exceeding the size of the largest boulders moved by recent severe hurricanes (Khan et al., 2010, Scheffers and Scheffers, 2006), e.g. on Aruba, Bonaire and Curaçao (ABC Islands), the Antillean Arc, Anegada, Barbados, Jamaica, the Grand Caymans and the Bahamas (Jones and Hunter, 1992; Scheffers, 2004, 2005; Kelletat et al., 2005; Robinson et al., 2006; Atwater et al., 2011). The high tsunami risk is also confirmed by O'Loughlin and Lander (2003) who compile 53 reliable tsunami occurrences in the Caribbean region within the last 500 years of written history.

On the island of Bonaire in the southern Caribbean (Fig. 29), the lack of historical accounts of tsunamis (O'Loughlin and Lander, 2003) stands in a remarkable contrast to the massive circumlittoral boulder deposits some of which have been associated with tsunamigenic dislocation (Scheffers, 2004, 2005). Moreover, the interpretation of these boulders as storm or tsunami deposits remains in question, partly due to the range of dates derived from clasts, and also due to differences in sedimentary analysis (cf. Morton et al., 2008; Spiske et al., 2008). For this reason, we have chosen to use coastal stratigraphical contexts (lagoons, alluvial flats) of Bonaire's coastline in order to examine the extreme wave history of the southern Caribbean and to evaluate the impact of these waves on shoreline dynamics.

The main goals of this paper are to reconstruct Mid- to Late Holocene coastal environments and to identify and date extreme wave deposits, as well as to differentiate between sedimentary signatures of tsunamis and tropical cyclones of west (leeward) Bonaire. The signatures are compared with those of fine-grained extreme wave deposits from the eastern (windward) coast (cf. Engel et al., 2009, 2010b) and with implications of the supralittoral coarse-clast record (Scheffers, 2005; Scheffers et al., 2006; Morton et al., 2008; Watt et al., 2010). Research on palaeotsunami deposits in coastal areas where tsunami occurrence has never been documented may provide a scientific basis for:

(i) the designation of high-risk areas,

(ii) the creation of public awareness for a generally underestimated coastal hazard, and

(iii) local disaster mitigation planning.

6.2 Study sites

The island of Bonaire (Fig. 29) comprises a volcanic core (Late Cretaceous, Washikemba Formation) and a series of surrounding palaeo-reef terraces (Neogene-Quaternary) forming steep cliffs along the coast as well as minor relics of Palaeogene deposition. Slow tectonic uplift (around 5 cm ka^{-1}), tilting and Quaternary sea level fluctuations drove the development of a sequence of reefal limestone terraces. The lowermost palaeo-reef stages, the Middle Terrace (MT) and the Lower Terrace (LT), relate to MIS 7 or earlier and 5e, respectively (Herweijer and Focke, 1978).

Bonaire has an arid climate and experiences persistent tradewinds from the east, with easterly storms and occasional hurricanes during the period of June and November. The coasts have a microtidal regime (c. 0.3 m) (Bak, 1977). While the eastern shore is exposed constantly to high wave energy, the western, leeward shore – including the study sites of Saliña Tam and Klein Bonaire – is calmer and thus characterised by a vertically narrow intertidal notch and a flourishing fringing reef (Focke, 1978a). Nevertheless, increased wave action triggered by tropical cyclones in the last decade, e.g. Hurricane Lenny in 1999, taking an unusual west-to-east track, had significant morphological effects on the coral rubble beaches (Scheffers, 2005) and destroyed large parts of the living reef (Bries et al., 2004). The southern part of the western (leeward) coastline from Lacre Punt to Punt Vierkant is covered by coral debris and boulders of up to 2 t, most of which were washed onshore in 1999. Several boulders of up to 20 t lie on top of the LT between Kralendijk and Goto Meer (Scheffers, 2005).

In search of subsurface extreme wave deposits along the leeward side of Bonaire, the former inland bay of Saliña Tam and the shallow back-barrier lagoon of southern Klein Bonaire (Fig. 29) were chosen for stratigraphical investigations. The sites are characterised by background sedimentation from shallow standing water (brackish to hypersaline) and occasional fluvial input (Saliña Tam) behind a barrier of coral rubble. At some places, thick beds of mangove peat are present. Event layers consist of shallow marine sands, shells, and coral fragments.

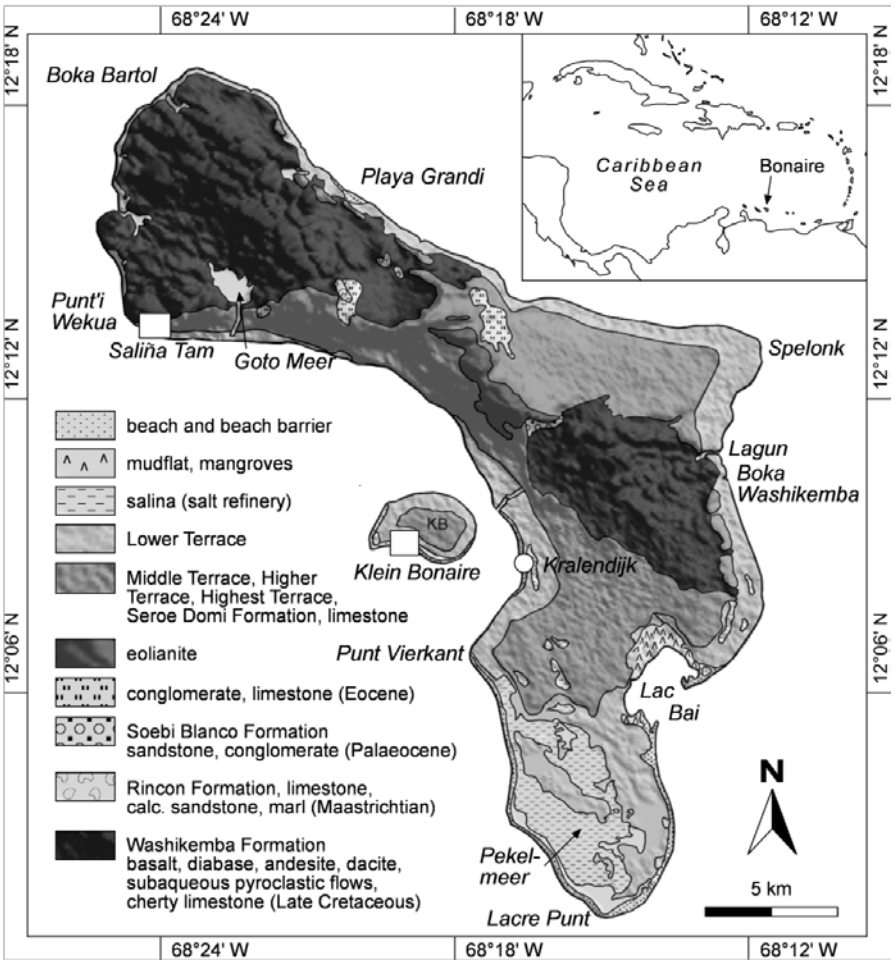

Fig. 29: Geological overview of Bonaire based on mapping by Pijpers (1933), Westermann and Zonneveld (1956) and De Buisonjé (1974), as well as SRTM elevation data (http://dds.cr.usgs.gov/srtm). The map shows sites from this study (white rectangles) and Engel et al. (2010b).

6.2.1 Saliña Tam

Saliña Tam is a ria-like landform (Scheffers, 2004, 2005) locally referred to as boka (Fig. 30), a valley draining a part of the undulating topography of northwestern Bonaire (Washikemba Formation, Fig. 29) and intersecting the LT and MT. The main morphodynamic processes are linear erosion during the latest Pleistocene base level fall. At the entrance of Bonaire's bokas, LT incision amounts up to 16 m below present sea level (De Buisonjé, 1974).

Postglacial sea level rise flooded Saliña Tam. The boka is separated from the open sea by a barrier of sand, coral rubble and beachrock reaching a width of up to 70 m and a height of up to 3 m above present mean sea level (a.s.l) (Figs. 30 and 31). At what time this bar formed and whether it formed due to long-term morphodynamic processes (e.g. longshore drift) (Zonneveld et al., 1977), or was triggered by extreme wave events (Scheffers, 2005; Morton et al., 2008), is a subject of this paper. Today, salinity of the bokas is high (up to 120‰ below the halocline of Goto Meer during summer [Kobluk and Crawford, 1990]) and the water table is low due to low permeability of the seaward barrier, low precipitation most time of the year, and due to high evaporation (De Buisonjé, 1974).

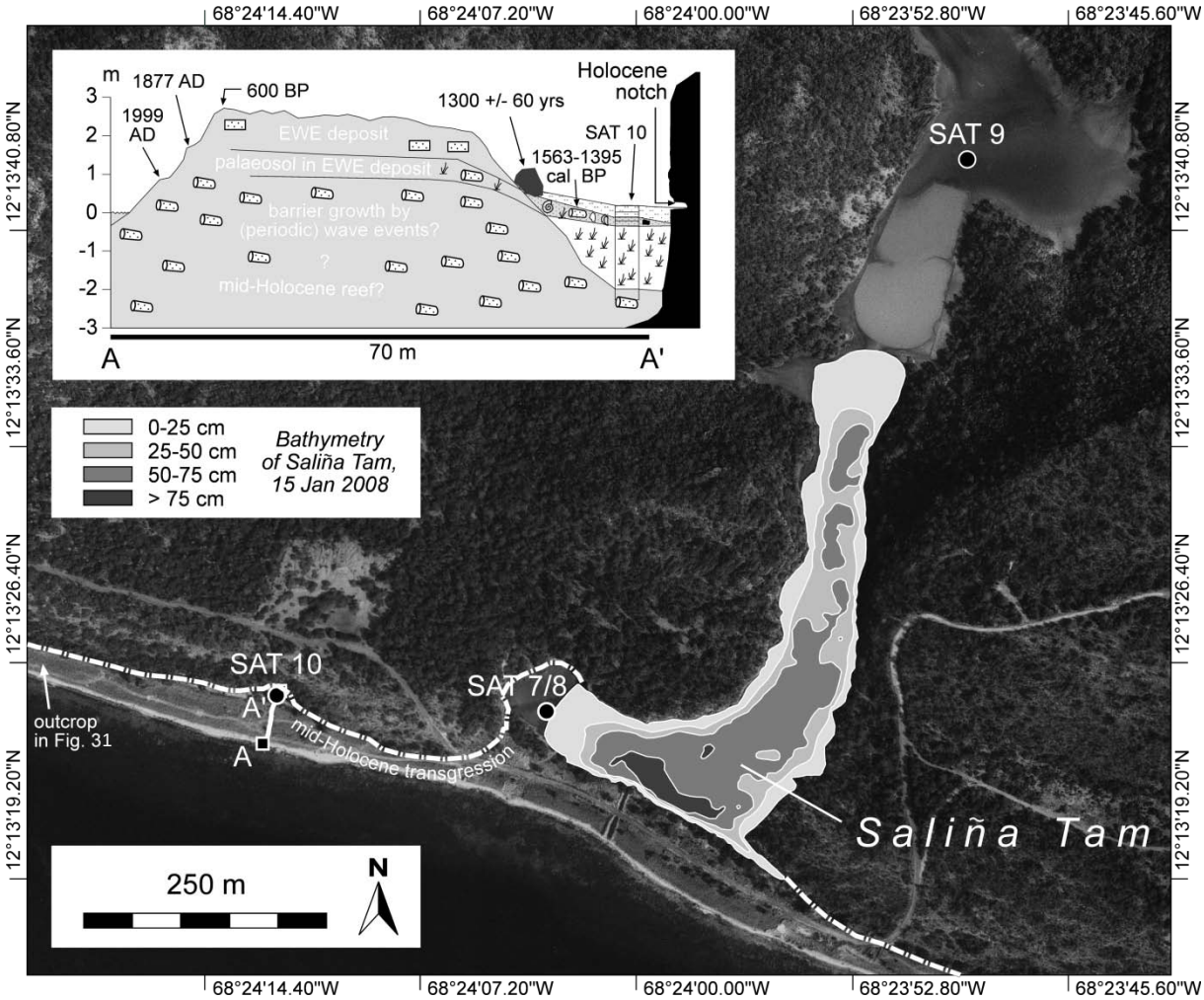

Fig. 30: Aerial photograph of Saliña Tam (1996), western Bonaire (Fig. 29), providing information on coring sites and bathymetry of the water body. The elevation profile A-A' was measured by DGPS. The internal structure of the barrier is also shown on Fig. 31. The ESR age of a large head coral (1300±60 a) is taken from Scheffers (2005). The back-barrier stratigraphy is based on SAT 10 (Fig. 37). A key to symbols is on Fig. 34. EWE = extreme wave event.

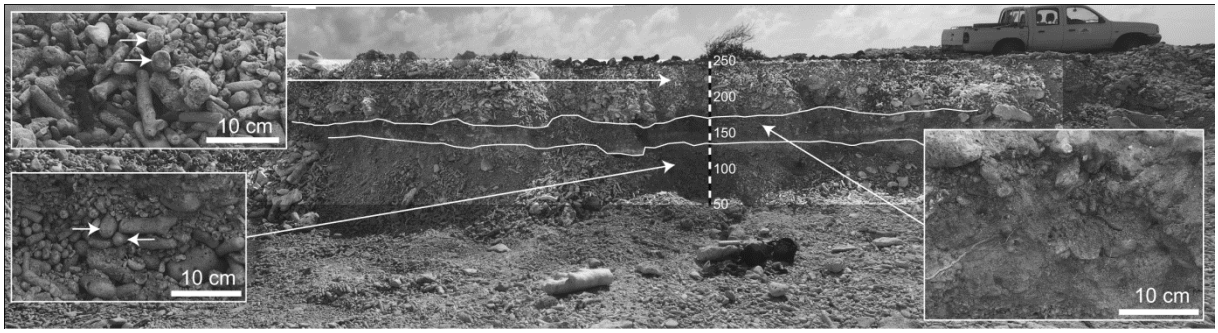

Fig. 31: Outcrop of the ridge of coral rubble near Saliña Tam (Fig. 30). Its stratigraphy is divided into three parts. On top there is a unit of well sorted angular fragments of *Acropora cervicornis* (c. 80 cm, upper left close-up foto). It is separated from the basal unit of well-sorted and well-rounded coral rubble (lower left close-up foto) by a palaeosol developed in a layer of poorly sorted carbonate sand and coral material (close-up foto on the right). The elevation is shown in cm above mean sea level.

Approximately 250 m west of Saliña Tam, the coastal barrier of coral rubble is separated from the inactive cliff of the LT by a morphological depression filled with sediment (site SAT 10). At ground level, the uppermost part of a bioerosive notch is visible. Numerous coral boulders (a-axes up to 2 m) are clustered at the landward avalanching face of the barrier (Fig. 30) (Scheffers, 2005; Morton et al., 2008).

6.2.2 Southern Klein Bonaire

Klein Bonaire is a small and flat island off the leeward coast of Bonaire, entirely consisting of MT and LT limestone. It is surrounded by ridges of sand and coral rubble (De Buisonjé, 1974). The MT and LT deposits lie significantly lower compared to their counterparts on the main island. In the southern part, the surface of the LT gently slopes towards the barrier forming an area of shallow water and backbarrier sedimentation (Fig. 32).

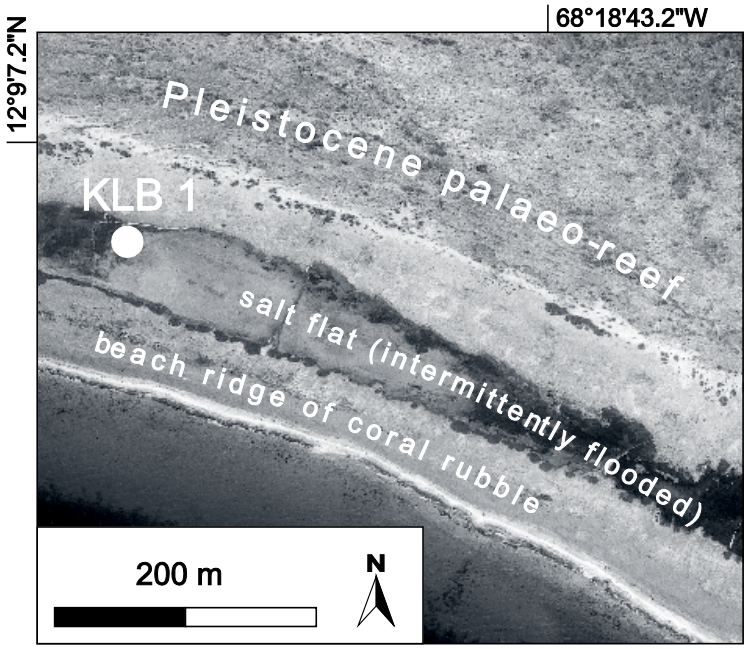

Fig. 32: Aerial view of coring site KLB 1 on southern Klein Bonaire (Fig. 29) at the back of a broad ridge of coral rubble.

6.3 Methods

In order to reconstruct sedimentation processes and palaeoenvironments at the two sites, we examined five sediment cores for their sedimentological, geochemical and faunal composition. Cores allow for sampling relatively great depths regardless of the shallow groundwater table, though they only provide one-dimensional insights into the stratigraphy and may hamper the identification of certain lateral sedimentological features indicative of tsunami or storm deposition. Four vibracores (d = 6.0 and 5.0 cm) were taken at Saliña Tam with an engine-driven Atlas Copco 248 coring device. The maximum coring depth was 11 m b.s. (below surface). Two cores were taken with open steel probes (SAT 7 and 10). These cores were cleaned, photographed, documented and sampled in the field for multi-proxy analyses. Two vibracores were preserved in closed PVC tubes, which were split in the laboratory (SAT 8 and 9). The fifth core was a 1.28-m push core (d = 7.5 cm) also split in the laboratory (KLB 1).

6.3.1 Non-destructive core analysis

The inorganic element composition of KLB 1 and SAT 8 was determined using an ITRAX X-ray fluorescence (XRF) core scanner (Cox Analytical Systems). The device was prepared with a 3 kW Mo X-ray tube set to 30 kV and 30 mA. It enables analyses of semi-quantitative variations of elements from Al to U by scanning 1 mm steps for 20 s each. Element amounts are shown as count rates (cr) representing estimates of the relative concentrations in the sediment (Croudace et al., 2006).

6.3.2 Analyses using core samples

For a sufficient amount of sediment material, each sample from the open cores (SAT 7 and 10) represents sections of 5-10 cm from significant stratigraphical units. The closed cores (SAT 8 and 9, KLB 1) were sampled selectively in 1-2 cm sections. Samples were air-dried and carefully broken up by hand with a mortar and pestle. The carbonate content of the fine-grained fraction (<2 mm) of all vibracores was gas-volumetrically measured following the Scheibler method. Loss-on-ignition (LOI) was determined by oven-drying at 105 °C for 12 h and ignition in a muffle furnace at 550 °C for 4 h (Beck et al., 1993). The wet sieve-pipette technique (Köhn, 1928) was applied for analysing the grain size distribution after pre-treatment of the aliquots with $Na_4P_2O_7$ (55.7 g/l) for aggregate dispersion. Shell material was not removed. Results were processed with GRADISTAT software (Blott and Pye, 2001). Mean grain size was calculated after Folk and Ward (1957) and grain sizes were classified after Ad-hoc-Arbeitsgruppe Boden (2005).

Selected samples were treated with H_2O_2 (3%) and fractionated by sieving (mesh sizes of 0.063 mm, 0.2 mm and 1.0 mm) for quantitative microfossil investigations. Microfaunal remains were picked from residue splits containing at least 300 specimens, if present within the sample, and were taxonomically identified using a low-power binocular microscope. High magnification light microscopy and scanning electron microscopy (SEM) supported photographic documentation and taxonomic identification (Fig. 33). Ostracods and foraminifers were identified to the species level if possible; all other fossils were identified to group level. The state of preservation of fossil groups was documented for distinguishing reworked and (par-)autochthonous specimens.

In order to identify sediment provenance areas (marine, terrestrial-autochthonous, terrestrial-allochthonous), the mineralogical spectrum of selected powder samples was investigated by means

of a Siemens 5000D X-ray diffractometer. XRD investigations were carried out using Cu Kα radiation (40 kV, 40 mA). Samples were run from 10° to 70° 2Θ. For semi-quantitative interpretation, X'Pert HighScore Plus software (PANalytical) was used, which is based on the Rietveld refinement technique by fitting a calculated XRD profile to the measured pattern and assigning abundances of minerals.

The chronostratigraphy of all sites is based on ^{14}C-AMS analyses (Table 10). Radiocarbon dates of marine shells were corrected for a regional marine reservoir effect of ΔR = -49 (Radtke et al., 2003). ^{14}C-AMS data were converted to sidereal years by means of CALIB 6.0.1 software (Reimer et al., 2009). For age interpretation the 2σ error was taken into account.

6.4 Sedimentary record of Saliña Tam

6.4.1 The back-barrier record – SAT 7/8

Sediment cores SAT 7 and SAT 8 represent the stratigraphy directly behind the broad ridge of coral rubble separating Saliña Tam from the open sea (Figs. 30 and 31). One open (SAT 7) and one closed (SAT 8) core were taken at the same site. Environmental interpretation of the cores is given on Figs. 34 and 35.

The lower 7.75 m (11.00-3.25 m b.s.) at site SAT 7/8 consist of a coquina of shell debris (light grey bivalves, mainly *Ctena orbiculata*, and gastropods, mainly *Bulla striata, Caecum* sp.), carbonate sand (on Bonaire predominantly represented by fragments of *Halimeda* sp.) and bryozoan fragments showing a high degree of abrasion. Ca and Sr concentrations are high and slightly decrease in the uppermost part. At 3.35-3.25 m b.s., the coquina contains lagoonal ostracods (*Cyprideis beaveni* [partly noded], *Cyprideis* sp., *Perissocytheridea cribrosa*; Fig. 33), small benthic foraminifers (miliolinids), and remains of small fish and echinoderms.

The overlying deposit of very dark brown sandy silt (3.25-2.82 m b.s.) shows an abrupt decrease in $CaCO_3$ and increasing LOI values. From 3.00-2.82 m b.s., the unit is stratified and contains thin layers of calcite, aragonite and gypsum. Concentrations of K, Ti and Br increase. *Cyprideis beaveni* (partly noded), *Cyprideis* sp., *Perissocytheridea cribrosa* and miliolinid foraminifers are still present. Mollusc shells, bryozoan and echinoderm remains are absent.

Between 2.82-2.60 m b.s., there are ten graded sequences with a thickness of 1-6 cm (Fig. 35). The lower boundary of each bed is sharp. The bottom parts of the sequences contain partly fragmented shells of *Cerithium* sp. and coarse carbonate sand. The upper parts consist of silty mud containing rafted plant material. Most of the graded sequences start with a sudden increase in Ca, which gradually decreases upwards (Fig. 35). Peaks of Br correlate with the upper parts of the graded beds and identify high concentration of organic matter (Chagué-Goff et al., 2002; Pérez et al., 2010a). Similar to the underlying unit, bulk samples of the entire unit contain high amounts of brackish foraminifers and ostracods, but also scattered fragments of corals, mollusc shells, bryozoans and echinoderms. It is noteworthy that only the lowermost sequence contains planktonic foraminifers and high abundances of reworked ostracods (thick carbonate encrustations). A shell of *Cerithium* sp. (2.72 m b.s., bed EWE V) was radiocarbon dated to 3039-2857 cal BP.

The overlying unit (2.60-2.38 m b.s.) is pale white and almost entirely consists of $CaCO_3$. Four sequences – three normally graded beds containing shells of *Cerithium* sp. and coarse sand at the bottom, and one inversely graded bed (Fig. 35) – were identified. A very thin mud drape covers the

second graded sequence. The section contains reworked valves of brackish ostracods as well as miliolinid foraminifers, *Amphistegina*, *Discorbis,* Alcyonaria and fragments of Malacostraca, Scleractinia and several other marine forms. Planktonic foraminifers (*Globigerinoides* cf. *immaturus*) were also found (Figs. 33 and 34). Aragonite is the dominating mineral. The amount of quartz is very low. From the lower part of this unit (in SAT 7) as well as from 2.43 m b.s. (in SAT 8) cerith shells were radiocarbon dated to 2607-2462 and 2021-1869 cal BP (Table 10, Figs. 34 and 35).

Between 2.38 and 2.30 m b.s. are three fining-up sequences, with distinct lower contacts consisting of a very thin basal layer of carbonate sand and a thicker muddy, organic-rich part. The spectrum of microfossils covers *Cyprideis* sp. and *P. cribrosa*, and some tests of miliolinid foraminifers and *Amphistegina*. The amount of marine biogenic particles is significantly reduced compared to the underlying graded beds.

The overlying units represent the background sedimentation: Ca and Sr are lower than previously, whereas LOI, Ti, Br and K values are higher. The most abundant mineral is quartz. Several plant remains (leaf fragments, wood) and angular stones were found. A thin unit of alternating silt layers of carbonate and gypsum occurs between 2.30 and 2.26 m b.s. From 1.00-0.76 m b.s., $CaCO_3$ values and mean grain size are higher than background and the sediment is more poorly sorted.

6.4.2 The landward alluvial plain – SAT 9

SAT 9 is located c. 800 m from the shoreline, on the alluvial plain north of the boka (Fig. 30). The area is seasonally flooded by the intermittent river. Proxy data and core interpretation are shown in Fig. 36.

From the base, 5.00 m, to 3.49 m b.s., there is a unit of black peat with high LOI and low $CaCO_3$ concentrations as well as a large number of juvenile smooth bivalves and several specimens of miliolinid foraminifers and *Ammonia* spp. (Fig. 33). Plant fragments from 3.60 and 3.55 m b.s. were dated by ^{14}C-AMS to 4826-4584 and 4568-4424 cal BP.

The peat is overlain by half a meter of light olive brown carbonate mud with an erosive basal contact (3.49-2.94 m b.s.) and numerous gypsum minerals. Carbonate content reaches up to 60%. Angular stones and well-preserved cerith shells are present in the matrix. *C. beaveni* (partly noded) and *P. cribrosa* as well as several miliolinid foraminifers compose the microfauna. Juvenile smooth bivalves are rare. No shell material indicating open marine or reefal origin was identified.

From 2.94 to 2.77 m b.s., the sediment consists of thin alternating beds of carbonate sand (light brown) and grey layers of silty clay, both containing gypsum and halite minerals. While sand layers are linked to small peaks in $CaCO_3$, silty clay layers coincide with peaks in LOI. *C. beaveni* (partly noded), *Cyprideis* sp. as well as miliolinid foraminifers are abundant, whereas *P. cribrosa* is rare. Several ostracods show signs of reworking.

The overlying unit (2.77-1.74 m b.s.) consists of olive grey sandy silt showing an upward decrease in $CaCO_3$. At 1.74-1.65 m b.s., there are three layers of coarse gypsum minerals. Above them, the uppermost unit of SAT 9 consists of very dark grey clayey silt with several reddish dark brown sections. The ostracod fauna is brackish, noded *C. beaveni* decrease. A minor peak in $CaCO_3$ occurs at 1.00-0.90 m b.s.

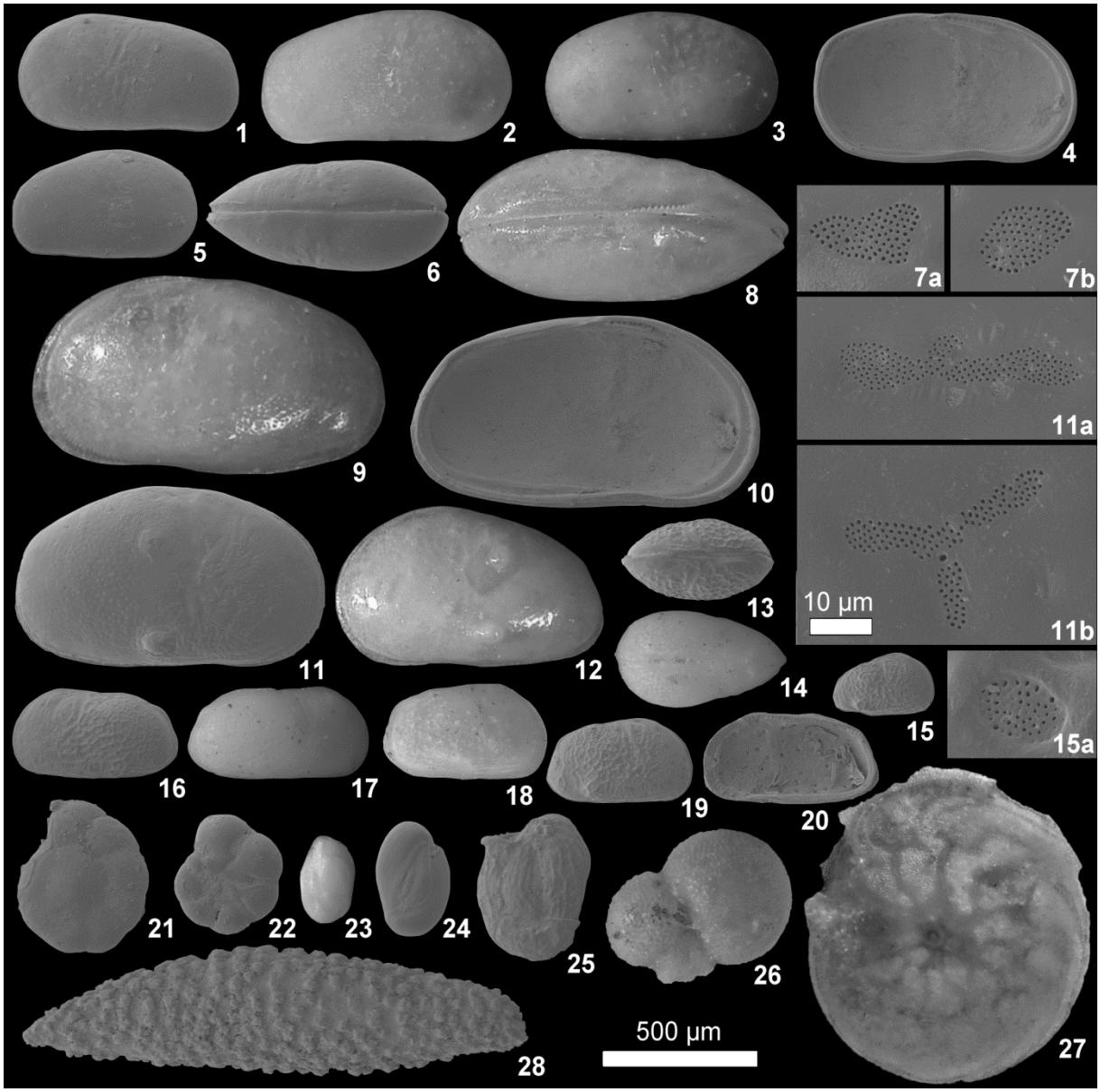

Fig. 33: Characteristic microfossils from Saliña Tam and Klein Bonaire: 1)-20) Ostracoda, 21)-27) Foraminifera, 28) Octocorallia. 1)-7) *Cyprideis* sp.: 1) left side of a male carapace, SAT 9 (2.61-2.50 m b.s.); 2) right side of a male carapace, SAT 8 (2.51-2.43 m b.s.); 3) right side of a female carapace, SAT 8 (1.75-1.65 m b.s.); 4) interior of a female left valve, SAT 9 (2.61-2.50 m b.s.); 5) juvenile right valve, SAT 9 (2.61-2.50 m b.s.); 6) dorsal view of a female carapace, SAT 9 (2.61-2.50 m b.s.); 7) sieve pores of a female left valve, SAT 9 (2.61-2.50 m b.s.). 8)-12) *Cyprideis beaveni* (Tressler and Smith 1948): 8) dorsal view of a female carapace, SAT 8 (2.43-2-2.38 m b.s.); 9) male left valve, SAT 8 (2.18-2.12 m b.s.); 10) interior view of a male left valve, SAT 9 (2.61-2.50 m b.s.); 11) noded female right valve and two sieve pores, SAT 9 (2.61-2.50 m b.s.); 12) noded juvenile left valve, SAT 8 (2.57-2.51 m b.s.). 13)-20) *Perissocythere cribrosa* (Klie 1933): 13) dorsal view of a female carapace, SAT 8 (3.00-2.90 m b.s.); 14) dorsal view of a male carapace, SAT 8 (3.05-2.95 m b.s.); 15) right side of a juvenile valve and a sieve pore, SAT 8 (2.86-2.81 m b.s.); 16) left side of a male carapace, SAT 8 (3.25-3.20 m b.s.); 17) right side of a male carapace, SAT 8 (3.05-2.95 m b.s.); 18) right side of a female carapace, SAT 8 (2.09-2.00 m b.s.); 19) female right valve, SAT 8 (3.25-3.20 m b.s.); 20) internal view of a male right valve, SAT 8 (3.00-2.90 m b.s.). 21)-22) *Ammonia tepida*? (Cushman 1926): 21) spiral view, last chamber missing, KLB 1 (0.69-0.68 m b.s.); 22) umbilical view, KLB 1 (0.69-0.68 m b.s.). 23-25) Miliolinids, lateral views: 23) *Quinqueloculina seminula* (Linnaeus 1758), SAT 8 (2.29-2.25 m b.s.); 24) *Miliolinella* sp. I, SAT 8 (2.80-2.73 m b.s.); 25) *Miliolinella* sp. II, KLB 1 (0.58-0.57 m b.s.). 26) *Globigerinoides* cf. *immaturus* (Leroy 1939), SAT 8 (2.59-2.40 m b.s.). 27) *Amphistegina* sp., SAT 8 (2.59-2.40 m b.s.). 28) Sclerite of an alcyonarian coral, SAT 8 (3.25-3.20 m b.s.). Photos 2, 3, 8, 9, 12, 14, 17, 18, 23, 26, and 27 are light microscope photos, all others are scanning electron microscope (SEM) pictures (photographs: P. Frenzel).

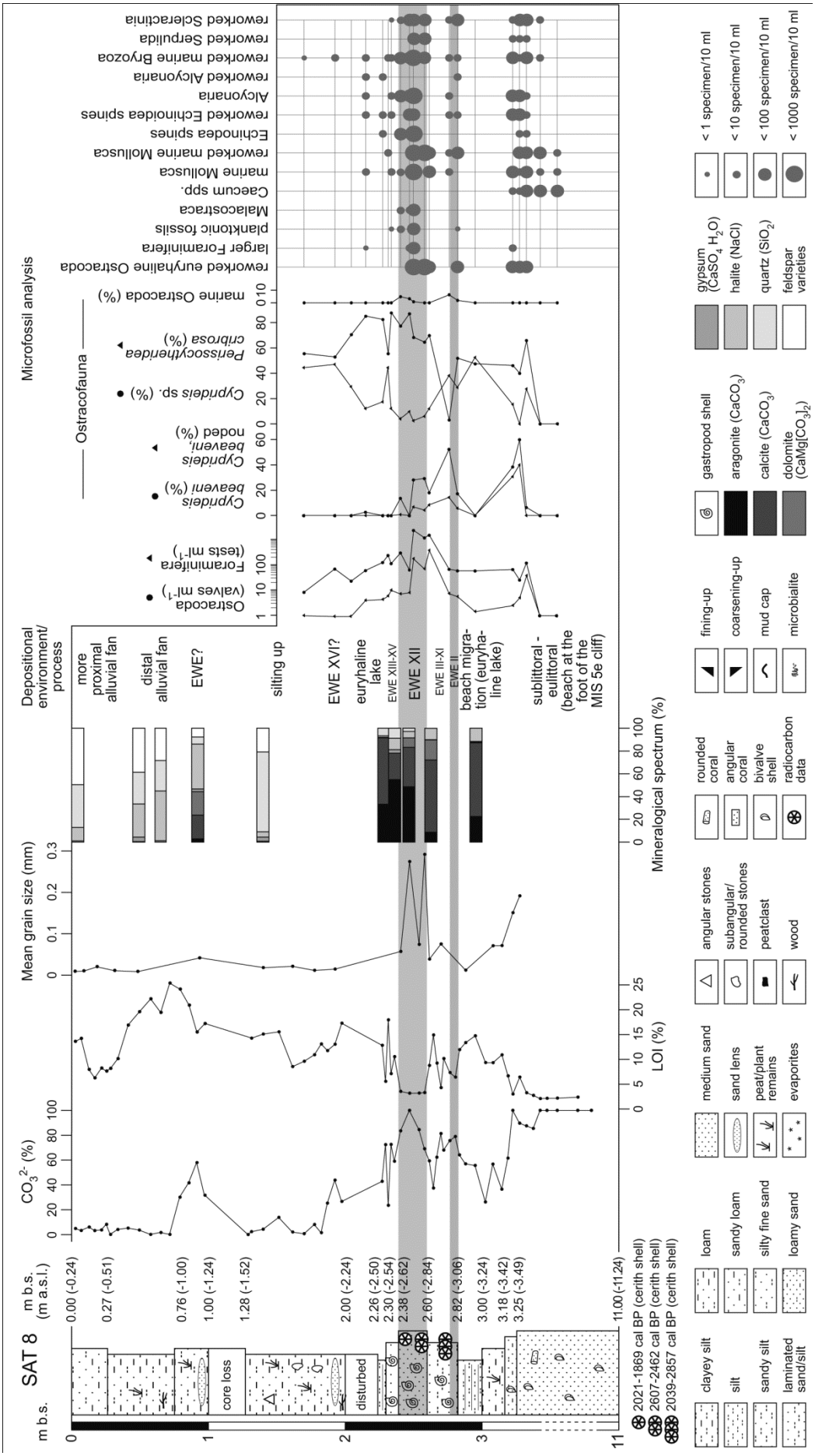
SAT 8
m b.s.
m b.s. (m a.s.l.)
0.00 (-0.24)
0.27 (-0.51)
0.76 (-1.00)
1.00 (-1.24)
1.28 (-1.52)
2.00 (-2.24)
2.26 (-2.50)
2.30 (-2.54)
2.38 (-2.62)
2.60 (-2.84)
2.82 (-3.06)
3.00 (-3.24)
3.18 (-3.42)
3.25 (-3.49)
11.00 (-11.24)
core loss
disturbed
CO_3^{2-} (%)
Mean grain size (mm)
LOI (%)
Mineralogical spectrum (%)
Depositional environment/ process
more proximal alluvial fan
distal alluvial fan
EWE?
silting up
EWE XVI?
euryhaline lake
EWE XIII-XV
EWE XII
EWE III-XI
EWE II
beach migration (euryhaline lake)
sublittoral - eulittoral (beach at the foot of the MIS 5e cliff)
Microfossil analysis
Ostracofauna
Ostracoda (valves ml^{-1})
Foraminifera (tests ml^{-1})
Cyprideis beaveni (%)
Cyprideis beaveni, noded (%)
Cyprideis sp. (%)
Perissocytheridea crbrosa (%)
marine Ostracoda (%)
reworked euryhaline Ostracoda
larger Foraminifera
planktonic fossils
Malacostraca
Caecum spp.
marine Mollusca
reworked marine Mollusca
Echinodea spines
reworked Echinoidea spines
Alcyonaria
reworked Alcyonaria
reworked marine Bryozoa
reworked Serpulida
reworked Scleractinia
2021-1869 cal BP (cerith shell)
2607-2462 cal BP (cerith shell)
2039-2857 cal BP (cerith shell)
clayey silt
silt
sandy silt
laminated sand/silt
loam
sandy loam
silty fine sand
loamy sand
medium sand
sand lens
peat/plant remains
evaporites
angular stones
subangular/ rounded stones
peatclast
wood
rounded coral
angular coral
bivalve shell
radiocarbon data
fining-up
coarsening-up
mud cap
microbialite
gastropod shell
aragonite ($CaCO_3$)
calcite ($CaCO_3$)
dolomite ($CaMg[CO_3]_2$)
gypsum ($CaSO_4 \cdot H_2O$)
halite (NaCl)
quartz (SiO_2)
feldspar varieties
< 1 specimen/10 ml
< 10 specimen/10 ml
< 100 specimen/10 ml
< 1000 specimen/10 ml

Fig. 34: Sediment core SAT 8 (= SAT 7; location on Fig. 30) from the seaward margin of Saliña Tam with data on carbonate content, LOI, mean grain size, mineralogy, chronology (^{14}C data in cal BP) and microfaunal remains, as well as interpretation of depositional environments and processes. Width of the core log positively correlates with mean grain size. The core section of 2.86.-2.28 m b.s. is presented in detail in Fig. 35. EWE = extreme wave event.

6.4.3 Between Saliña Tam and Punt'i Wekua – SAT 10

SAT 10 (Fig. 37) is located on a narrow alluvial plain between the ridge of coral rubble and the LT cliff (Fig. 30). At ground level, this cliff is cut horizontally by a sea level-related bioerosive notch (c. 0.00-0.20 m a.s.l.). The core reached only 2.45 m due to a thick layer of coral rubble underneath (mainly *Acropora cervicornis*).

The coral rubble is overlain by a unit of very dark brown mangrove peat (2.17-0.52 m b.s) dated to 2295-2004 cal BC at 2.10 m b.s. An erosional boundary separates the peat from a carbonate sand layer (0.52-0.40 m b.s., layer A in Fig. 37) containing reworked peat remains, shell debris and two 4 cm-fragments of *Diploria* sp. (1563-1395 cal BP). In a trench at the site (photo inset in Fig. 37), even coarser coral shingle and beachrock slabs containing branches of *A. cervicornis* were present in this layer. At 0.40-0.30 m b.s. (layer B in Fig. 37) the sediment consists of poorly sorted, grey silty sand with shell debris. The overlying strata consist of dark grayish brown (0.30-0.17 m b.s.) to dark yellowish brown (0.17-0.00 m b.s.) silty matrix with reduced carbonate sand components (layers C and D in Fig. 37).

Table 10: ^{14}C-AMS dates for samples from Saliña Tam and Klein Bonaire were carried out at the radiocarbon laboratory of the University of Georgia at Athens (USA).

Sample	Depth (cm b.s.)	Lab ID UGAMS#	Material	δ^{13}C (‰)	^{14}C age	Age cal BP (2σ)
SAT 7/11	273*	3212	gastropod	-3.74	2740±25	2607-2462
SAT 8/7	243	5996	gastropod	0.3	2280±20	2021-1869
SAT 8/28	272	7577	gastropod	-2.8	3110±20	3039-2857
SAT 9/1	355	5999	peat	-24.4	4030±25	4568-4424
SAT 9/2	360	6000	peat	-26.4	4160±25	4826-4584
SAT 9/a	325	7578	gastropod	-3.8	3360±25	3359-3206
SAT 10/4 Ko	50	7579	coral	-3.0	1890±25	1563-1395
SAT 10/10	210	7580	peat	-26.9	2080±25	2295-2004
KLB 1/a 43	43	7588	gastropod	-4.1	3240±25	3236-3028
KLB 1/c 70	70	7589	gastropod	-5.3	3570±30	3614-3426

*Depth information is as recorded in core SAT 7. However, the sediment layer lies approx. 15 cm deeper compared to parallel core SAT 8, most likely due to compaction differences between open and closed coring techniques.

6.4.4 The sedimentary record of southern Klein Bonaire – KLB 1

Core KLB 1 (Fig. 38) was recovered behind the coastal barrier of southern Klein Bonaire (Fig. 32), less than a 100 m from the swash zone. The site is a shallow pond characterized by algae mats, mud sedimentation, and carbonate precipitation.

The basal part (1.28-1.20 m b.s.) consists of light olive gray sandy silt containing several gastropod shells, a lens of root material, and a brackish-marine foraminifer assemblage dominated by miliolinid foraminifers and *Ammonia* spp. (both genera highly abundant), marine mollusc shells, and only few ostracods. Between 1.20 and 0.70 m b.s. is a layer of pure mangrove peat void of Ca and Sr and exhibiting a high plateau in the Br curve. The peat is unconformably overlain by two thin graded beds

(0.70-0.67 cm b.s.; 0.67-0.66 cm b.s.), both characterized by basal carbonate sand with well-preserved gastropod shells and shell fragments, an upward decrease in Ca, a Br peak in the upper part corresponding to a mud cap (Chagué-Goff et al., 2002; Pérez et al., 2010a) and a large number of reworked brackish ostracods. The amount of aragonite is more than 60%. Radiocarbon dating of a cerith shell (0.70 m b.s.) yielded an age of 3614-3426 cal BP. The thin sand beds are overlain by a well sorted layer of light yellowish brown sandy silt (0.66-0.64 m b.s.) rich in Ca and Sr. Aragonite is significantly reduced in favour of calcite. A thin layer of mangrove peat resembling the lower peat is present at 0.64-0.60 m b.s. A sharp upper boundary separates it from a massive layer of loamy carbonate sand (0.60-0.35 m b.s.), which is divided into three subunits:

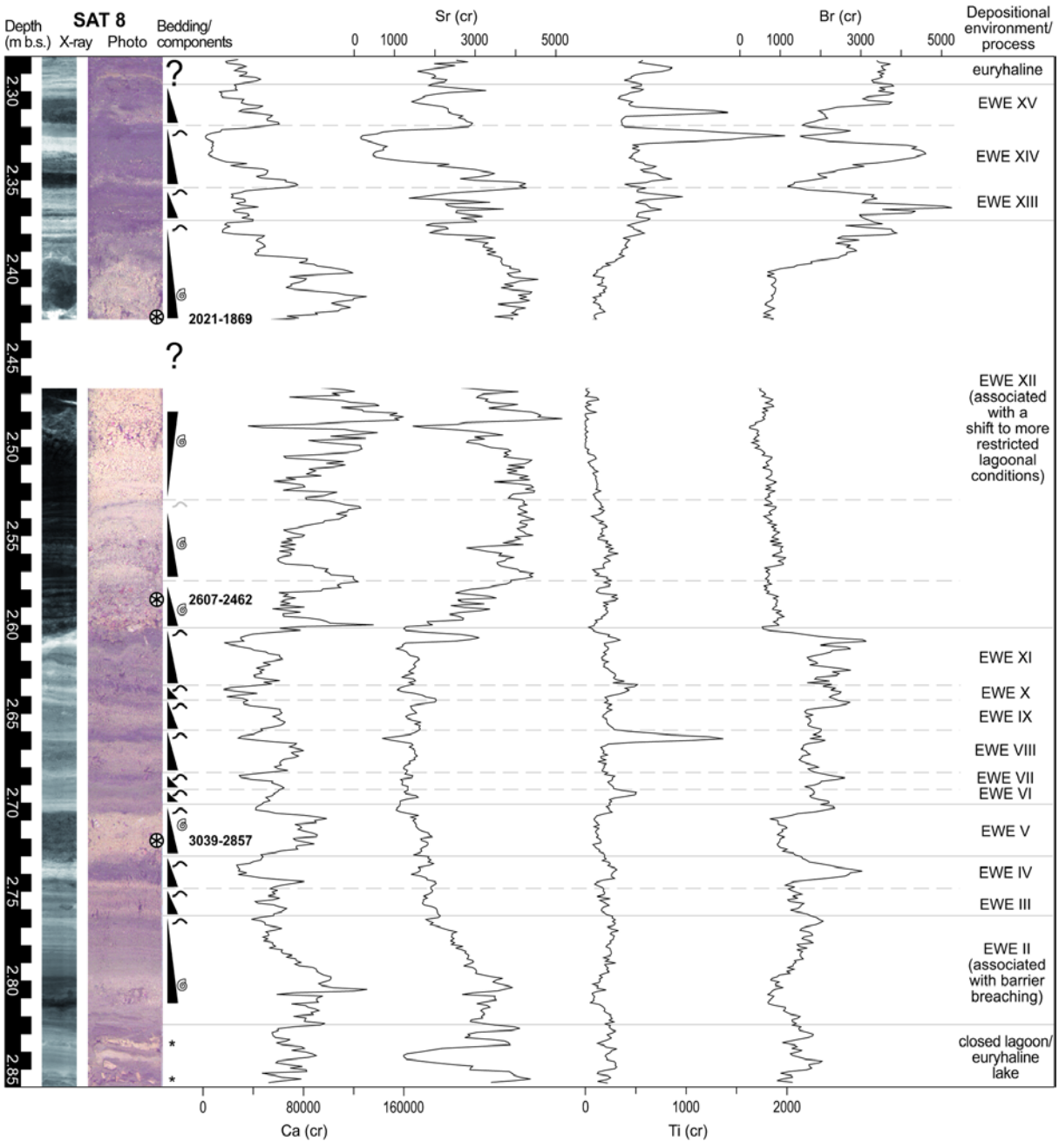

Fig. 35: X-ray, photograph, and high-resolution XRF data (Ca, Sr, Ti, Br; cr = XRF count rates) of core section 2.86.-2.28 m b.s. from SAT 8 (Figs. 30 and 34), labelled with basic interpretation of depositional environments and processes. ^{14}C data are displayed as cal BP. A key to symbols is on Fig. 34. EWE = extreme wave event.

(i) a lowermost normally graded sequence with shells and shell fragments (0.60-0.50 m b.s.);

(ii) a coarsening-up sequence (0.50-0.43 m b.s.) associated with increasing values of Ca and Sr, a large peat clast, most likely from the underlying peat, and shells of *Cerithium* sp. in the upper part;

(iii) a normally graded bed (0.43-0.35 m b.s.) with basal shell material and another large peat clast.

The overlying stratum (0.35-0.15 m b.s.) also has a normally graded bed and contains *Cerithium* sp. shells. At 0.14-0.02 m b.s. is a pale yellow, silty fine sand consisting of calcite, dolomite, gypsum and halite with no larger components. The surface is composed of a very dark brown aragonite-rich crust.

6.5 Discussion

Interpretation of these cores is based on the assumption that sedimentary patterns are predominantly determined by relative sea level evolution (*Chapter 8*), intermittent river input, typical yearly wave action as well as hurricanes and tsunamis. The frequency of strong hurricanes is considered as periodic (in the order of 10-500 years), the one of major tsunamis as episodic (in the order of 500-5000 years). Both are summarized under the term extreme wave event (EWE). Even though long-term fluctuations in temperature and precipitation were considered to be very important in other palaeo-environmental investigations along Caribbean shorelines (e.g. Bertran et al., 2004), they appear rather negligible in this study, at least concerning the prehistoric core sections. Evaporation rates throughout the time of deposition seem to have been consistently high, often resulting in stressful ecological conditions, reflected by the low diversity of the *in-situ* ostracofauna (cf. Frenzel and Boomer, 2005). Increased sedimentation rates in the last millenium on Bonaire (Engel et al., 2010) may be the result of a combination of anthropogenic impact on the vegetation – e.g. livestock breeding since the 16th century AD (Hartog, 1978) – and a regional aridification impulse (Haug et al., 2003).

Chapter 6.5.1 provides a chronology of coastal evolution and EWEs based on core data. It is separated into evidence from Klein Bonaire (KLB) and Saliña Tam (SAT). The nature of EWEs (tsunami or tropical cyclone) is discussed in *Chapter 6.5.2*, a synopsis of the cores is shown in Fig. 39.

6.5.1 High energy wave impacts and shoreline change

6.5.1.1 Klein Bonaire (KLB)

In the south of Klein Bonaire, the lowermost calcareous deposit (pre-3.6 ka BP) is associated with a calm lagoon connected to the open ocean according to the presence of a large number of shallow marine to brackish foraminifers (*Quinqueloculina* spp., *Ammonia* spp.) and ostracods (*C. beaveni*) (e.g. Culver, 1990). Several well-rounded shell fragments point to temporarily intensified energetic conditions. Thus, the mangrove peat overlying this carbonate mud may be interpreted as a regressive process where prograding mangroves colonised marginal marine sediments, similar to findings made by Woodroffe (1981) on North Sound, Grand Cayman.

At around 3.6 ka BP or later (cerith shell: 3614-3426 cal BP) a high-energy wave event (which we label EWE I) possibly destroyed the mangroves, as indicated by an erosional unconformity and two thin fining-up sequences, each capped by rafted plant fibres from the underlying peat. Ostracod

valves from the beds indicate reworking. The event significantly contributed to the formation of a barrier of coral rubble fringing the entire coast of southern Klein Bonaire and which limited access to the open ocean. This is inferred from the subsequent layer of carbonate mud resembling recent deposition at KLB 1. High amounts of dolomite (>25%) within this lithofacies result from increasing Mg/Ca ratios due to evaporation of the supratidal sea water and withdrawal of Ca due to gypsum precipitation and secondary replacement of pre-existing $CaCO_3$ (Deffeyes et al., 1965; Klosowska et al., 2004).

Subsequently, mangroves began to recolonize the site. The mangrove stands, which reestablished at KLB 1 after EWE I were irreversibly destroyed by a major wave impact (EWE II) overtopping the barrier. EWE II left a deposit, which unconformably overlies the mangrove peat. It is divided into three beds of marine sediment and contains large reworked clasts of the underlying peat causing excursions in the Br curve (Fig. 38). EWE II struck the coastline of Klein Bonaire 3.2-3.0 ka BP or later (cerith shell: 3236-3028 cal BP).

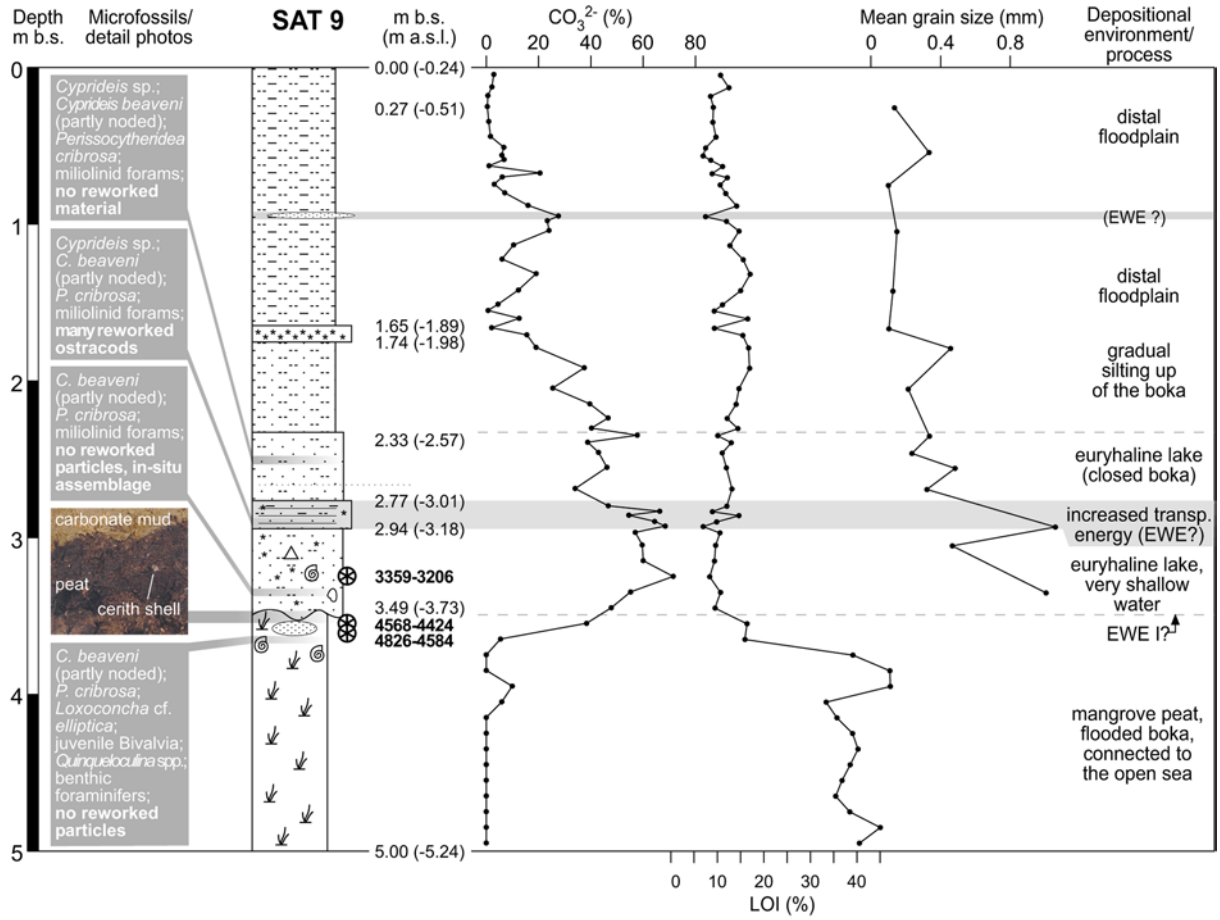

Fig. 36: Sediment core SAT 9 (located on Fig. 30) from the landward margin of Saliña Tam with data on carbonate content, LOI, mean grain size, microfaunal remains and chronology (^{14}C data in cal BP), as well as interpretation of depositional environments and processes. Width of the core log positively correlates with mean grain size. A key is provided in Fig. 34. EWE = extreme wave event.

6.5.1.2 Saliña Tam (SAT)

The deepest and oldest sediment unit reached at Saliña Tam is between 11.00 and 3.25 m b.s. right behind the barrier of coral rubble (SAT 7/8). High amounts of Ca and Sr, well rounded carbonate particles and shell debris as well as its extraordinary thickness relate to a sublittoral environment or –

regarding the upper part of the unit – to the beach ridge of a shoreline, which ran landward in a sheltered position right at the foot of the MIS 5e cliff (Mid-Holocene transgression in Fig. 30). Since long-term littoral sedimentation is connected to the sea level, an age of c. 8 ka for the base of core SAT 8 may be inferred from the model of southern Caribbean sea level evolution by Milne et al. (2005). The Early to Mid-Holocene transgression is assumed to have flooded the near-shore parts of the island's drainage network creating bokas with full sea access and a landward fringe of mangroves comparable with the present inlet of Lagun, east Bonaire (cf. Engel et al., 2010b). Mangroves established when relative sea level rise decelerated c. 7-6 ka ago (*Chapter 8*; Milne et al., 2005; McKee et al., 2007) and compensation through subsurface accumulation of resistant roots and rhizomes was possible (Woodroffe 1981; McKee et al., 2007). The mangrove populations at Saliña Tam were probably dominated by *Rhizophora mangle* according to Mid-Holocene pollen spectra (*Chapter 5*; Engel et al., 2009) and recent mangrove stands (De Freitas et al., 2005) from the east coast of Bonaire. Small but stable mangrove populations persisting at Saliña Tam until at least 4.5 ka BP are represented by thick fibrous peat accumulations in the landward core SAT 9 (5.00-3.49 m b.s.). Their microfaunal assemblage of brackish ostracods and foraminifers, both of which show relatively high abundance and diversity, as well as numerous juvenile bivalves, reflect low-energy environmental conditions of a distal lagoon connected to the open sea.

Isolation of the boka some time before 3000 BP is reflected by thin alternating layers of organic rich sediment, platy aragonite and gypsum, which cover the littoral lithofacies in SAT 8 (Fig. 34). The evaporites relate to autochthonous sedimentation and a negative water balance due to limited water input either from the sea or inland in combination with high evaporation as also observed on Curaçao (Klosowska et al., 2004). Mg, Na, Cl and Ca ions indicate high evaporation rates and isolation from the sea similar to recent conditions, but also continuous sea water supply through the permeable seaward barrier. Depending on fluctuating concentrations of soluble salts, different evaporite types precipitated forming the cyclic laminated depositional pattern. Surface runoff at that time was reduced since the amount of detrital material from the volcanic catchment area (quartz, plagioclase) is very low (SAT 8, 3.00-2.82 m b.s.). Euryhaline to polyhaline conditions are supported by the sole presence of *Cyprideis* sp. and *Perissocytheridea cribrosa* within the ostracofauna (Keyser, 1977b).

No sedimentary evidence for an abrupt closure of the boka during an episodic wave event was found at SAT 8. It seems likely that the barrier was formed gradually due to the low rate of sea level rise (*Chapter 8*; Milne et al., 2005), a moderate longshore current from south to northwest (Zonneveld et al., 1977) and the effects of periodic tropical cyclones, which are capable of moving coral rubble onshore (Schubert and Valastro, 1976; Scheffers and Scheffers, 2006; Spiske and Jaffe, 2009). The stratigraphy of the lower part of the barrier (Fig. 30, 31) also supports a gradual closure of Saliña Tam due to the very well rounded particles in its entire lower part (pre-1300 BP according to Scheffers et al., 2009a) resembling the degree of roundness of *A. cervicornis* fragments at the present beach face. They differ significantly from the angular coral rubble, which builds up the uppermost part of the barrier (Fig. 31) and was removed and transported onshore by a major hurricane (EWE XVI or later?) according to Scheffers (2005) and Scheffers et al. (2009a). For the period when Saliña Tam closed (c. 3.5-3.4 ka BP), a gradual barrier formation was also reconstructed for the St. Michiel lagoon at leeward Curaçao, which shares similar morphodynamic boundary conditions (Klosowska et al., 2004). However, the isolation of Saliña Tam is in the same time window as EWE I (inferred from the core at Klein Bonaire) which may have accumulated coral material at the outlet of the boka as well.

Isolation of the small basin of Saliña Tam resulted in a demise of the mangrove population in the landward part of Saliña Tam (SAT 9), which strongly depends on the circulation of sea water. The deposition of autochthonous carbonate mud at SAT 9 started before 3359-3206 cal BP and correlates with the evaporite facies in SAT 8 (3.00-2.82 m b.s., pre-3039-2857 cal BP). The carbonate mud in SAT 9 is not related to an EWE since it is very homogeneous and marine sand, faunal remains or reworked material of the underlying peat are absent. However, the erosional unconformity might be induced by purely erosional processes during EWE I – the relevance of which has been demonstrated by MacInnes et al. (2009a) on the Kurils, northeastern Pacific. The abundant valves of noded *Cyprideis beaveni* (75%) and *Perissocytheridea cribrosa* as well as several miliolinid foraminifers within the carbonate mud indicate euryhaline to polyhaline still water conditions (Keyser, 1977b) and show no signs of reworking.

We interpret the basal part of the coarse shell-rich sequence in SAT 8 (2.82-2.76) to be a deposit of EWE II (cf. KLB 1, *Chapter 6.5.1.1*); the age control (minimum age) is from an overlying bed (2.72 m b.s.) of 3039-2857 cal BP. This basal unit is a fining-up sequence, which has a partly marine micro-fauna, an upward decrease in Ca and Sr and is capped by organic-rich mud. The mud layer, marked by a small Br peak (Fig. 34), we interpret to have been deposited after flow attenuation.

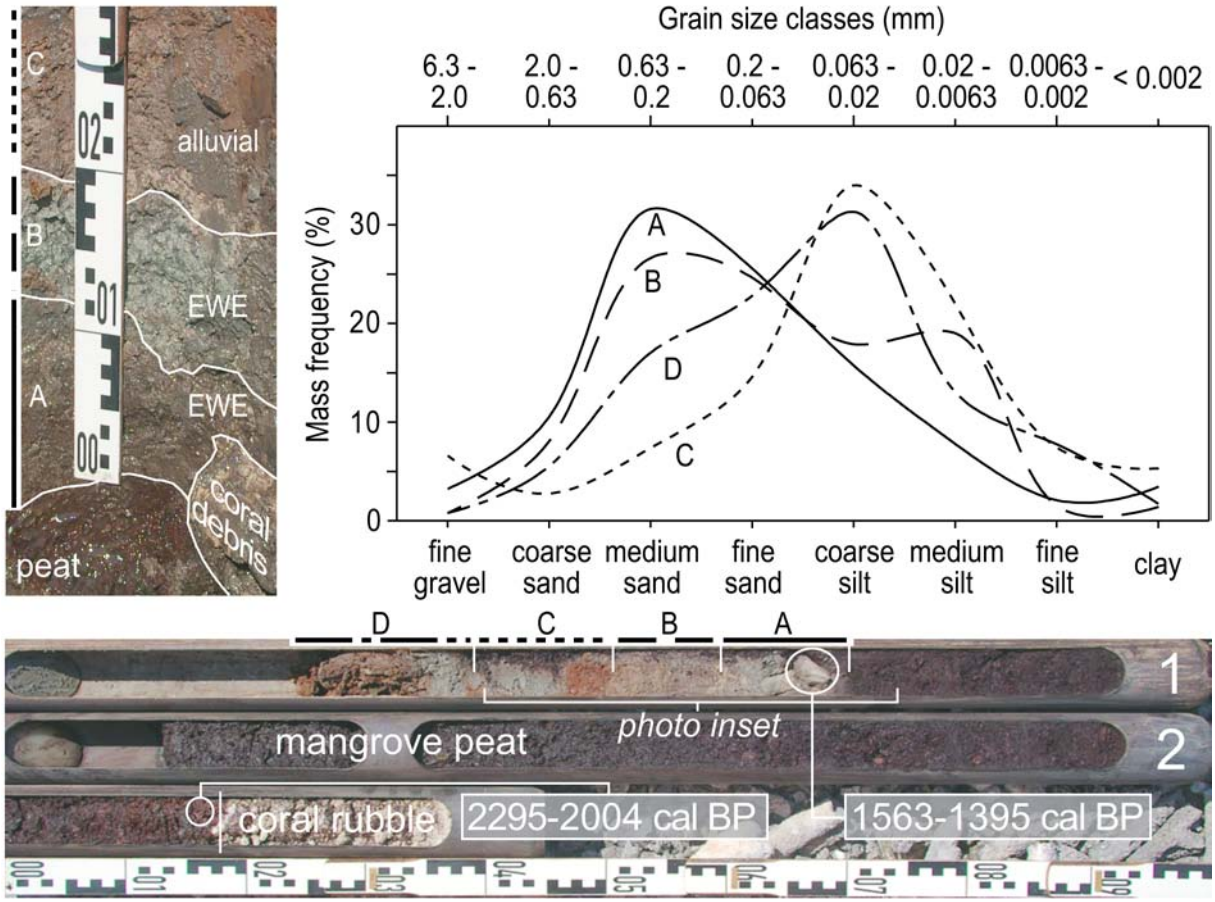

Fig. 37: Sediment core SAT 10 (2.45 m) west of Saliña Tam (Fig. 30) with ^{14}C data and grain size distribution of the upper four clastic sediment units. Grain size samples represent the centre of each layer A-D. Each line style indicates a particular grain size distribution of one of the four carbonate sand/mud units (A-D) in the core. Correlating line styles of the core units are displayed on top of the core photo. The photo inset at the top left shows a profile within a trench at the same site, displaying the uppermost part of the peat and three of the overlying carbonate sand/mud units (A-C) as indicated on the core photo as well as a massive coral branch. Correlating line styles are plotted on the left. EWE = extreme wave event.

We also interpret the following nine sequences (2.76-2.60 m b.s. in Fig. 35) as deposits of overwash events (EWE III-XI) affecting the interior of Saliña Tam due to the partial destruction of the barrier during EWE II. Within the entire section EWE III-XI, increased marine influence is reflected by abraded sand-sized shell particles. Each of the nine depositional cycles comprises basal sand with increasing phytomass and mud content upward. Accordingly, nine significant overwash events may be inferred between c. 3.0 ka BP and the overlying age 2.0-1.8 ka BP based on radiocarbon dates of cerith shells (Table 10, Fig. 34).

The depositional sequence containing a radiocarbon age of 2021-1869 cal BP unconformably overlies the EWE III-XI unit and consists of a wide variety of marine microfossils (benthonic and planktonic) indicating that it was generated by an EWE (which we label XII) of stronger traction force at the shelf bottom than EWE III-XI.

After EWE XII, three minor overwash deposits separated by relatively thick mud sections (EWE XIII-XV) indicate a lower frequency of major tropical cyclones) compared to the phase of EWE III-XI.

Above the EWE sequences associated with a partial destruction of the barrier and a higher susceptibility to overwash deposition, still-water conditions very similar to the period before EWE II (pre-3.2-3.0 ka BP) indicate that the barrier closing the boka recovered. We assume that reshaping the barrier represents development towards an equilibrium defined as “stability of form” (Woodroffe, 2002: p. 32) after disturbances (EWE II-XII) manifested by cyclic carbonate sequences spanning a period of c. 1 ka. This is a long time given the fact that beaches of Sumatra and Thailand have reorganised only a few years after the Indian Ocean Tsunami of 2004 (IOT) (Choowong et al., 2009; Liew et al., 2010). Nevertheless, Kraus (2005: p. 171) describes barrier breachings, which did “not recover on the time-scale of human lifetime” in case the event was so strong that the sediment was transported into deeper water – consider the narrow reef and steep offshore slope of Bonaire! – where it was out of reach for long-term wave action. Temporary changes in external boundary conditions, e.g. an interruption of the longshore current, increased hurricane frequency, and, most importantly, limited sediment sources, also have to be taken into consideration. In addition to the coring results, the re-establishment of the barrier after 2.0 ka BP is corroborated by ESR ages from the Saliña Tam barrier, all of which are younger than 1.3 ka (Scheffers, 2005).

The period of increased susceptibility to overwash impact at Saliña Tam (EWE III-XI) or EWE II both inferred from SAT 8, might correlate with layer 2.94-2.77 m b.s. in SAT 9 where reworked ostracods were identified; however, this is a tenuous assumption since age control is not available. Apart from that, SAT 9 has no clear event deposits.

West of Saliña Tam, at SAT 10, a mangrove population established around 2.0 ka BP. Below the mangrove peat, the coral rubble from the basal core unit is interpreted to derive from a major EWE (II or XII?). After the event, the area was sheltered by the coastal barrier but still had access to the sea providing a suitable habitat for mangroves. The demise of the mangroves is associated with the two overlying units of medium sand (layers A and B in Fig. 37), which most probably represent one or two EWE. The age of a coral boulder found at the landward foot of the broad ridge of coral rubble adjacent to SAT 10 was dated to 1300±60 (Fig. 30; Scheffers, 2005). Since a *Diploria* sp. fragment from the sand layer yielded a similar age (1563-1395 cal BP), boulder transport and deposition of the sand layers may be linked to one EWE (which we label XVI). The overlying silt-dominated alluvial lithofacies (C and D in Fig. 37) contains several carbonate sand components testifying to periodic small overwash processes.

The upper sediment column of SAT 8 (2.00-0.00 m b.s.) and SAT 9 (2.78-0.00 m b.s.) is dominated by detrital sedimentation as indicated by increased amounts of quartz, anorthite and albite (feldspar varieties) in the mineralogical spectrum. Mean grain size is small reflecting the interface between the fluctuating still water body and distal alluvial fans (inferred from changing LOI percentages). At SAT 8, two candidate overwash deposits occur at 1.96-1.87 m b.s., where several bryozoan fragments are preserved, and at 0.97-0.77 m b.s. (EWE XVI?). The upper one might correlate with a peak in $CaCO_3$ at SAT 9 (1.00-0.90 m b.s.). However, both layers are heavily altered by capillary evaporites from interstitial pore waters.

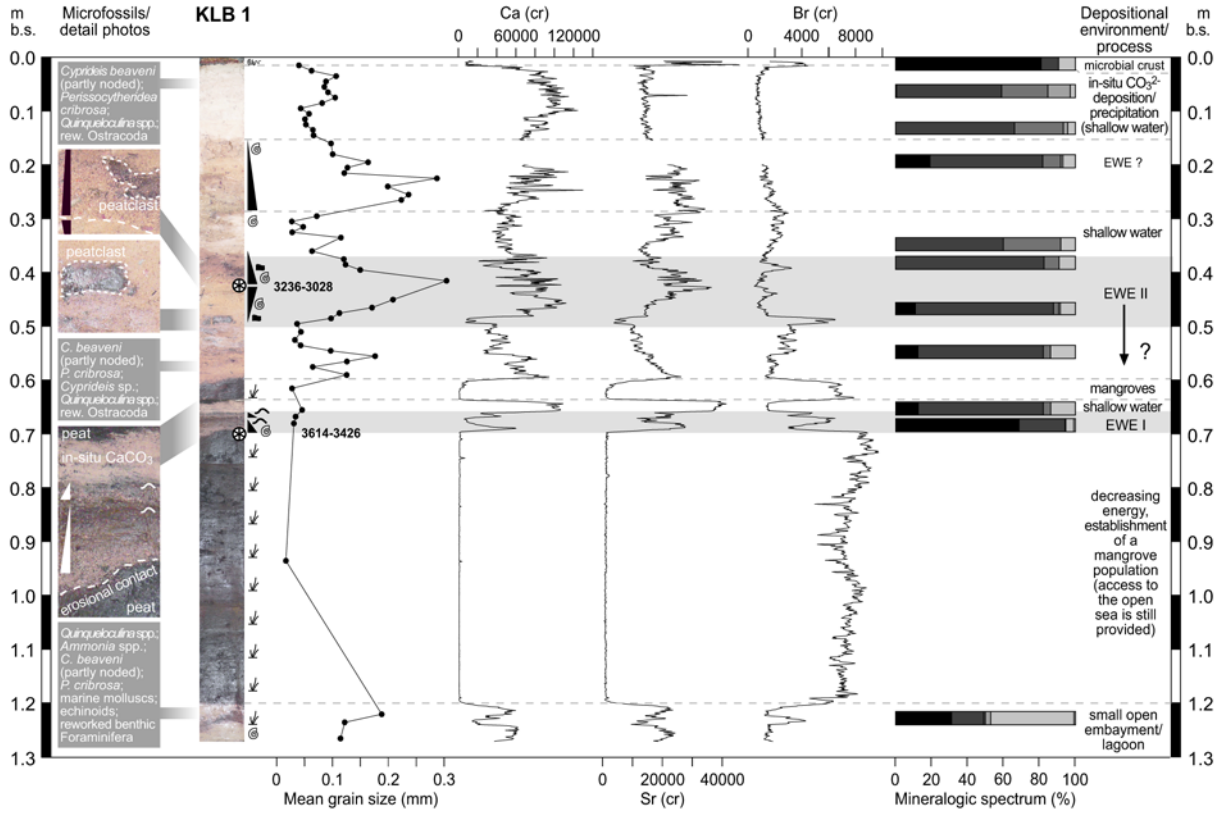

Fig. 38: Push core KLB 1 (Fig. 32) with mean grain size variations, high-resolution XRF data (Ca, Sr, Br; cr = XRF count rates), mineral spectra, microfaunal remains and ^{14}C data (cal BP). A key is provided in Fig. 34. EWE = extreme wave event.

6.5.2 Extreme wave events (EWE): tsunamis or tropical cyclones?

Sediment layers from Saliña Tam and Klein Bonaire interpreted as extreme wave deposits fulfill several criteria commonly associated with tsunami and/or storm wave impacts, such as a basal unconformity, reworked underlying material, graded bedding, increased mean grain size, peaks in marine indicator ions (Ca, Sr), increased $CaCO_3$ content as well as marine microfossils showing signs of reworking (Switzer and Jones, 2008a; Mamo et al., 2009; Peters and Jaffe, 2010a). However, in the sedimentary record, differentiating between deposits of tsunamis and waves generated by extraordinary storms is challenging (Bridge, 2008), since most onshore sedimentary features attributed to either one may be generated by both hydrodynamic processes (Sugawara et al., 2008). Further problems in deducing a chronology of extreme wave events from the stratigraphical record include the possibility that events may not leave sedimentary traces, that sediments may be eroded or heavily disturbed, e.g. by bioturbation (Szczuciński, 2012), and that radiometric ages obtained

from the deposit may not represent the age of the event (Sugawara et al., 2008) due to possible previous reworking or local reservoir ages. The sedimentary pattern a tsunami creates is hard to predict and site-specific. However, interpretations may be enhanced by identifying the presence of a high number of common tsunami signature types, by careful analyses of the local sedimentary environment and "the geological potential for tsunamis" (triggering processes) at a particular site (Peters and Jaffe, 2010a: p. 22), by comparing a candidate tsunami deposit with local modern analogues (either recent tsunami or severe storm deposits), and by also considering the coarse-clast record (e.g. Yu et al., 2009; Peters and Jaffe, 2010a). On Bonaire, no historical tsunamis are documented, but category 5 hurricanes passed the island several times within close distance during the recent past (Meteorological Service of the Netherlands Antilles and Aruba, 2010c) leaving very little to no sediment at coastal depressions such as alluvial plains and bokas (*Chapter 4*; Engel et al., 2010b).

6.5.2.1 EWE I (→ KLB 1)

Tsunami. EWE I was only found in KLB 1 where it is represented by two thin graded beds of 2 and 1 cm thickness. It may also be associated with an erosional unconformity above the peat in SAT 9. The graded beds are dated to c. 3.6 ka BP or later (Fig. 39). Both graded beds are characterized by plant remains and finer material covering basal marine sand. These findings indicate a long wave period of at least several minutes of flow attenuation. Similar observations were made following the tsunamis of Papua New Guinea 1998, Peru 2001 (Morton et al., 2007) and the IOT 2004 (Choowong et al., 2008; Naruse et al., 2010). Thus, storm wave origin after a long period of undisturbed mangrove growth seems unlikely though not impossible.

6.5.2.2 EWE II (→ SAT 8, KLB 1)

Tsunami. Barrier destruction or breaching by the EWE II at Saliña Tam c. 3.2-3.0 ka BP is a phenomenon commonly associated with extraordinary storms or tsunamis (Andrade et al., 2004; Kortekaas and Dawson, 2007; Atwater et al., 2011). Even though it is difficult to infer the exact origin of the EWE II deposit in SAT 8, the presence of open marine planktonic formanifera, which are absent in the overlying deposits of periodic events may point to tsunami (cf. Luque et al., 2002; Uchida et al., 2010). At Klein Bonaire, two normally and one inversely graded sequence are associated with EWE II. Large intraclasts of the underlying peat are a typical feature of tsunami deposits (Kortekaas and Dawson, 2007; Morton et al., 2007; Choowong et al., 2008; Switzer and Jones, 2008a; Bourgeois, 2009; Mamo et al., 2009; Peters and Jaffe, 2010a), even though they have also been observed within storm deposits (Wang and Horwitz, 2007). At Playa Grandi, northeast Bonaire, a coeval deposit was interpreted as tsunamigenic based on taphonomic characteristics and the comparison with the marginal sediment input during recent hurricanes (*Chapter 4*; Engel et al., 2010b). Scheffers (2005) and Scheffers et al. (2006, 2009a) deduced a major tsunami around 3.3-3.1 ka BP based on ^{14}C and ESR ages of onshore coral debris from eastern Bonaire even though this chronological interpretation has recently been challenged by Morton et al. (2008).

6.5.2.3 EWE III-XI (→ SAT 8)

Tropical cyclones. Depositional cycles of sand and organic-rich mud present in SAT 8 relate to periodically recurring inundation pulses during EWE III-XI in the order of decades to centuries. The lower sequences might also be associated with a tsunami wave train of EWE II creating several fining-up layers (cf. Morton et al., 2007; Switzer and Jones, 2008a).

However, nine (EWE III-XI) thin graded sequences implying c. 1 ka of deposition correspond to the approximate recurrence rate of severe tropical cyclones on Bonaire, which is about 100 years (Meteorological Service of the Netherlands Antilles and Aruba, 2010c). It is assumed that storm waves transported reworked particles from the surf zone and shallow marine ostracods into the partly opened southern section of Saliña Tam, each time followed by ponding conditions resulting in sedimentation of organic-rich mud and plant debris, and algae growth (cf. Morton, 1978). This interpretation is in accordance with that of sand layers in a hypersaline lagoon of southern Puerto Rico by Donnelly and Woodruff (2007). A series of thin normally graded sequences may only be attributed to one single storm event if the graded layers are not separated by mud strata due to the short periods of storm wave pulses (Morton et al., 2007). No planktonic or larger foraminifera were identified in these beds, also indicating a different, more limited source area of the sand than in the sediments of EWE II and XII.

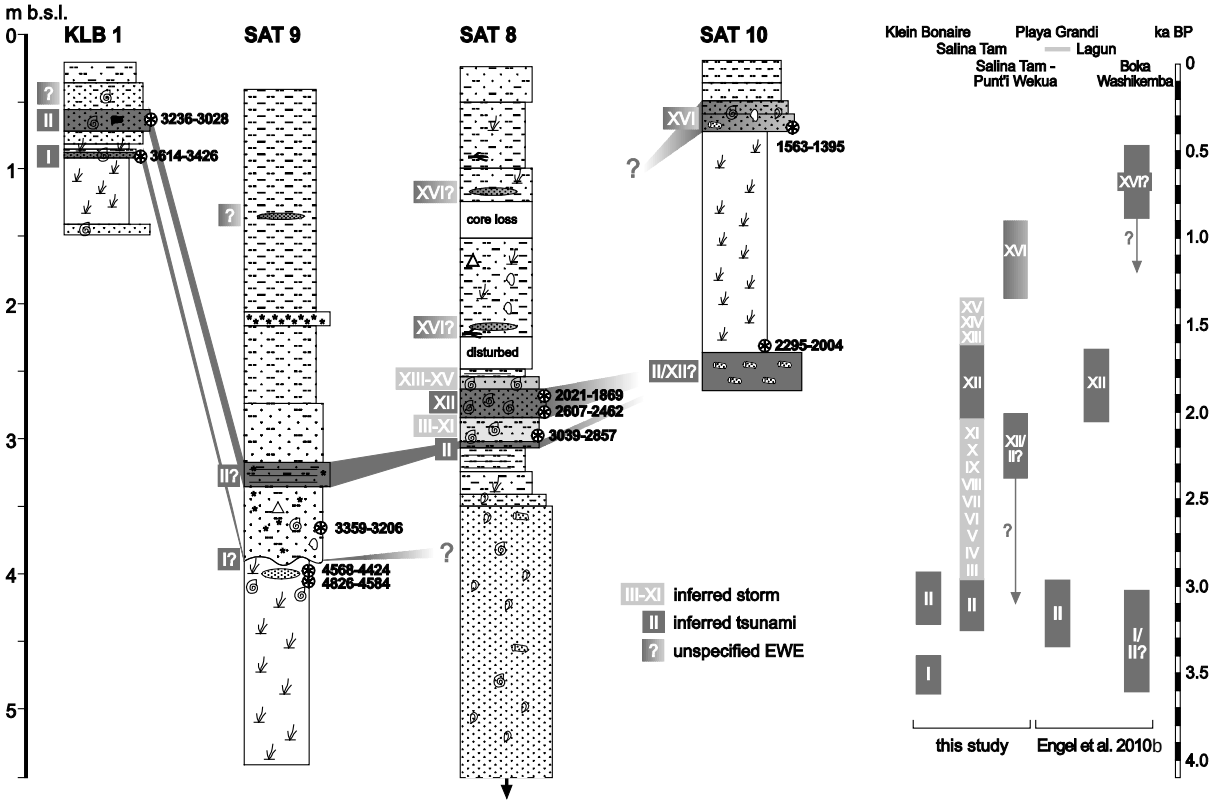

Fig. 39: Left: Synopsis of the cores used in this study including tentative correlations of extreme wave deposits (EWE). Right: Chronology of EWE including the sites of windward Bonaire investigated in Engel et al. (2010b). Position and width (time frame) of the EWE is inferred from ^{14}C data which provide either maximum (in case the date derives from an object incorporated into the EWE deposit or from beneath the EWE deposit) or minimum (in case the date derives from the layer above the EWE deposit) ages.

6.5.2.4 EWE XII (→ SAT 8, SAT 10[?])

Tsunami. Around 2.0-1.8 ka BP, EWE XII struck Bonaire's coastline. For the same time, a tsunami impact was inferred from a massive shell debris layer on the eastern shore (*Chapter 4*; Engel et al., 2010b). The high diversity of marine particles including planktonic foraminifers and marine ostracods recorded in this bed at SAT 8 (Fig. 34) indicates a wider source area compared to the underlying beds interpreted as storm deposits (EWE III-XI) and may support the tsunami hypothesis. Larger foraminifers such as *Amphistegina* sp., for instance, relating to a reefal sediment source were also

found in deposits of the IOT 2004 on the Andaman Islands (Hussain et al., 2006). In a sediment sequence from Martinhal (Algarve, Portugal) containing deposits from the 1755 AD Lisbon tsunami and subsequent storm events, slightly increased microfossil diversity within the tsunami sediments was one of the few features differentiating the layers (Kortekaas and Dawson, 2007). The bedding structure including shell debris at the bottom and two fining-up sequences, followed by inverse grading and a relatively thick normally graded sublayer, rather corresponds to tsunamigenic deposition than to cyclone-induced waves (Morton et al., 2007).

6.5.2.5 EWE XIII-XV (→ SAT 8)

Tropical cyclones. Sediment layers of EWE XII-XV (SAT 8) show a structure similar to those of EWE III-XI, even though thicker subunits of organic-rich mud indicate lower frequency, which could be related to barrier re-growth. Cyclic hurricane impacts are assumed to be responsible for their deposition since diversity and abundance of marine microfossils decreases compared to EWE XII.

6.5.2.6 EWE XVI (→ SAT 10, SAT 8[?])

Tsunami? A sand deposit unconformably overlying mangrove peat at SAT 10, containing shell debris and coral rubble (1563-1395 cal BP), and an adjacent ESR-dated coral boulder (1300±60 a according to Scheffers, 2005) indicate that around 1.3 ka BP or later, a major wave (EWE XVI) impacted the leeward shore of Bonaire. EWE XVI is the youngest EWE that is well-preserved in the local stratigraphy. Major historical hurricanes, e.g. in 1877 or 1999, only modified the higher berm (Scheffers, 2005; Fig. 30), but did not leave distinct sand sheets in the backbarrier, what may indicate that EWE XVI was a tsunami.

6.6 Conclusions

The stratigraphy of Saliña Tam at the leeward coast of Bonaire reflects an interplay of long-term sea level rise, gradual sediment dynamics as well as periodic (tropical cyclones) and episodic (tsunamis) strong wave impacts. Fig. 39 provides a synopsis of the cores of this study focussing on the distribution of extreme wave deposits. Clear sedimentary evidence for EWE I (tsunami) is only provided on Klein Bonaire, though it may be associated with the erosional unconformity in SAT 9. The scale on the right on Fig. 39 shows that EWE II (around 3.2-3.0 ka BP) which we also interpret as tsunamigenic is well represented at several sites on the island including the windward coast. A third candidate tsunami deposit (EWE XII) from c. 2.0-1.8 ka BP is preserved at Saliña Tam (SAT 8) and Lagun (Engel et al., 2010b). EWE XVI (post-1.3 ka BP) had a major impact on barrier accumulation at Saliña Tam. It may also correspond to a tsunami since recent strong hurricanes (W-E-tracking Hurricane Lenny in 1999) caused no changes on the top and back of the barrier. However, sedimentary evidence of this event is limited at other sites. Today, i.e. in case of a stable barrier of coral rubble, marine sediment deposition at Saliña Tam tends to zero during tropical cyclone conditions. Thus, the graded sequences of EWE III-XI and XIII-XV, which we interpret as storm wave deposits, are associated with a breach of the barrier.

The geographical distribution of event deposits was found to be very irregular and difficult to predict, even on a small spatial scale. The same applies to the impact of tsunamis and extraordinary storms on the coastal morphology. However, the outcome of this study is that high-energy wave events do have long-lasting effects on the coastal morphology and ecosystem of Bonaire. This influence

includes century-scale destruction of coastal ridges and may even trigger or drive ridge formation (cf. Scheffers, 2005; Scheffers et al., 2009a). This process has recently been observed during Hurricane Lenny, when a spit of coral rubble (c. 100 m long) was accumulated in the foreshore of north Bonaire (Scheffers and Scheffers, 2006; Morton et al., 2008). EWEs seem to control the formation of coastal sedimentary landforms to a certain extent, as already been emphasised by Scheffers (2004, 2005), Scheffers et al. (2009a), Morton et al. (2008), and Watt et al. (2010), and thus, they shift ecological and morphodynamic boundary conditions of the circumlittoral bokas.

7 Prehistoric Caribbean tsunamis in coastal sedimentary archives – new data from Washington-Slagbaai National Park, Bonaire, and a tentative synthesis of published records*

Abstract: Caribbean societies face a high vulnerability to coastal hazards. Based on their short (and shortening?) recurrence intervals over the intra-American Seas, tropical cyclones and their associated effects of elevated storm surge, heavy wave impacts, mudslides and floods represent the most serious threat. Furthermore, tsunamis must be considered due to the abundance of trigger mechanisms (strike slip motion and oblique collision at the northern and southern Caribbean plate boundaries, submarine and coastal landslides, volcanism, far-field tsunamis) and indicated by available historical accounts. This paper presents results of a multi-proxy investigation (grain size distribution, carbonate, loss-on-ignition, magnetic susceptibility, microfauna, macrofauna) from Washington-Slagbaai National Park, Bonaire, which seeks to infer potential tsunamis and to evaluate their impact on the littoral ecosystem. A large set of sedimentary criteria typically linked with modern tsunami deposits obtained from the stratigraphy of Boka Bartol and calibrated ^{14}C data point to a palaeotsunami with a maximum age of 3300 years. The setting of Boka Bartol changed from an open mangrove-fringed embayment into a poly- to hypersaline lagoon due to the establishment or closure of a barrier of coral rubble with low permeability during the event. The timing of the event is supported by further sedimentary evidence from other lagoonal and alluvial archives on Bonaire. A review of sedimentary evidence of palaeotsunamis from other Caribbean sites is scarce, though urgently needed when aiming to reconstruct reliable patterns of frequency and magnitude over longer time scales.

Keywords: *Palaeotsunamis, Caribbean Sea, Tsunami vs. storm deposits, Coastal evolution, Hazard assessment, Foraminifera, Ostracoda*

7.1 Introduction

A large number of studies based on sediment cores has been undertaken in the Caribbean region in order to reconstruct Holocene coastal geo-ecosystems (Weiss, 1979; Gischler, 2003; Klosowska, 2003) and vegetation (Monacci et al., 2009; Gonzalez et al., 2010), relative sea level rise (Toscano and Macintyre, 2003), or climate (Higuera-Gundy et al., 1999). Several studies have applied marine overwash deposits in coastal ponds to infer fluctuations in millennial hurricane frequency (Donnelly, 2005; Donnelly and Woodruff, 2007; Malaizé et al., 2011). Using coastal sediment cores or trenches to reconstruct pre-historical tsunami occurrence and differentiating between tsunami and storm deposits is a task which has only recently been addressed in the Caribbean (Moya and Mercado, 2006; Hornbach et al., 2008; Atwater et al., 2011; Palmer and Burn, 2011; Scheucher et al., 2011) for

*This chapter is based on: Engel, M., Brückner, H., Fürstenberg, S., Frenzel, P., Konopczak, A.M., Scheffers, A., Kelletat, D., May, S.M., Schäbitz, F., Daut, G., subm. Prehistoric Caribbean tsunamis in coastal sedimentary archives – new data from Washington Slagbaai National Park, Bonaire (Leeward Antilles), and a tentative synthesis of published records. The Holocene.

the purpose of extending the relatively short written record of intra-American tsunami impacts into the Mid-Holocene and to improve regional risk assessment.

A recent example for this relationship is the 869 AD Jogan Tsunami deposit buried within the Sendai plain, Japan, which represents a comparable predecessor of the devastating Tohoku-oki tsunami of 2011. Sediments from both tsunamis share a number of characteristics (Goto et al., 2011).

The island of Bonaire, off the coast of northern Venezuela (Figs. 40 and 41), has one of the most extensively studied coarse-clast records of extreme wave events in the Caribbean (e.g. Scheffers 2002, 2004, 2005; Scheffers et al., 2006; Morton et al., 2006; Spiske and Jaffe, 2009; Engel and May, 2012). It has recently been complemented by findings of marine sand and shell deposits buried in floodplains and coastal ponds (*Chapters 4* and *6*; Engel et al., 2010, in press). Despite a lack of historical accounts on tsunami occurrence on Bonaire during the past 500 years (O'Loughlin and Lander, 2003) and the often very similar nature of both storm and tsunami sediments (*Chapter 3*; Switzer and Jones, 2008a; Lario et al., 2010; Engel and Brückner, 2011), Late Holocene tsunami occurrence on Bonaire has been inferred from the sedimentary record.

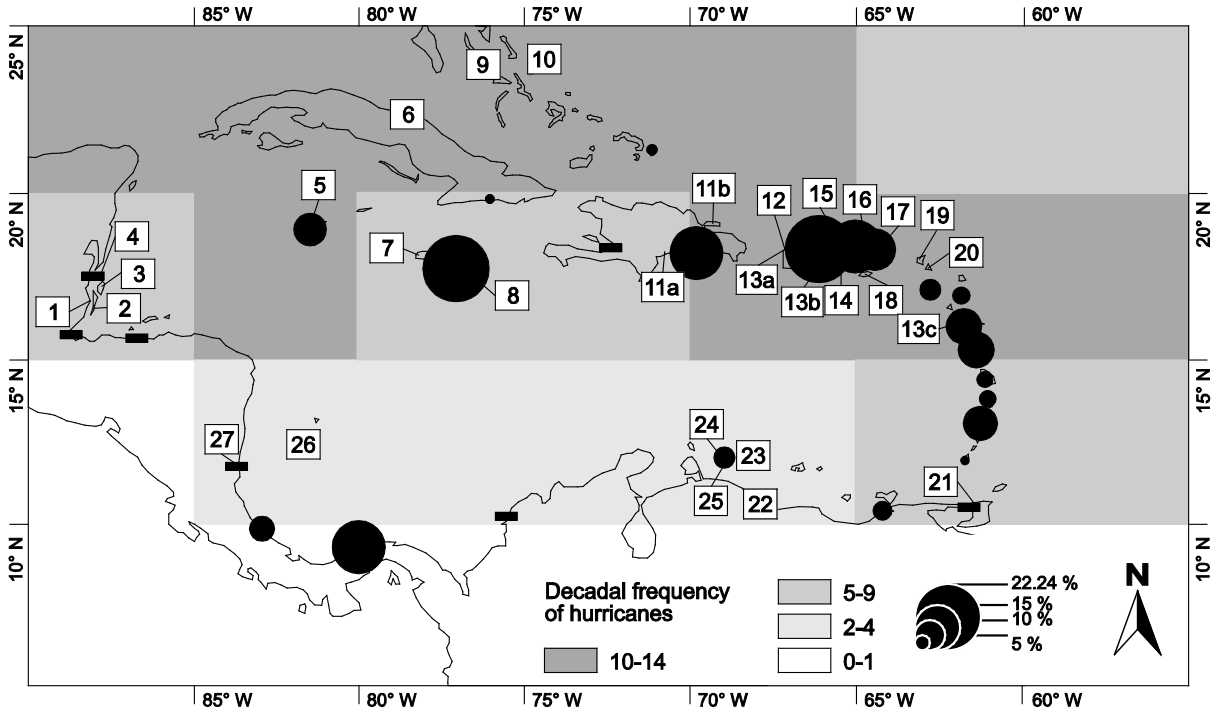

Fig. 40: Overview of the Caribbean basin displaying the study site of Bonaire (23) as well as sites of other palaeoenvironmental records reviewed in this paper (see Table S1, supplementary material). Greyscale quadrants indicate decadal frequencies of tropical cyclones based on instrumental records (Reading, 1990). Circles show the probabilities of tsunami occurrence (run-up >0.5 m) within a period of 30 years (Parsons and Geist, 2009).

In this paper, new sedimentary evidence for high-energy wave impacts (tsunamis or tropical cyclones) from bokas (enclosed coastal ponds) inside Washington-Slagbaai National Park on northwest Bonaire is presented. It is compared with findings from the windward (Engel et al., 2010b) and the leeward (Engel et al., in press) coasts as well as a large set of chronological data derived from supralittoral coral rubble deposits (Scheffers, 2005; Scheffers et al., 2006) in order to establish and discuss a potential chronology of palaeotsunamis for the area of the ABC Islands (Aruba, Bonaire, Curaçao) in the southern Caribbean. By considering other Holocene coastal sediment records, we evaluate the general potential of fine-sedimentary geoarchives for reconstructing tsunami events in the Caribbean.

7.2 Study area

7.2.1 Tectonic and geological setting of Bonaire

Eastward migration of the Caribbean Plate (CP) relative to the North (Cenozoic offset c. 1000 km) and South American Plates (NAP, SAP) resulted in a major subduction zone in the east and complex patterns of strike-slip processes in the north and south (Meschede and Frisch, 1998). Though being part of the Caribbean geographical region, the ABC islands are located on the Bonaire microplate, which is a component of the Late Cretaceous-Early Cenozoic Leeward Antilles ridge (LAR), in the active transpressional boundary zone between the CP and the SAP (Audemard et al., 2005). The LAR involves NE-SW extension creating a roughly NW-SE-striking normal fault pattern (Hippolyte and Mann, 2011). Bonaire itself experiences tectonic uplift and tilting, with the highest uplift rates occurring in the northwest (Herweijer and Focke, 1978). The island's core consists of a volcanic sequence of Middle to Late Cretaceous age comprising basalt, andesite, dacite, pelagic cherts and cherty limestones (Washikemba Formation [WF]) (Beets et al., 1977). A striking feature along the coastline is a series of elevated palaeo-reef terraces associated with Pleistocene sea level highstands (Fig. 41) (for details see De Buisonjé, 1974).

7.2.2 Sampling sites

The area of Washington-Slagbaai National Park, northwest Bonaire, is characterized by the undulating topography of the Washikemba Formation (WF). Along the coast, the MIS 5e limestone terrace is only present at a width of 20-200 m. Torrential drainage channels gather near the coast where they incised the terrace as well as adjacent parts of the WF during sea level lowstands. These coastal indentations are flooded at present forming narrow embayments (bokas) which are separated from the ocean by broad barriers of coral rubble (Fig. 42A).

Boka Bartol has a depth of up to 6 m (Fig. 42B) and is saline with substantial seasonal changes in water level and salinity. We studied its sedimentary infill at the distal alluvial fan entering the water body at the landward side (mastercore BBA 10, BBA 8) and at the shallow tributary basin (BBA 11). South of Boka Bartol, we investigated Wayaka, another flooded channel system. Two sediment cores were taken at its landward shore (WAY 1) and close to the seaward barrier (WAY 2) in order to document spatial variations in marine washover deposition and preservation. At Boka Funchi, one sediment core was taken at the landward shore (BFU 1).

Present continuous sedimentation (background sedimentation) of the bokas is determined by torrential fluvial input and autochthonous precipitation of open water evaporites. Marine influence during recent hurricanes, such as Ivan in 2004, was limited to modifications of the seaward part of the coral rubble ridges at Boka Bartol and Wayaka (Scheffers, 2005; Scheffers and Scheffers, 2006). At Boka Funchi, waves of Hurricane Lenny 1999 washed over the barrier and deposited an entirely new ridge of coral material on top of the pre-existing broad barrier as well as lobe-like overwash structures reaching into the boka waters (Spiske and Jaffe, 2009). Whereas Boka Bartol has a northwesterly exposition, the coast of Boka Funchi and Wayaka is exposed to the west. The mean tidal range on Bonaire amounts to c. 30 cm (Bak, 1977).

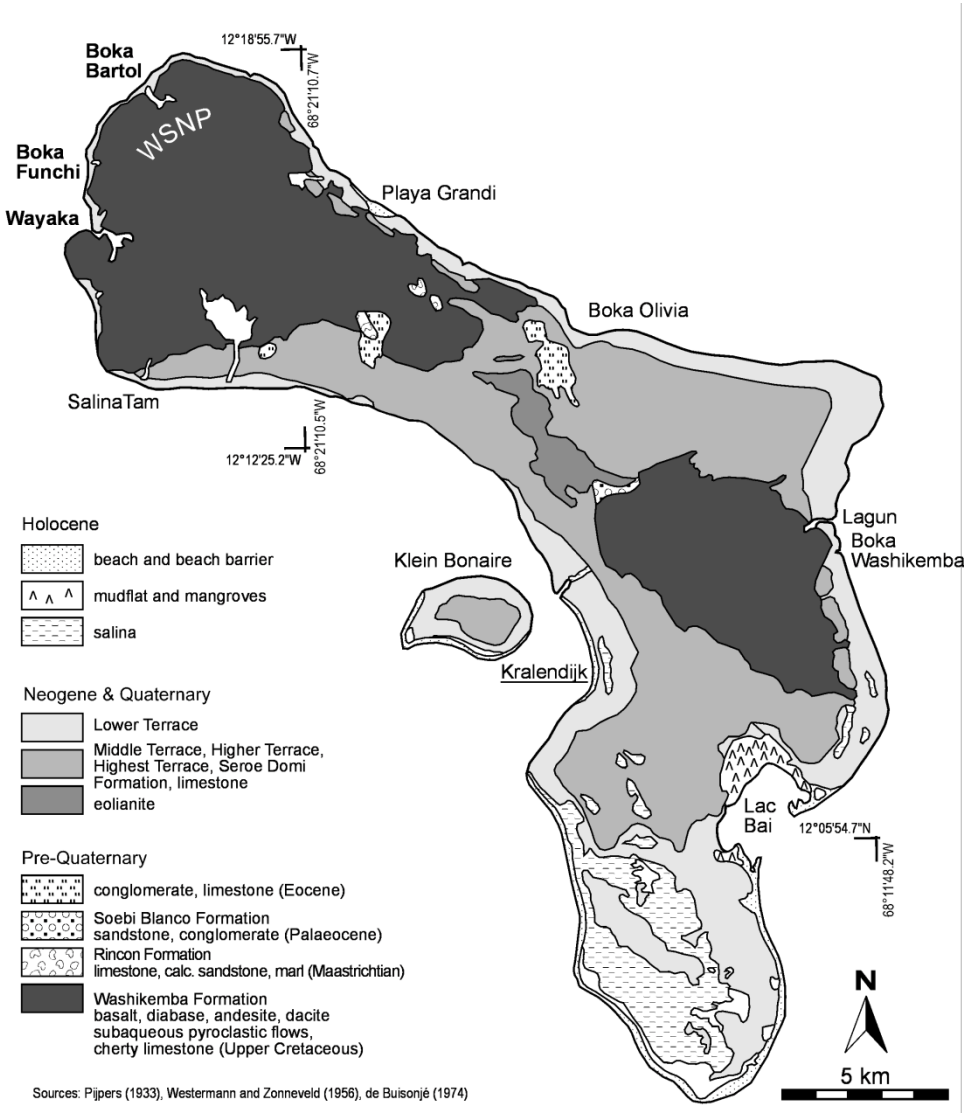

Fig. 41: Simplified geological map of Bonaire based on mapping by Pijpers (1933), Westermann and Zonneveld (1956) and De Buisonjé (1974) showing sites from this study and Engel et al. (2010b, in press).

7.2.3 Tropical cyclones and tsunamis

The Caribbean region is regularly crossed by tropical cyclones (locally known as hurricanes) and, with much lower frequency, impacted by autochthonous tsunamis and teletsunamis. Most cyclones, particularly during late summer and early autumn, belong to the Cape Verde type (CV) cyclones triggered by atmospheric easterly waves crossing the North Atlantic between 10 and 20° (Goldenberg and Shapiro, 1996). At the time of peaking sea surface temperatures and decreasing wind shear, these tropical waves may grow into tropical cyclones and cross the Caribbean. When reaching the western edge of the associated subtropical high they are usually directed polewards (Hobgood, 2005). Their effects on lives and economies in Central America in the form of waves, storm surges, winds, rainfall and mass wasting are severe and have a very uneven spatial distribution. Cyclones most frequently affect the Bahamas, Cuba and Jamaica, and the Antilles island arc, where most CV systems enter the Caribbean from the open Atlantic. The entire southern Caribbean from Venezuela to Nicaragua including the ABC islands is less threatened (Fig. 40) (Reading, 1990).

Most Caribbean tsunamis are triggered by tectonic processes including subduction, strike-slip motion and oblique convergence along the northern plate boundary as well as subduction in the east,

though submarine mass failure at steep slopes and explosive volcanism also proved to be tsunamigenic on a local (affected area is located within a radius of <100 km from the source) to regional (100-750 km) scale (Cotilla Rodriguez and Córdoba Barba, 2011). A far-field or teletsunami (>750 km) with widespread effects in the Caribbean was triggered by the 1755 Lisbon earthquake (O'Loughlin and Lander, 2003). In the southern Caribbean, faults along the Venezuelan coast generated tsunamis in historical times (Audemard, 2007). Based on the Caribbean historical tsunami catalogue of O'Loughlin and Lander (2003) and numerical models of tsunami run-up (r), a 30-year probability of for $r \geq 0.5$ m of c. 7% was calculated for northern and eastern Bonaire (Fig. 40). Towns with highest values include San Juan, Puerto Rico, and Kingston, Jamaica (both c. 22 %) (Parsons and Geist, 2009).

7.3 Methods

The methods involved in this study are similar to those successfully applied at the windward (*Chapter 4*; Engel et al., 2010b) and leeward (*Chapter 6*; Engel et al., in press) coasts of Bonaire. Open (BBA 8, BBA 11, WAY 1, WAY 2, BFU 1) and closed (BBA 10) vibracores with diameters of 5 and 6 cm were carried out using an Atlas Copco Cobra 248 device. The purpose was

(i) to deduce ecological and geomorphological changes from long-term background sedimentation,

(ii) to discriminate these sediments from allochthonous marine layers and

(iii) to use multi-proxy data from the allochthonous layers for a tentative differentiation between storm and tsunami impact.

A discussion on possibilities and pitfalls in differentiating between storm and tsunami deposit is presented in *Chapter 3* and e.g. by Kortekaas and Dawson (2007), Morton et al., (2007), Switzer and Jones (2008a), Mamo et al. (2009), Engel and Brückner (2011), or Goff et al. (2012).

Mastercore BBA 10 (9 m long) was brought to the laboratory as a whole and split in order to perform high-resolution sedimentological investigations. Magnetic susceptibility reflecting the magnetisability of mineral components and thus supporting the differentiation of sediment source areas was measured by means of a Bartington MS2B sensor in steps of 2 mm. One cm sections of the core were taken selectively, air-dried, and carefully disintegrated by mortar and pestle. Loss on ignition (LOI) was determined by oven-drying at 105 °C for 12 h and ignition in a muffle furnace at 550 °C for 4 h. the carbonate content was measured using a Scheibler-type calcimeter (Beck et al., 1993). After pretreatment with H_2O_2 (30%) and $Na_4P_2O_7$ (55.7 g/l), grain size distribution was investigated by means of a Beckman Coulter LS 13320 Laser Particle Analyzer and dry sieving. Sections bearing high amounts of gypsum crystals were skipped for grain size analyses. Statistical measures of grain size distribution were calculated using GRADISTAT software (Blott and Pye, 2001).

Foraminifers and ostracods are highly indicative of past sedimentary processes and ecological conditions (Frenzel and Boomer, 2005; Murray, 2006; Mamo et al., 2009). Their abundance was investigated using the grain size fraction 200-1000 µm (wet sieving) under a reflected-light microscope. Correlation and biofacies determination based on multivariate statistics was performed using PAST software (Hammer et al., 2001). High magnification light microscopy and scanning electron microscopy (SEM) enabled photographic documentation and further taxonomic identification. The state of preservation of fossil groups was documented semi-quantitatively for distinguishing reworked and (par-)autochthonous specimens.

The open cores were documented and sampled in the field. Samples were analyzed in the laboratory for macrofaunal content, LOI, and carbonate content.

All cores were levelled by differential GPS (Leica SR 530). The bathymetry of Boka Bartol was surveyed using a zodiac and a fishfinder (Lowrance LMS-522 C iGPS).

Age estimates derive from ^{14}C-AMS dating. ^{14}C ages were calibrated using Calib 6.0.1 software (Reimer et al., 2009) considering the 2σ error. For marine objects a regional reservoir effect of ΔR = -49 was applied (Radtke et al., 2003).

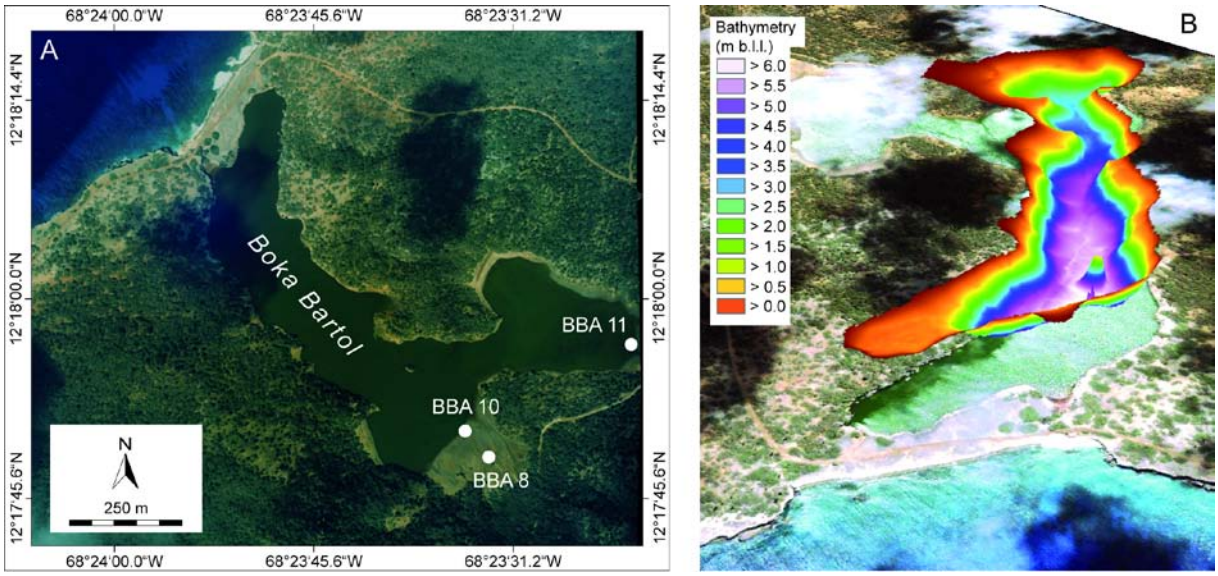

Fig. 42: A) Rectified aerial photograph of Boka Bartol (1996) showing sediment cores BBA 10 and BBA 8 on the distal alluvial fan entering the main basin and BBA 11 at the margin of the shallow tributary basin. B) Bathymetry of the main basin of Boka Bartol projected on an oblique Google Earth image (b.l.l. = below lagoon level). The view is directed towards southeast (GPS data processing and design: A. Bolten).

7.4 Results

Mastercore BBA 10 represents the backbone of this study. Proxy data are presented in detail in Fig. 43 and stratigraphical descriptions are depicted in Table 11. All other cores are described in the text and presented in the synopsis of Fig. 46. Further documentation can be accessed in the supplementary material (*Chapter 7.7*).

7.4.1 Boka Bartol

7.4.1.1 Stratigraphy of the mastercore (BBA 10)

Mastercore BBA 10 was taken on the distal, seasonally flooded part of the alluvial fan entering Boka Bartol (Fig. 42A). The stratigraphy of BBA 10 is presented in Table 11, and Figs. 43 and S1 (see supplementary material). Additional stratigraphical information on the site can be inferred from open core BBA 8, 100 m to the north (Engel et al., 2009a, and Figs. S2 and S3). Based on proxy data (Fig. 43) and sedimentary characteristics (Table 11), four different units (I-IV) and further subunits (IIIa, IIIb, IVa, IVb) were identified.

7.4.1.2 Biofacies of BBA 10

All meso- and microfaunal components and semi-quantitative data on their abundance are summarized in Fig. 43. Figs. 44 and 45 show SEM pictures of relevant taxa, mostly foraminifers and ostracods. Biofacies A correlates with stratigraphical unit I (Table 11). It is characterized by moderate abundance of both ostracods and foraminifers. Biofacies B shows highest diversity and abundance of microfaunal remains and is congruent with unit II. Its percentage of broken tests is significantly increased. Biofacies C is represented by two samples from units IIIa and IIIb including a darker organic-rich layer as well as a lighter carbonate stratum. Both abundance and diversity of ostracods are low. Foraminifers are absent.

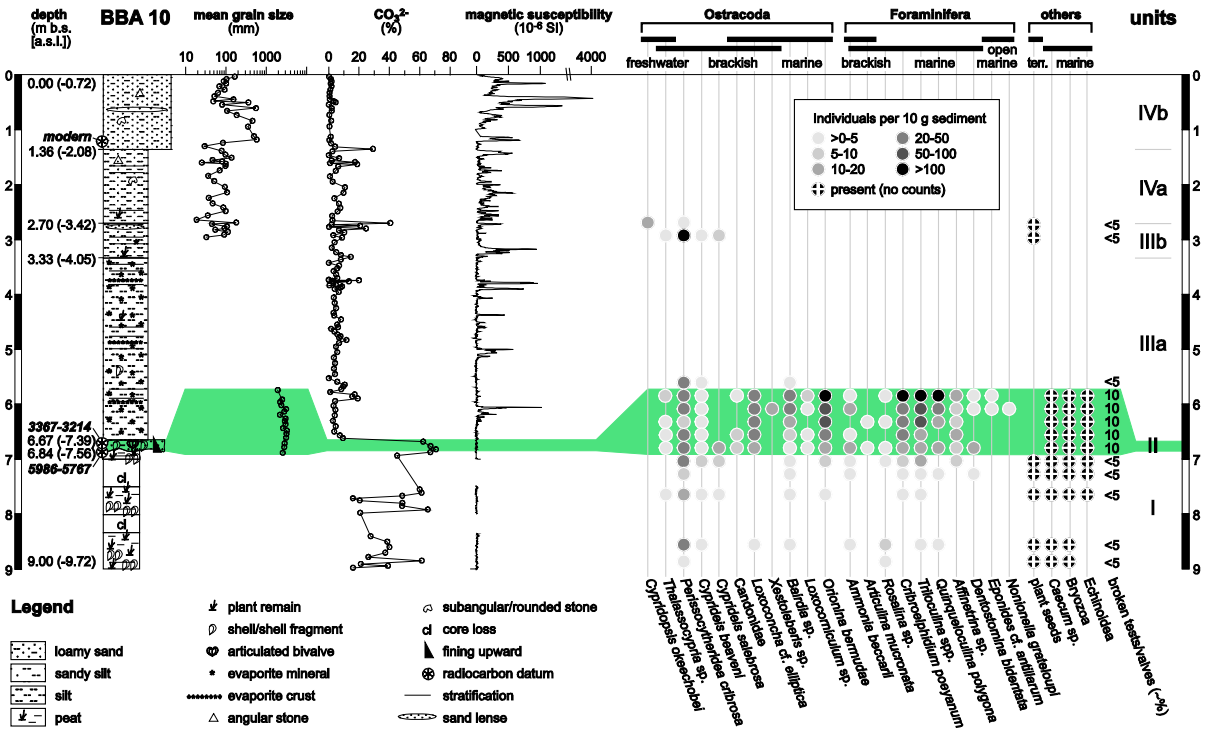

Fig. 43: Stratigraphy of sediment core BBA 10 and proxy data. See Fig. 42A for the coring site. Sections containing peat or significant amounts of evaporite minerals were rejected for grain size analysis. The depiction of mean grain size and microfossil analysis within unit II is vertically exaggerated.

7.4.1.3 BBA 11

Sediment core BBA 11 was taken at the eastern margin of the shallow tributary basin of Boka Bartol. It reached a depth of 3 m. Details on the stratigraphy are summarised in Fig. S4. BBA 11 is also depicted in the synopsis of Fig. 46.

Sandy silt and numerous stone components were found in the lowermost section (3.00-2.26 m b.s.) of BBA 11. In the upper part, it contains several plant fragments. The overlying unit (2.00-1.61 m b.s.) consists of silt, plant remains, juvenile bivalves and only few stones at the base. A mixture of organic-rich silt matrix, carbonate sand particles and a high number of mollusc shells and their fragments were identified between 1.61 and 1.47 m b.s. Bivalve shells were dated to 3329-3204 and 3390-3236 cal BP and a plant fragment was dated to 3339-3162 cal BP (Table 12). The chaotic layer is vertically confined by a thin, mollusc-free silt unit (1.47-1.33 m b.s.) and a pale olive muddy deposit dominated by evaporate crystals, anorganic carbonate, and a small number of plant remains and stones (1.33-0.44 m b.s.). The top layer consists of silty sand and several angular stones.

Table 11: Field log of mastercore BBA 10 (Fig. 43) and correlation with biofacies.

Layer	Depth in cm b.s. (b.s.l)	Colour	Matrix	Sorting	Texture	Components	Others	Bio-facies
I	9.00-6.84 (9.72-7.56)	Black (7.5YR 2/5) to very dark grey (5YR 3/1)	Muddy peat	-	Unstructured apart from 6 distinct layers of *Crassostrea rhizophorae* (Guilding 1828) shells	Macroscopic plant remains; Shell fragments and shells of *C. rhizophorae* and *Chione cancellata* (Linnaeus 1767)	H_2S odour	A
II	6.84-6.67 (7.56-7.39)	Greenish grey (5GY 6/5)	Sand to coarse silt	Poor	One normally graded sequence, erosive basal contact	Many bivalve shells (some articulated) and shell fragments	-	B
IIIa	6.67-3.33 (7.39-4.05)	Very dark grayish brown (10YR 5/8) to yellowish brown (10YR 3/2)	Gypsum and halite crystals, aragonite mud, and organic matter	Moderate to good	Alternate lamination of matrix materials (mm- to cm-scale layers)	Plant remains; very few shell fragments; gypsum crystals up to 1 cm	H_2S odour	C
IIIb	3.33-2.70 (4.05-3.42)	Pale brown (10YR 4/3)	Fine sandy silt, sand, organic-rich mud	Moderate to good	Lamination	Low concentration on capillary evaporites	-	C
IVa	2.70-1.36 (3.42-2.08)	Very dark grey (5Y 3/1)	Fine to medium silt	Moderate to good	Lamination; 9 sand lenses	-	-	(C)
IVb	1.36-0.00 (2.08-0.72)	Very dark grey (5Y 3/1) to very dark brown (10 YR 2/2)	Silty fine sand	Poor	No structure	Very few plant fragments	-	(C)

7.4.2 Boka Funchi

Sediment core BFU 1 was taken at the landward margin of Boka Funchi (Fig. S6). The core reached bedrock at 6.45 m b.s. Its stratigraphical pattern is displayed in Figs. 46, S7 and S8.

A bluish grey to black loamy deposit with low carbonate content overlies the bedrock (6.40-3.37 m b.s.). The amount of angular stones decreases upwards, while plant remains increase. Very few shell fragments are present in the upper part. Sedimentation is interrupted by a normally graded layer of fine sand and a diverse mixture of shells including an articulated bivalve (3.37-3.19 m b.s.). Its basal contact is erosive. A bivalve shell was dated to 4143-3951 cal BP. The graded sand is vertically confined by a laminated deposit of organic-rich silt and evaporites (gypsum crystals, carbonate) (3.19-0.57 m b.s.). Between 2.59-2.49 m b.s., a monotonous assemblage of juvenile bivalves including articulated specimen was identified. The top layer consists of poorly sorted silt and sand layers with several anoxic spots.

7.4.3 Wayaka

Sediment core WAY 1 is located close to the coral rubble ridge separating Wayaka from the open sea, though still protected by the limestone terrace (Fig. S9). WAY 1 reached a depth of 5.70 m (Figs. 46, S10, S11).

Poorly sorted sandy silt containing many angular and subangular stones and some shell and plant material was encountered at the bottom (5.70-4.76 m b.s.). Overlying is a section of clastic silt and clay with varying amounts of fine angular shell debris, stones and organic matter. The upper part is normally graded and capped by a massive piece of consolidated sand (beachrock?). A plant fragment from 4.63 m b.s. was dated to 5727-5608 cal BP. A sharp boundary separates this section from a muddy matrix dominated by gypsum and salt crystals, and thin strata of anorganic carbonate. Gypsum precipitation has destroyed primary lamination (3.64-1.30 m b.s.). Apart from the lowermost 15 cm, the unit is void of plant remains and mollusc shells. The top layer consists of silt and sand and very few additional components such as precipitated minerals and bivalve shell and plant fragments.

WAY 2 (Figs. 46, S12, S13) reflects the stratigraphy of Wayaka's landward margin and reached 6 m b.s. Loamy sediments containing subangular to angular stones were encountered from the bottom to 2.61 m b.s. They are overlain by sandy silt and consolidated sand (beachrock?) as well as olive grey mud with relatively large fragments of bivalve shells (2.61-2.28 m b.s.). A ^{14}C age of 4932-4797 cal BP was obtained from a plant fragment (2.55-2.49 m b.s.). The shelly mud is overlain by a laminated sequence of clastic mud and evaporites (1.80-1.25 m b.s.) and a deposit of pale yellow gypsum and salt crystals (0.98-0.47 m b.s.). The poorly sorted uppermost unit contains sand and silt strata and anoxic spots.

Table 12: ^{14}C-AMS ages presented in this study. Measurements were carried out at the radiocarbon laboratory of the University of Georgia at Athens (USA).

Sample	Depth (m b.s.)	Lab ID UGAMS#	Material	δ^{13}C	^{14}C age	Age cal BP (2σ)
BBA 8/6 PF	2.43	3201	Plant fragment	-25.0	840±25	789-693
BBA 8/22	5.78	3202	Plant fragment	-24.6	5860±25	6742-6636
BBA 8/32	8.36	3203	Plant fragment	-27.8	6730±25	7657-7525
BBA 10-124	1.24	6007	Plant fragment	-28.7	190±20	289-0 (modern)
BBA 10-680	6.80-6.64	6009	Articulated *Corbula* sp.	1.0	3370±25	3367-3214
BBA 10-690	6.90-6.84	6010	Wood	-25.7	5150±25	5986-5767
BBA 11/9 ^{14}C	1.47	6005	Plant fragment	-24.9	3030±25	3339-3162
BBA 11/10 Venus	1.58	6006	*Chione cancellata*	-0.1	3320±25	3329-3204
BBA 11/10	1.60-1.55	7584	*Corbula* sp.	-0.1	3390±25	3390-3236
WAY 1/20 ^{14}C	4.63	7585	Plant fragment	-24.2	4900±25	5727-5608
WAY 2/10 F	2.55-2.49	7586	Plant fragment	0.8	4580±25	4932-4797
BFU 1/17 ^{14}C	3.28-3.20	7587	*Chione cancellata*	-1.8	3980±25	4143-3951

7.5 Discussion

7.5.1 Boka Bartol

Stratigraphical units I-IV of BBA 10 (and BBA 8) reflect distinct consecutive environmental conditions and morphodynamic processes at Boka Bartol. Tentative correlations with strata of BBA 11 are presented.

7.5.1.1 Unit I: The open embayment (early Holocene until c. 3300 BP)

High values of carbonate, abundant shell remains of *Crassostrea rhizophorae* and plant material indicate a calm marine embayment which formed due to rapid early to Mid-Holocene relative sea level rise. Unit I most likely represents fringing mangroves where *C. rhizophorae* populate the root system in the intertidal zone. Both mangroves and *C. rhizophorae* require a permanent connection to the

ocean throughout the year (Mattox, 1949). Low magnetic susceptibility indicates negligible influence of terrestrial sedimentation from the inner igneous complexes of Bonaire. An articulated specimen of *Chione cancellata* in living position supports the interpretation of a shallow seagrass-covered, soft-bottom environment (Moore and Lopez, 1969). Comparable to the "wooden shoreline" of mangroves described by Thom (1967: pp. 326 ff.), the stable shoreline of Boka Bartol was dominated by *Rhizophora* stands. Similar inferences were made for the Mid-Holocene open embayment of Lagun, east Bonaire (*Chapter 4*; Engel et al., 2010b). At Boka Bartol, post-glacial ingression occurred not later than the 8th millennium BP (see datings of lagoonal deposits in BBA 8, Fig. 46). The relative sea level reached a position of approx. 1 m below present level c. 5000 years ago and rose asymptotically since then (*Chapter 8*; Milne et al., 2005). Biofacies A, congruent with unit I, is dominated by brackish and marine ostracods and foraminifers. Highest abundance is reached by the ostracod *Perissocytheridea cribrosa* (Fig. 44), tolerating a broad range of salinity (5-48‰) and preferring hard-bottom substrate with detritus cover (Keyser, 1977a). A reliable indicator of open access to the sea is the presence of *Orionina bermudae* (Fig. 44), which is associated with shallow marine environments and a salinity of 32-36‰ (Swain and Gilby, 1967), as well as several foraminiferal taxa such as *Cribroelphidium poeyanum* and *Quinqueloculina polygona* (Fig. 45), which are restricted to open lagoons and shallow marine habitats (Hart and Kaesler, 1986; Havach and Collins, 1997). Abundance and diversity of microfossils increase upwards, indicating enhanced exchange with the ocean rather than a gradual closure of the connection.

At least during the latest stage of the open embayment, the shallow tributary basin of Boka Bartol (core BBA 11, Fig. 46) was also flooded. Thin-walled, autochthonous juvenile bivalves in layer 2.00-1.61 m b.s. indicate a connection to the marginal-marine environment of the main basin.

7.5.1.2 Unit II: A high-energy wave event – tsunami or hurricane? (c. 3300 BP or shortly after)

High carbonate content, low magnetic susceptibility, and many bivalve shells (including articulated specimens) and shell fragments indicate a marine origin of the deposit. The sharp lower contact and quasi-graded bedding point to a high-energy wave event (Fig. 47), most likely a tsunami or strong storm wave impact (Switzer and Jones, 2008a; Brill et al., 2011). The large discrepancy between the ^{14}C dating from the upper part of unit I (5986-5767 cal BP) and unit II (3367-3214 cal BP) is interpreted to be the result of erosion of the striking wave and is rather associated with tsunamis than storm waves (Morton et al., 2007; Switzer and Jones, 2008a; Mamo et al., 2009). Articulated bivalve shells of *Corbula* sp. indicate proximal dislocation from a sandy, shallow marine (reefal?) environment (cf. Treece, 1980; García-Cubas and Reguero, 1995), which can be found just seaward of Boka Bartol, rather caused by a tsunami than a storm, since stepwise transport by storm waves would possibly have caused separation and/or fragmentation of the valves (Donato et al., 2008). The interpretation of tsunami occurrence is furthermore supported by a lack of sediment deposition at BBA 10 during recent high-category hurricanes.

Microfaunal samples of unit II were clustered as biofacies B. Ostracods and foraminifers are highly abundant ranging from brackish to open marine taxa. The ostracofauna indicates a sediment source comprising the marine inner shelf, i.e. the narrow reef in front of Boka Bartol (*Orionina bermudae, Bairdia* [Benson, 1959; Swain and Gilby, 1967]) and marginal lagoons such as Boka Bartol during the phase of unit I (*Perissocytheridea cribrosa, Cyprideis beaveni* [Benson, 1959; Keyser, 1977a]). Increased abundance and diversity of ostracods has repeatedly been reported from tsunami deposits,

e.g. in southern Portugal (Hindson and Andrade, 1999) or on the Boso and Miura peninsulas, Japan (Fujiwara et al., 2000).

The presence of the foraminiferal taxa *Eponides* cf. *antillarum* and *Nonionella grateloupi*, both usually dwelling on the outer shelf in water depths of up to 180 m (Brooks, 1973; Corliss, 1991), provides evidence for the transport of deeper shelf sediment to the coast. The majority of foraminiferal taxa is associated with brackish and lagoonal waters (*Ammonia beccarii* [Havach and Collins, 1997; Dix et al., 1999]) and the inner shelf (*Cribroelphidium poeyanum* and *Quinqueloculina polygona* [Hart and Kaesler, 1986; Havach and Collins, 1997]). Mixed marine foraminiferal assemblages dominated by but not restricted to inner shelf species were also identified in deposits of the Indian Ocean Tsunami of 2004 in Thailand (IOT), Malaysia, and India (Hawkes et al., 2007; Nagendra et al., 2005) or the 1755 Lisbon Tsunami (Hindson and Andrade, 1999). The presence of species from a greater shelf depth, i.e. below the storm wave base, has often been observed in tsunami deposits and may represent a key diagnostic criterion to rule out storm wave deposition (Mamo et al., 2009; Uchida et al., 2010). It is explained by the ability of tsunamis to entrain sand-sized particles from water depths of up to several hundred metres due to their long period and amplitude (Weiss, 2008). An upward increase in abundance of foraminifers, as recorded in unit II, was also observed in IOT deposits from Khao Lak and Phi Phi Don, Thailand (Hawkes et al., 2007) as well as in 1755 Lisbon tsunami deposits (Dawson, 1996; Hindson and Andrade, 1999). This might correspond with their below average size compared to other constituents of unit II and their preferential deposition out of suspension during a later stage of inundation. A higher number of broken tests in unit II compared to background sediments is the result of a high-energy depositional process, though it is not diagnostic for either storm or tsunami (Kortekaas and Dawson, 2007).

The fining-up pattern of unit II is typical for tsunami deposits, where most sediments derive from suspension. As current velocities during onshore inundation gradually decrease due to bottom friction and internal turbulent flow, coarser sediments settle first, followed by finer particles (Morton et al., 2007). Similar conclusions were drawn from a study on inundation patterns during the IOT at Phra Tong Island, Thailand, based on diatoms. High flow velocities during the initial phase of inundation were associated with coarser particles from a littoral or sublittoral source area within the basal deposit (Sawai et al., 2009). At Boka Bartol, a similar pattern is reflected by foraminifers and ostracods of brackish and sublittoral habitats as well as shells and shell fragments and carbonate sand grains (*Halimeda* sp.) in the basal part indicating a sediment source located at the narrow shallow reef zone and the formerly open embayment.

Sawai et al. (2009) recorded marine plankton towards the central part of the IOT deposit, which might correspond to the occurrence of outer shelf foraminiferal taxa (*Eponides cf. antillarum, N. grateloupi*) towards the upper part of unit II. They are interpreted to have jointly fallen out from suspension with the finer sediment fraction deriving from deeper environments at a later stage of tsunami inundation. Comparable to the findings of Sawai et al. (2009), the uppermost microfaunal sample of unit II shows a higher abundance and slightly higher diversity including more freshwater and brackish taxa.

Unit II is represented by layer 1.61-1.47 cm b.s. in the shallow tributary basin of Boka Bartol (Fig. 46, S4, S5). Angular shell fragments of allochthonous taxa, such as *Corbula* sp., which is most abundant in regions of 20-40 m depth (Treece, 1980), also indicate the input of shelf sediment by an extreme wave event. Remarkably consistent ^{14}C datings of 3339-3162 (plant fragment), 3329-3204 (*C. cancel-*

lata) and 3390-3236 (*Corbula* sp.) furthermore justify the assumption that this layer has been deposited by the inferred tsunami around 3300 BP or a bit later.

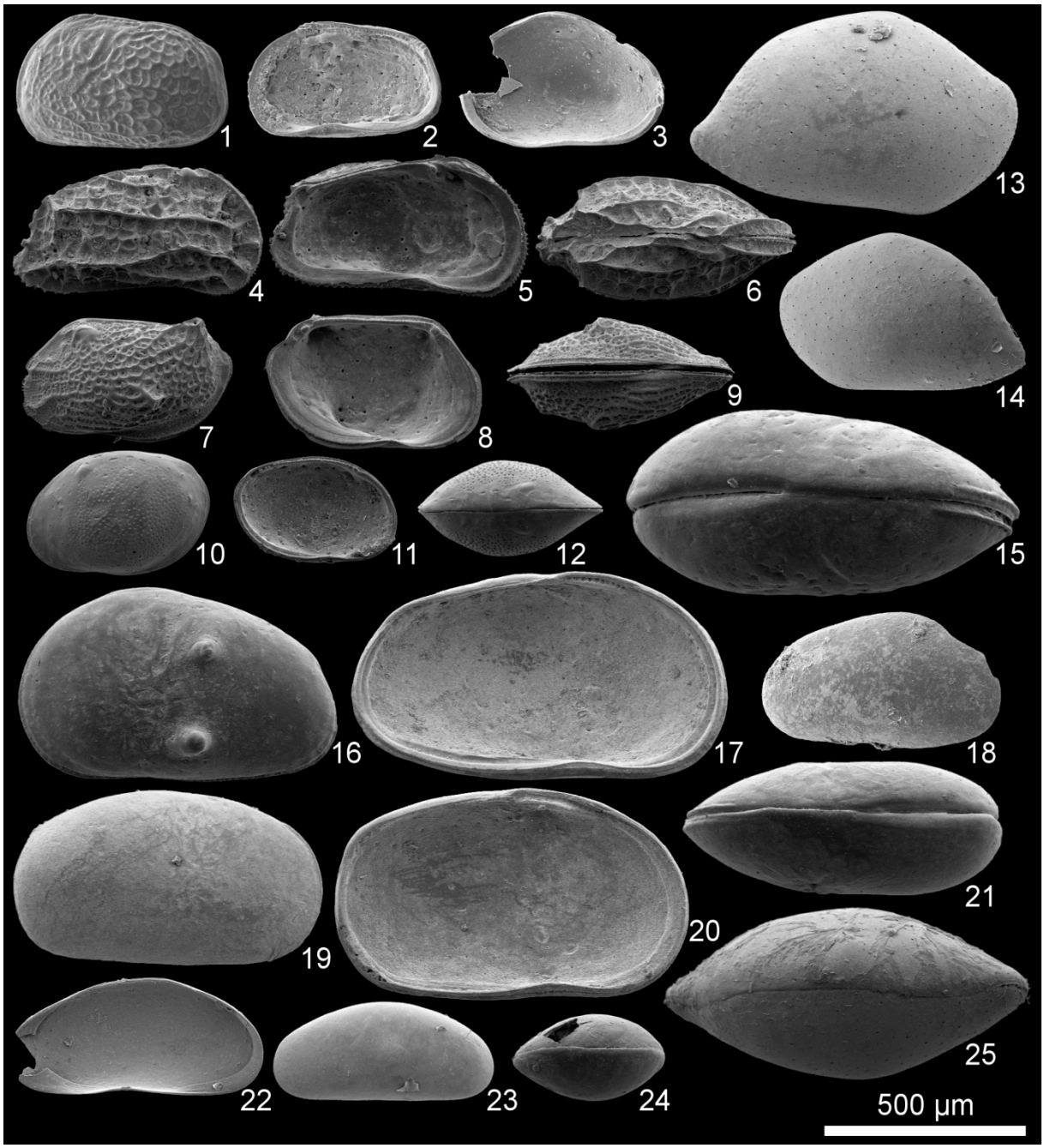

Fig. 44: Scanning electron microscope photographs of ostracods from core BBA 10. 1) *Perissocytheridea cribrosa* (Klie 1933), left valve (LV), lateral; 2) *P. cribrosa*, right valve (RV), intern; 3) *Cypridopsis okeechobei* (Furtos 1936), RV, intern; 4) *Orionina bermudae* (Brady 1880), RV, lateral; 5) *O. bermudae*, LV, intern; 6) *O. bermudae*, dorsal; 7) *Loxocorniculum* sp., LV, lateral; 8) *Loxocorniculum* sp., LV, intern; 9) *Loxocorniculum* sp., dorsal; 10) *Loxoconcha aff. elliptica*, LV, lateral; 11) *Loxoconcha aff. elliptica* (Brady 1868), LV, intern; 12) *Loxoconcha aff. elliptica*, dorsal; 13) *Bairdia* sp., RV, lateral; 14) *Bairdia* sp., LV, lateral; 15) *Cyprideis beaveni* (Tressler & Smith 1948), dorsal; 16) *C. beaveni*, LV, lateral; 17) *C. beaveni*, LV, intern; 18) *Candonidae* sp., LV, lateral; 19) *Cyprideis salebrosa* (van den Bold 1963), RV, lateral; 20) *C. salebrosa*, LV, intern; 21) *C. salebrosa*, dorsal; 22) *Thalassocypria* sp., RV, intern; 23) *Thalassocypria* sp., LV, lateral; 24) *Xestoleberis* sp., dorsal; 25) *Bairdia* sp., dorsal (photographs: S. Fürstenberg, P. Frenzel).

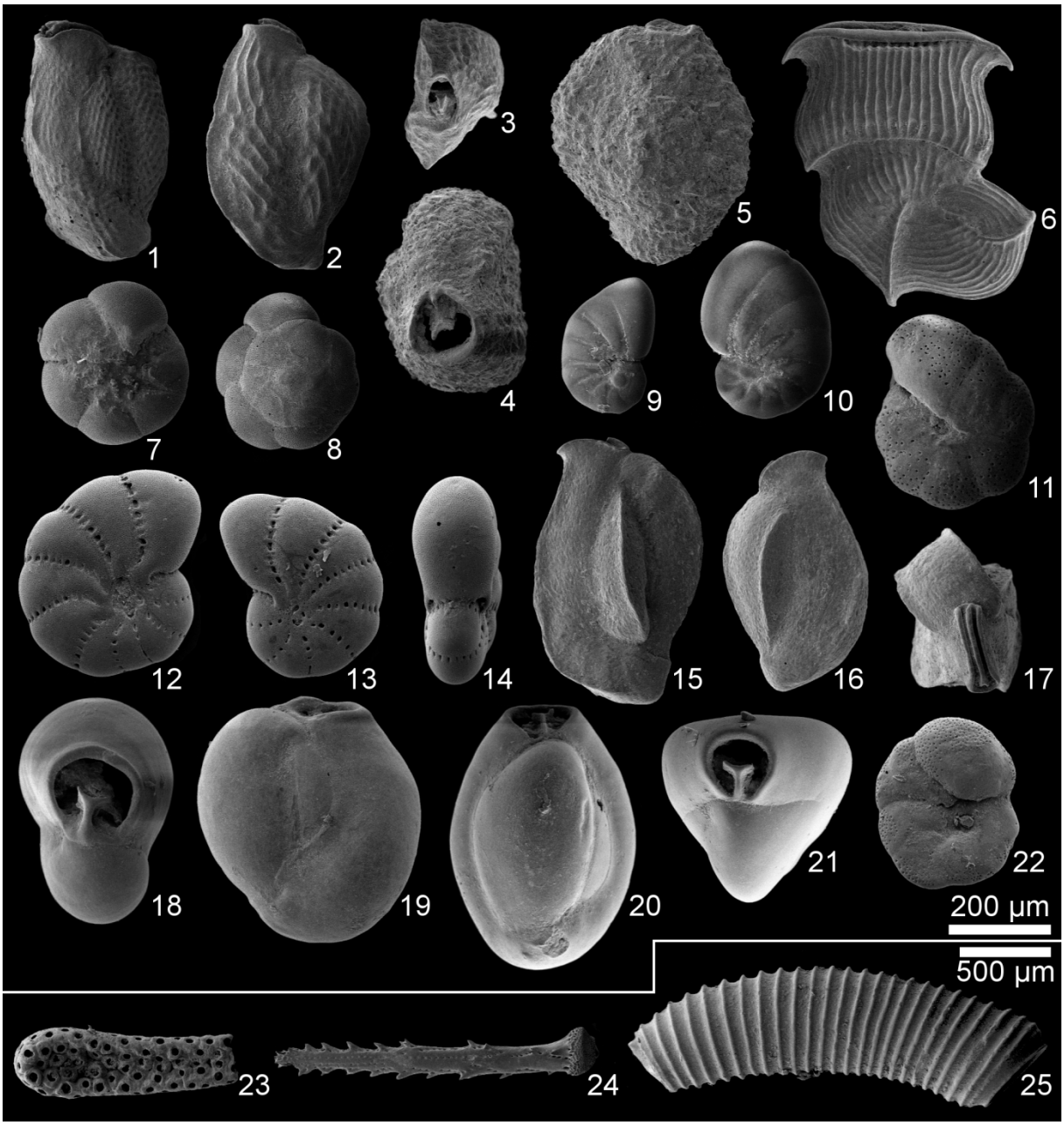

Fig. 45: Scanning electron microscope photographs of foraminifers and other faunal remains from core BBA 10. 1-3) *Affinetrina* sp.; 4-5) *Dentostomina bermudiana* (Carman 1933); 6) *Articulina mucronata* (d'Orbigny 1839); 7-8) *Ammonia beccarii* (Linnaeus 1758); 9-10) *Nonionella grateloupi* (d'Orbigny 1836); 11) *Eponides cf. antillarum* (d'Orbigny 1839); 12-14) *Cribroelphidium poeyanum* (d'Orbigny 1826); 15-17) *Quinqueloculina polygona* (d'Orbigny 1836); 18-19) *Triloculina rotunda* (Schlumberger 1893); 20-21) *Triloculina trigonula* (Lamarck 1804); 22) *Rosalina* sp.; 23) Bryozoa; 24) Echinoidea; 25) *Caecum* sp. (photographs: S. Fürstenberg, P. Frenzel).

7.5.1.3 Unit III: The landlocked lagoon (c. 3300 BP until today)

A sharp non-erosional boundary between unit II and unit III and the sudden occurrence of alkaline earth carbonates (aragonite), gypsum, and halite indicate a substantial modification of the ecosystem after the inferred tsunami impact with a maximum age of 3300 years. Evaporites precipitate from hypersaline surface waters in the order of their solubility (see listing in previous sentence). This occurs due to excess evaporation most likely related to the establishment or subaerial growth of the broad barrier of coral rubble separating Boka Bartol from the open sea. The general contribution of extreme wave events to barrier growth is indicated by lobe-like overwash structures dipping into Boka Bartol (Fig. 42A). A limited input of water is provided by torrential rains during the winter

months and low permeability of the seaward barrier. Large gypsum crystals (>1 cm) may also be the result of interstitial growth (Klosowska, 2003). Lamination reflects strong fluctuations in water input, salinity and lake level (Fig. S1 and S3). During the relatively arid winter of 2008, for instance, the lake level was more than 70 cm b.s.l., whereas after excessive rains one year later it was c. 5 cm a.s.l. based on DGPS measurements. Torrential events are reflected by laminae of clastic silt in the stratigraphy causing peaks in magnetic susceptibility, and the presence of *Cypridopsis okeechobei* (2.73 m b.s.), an ostracod genus associated with the phytal zone of freshwater to oligohaline environments (Pérez et al., 2010b). In general, faunal remains are very scarce compared to units I and II. An aragonite layer from the upper part of unit III (sample 2.74 m b.s.) contains a non-diverse ostracofauna dominated by *Perissocytheridea cribrosa*, a species highly adapted to a broad range of environments and fluctuating salinities (Keyser, 1977a). *Cyprideis beaveni* and *C. salebrosa*, also competitive in poly- and hypersaline habitats, were found as well (Benson, 1959; Keyser, 1977a). The light grey layers (Fig. S1) do not represent overwash events since foraminifers and other marine indicators (bryozoans or echinoid remains, *Caecum* sp.) are entirely absent.

Limited inflow and excess of evaporation is also reflected by core BBA 11. A whitish evaporite layer occurs at 1.33-0.44 m b.s. correlating with unit III.

7.5.1.4 Unit IV: Progradation of the alluvial fan

Unit IVa is void of large crystals of gypsum and halite and mainly consists of clastic silt delivered by the distal alluvial fan entering Boka Bartol at its landward side. This silting up process reached coring site BBA 10 around 1000 BP. Magnetic susceptibility as an indicator of terrestrial sedimentary input is increased. Only few peaks in carbonate indicate inorganic carbonate layers. The uppermost unit (IVb) represents the rapidly prograding, more proximal part of the alluvial fan with coarser and more poorly sorted sediments, and several angular stones indicating subaerial transport over short distances. The facies is purely terrestrial (erosional product of the igneous interior of NW Bonaire) and almost void of carbonate and faunal remains. We link the rapid alluvial sedimentation in post-Columbian times with “reckless cutting” of naturally grown dye-wood and later on cultivated *Guaiacum* trees (known locally as Wayaca) since the arrival of the Dutch in 1623. These activities evolved into a rigorous timber trade business in the mid-17th century, and the intense former use of today’s Washington-Slagbaai National Park for planting aloe, charcoal production as well as livestock breeding (Hartog, 1978: pp. 15 ff.). All these activities must have significantly increased erosion rates. Young alluvial infill of the tributary basin of Boka Bartol was also recorded in BBA 11 driven by the torrential channel in the east.

7.5.2 Wayaka and Boka Funchi

Sediment cores from the vicinal bokas (Boka Funchi, Wayaka) were taken in order to compare inferences on extreme wave events from the sedimentary record of Boka Bartol. The stratigraphy of landward Boka Funchi is similar to BBA 10, including dark loamy deposits of an open embayment at the bottom, possibly fringed by mangroves, which is indicated by a rising amount of organic matter. This section is vertically confined by a normally graded layer of fine carbonate sand and marine shell fragments presumably indicating a high-energy wave impact. The age 4143-3951 cal BP obtained from a *Chione cancellata* shell does not match the consistent age estimations (3300 BP or later) of unit II (BBA 10). It may either be that

(i) the graded sand sequence represents an earlier, unspecified high-energy wave event; or that

(ii) the shell used for ^{14}C dating remained c. 800 years in the sublittoral zone before dislocation by a tsunami.

Dating problems (interpretive approach [ii]) cannot be excluded, though selective formation of high-energy wave deposits (interpretive approach [i]) depending on available source material and coastal relief as well as post-depositional erosion (Szczuciński, 2012) are the main sources of uncertainty in interpreting coastal event stratigraphies. In this context, MacInnes et al. (2009a) assume that higher-relief coastlines, such as the northwestern western tip of Bonaire which is characterized by the undulating topography of the Washikemba Formation, induce net offshore sediment transport compared to net onshore sediment transport on low-lying coastlines, tantamount to a reduced probability of deposit formation after tsunami flooding in the study area.

Core WAY 1 close to the entrance of Wayaka can also be divided into a section representing a marginal marine embayment (5.70-3.64 m b.s.) correlating with unit I in BBA 10, an evaporate-rich unit representing a poly- to hypersaline closed lagoon (3.64 to c. 1.30 m b.s.) correlating with unit III in BBA 10, and sediments of both shallow water cover during rainy seasons and the prograding alluvial fan (1.30-0.00 m b.s.) related to intense land use in historical times (unit IV in BBA 10). Several subsections of the open embayment facies are enriched with bivalve shells. Whether the uppermost part of this facies (3.89-3.64 m b.s.) including its beachrock-like cap showing an upward decrease in shell remains is related to the tsunami inferred at 3300 BP or later remains uncertain.

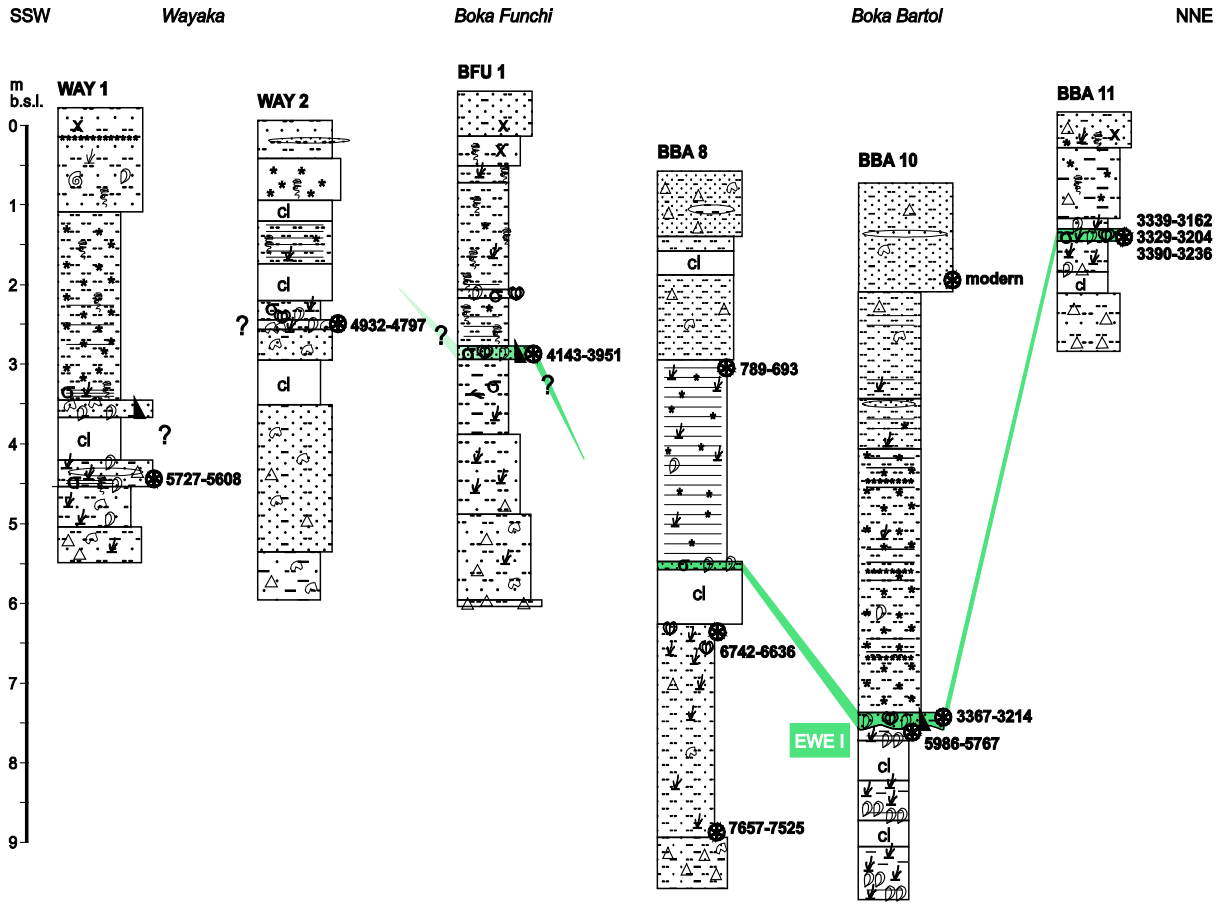

Fig. 46: Synopsis of the cores used in this study (see Fig. 43 and supplementary material) including tentative correlations of deposits of extreme wave events (EWE). A legend is provided in Fig. 43.

Similarly, WAY 2 further landward comprises an open embayment facies (2.61-2.28 m b.s.), dated to around 4800 BP and indicating the maximum Holocene transgression, a closed lagoon facies (2.28-0.47 m b.s.), and sediments of the prograding alluvial fan on top. The lowermost part of WAY 2 consists of weathered bedrock and pre-transgressive colluvial input (slope debris). Sediments related to high-energy wave impacts were not detected.

At both sites, a significant increase in salinity was inferred for some time after c. 4000 BP (Boka Funchi) and after c. 4800 BP (Wayaka). We relate this to the establishment of the barrier of coral rubble, which persists until today at both sites. Whether this barrier built up gradually or, as suggested for Boka Bartol based on the presence of a correlating *ex-situ* marine deposit (unit II), was generated by a tsunami around 3300 BP, cannot be resolved completely with the currently available data.

7.5.3 A Bonairean synthesis

Geoarchives of Washington-Slagbaai National Park on Bonaire, in particular at Boka Bartol, provide evidence for an extraordinary wave impact around 3300 BP or later, which entirely changed the coastal ecosystem and sedimentation patterns. Traces of previous high-energy wave events might have been preserved in BFU 1 and possibly WAY 1, though no precise indication on age, magnitude and type of event could be inferred. Here, we compare these findings with deposits related to extreme wave events (EWE) from the windward (Engel et al., 2010b) and leeward (Engel et al., in press) coast of Bonaire by referring to the numeration of extreme wave events (EWE) used in Engel et al. (in press) (Fig. 48).

EWE I: The oldest extreme wave deposit (EWE I) found so far in Bonaire's coastal stratigraphies is from Klein Bonaire (around 3600 BP). Any correlation of this deposit with traces from BFU 1 or WAY 1 is speculative.

EWE II: The well-preserved candidate tsunami deposit from Boka Bartol with a maximum age of 3300 BP (unit II = EWE II) has counterparts on the leeward coast (Klein Bonaire, Saliña Tam, possibly between Saliña Tam and Punt'i Wekua) and the windward coast (Playa Grandi, possibly Boka Washikemba). EWE II can be identified as the best-documented potential palaeotsunami on Bonaire.

EWE II-XI: A sequence of normally graded strata separated by thin mud laminae at Saliña Tam, spanning a time of roughly 1000 years, has been interpreted as relics of tropical cyclones (EWE III-XI).

EWE XII: EWE XII, 2000 BP or later, left massive shell-dominated deposits at Lagun (windward side) and Saliña Tam, both of which were interpreted as tsunamigenic.

EWE XIII-XV: Deposits of EWE XIII-XV exhibit the same sedimentary pattern as EWE III-XI and were also only identified at Saliña Tam, which is the only location on Bonaire where a sequence of palaeo-tempestites has been identified. The only site where thin modern deposits of marine flooding caused by hurricanes were found is Playa Grandi, representing one link in the line of arguments pro tsunami for EWE II and XII.

EWE XVI: Deposits of another younger unspecified EWE XVI (pre-500 BP) were found between Saliña Tam and Punt'i Wekua and Boka Washikemba.

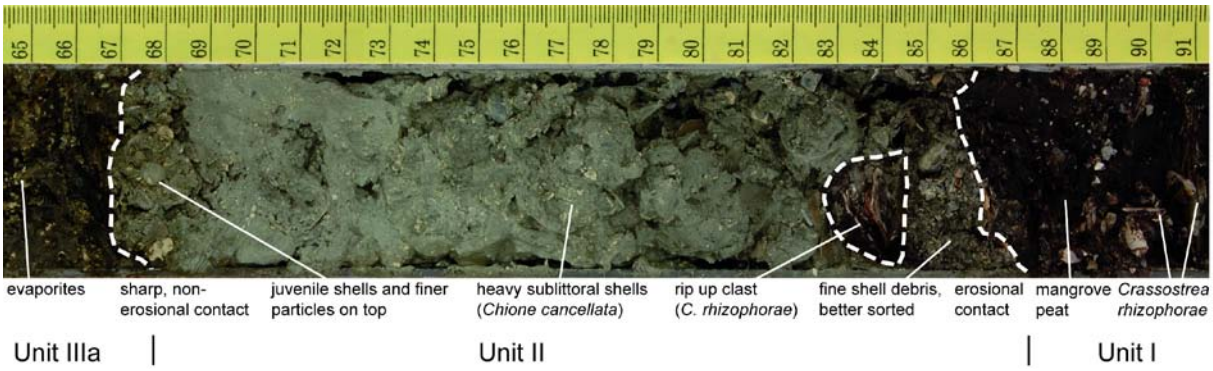

Fig. 47: Section 6.91-6.65 m b.s. (below surface) of sediment core BBA 10 (Fig. 43) showing the candidate tsunami deposit (unit II), its lower and upper boundaries and parts of the underlying and overlying units I and IIIa. The photograph depicts several sedimentary features which are often – though not exclusively – reported from tsunami deposits: erosional lower contact, varying degrees of sorting, rip-up clast or heavy ex-situ shells. It also illustrates the significant differences in sedimentation after the event (compare units I and IIIa) indicating strong and long-duration changes of the geo-ecosystem due to the final closure of Boka Bartol.

The coastal coarse-clast record on Bonaire indirectly supports the interpretation that some overwash sand layers on Bonaire were deposited by palaeotsunamis since storm waves were ruled out for dislocation of the largest blocks (Scheffers, 2002, 2004, 2005; Watt et al., 2010; Engel and May, 2012). Uncertainties in age estimations of the sandy overwash layers based on ^{14}C, which mainly include the possibility that the age of the dated object within a marine flooding deposit does not represent the age of the depositional process and fluctuations of the reservoir effect, are even more severe when coarse-clast objects (e.g. coral rubble) are used for dating. Lacking stratigraphical contexts hamper the correlation of boulders and depositional units of coral rubble. However, a dataset of 32 U-Th datings of coral rubble deposited during the Cyclone Hamish (2009) showed clustering ages of only 20-170 years (J.-X. Zhao, pers. comm.) indicating that a large number of datings from the same depositional unit potentially reduces uncertainties. Scheffers (2005) tentatively clustered uncalibrated ^{14}C and ESR data derived from coarse-clast deposits on Bonaire and inferred tsunamis around 4300 BP, 3900 BP, 3300 BP, 1200 BP, and 500 BP (Fig. 48). Before calibration using a homogeneous reservoir error and statistical analysis of the dataset definite correlation with the stratigraphical data presented in this study is not possible. However, it is evident, that a high amount of dead coral material from the 4^{th} millennium BP has been transported onshore, possibly during EWE II.

7.5.4 A Caribbean synthesis

Geological evidence for palaeotsunamis in the Caribbean region is manifold and comprises:

(i) Mass wasting processes at the continental margin, e.g. east of Trinidad and Venezuela (Moscardelli et al., 2010);

(ii) signs of potentially tsunami-triggering submarine mass failures in the coastal zone, e.g. on Curaçao (Hornbach et al. 2010);

(iii) flank-collapse structures and associated debris avalanches, e.g. off the coast of St. Vincent (Le Friant et al., 2009);

(iv) coarse-clast coastal deposits on Bonaire (see *Chapter 7.5.3*) and other islands (e.g. Kelletat et al., 2004; Scheffers and Kelletat, 2006; Khan et al., 2010).

We reviewed published Holocene stratigraphical records for potential tsunami deposits (Table S1, Fig. 40) in order to initiate the work on a synoptic regional palaeotsunami history. Thereby, we generally relied on the authors' interpretation of the sedimentary record. Stratigraphical contexts thus far represent the most promising archives for age inferences and the establishment of event chronologies. For the Caribbean, a large number of palaeoenvironmental studies based on coastal stratigraphies exist, but tsunamis have only rarely been considered as sediment suppliers or processes capable of generating erosional hiatuses. Thus, not much is known about prehistoric tsunami recurrence intervals or the spatial distribution of their impacts (Fig. 48).

On Puerto Rico in the northern Caribbean (site 12 in Figs. 40 and 48), Moya and Mercado (2006) found three marine overwash deposits in a sediment sequence of a coastal swamp, all of which were linked to tsunamis. Maximum ages for these events were inferred from two ^{14}C ages to be about 2770-2350 BP and 680-540 BP, whereas the youngest deposit was associated with the regional tsunami of 1918 (cf. O'Loughlin and Lander, 2003).

A thorough multi-proxy study of disturbed beach ridges and backbarrier sediments of Anegada, British Virgin Islands (site 15), either points to the impact of a known tsunami (Antilles tsunami 1690 or Lisbon teletsunami 1755), a previously undocumented tsunami, or a storm surge with a greater magnitude than the most severe hurricane of the past decades (Atwater et al., 2011).

Studies from the northwestern Lesser Antilles and the Antilles island arc are scarce. Malaizé et al. (2011) present proxy records from a coastal pond on St. Martin (site 19) containing several marine overwash deposits. These carbonate sand layers were linked to phases of increased storminess. However, tsunamis are not entirely excluded by the authors.

Weiss (1979) reports an *ex-situ* sandy mud deposit from Cayo Sal (site 22), off the coast of Venezuela in the southern Caribbean, likely to be associated with a tsunami. Age constraints are imprecise. Calibration of the ^{14}C ages using Calib 6.0.1 (Reimer et al., 2009) indicates that the deposit derives from an event of the last 600 years.

A palaeoenvironmental record from St. Michiel lagoon on Curaçao (site 24) indicates an abrupt closure by a barrier of coral rubble during an extreme wave event. This observation is similar to inferences from Boka Bartol in this study. ^{14}C ages indicate a closure around 3500 BP (or later), possibly due to a tsunami (Klosowska, 2003).

An underwater sediment core from Spaanse Waters bay, also on Curaçao (site 25), contains a "chaotic mixed layer", 460-310 cal BP (or younger), which was linked to a tsunami by Hornbach et al. (2008: p. 44).

A sand layer buried in a swamp lagoon on the Caribbean coast of Nicaragua (site 27) is inferred to be the result of flooding during a hurricane since no historical accounts on tsunamis are available for the area. The deposit dates to 3680-3490 cal BP (or later) (Urquhart, 2009). However, one single marine overwash deposit in an 8000-yr peat sequence in an area where strong hurricanes occur frequently (and do not regularly provide marine sediment input), but tsunamis have never been reported in historical times, does not necessarily exclude the impact of a major far-field tsunami.

From the Dominican Republic, sand deposits associated with the historical tsunamis of 1751 and 1946 were reported by Scheucher et al. (2011). On Isla de Culebrita, east of Puerto Rico, Donnelly (2005) documents several marine overwash events within a salt pond stratigraphy referring to intense hurricanes. The uppermost sand layer is linked to a category 4 hurricane in 1867 rather than the 1867 Virgin Island Tsunami by the author. The salt pond on the northwestern tip of Culebrita is

located in the lee of the propagating tsunami of 1867, which was generated 20 km south of the island. Age estimates are based on extrapolation of ^{14}C data.

In the Caribbean, local, regional, and far-field tsunamis occur. Major earthquake-induced events (far-field tsunamis) potentially affect large parts of the Caribbean, as for instance the 1867 Virgin Islands Tsunami for which historical accounts and models of run-up >0.5 m comprise the entire area between Puerto Rico, the Antilles island arc, and Venezuela (O'Loughlin and Lander, 2003; Zahibo et al., 2003). The high magnitude and broad spatial impact of teletsunamis generated in the east Atlantic basin has been historically proven by the 1755 Lisbon Tsunami (O'Loughlin and Lander, 2003). It is furthermore indicated by extraordinary coarse-clast accumulations concentrated along the east coasts of several of the eastern Lesser Antilles (e.g. Barbados, Anguilla) as well as Long Island and Eleuthera (Bahamas) (Kelletat et al., 2004; Scheffers and Kelletat, 2006). In contrast, most tsunamis from submarine landslides or lower-magnitude earthquakes may only affect a very small area. Thus, many deposits are likely to indicate local and regional tsunamis only and a Caribbean-wide correlation of candidate tsunami deposits would only work for major events.

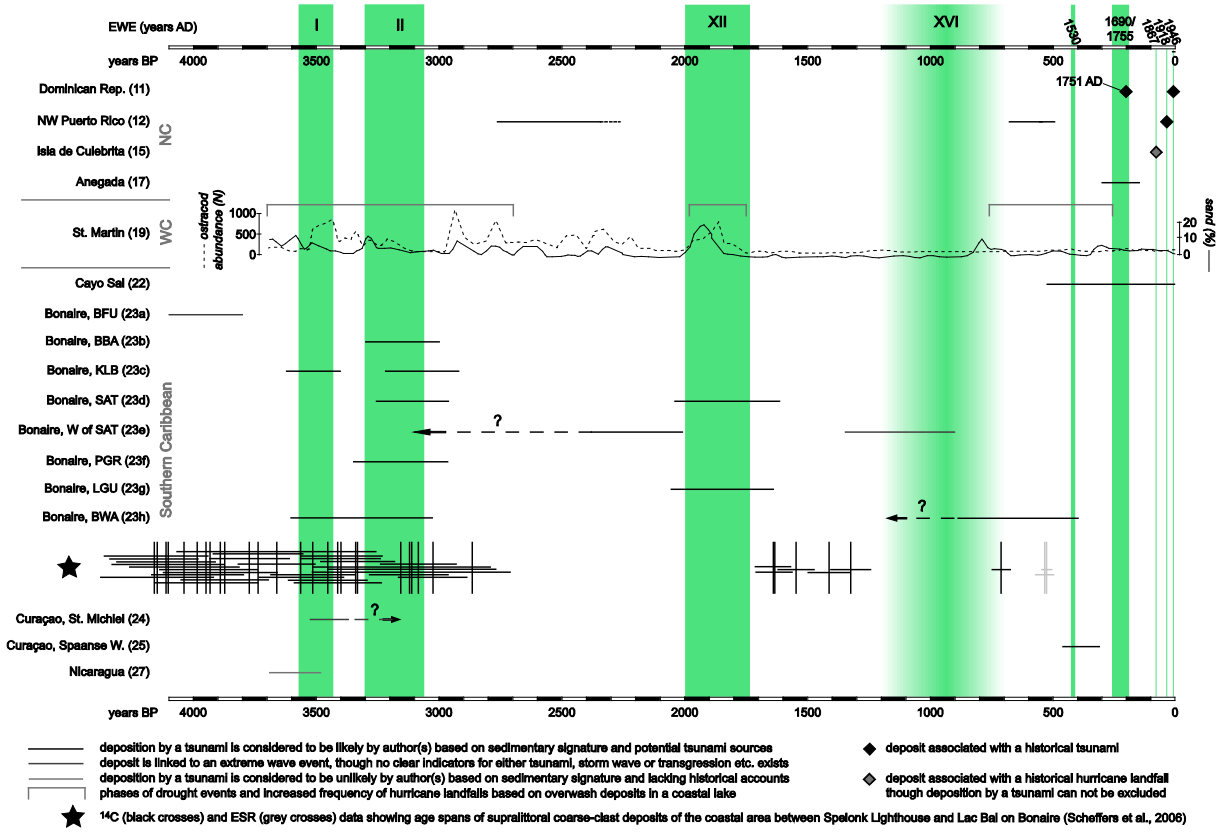

Fig. 48: Compilation of published Holocene stratigraphical records of the Caribbean region where deposition by tsunamis is considered to be likely or at least discussed by the authors and where chronological information is available. Radiometric ages of the coarse-clast record of Bonaire (Scheffers et al., 2006) is also shown (black star). Green bars labelled as EWE (extreme wave event) I, II, XI and XVI (for numeration see text and Engel et al., in press) mark potential palaeotsunamis inferred from the stratigraphical record of Bonaire. WC = Western Caribbean; NC = Northern Caribbean; 11 = Scheucher et al. (2011); 12 = Moya and Mercado (2006); 13 = Donnelly (2005); 16 = Atwater et al. (2011); 19 = Malaizé et al. (2011); 22 = Weiss (1979); 23a-b = this study; 23c-e = Engel et al. (in press); 23f-h = Engel et al. (2010b); 24 = Klosowska (2003); 25 = Hornbach et al. (2008); 27 = Urquhart (2009). Study sites are indicated in Fig. 40.

From a southern Caribbean perspective, correlations can be established for the possible tsunami inferred at St. Michiel (Klosowska, 2003) and EWE I or II on Bonaire. Likewise, the singular sand layer

reported by Urquhart (2009) could be related to EWE I or II. Furthermore, younger deposits at Cayo Sal (Weiss, 1979), Spaanse Waters, Curaçao (Hornbach et al., 2008) and Boka Washikemba, Bonaire (*Chapter 4*; Engel et al., 2010b), may stem from one and the same event (EWE XVI). A possible candidate is the tsunami of 1530, which affected almost the entire northern coast of Venezuela according to historical accounts (O'Loughlin and Lander, 2003).

It is remarkable, that phases of increased hurricane activity on St. Martin, inferred by Malaizé et al. (2011) from marine overwash deposits, chronologically coincide with deposits of EWE II and XII on Bonaire, both interpreted as palaeotsunamis (Fig. 48). However, due to a lack of further sedimentary evidence from western and southern Caribbean coastal archives, it remains open if both localities store sediments of the same regional or far-field events. Hence, further palaeotsunami studies are urgently needed in order to reconstruct long-term patterns of frequency, magnitude and spatial impact of tsunamis in the Caribbean.

7.6 Conclusions

We present the sedimentary record of three saline lagoons (bokas) of NW Bonaire, which are separated from the open sea by broad barriers of coral rubble. At Boka Bartol, four distinct sedimentary environments and processes were identified:

Unit I: Open embayment fringed by mangroves.

Unit II: High-energy wave event destroying the mangroves and probably resulting in the establishment of a barrier of coral rubble separating the embayment from the sea and transforming it into a high-salinity lagoon.

Unit III: Poly- to hypersaline lagoon with fluctuating hydrochemistry.

Unit IV: Silting up of the lagoon indicated by an active prograding alluvial fan.

The sites of Boka Funchi and Wayaka reflect a similar environmental history, even if they do not provide clear evidence for extreme wave impacts. Although no sedimentary criterion exists, which unambiguously evidences tsunami deposition (Switzer, 2010), unit II (Fig. 47) was interpreted as tsunamigenic based on the parallel occurrence of a set of signatures often associated with modern tsunami sediments (e.g. Mamo et al., 2009; Goff et al., 2012):

(i) The presence of allochthonous reefal bivalve shells including articulated specimen and shell fragments with predominantly angular breaks;

(ii) marine geochemical (CO_3^{2-}) and non-terrestrial geophysical (magnetic susceptibility) sediment properties;

(iii) a basal unconformity → large hiatus according to ^{14}C ages of BBA 10;

(iv) a fining-up sediment pattern (grain size means);

(v) the lack of sediment deposition at BBA 10 during recent high-category hurricanes;

(vi) significantly increased abundance and diversity of ostracods and foraminifers including brackish to open marine taxa;

(vii) foraminiferal taxa from the deeper shelf, which indicate a partial sediment source below the storm wave base;

(viii) a proximal sediment source in the lower part (shallow marine and lagoonal microfaunal taxa) and increased microfossil diversity in the upper part including deeper dwelling taxa, which reflect the final suspension stage of tsunami sedimentation.

Unit II is dated to 3300 BP or shortly after according to four remarkably similar ^{14}C ages of different materials from two different cores. This supports the tentative local tsunami chronology of two well-documented events with maximum ages of 3300 BP (EWE II) and 2000 BP (EWE XII) based on coastal stratigraphical records (Engel et al. 2010b, in press, this study). An event with a maximum age of 3600 BP (EWE I) was only documented on Klein Bonaire. Another one with a maximum age of 1300 BP (EWE XVI) was identified west of Saliña Tam. A high-energy wave deposit at Boka Washikemba may correspond either to EWE XVI, an unknown event, or the historical tsunami of 1530 AD. Based on these results, a preliminary estimation of the recurrence interval of high-energy wave events on Bonaire, which reveal magnitudes significantly exceeding those of recent high-category hurricanes and which are therefore likely to be major tsunamis, is in the order of roughly 1000 years or less.

This study confirms that the sedimentary record of tsunamis is very site-dependant and difficult to predict as also indicated by modern deposits (e.g. Szczuciński, 2012). Even though the stratigrapical order of the lagoonal geoarchives provides a more promising context for radiocarbon dating event layers than subaerial coarse-clast deposits, a larger number of investigated archives are required to infer a palaeotsunami chronology. The review of fine sediment-based palaeoenvironmental records of further Caribbean sites revealed that tsunamis as depositional or erosional processes were considered in very few cases only. For the southern Caribbean, records from Cayo Sal (cf. Weiss, 1979) and Curaçao (Klosowska, 2003; Hornbach et al., 2008) were tentatively correlated with data from Bonaire. Thus, further palaeotsunami studies using well-dated coastal deposits are required to reconstruct reliable patterns of magnitude and frequency of palaeotsunamis in the Caribbean. To date, known palaeotsunami deposits from the Caribbean probably represent a fraction of real prehistoric tsunamis only, and may be solely reflecting major tsunamis inundations.

7.7 Supplementary material

Fig. S1: Photograph of sediment core BBA 10. For geographical contexts see Figs. 41 and 42 in the main text. Sedimentary documentation and proxy data are shown in Table 11 and Fig. 43 (main text).

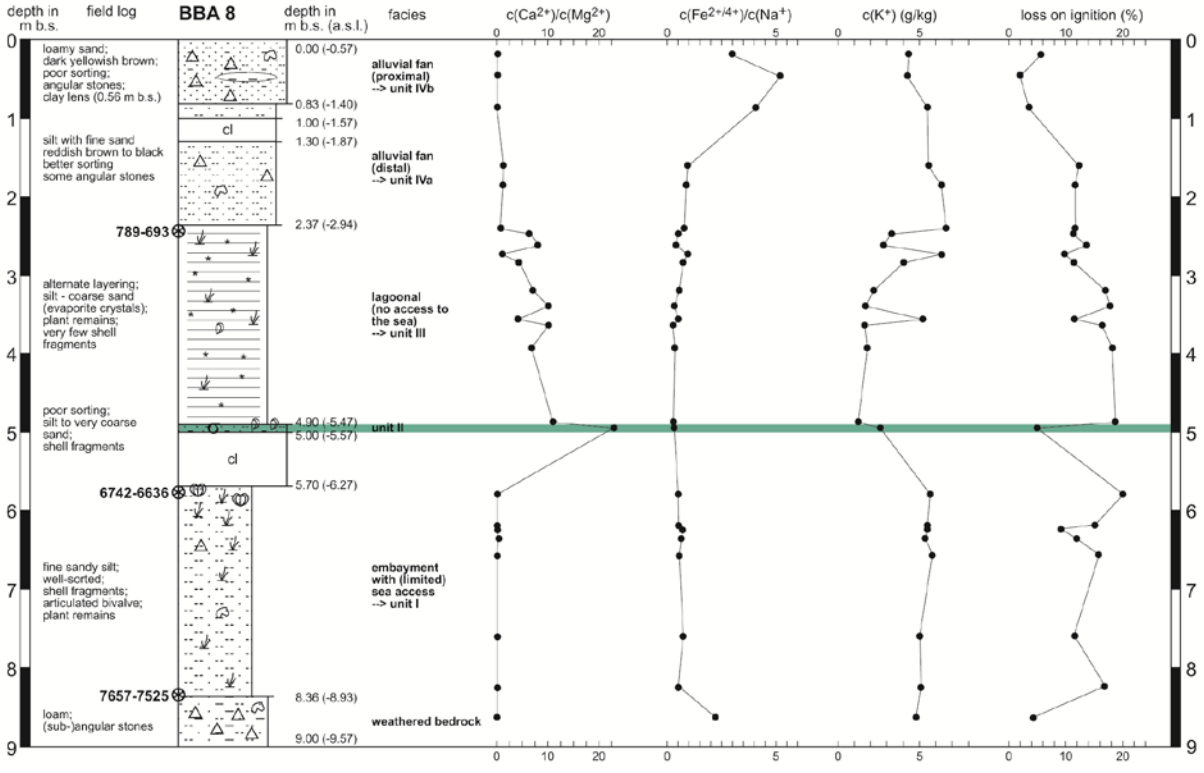

Fig. S2: Field log, stratigraphical interpretation and proxy data of BBA 11 (modified after Engel et al., 2009a). The stratigraphy is well comparable to mastercore BBA 10. For geographical contexts see Figs. 41 and 42 in the main text. For details on proxy data see Engel et al. (2009a).

Fig. S3: Photograph of sediment core BBA 8. For geographical contexts see Figs. 41 and 42 in the main text. Sedimentary documentation and proxy data are depicted in Fig. S2.

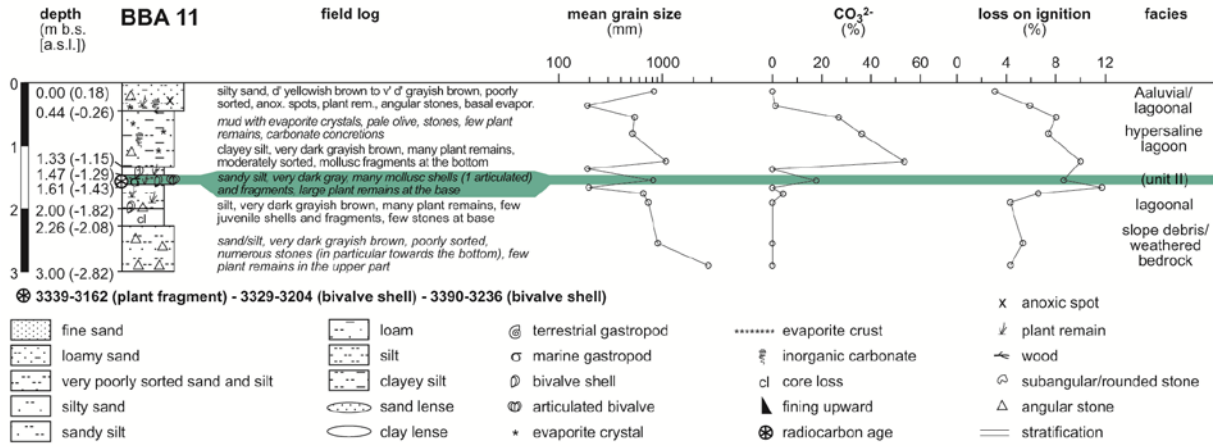

Fig. S4: Field log, stratigraphical interpretation and proxy data of BBA 11. For geographical contexts see Figs. 41 and 42 in the main text.

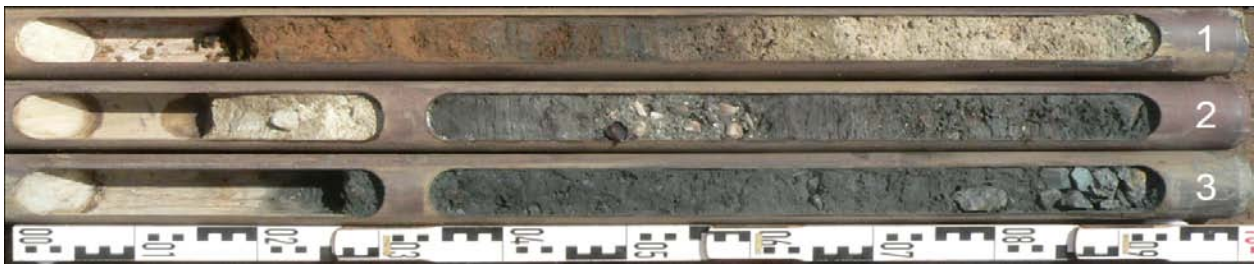

Fig. S5: Photograph of sediment core BBA 11. For geographical contexts see Figs. 41 and 42 in the main text. Sedimentary documentation and proxy data are depicted in Fig. S4.

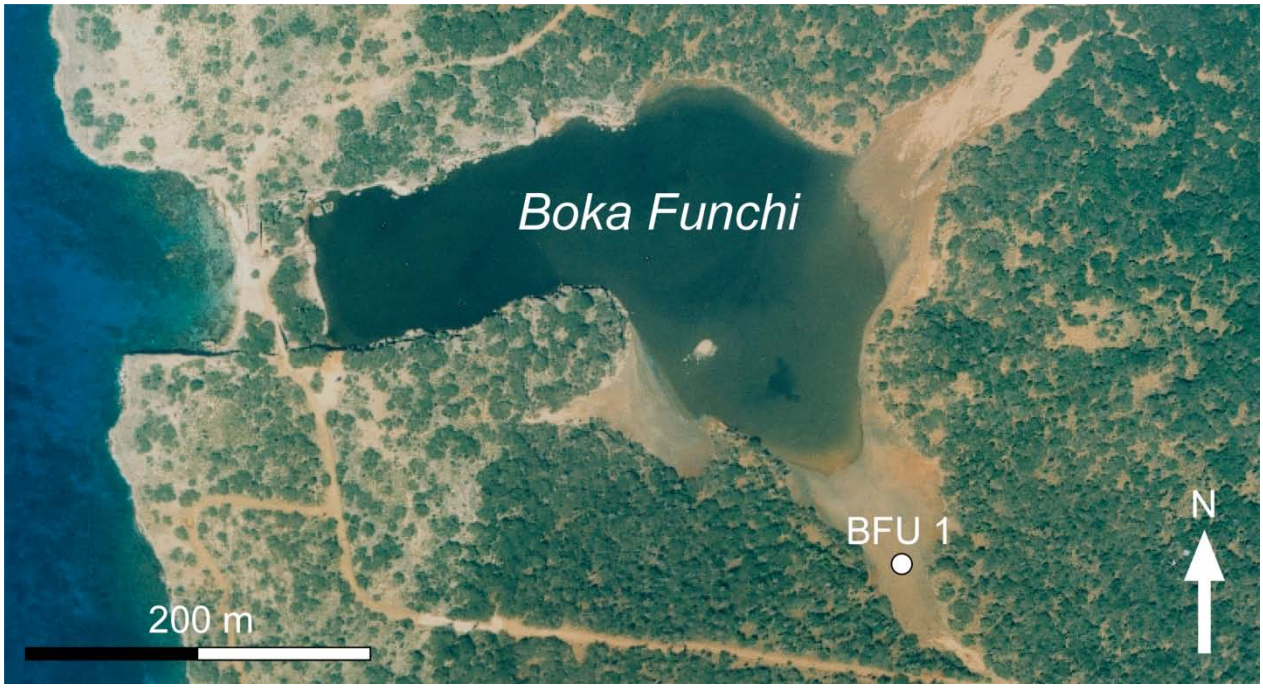

Fig. S6: Aerial photograph of Boka Funchi (1996) showing site BFU 1. For geographical contexts see Fig. 41 (main text).

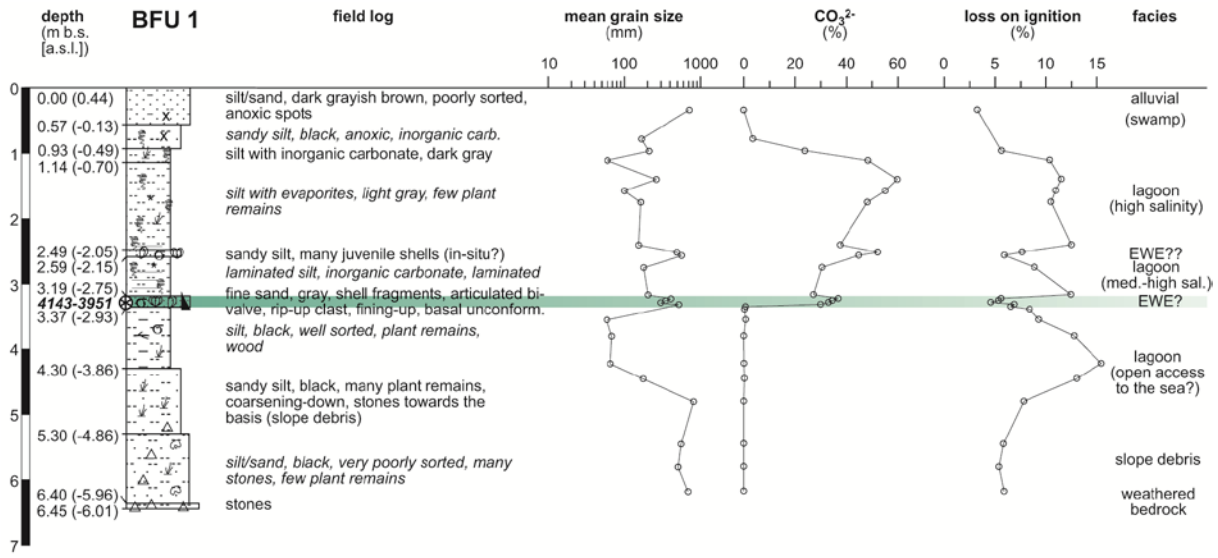

Fig. S7: Field log, stratigraphical interpretation and proxy data of BFU 1. For geographical contexts see Figs. 41 (main text) and S6.

Fig. S8: Photograph of sediment core BFU 1. For geographical contexts see Figs. 41 (main text) and S6. Sedimentary documentation and proxy data are shown in Fig. S7

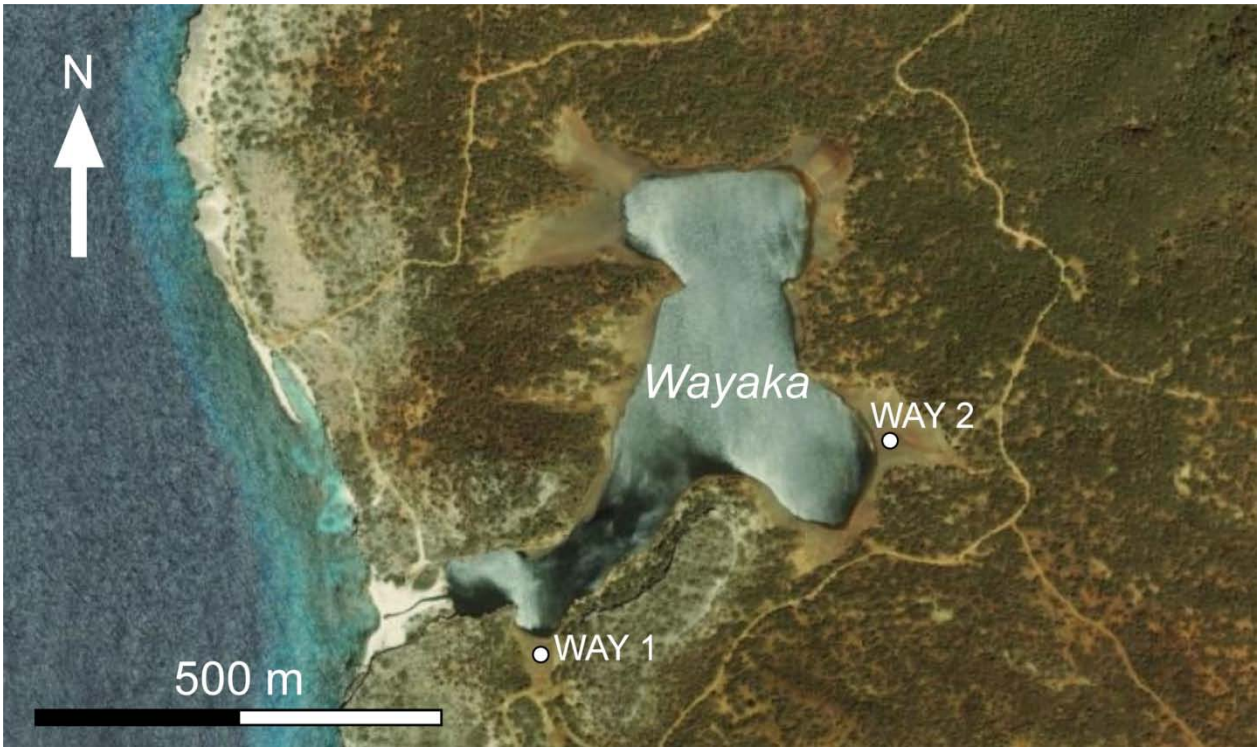

Fig. S9: Google Earth image of Wayaka indicating sites WAY 1 and WAY 2. For geographical contexts see Fig. 41 (main text).

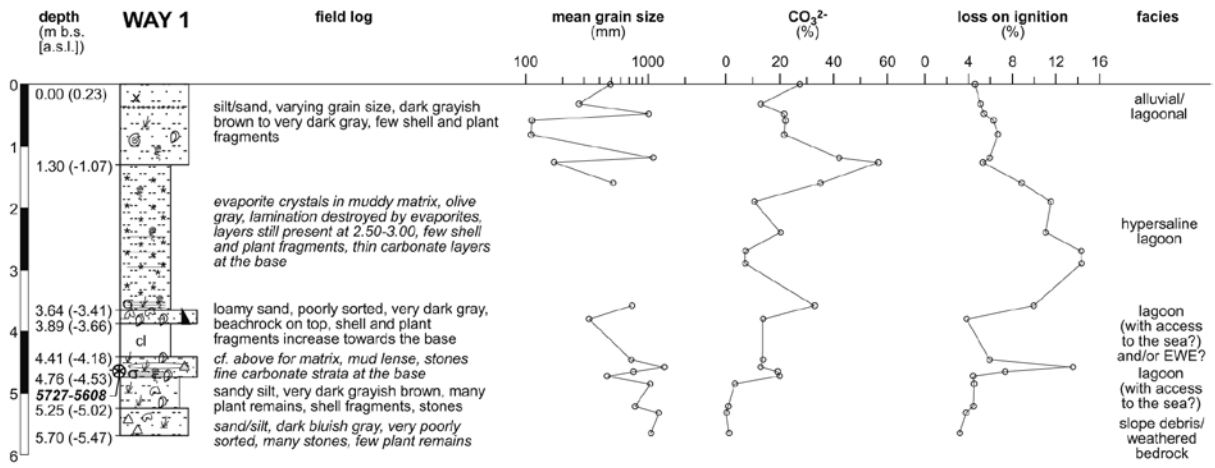

Fig. S10: Field log, stratigraphical interpretation and proxy data of WAY 1. For geographical contexts see Fig. 41 (main text) and Fig. S9.

Fig. S11: Photograph of sediment core WAY 1. For geographical contexts see Figs. 41 (main text) and S9. Sedimentary documentation and proxy data are shown in Fig. S10.

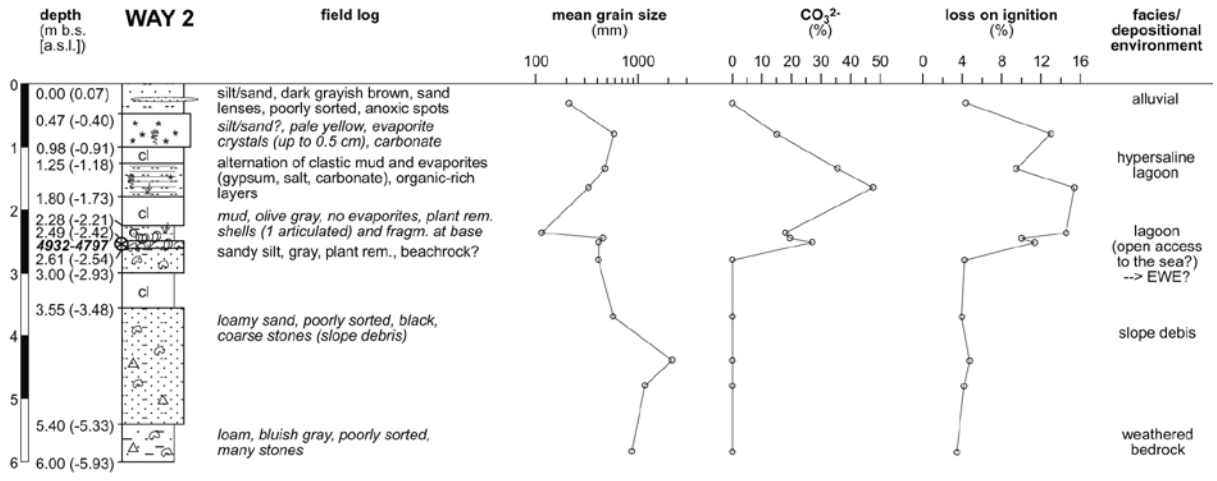

Fig. S12: Field log, stratigraphical interpretation and proxy data of WAY 2. For geographical contexts see Fig. 41 (main text) and Fig. S10.

Fig. S13: Photograph of sediment core WAY 2. For geographical contexts see Figs. 41 (main text) and S9. Sedimentary documentation and proxy data are shown in Fig. S12.

Table S1: Sediment-based reconstructions of palaeoenvironments and processes reviewed for evidence of extreme wave events. All sites are indicated in Fig. 40 (main text). For all sites, the 30-yr probability of tsunami run-up >0.5 m (Parsons and Geist, 2009), the calculated amplitude of the Virgin Island Tsunami of 1867 (Zahibo et al., 2003), and the decadal number of hurricanes (Reading, 1990) is shown.

No.	Author(s)	Goal of the study	Location	Time covered by the sediment archive (years BP)	Type of sediment archive	Evidence for extreme wave events	30-year prob. of tsunami run-up > 0.5 m	Amplitude 1867 tsunami	De-cadal num-ber of hurri-canes
1	McCloskey and Keller (2009)	Reconstruction of palaeotempestol.	Gales Point/Mullins River (Belize)	5000-0	Swamp/ marsh	Hurricanes inferred, since absence of historical accounts on tsunamis	0 (Belize City)	-	5-9
2	McKee et al. (2007)	Reconstructing rates of peat formation	Twin Cays (Belize)	c. 5600-0	Man-grove island	Sand lenses interpreted as shoreline migration	0 (Belize City)	-	5-9
3	Gischler (2003)	Reconstructing lagoonal develop-ment	Turneffe Islands, Glovers Reef, Lighthouse Reef (Belize)	8500-0	Man-grove island, shallow reef	Shell beds interpreted as reworking by storms and/or bioturbation, e.g. approx. 4500 BP ago	0 (Belize City)	-	5-9
4	Monacci et al. (2009)	Reconstructing mangrove dynam-ics	Spanish Lookout Cay (Belize)	8000-0	Man-grove island	Continuous peat record, no disturbance detected	0 (Belize City)	-	5-9
5	Woodroffe (1981)	Spatio-temporal reconstruction of marine transgres-sion	North Sound (Grand Cayman)	more than 2100-0	Man-grove swamp	No extreme wave impact inferred	10.79	-	10-14
6	Peros et al. (2007)	Reconstructing palaeoenvironmen tal change	Laguna de la Leche (Cuba)	c. 8000-0	Coastal lake	No extreme wave impact inferred	c. 0	-	10-14
7	Hendry (1987)	Determining tectonic and eustatic influence on sedimentation	The Great Morass (NW Jamaica)	Holocene	Sublit-toral, beach, wetland	No extreme wave impact inferred	c. 5	-	5-9
8	Palmer and Burn (2011)	Identifying marine washover events	Manatee Bay (Jamaica)	"Millenni-al scale"	Enclosed lagoon	Several overwash strata, overwash fan in the E	c. 22	-	5-9
9	Dix et al. (1999)	Reconstructing palaeoenvironmen tal change	Lee Stocking Island (Bahamas)	1500-0	Shallow ponds	Possible storm surge overwash inferred from *ex-situ* marine deposits	c. 0	-	10-14
10	Park et al. (2009)	Evaluating ecologi-cal response to hurricane impacts	San Salvador Island (Bahamas)	>1300-0	Shallow pond	Tsunami overwash possible, but considered to be unlikely, due to lack of modern tsunami deposition and presence of correlating freshening (rainwater input); 19 events marked by peaks in sand	c. 3-5	-	10-14
11	Scheucher et al. (2011)	Detecting tsunami deposits and foraminiferal characterization	a) Puerto Viejo (SW Dominican Rep.); b) Playa Cosón (NE Dom. Republic)	a) 300-0? b) ?	Beach (?)	Sand layers are ascribed to Oct 1751 (a) and 8 Aug 1946 (b) tsunamis	a) 5-7; b) c. 10	0.3-0.4 (Santo Domingo, southern coast)	a) 5-9; b) 10-14
12	Moya and Mercado (2006)	Reconstructing pre-historical tsunamis	Aguadilla—Rincón (NW Puerto Rico)	>2500-0	swamps	Overwash deposits correlated with (post-) 2770-2350 BP, (post-) 680-540 BP, and Oct 1918 tsunamis	c. 10-20	Run-up 11 Oct 1918 tsunami: 3-5 m	10-14
13	Morton et al. (2006)	Evaluating coastal hazards using sedimentary records	a) NW Puerto Rico; b) SE Puerto Rico; c) NW Basse-Terre (Guadeloupe)	?	Coastal plains and wetlands	a+b) 1-2 thin tsunamigenic sand layers in various depths at different locations, no datings; c) no marine overwash identified	a) c. 5; b) c. 12-15 ; c) c. 10-12	c) 0.6-1.6 m (Basse-Terre)	10-14
14	Donnelly and Woodruff (2007); Woodruff et al. (2008)	Reconstructing fluctuations in Hurricane frequen-cy	SW Vieques, Puerto Rico	5000-0		Periodic hurricane overwash inferred; tsunamis excluded	c. 15	3.0-3.5 m tsunami ampitude (SE coast of Vieques), 3 main waves within 30 min.	10-14
15	Donnelly (2005)	Reconstructing severe cyclones	Isla de Culebrita (Puerto Rico)	2200-0	Back-barrier salt pond	Massive sand layer interpreted as 1867 hurricane-borne; 1867 tsunami also possible	c. 15	6.1 m at adjacent Culebra	10-14

16	Brooks et al. (2007)	Identifiying human influence on sedimentation	Coral Bay (St. John, USVI)	>5000-0	Marginal marine embay-ment	No extreme wave impact inferred	13.85 (Road Town, BVI)	3.2-7.5 m (Cruz Bay, St. John)	10-14
17	Atwater et al. (2011)	Identifying marine overwash	Central and W Anegada (BVI)	c. 400-0	Coastal ponds	Tsunami or storm overwash inferred at 1650-1800 AD	c. 10-15	2.3-5.2 m (Road Town, Tortola)	10-14
18	Jessen et al. (2008)	Reconstructing palaeoenvironmen ts	Altona Bay (St. Croix, USVI)	c. 4500-0	Lagoon	One event inferred, post-1960 AD, hurricane	c. 10-15	3.0-3.9	10-14
19	Bertran et al. (2004) ; Malaizé et al. (2011)	Determining in hurricane frequen-cy	Grand-Case (St. Martin)	c. 4000-0	Coastal pond	Up to 21 event layers; sand layers ascribed to hurricanes (authors "cannot exclude that some sand layers corre-spond to tsunamis")	c. 3-5	Run-up 1867 tsunami: c. 1.5 m	10-14
20	Caron (2011)	Evaluating the preservation potential of extreme wave deposits by beachrock	St. Bartholomew (Guadeloupe)	?	Beach-rock	Considered as unlikely to be tsunamigenic	< 10	-	10-14
21	Ramchara n (2004); Ramchara n and MacAn-drews (2006)	Reconstructing Holocene wetland development	Maracas Bay (Trinidad)	7000-0	Swamps	No marine sedimentary impact	0 (Port-of-Spain)	0.5-1.2 (Port-of-Spain)	5-9
22	Weiss (1979)	Sedimentological and geomorpho-logical characteri-zation	Cayo Sal (Vene-zuela)	3800-0	Enclosed lagoon	Hurricane or tsunami is suggested to have dis-turbed sedimentation of Cayo Sal, 770-500 BP	c. 3-5	0.6-0.8 m (Puerto Cabello)	2-4
23	Engel et al. (2010, in press, this study)	Evaluating the impact of extreme wave events on Holocene coastal ecosystems	Bonaire	8000-0	Enclosed lagoons, flood-plains	Potential tsunamis inferred for 3600 or later, 3300 or later, 2000 BP or later, plus one younger event	c. 7 (Willem-stad, Cura-çao)	0.1-0.8 m	2-4
24	Klosowska (2003)	Reconstructing coastal palaeoenvironmen ts	Lagoon St. Michiel (Curaçao)	5000-0	Saline lagoon	Rapid closure of lagoon at around 3500 BP might be related to tsunami impact	c. 5-10	-	2-4
25	Hornbach et al. (2008)	Reconstructing storm and tsunami events	Spaanse Waters, Lagoen Jan Thiel, Fuik Bay (Curaçao)	c. 1000-0	Sheltered coastal embaym ents	Surface Halimeda sand attributed to recent storms; "chaotic mixed" layer (460-310 cal BP) interpreted as tsunamigenic	7.04 (Willem-stad)	Negligible	2-4
26	González et al. (2010)	Reconstructing mangrove dynam-ics	Bahia Honda (San Andres, Colombia)	c. 3000-0 (hiatus from c. 2500-500/400)	Man-grove embay-ment	Major erosive disturbance event: 1605 hurricane?	c. 3	Negligible	2-4
27	Urquhart (2009)	Evaluating man-grove response to hurricane impacts	Laguna Negra, SE Nicaragua	8000-0	Lagoon, 17 km from the coast	Tsunami or hurricane (post-)3340 +/-40 BP	0	0-0.2 m (Puerto Cabezas)	2-4

8 Holocene sea levels of Bonaire (Leeward Antilles) and tectonic implications*

Abstract: Future relative sea level (RSL) rise is one of the most serious coastal hazards worldwide, in particular in the Caribbean region. RSL is a function of global (glacioeustasy, steric effect), regional (e.g. glacioisostatic adjustment [GIA], gravitational effects inducing deformation of the earth, upper/lower mantle viscosity etc.) and local (lithosome compaction, vertical neotectonic movement) factors which are connected via a complex pattern of interference. Information on past RSL supports inferences on upper limits of ice shield ablation, estimates of anthropogenic contribution to historical and future RSL rise and calibration of rheological models of the earth. We present the first RSL curve for the island of Bonaire (southern Caribbean). Forty-two ^{14}C ages from 20 sediment cores taken from nine different sedimentary archives along the coast were used. The sedimentary environment of each index point was linked to a palaeo-water depth based on literature and field observations. The index points trace a local RSL history of decelerating rise since 7000-6000 years ago and subsequent asymptotical approximation, similar to existing RSL curves from Curaçao and Venezuela. The results were compared to a simulation of Holocene sea level history (reference model) which considers global effects and regional GIA (including consequences for geopotential and vertical position of earth surface). Even though the central and northwestern parts of Bonaire experienced slow tectonic uplift of up to 50 cm since the Mid-Holocene and tentative correction for compaction was applied, the new RSL curve for Bonaire runs slightly below the reference model. A further outcome of this study is the detection of an unmapped micro-graben structure with a vertical slip rate of c. 1.5 mm yr^{-1} at Boka Bartol, which was identified based on depth discrepancies of well-dated isochronous high-energy wave deposits.

Keywords: *Local relative sea-level, Bonaire, Southern Caribbean, Mangrove peat, Holocene stratigraphy, Vibracoring*

8.1 Introduction

Sea level change is defined as a variation of the level of the sea compared to land, triggered by either fluctuations of water volume in ocean basins or vertical movement of landmass (Lambeck, 2002). Thus, it is often referred to as relative sea level (RSL) change. Today, the rising RSL is one of the most serious coastal hazards worldwide (Church et al., 2008; Milne et al., 2009). Caribbean islands are particularly under threat, since the majority of settlements, economic activities, industrial areas and infrastructure is located at or near the coast. Rising RSL increases the hazard posed by the frequent tropical cyclones in the Caribbean, locally known as hurricanes (McGregor and Potter, 1997; Biasutti et al., 2011).

The relevance of palaeo-RSL data, i.e. sea level reconstructions based on the sedimentary or geomorphological record, for projections of future RSL rise lies in possible inferences on upper limits of

* This chapter is based on: Engel, M., Brückner, H., Scheffers, A., May, S.M., Kelletat, D., subm. Holocene sea levels of Bonaire (Leeward Antilles) and tectonic implications. Zeitschrift für Geomorphologie N.F.

ice shield ablation, which used to be the most important determinant of sea level rise in late Pleistocene to early Holocene times (Milne et al., 2009). Furthermore, palaeo-RSL data

(i) provide information on the "preindustrial context" of sea-level evolution supporting estimations of present and future anthropogenic impact on sea-level rise (Gehrels et al., 2011: p. 289);

(ii) represent a reference for glacial isostatic adjustment (GIA) (Wahr and Davis, 2002);

(iii) are used for filtering eustatic and steric effects from satellite and tide gauge data (Church and White, 2006);

(iv) support the calibration of rheological models of the earth (Lambeck, 2002).

Post-LGM (Last Glacial Maximum) change of RSL is the result of many factors (see *Chapter 8.2.2*), including those of purely local significance. Hence, individual reconstructions of RSL change on a local scale based on local evidence are necessary (Vött, 2007). This paper presents the first Holocene RSL curve for Bonaire based on mangrove peat and other coastal deposits, filling a significant knowledge gap of the regional sea level history of the southern Caribbean. Accurate information on local RSL changes is an essential prerequisite for studies on extreme wave events based on overwash sand deposits and boulders (Liu, 2004), which is a branch of research with a strong foothold on Bonaire (e.g. Scheffers, 2002, 2005; Scheffers et al., 2006; Morton et al., 2008; Engel et al., 2010b, in press). Furthermore, the RSL references provide new implications on small-scale neotectonic activity.

Inferred RSL changes are compared to a reference model of Holocene RSL evolution calculated for and adjusted to Curaçao (Milne et al., 2005), the sister island of Bonaire. This reference model combines a number of dynamic geophysical parameters influencing RSL, which are determined by the redistribution of ice masses and ocean water during post-glacial climate change. The changes in ice masses and ocean water were simulated by the global ICE-3G deglaciation model by Tushingham and Peltier (1991), which represents the most important component driving the reference model. The parameters driven by the ice load model are perturbations of the geopotential, which are directly related to shifts in height of the equipotential surface of the earth's gravitational field (= "global mean sea level"). The perturbations include variations in gravity due to melting ice shields and deformation of the solid earth. Furthermore, the reference model considers eustatic sea-level change, GIA – including Holocene ocean syphoning (Mitrovica and Milne, 2002) –, a tentative value for lithospheric thickness, and an asthenospheric viscosity model adapted from literature. More details are provided by Milne et al. (2005) and references therein.

8.2 Drivers of RSL change

8.2.1 The general perspective

Drivers of Holocene RSL can be separated into global, regional and local processes. Global processes include mass exchanges due to accumulation and ablation of ice caps and glaciers (glacioeustasy), changes in ocean basin volume due to glacioisostatic rebound of the lithosphere after reduction of ice loads, and thermal response of ocean water (density changes/steric effect). Processes implying regional differences comprise glacioisostatic adjustment (GIA) of landmass. Isostatic deformation of the earth causes gravitational effects and influence ocean basin volume. These effects create a complex pattern of interaction; e.g. offloading of ice caps not only causes eustatic and isostatic RSL

changes, but also induces gravitational and rotational changes of the solid earth, such as shifts in the equipotential surface of the earth. Local processes include tectonic uplift/subsidence, changes in tidal range and compaction of coastal sediment bodies (Milne et al., 2009; Gehrels et al., 2011; Toscano et al., 2011). The effects of both regional and local processes are very site-specific (Vött, 2007).

8.2.2 Bonaire

Bonaire is one of the Leeward Antilles and, together with its neighbours Aruba and Curaçao, represents the ABC Islands. Its climate is semi-arid and surface discharge is bound to arroyos and periodic sheetwash (Zonneveld et al., 1977). Late Cretaceous igneous rocks (Washikemba Formation [WF]) are surrounded by a sequence of palaeo-reef terraces, the youngest of which was formed during MIS 5e (Lower Terrace [LT]) (Fig. 49) (Herweijer and Focke, 1978; Schellmann et al., 2004). Narrow valleys dissect the seaward WF as well as the limestone belt of the palaeo-reef terraces and provide drainage for the hinterland. These valleys (locally called bokas or saliñas) were incised during RSL lowstands and are flooded at present (Westermann and Zonneveld, 1956; Alexander, 1961; De Buisonjé, 1974; Scheffers, 2002, 2005; see also Fig. 49). Bokas/saliñas provide most of the geoarchives used in this study. Alluvial and lagoonal deposition dominates the coring sites. Marine overwash is rare. The tidal range on Bonaire amounts to 30 cm on average (Bak, 1977) and is considered to be of minor importance for RSL reconstruction. For more details on Bonaire's geology and geomorphology the reader is referred to De Buisonjé (1974) and Scheffers (2005).

Holocene RSL change ($\Delta\xi_{RSL}$) as experienced by the low-lying sedimentary archives on Bonaire for time (τ) and coastal section (ϕ) can be expressed as (e.g. Farrell and Clark, 1976; Horton and Shennan, 2009)

$$\Delta\xi_{\mathrm{RSL}}(\tau,\varphi) = \Delta\xi_{\mathrm{eus}}(\tau) + \Delta\xi_{\mathrm{iso}}(\tau) + \Delta\xi_{\mathrm{tec}}(\tau,\varphi) + \Delta\xi_{\mathrm{sed}}(\tau,\varphi). \quad (21)$$

$\Delta\xi_{eus}$ represents glacioeustasy and should also include isostatically induced ocean basin volume change. Currently, expansion of the ocean basin volume contributes to sea level fall (Gehrels et al., 2011). $\Delta\xi_{iso}$ includes GIA and gravitational effects. $\Delta\xi_{tec}$ represents vertical neotectonic movements of the island, dominated by tilting, i.e. very little subsidence to quasi-stability in the south and slow net uplift in the northwest (Alexander, 1961; Herweijer and Focke, 1978), which is most likely due to shallow subduction of the Caribbean Plate in the south (Hippolyte and Mann, 2011). The backslope surface of the LT is located at <2 m a.s.l. (above present mean sea level) in the south and at more than 10 m in the north. In between, the LT is unevenly uplifted and arched (Alexander, 1961). $\Delta\xi_{sed}$ refers to sediment compaction, which is a significant factor in peat-dominated sequences, but rather negligible in sand and gravel deposits (Bird et al., 2004; Vött, 2007; Horton and Shennan, 2009). The amount of compaction of a certain stratum, though difficult to predict, depends on the time since deposition, thickness of the sediment column and the type of sediment above and beneath. Peat compaction is rapid in the beginning and ceases asymptotically. Along the coast of Singapore, compaction of peat-bearing sequences was estimated to range between 17 and 55% (Bird et al., 2004). Horton and Shennan (2009) found average compaction rates of 0.4 ± 0.3 mm yr^{-1} for peats buried in Holocene sequences along the east coast of England.

8.3 Sea level indicators

8.3.1 The general perspective

Indicators of past sea-level stands are manifold. They include destructive geomorphological features, such as bioerosive notches, abrasion platforms, rock pools, boreholes of rock-boring molluscs and sponges. Accretional features comprise coastal dunes, lagoonal and wadden sediments, microfossils, bioconstructive organisms (oysters, vermetids, coral microatolls, etc.) or beach deposits. Archaeological remains may also provide RSL markers (Fairbanks, 1989; Brückner and Radtke, 1990; Gehrels, 1999; Kelletat, 1988, 2005; Pirazzoli, 2005, Switzer et al., 2010; Scheffers et al., accepted). During the last 200 years, tide gauge records and, since the 1990s, satellite altimetry became important (Church and White, 2006; Church et al., 2008; Milne et al., 2009).

Coastal or paralic peats and marshland deposits are among the most common indicators (= index points) used for RSL reconstruction worldwide since accurate age estimations can be obtained from their organic remains by ^{14}C (Gehrels, 1999; Lampe, 2005; Vött, 2007; Bungenstock and Schäfer, 2009; Engel et al., 2009b; Horton and Shennan, 2009; Brückner et al., 2010). For Caribbean coasts, intertidal mangrove peat (predominantly *Rhizophora mangle*) is widely used as RSL indicator. It builds up through organic accumulation controlled by RSL rise. Peat accumulation can compensate RSL rise of up to 3.5 mm yr^{-1} and provides reliable records for the Mid- to Late Holocene. However, peat records are rarely reflecting negative fluctuations, i.e. phases of RSL fall, unless a hiatus can be clearly identified in the stratigraphy (McKee et al., 2007). In other cases, the peat record might be disturbed/eroded by high-energy wave impact (tsunamis, hurricanes) (*Chapter 4*; Engel et al., 2010b). RSL indicators, particularly peat, set within a coastal stratigraphy, are susceptible to post-depositional compaction and lowering (Vött, 2007; Horton and Shennan, 2009).

8.3.2 Studying Holocene sea levels on Bonaire

In this study we used several ^{14}C-dated objects from sedimentary environments, which can be associated with a particularly range of water depth (see Table S2). The objects derive from 18 vibracores, two push cores and one trench. Sedimentology and facies interpretation have been presented previously for the sites of Lagun (LGU), Boka Washikemba (BWA), Playa Grandi (PGR) (all in Engel et al., 2010b), Saliña Tam (SAT, W of SAT), and Klein Bonaire (KLB) (both in Engel et al., in press). All cores and pits were leveled by DGPS (Leica 530 SR, Topcon HiPerPro) with a maximum vertical error of ±2 cm. Radiocarbon ages were generated by the Radiocarbon Lab Cologne, Institute of Prehistoric Archaeology, Universität zu Köln, the AMS C14-Labor Erlangen, Friedrich-Alexander-Universität Erlangen-Nürnberg, and the Center for Applied Isotope Studies, University of Georgia, Athens. The data were calibrated using Calib 6.0.1 software (Reimer et al., 2009). The 2σ error was dealt with as recommended for instance by Brückner et al. (2010). Marine samples ($\delta^{13}C > -18$ in Table S2) were corrected for a local average marine reservoir value ΔR = -49 (Radtke et al., 2003). The terrestrial snail of *Cerion uva* was corrected for an age anomaly of 1020±430 years according to Goodfriend and Gould (1996). Palaeo-sea levels associated with the sedimentary environment of the ^{14}C-dated objects/substrates were evaluated using literature data and observations of correlating modern environments, and are depicted in Fig. 49 and Table S2.

Mangrove peat can be associated with the intertidal zone, c. ±0.15 m a.s.l. in microtidal environments (Toscano and Macintyre, 2003; Zong, 2004). A large number of ^{14}C data from Bonairean

coastal stratigraphies are associated with high-energy wave deposits, several of which are considered to be tsunamigenic. Since strong erosion of mangroves and mangrove peat occurred during high-energy wave impacts and the overlying deposits are in all cases related to shallow standing water bodies (Engel et al., 2010b), they were linked with a higher sea level of 0-1 m.

The basin of Boka Bartol is an exception: Here, a corresponding higher sea level of +1-3 m was inferred due to its unusual water depth (up to 5.5 m) and the extraordinary amount of peat erosion. The unusual water depth is linked to active tectonic subsidence (see *Chapter 8.5.2.5*). Peat erosion due to a high-energy wave impact – probably a tsunami – is indicated by a hiatus of 2500 years between the peat and the overlying high-energy wave deposit (see sediment core BBA 10 in Figs. 50-51).

Lagoonal mud was also given a palaeo-sea level of +0-1 m (+0-2 m at Boka Bartol due to its greater depth; 0-0.5 m at landward Saliña Tam [SAT 9] due to its very shallow bathymetry; Figs. 30 and 42). Lagoonal deposits are defined here as sediments accumulated in calm and poly- to hypersaline waters of coastal water bodies, which are cut off from the sea by a barrier of coral rubble and beachrock. Zong (2004) links lagoonal organic sediment with mean low water to mean high water. However, on Bonaire, lagoonal water levels are significantly lower than sea level for most of the year (around 0.7 m b.s.l. [below present mean sea level] during field work in Jan 2009, right after the rainy season) due to high evaporation losses and low permeability of the seaward barriers of beachrock and coral rubble. It is noteworthy that, in general, the indicator value of high-energy wave deposits and lagoonal mud is much lower compared to mangrove peat.

At sites without mangrove remains in the sedimentary record such as Playa Grandi (Fig. 22) and Boka Washikemba, organic-rich layers represent coastal marsh environments. They are often linked to a range of 0-0.5 m a.s.l. (Vött, 2007) or local mean high water (Zong, 2004). On Bonaire, where back-barrier water levels were found to be significantly lower than sea level, we relate coastal marsh deposits to a position of -0.5-0 m a.s.l. A terrestrial snail (*Cerion uva*) at Boka Washikemba buried in a floodplain deposit indicates a lower palaeo-sea level of c. 0-1 m, according to the elevation of today's distal floodplain which was levelled by DGPS (see Table S2 for details).

8.4 Holocene sea levels of the Caribbean basin

During the LGM, the Caribbean sea level was 121±5 m b.s.l. as inferred from the coral record of Barbados (Fairbanks, 1989). Rates of sea level rise were high until the Early Holocene. A decrease in global ice melt led to the influence of regional (e.g. GIA) and local (e.g. vertical tectonic movement) factors becoming more significant and diverging local RSL histories evolved. In the wider Caribbean, Mid- to Late Holocene RSL curves based on field evidence exist for Jamaica (Digerfeldt and Hendry, 1987), Trinidad (Ramcharan, 2004), Belize (Macintyre et al., 2004; McKee et al., 2007) and St. Croix (Toscano et al., 2011). Peat and coral records of the wider Caribbean were compiled by Toscano and Macintyre (2003) to establish an RSL curve for the western Atlantic region. Peat-based RSL records from Venezuela (Rull et al., 1999) and Curaçao (Klosowska, 2003) as well as a reconstruction of Holocene reef growth from Curaçao (Focke, 1978a) provide the most important references for Bonaire so far. All records indicate a continuously ceasing RSL rise towards the present and reflect considerable deceleration after 7000 cal BP due to reduced melt water input and the direct effect of this process on the geopotential. None of the RSL curves indicate a Mid-Holocene sea level highstand; it is absent due to minor isostatic subsidence of the Caribbean lithosphere, which is located on the peripheral bulge of the Laurentide ice shield (Milne et al., 2005).

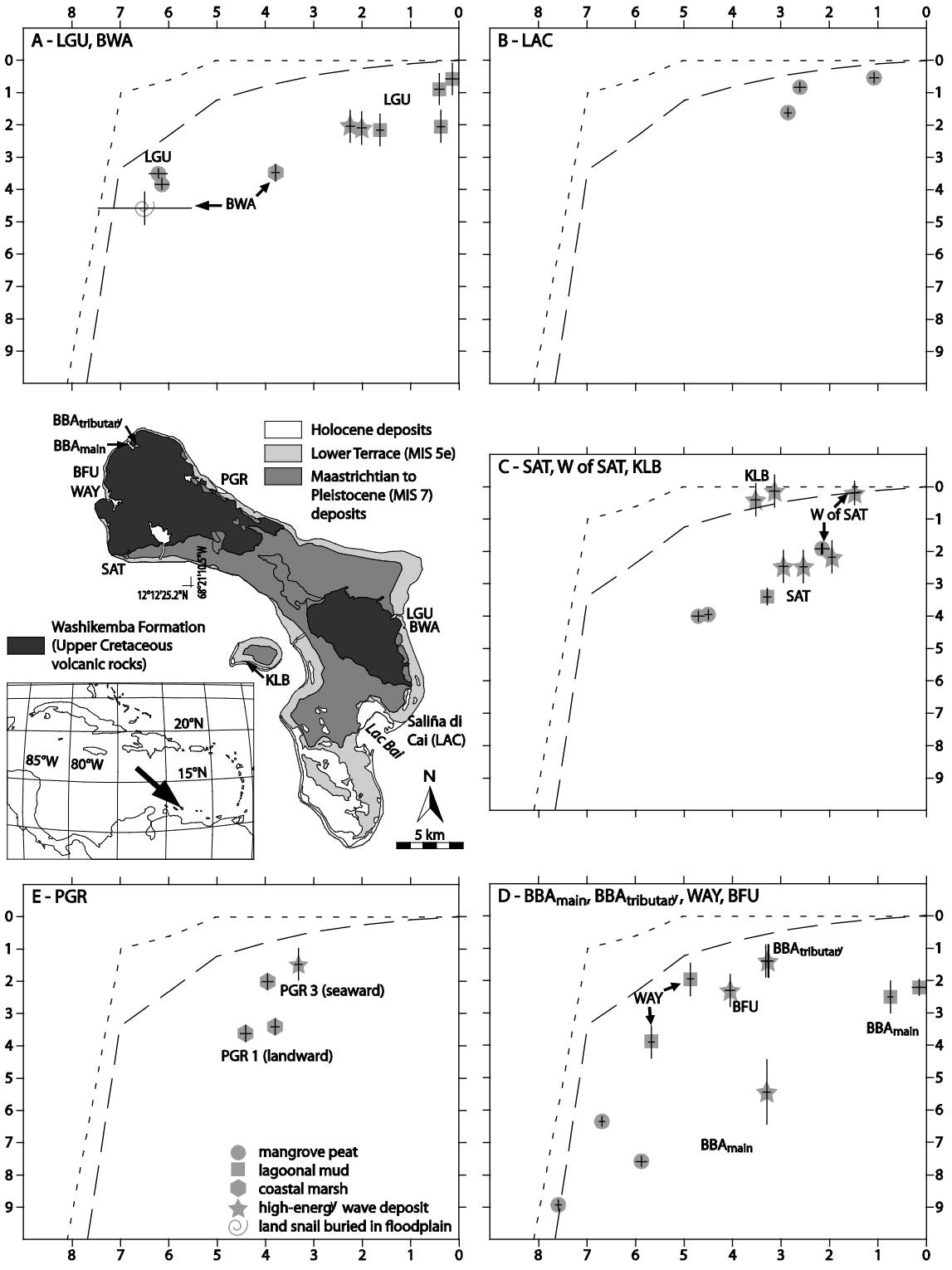

Fig. 49: Simplified geological map of Bonaire (based on Pijpers, 1933; Westermann and Zonneveld 1956; De Buisonjé 1974). The island's location in the southern Caribbean is marked by a black arrow in the overview map. LGU = Lagun; BWA = Boka Washikemba; KLB = Klein Bonaire; SAT= Saliña Tam; WAY = Wayaka; BFU = Boka Funchi; BBA_{main} = main basin of Boka Bartol (micro-graben); $BBA_{tributary}$ = tributary basin of Boka Bartol. Diagrams 1A-1E show index points (crosses) of relative sea level (RSL) stands (see text for details). The vertical extent of the crosses specifies the range of the assumed sea level position associated with the sedimentary environment of the sample (indicated by grey symbols). The lateral extent of the crosses indicates the 2σ range of calibrated radiocarbon ages. X-axes show calibrated 1000 years BP, y-axes show depth below present mean sea level in meters. Eustatic sea level is displayed according to the global ICE-3G deglaciation model by Tushingham and Peltier (1991) (dotted line) and the reference model of Milne et al. (2005) which also involves correction for $\Delta\xi_{iso}$ (glacioisostatic rebound and gravitational effects) and is tuned to reduced lithospheric thickness (dashed line).

8.5 Field evidence for Holocene sea levels on Bonaire

8.5.1 The cliff coast

Significant features of Bonaire's rocky coast are bioerosive notches and bioconstructive benches (Scheffers, 2002, 2005). The innermost point of the notches correlates with mean high water level (Kelletat, 1988). Algae and other microorganisms dwell in the intertidal zone causing biochemical erosion. Chitonidae and Patellidae graze on these algae and induce bio-mechanical abrasion using their radula. A bench formed by calcareous algae is present in the zone of maximum turbulence, whereas further down a second, less pronounced notch is present due to abrasion predominantly by echinoids (Zonneveld et al., 1977; Focke, 1978b). At sheltered sites, such as bokas, benches are absent. Some of the active notches at sea level have a vertical range that significantly exceeds the local tidal range indicating a slowly rising RSL for the last millennia.

8.5.2 The bokas and saliñas

The formation of coral rubble beaches containing beachrock sections in front of the bokas and saliñas also points to relatively stable or slowly rising RSL. Lagun and Boka Washikemba are exceptions in this regard, due to a lack of source material (corals) in the foreshore since at least 3100 BP (Scheffers et al., 2006).

8.5.2.1 Lagun and Boka Washikemba (Fig. 49A)

The most promising RSL indicators stem from the stratigraphy of the distal floodplain of Lagun which, together with the open inlet, cuts the Washikemba Formation (WF), as well as the Lower Terrace (LT). At Lagun, the LT has an elevation (E) of c. 7 m a.s.l. We estimate net uplift of this part of the island (ΔU) since its formation during MIS 5e (122,000±12,000 years after Schellmann et al., 2004) by

(22) $$\Delta U = E + \Delta R + D_{AP} - \Delta\xi_{eus}$$

to be in the range of 5.8-10.8 m, i.e. 4-8 cm per 1000 years. The subaerial erosion (downwearing) since reef exposure (ΔR) is inferred from the erosion rate of limestone terraces on the Leeward Antilles, c. 0.01-0.02 mm yr^{-1} (Focke, 1978b). A former water depth of 0-5 m (D_{AP}) is associated with the *Acropora palmata*-dominated palaeo-reef of the LT (cf. Fairbanks, 1989). $\Delta\xi_{eus}$ represents the difference in eustatic sea level between the peak of MIS 5e of c. 4 m a.s.l. (Schellmann et al., 2004) and today.

All RSL index points lie significantly below the reference model of Milne et al. (2005). This, of course, can be explained by syntectonic base level-driven incision in the area of the geoarchive of Lagun where a water course enters the sea, compensating ΔU. Incision ceased when accumulation at Lagun started around 7000-6000 years ago; thus post-depositional uplift amounts to ≤50 cm. Taking Eq. (21) as a base, $\Delta\xi_{eus}$ and $\Delta\xi_{iso}$ are represented by the reference model. $\Delta\xi_{sed}$, i.e. compaction of the sediment column, is most likely responsible for the large discrepancy, but even when maximum compaction (around 50% according to Bird et al., 2004) is assumed, there is still a gap of 0.8-1.0 m to fill between vertical position of index point BON 10/4-1 (Fig. 49A, Table S2), for instance, and the reference model. The following potential reasons should be considered regarding this disparity:

(i) Microtectonics: unlikely. $\Delta\xi_{tec}$, i.e. tectonic subsidence due to normal faulting of the low-lying area of the Lagun floodplain and embayment would be the remaining factor according to Eq. (21). However, to date there is no evidence for this process.

(ii) Root contamination: very occasionally. Root contamination, as described by Scholl and Stuiver (1967), occurs when root material – in this case: *Rhizophora mangle* – penetrates older peat strata, where its ^{14}C data leads to age underestimations. In this case, only LGU 7/8 ^{14}C (Table S2) as an outlier seems to represent such a stratigraphical contamination.

(iii) Compaction through coring: practically ineffective. Additional compaction during the coring process is relevant in the first meter, though small (<10 cm) further down.

(iv) Uncertainties in assigning palaeo-water depths: potentially applicable.

(v) Uncertainties in the reference model: potentially applicable. Milne et al. (2005) calculated the reference model for Curaçao using a range of rheological properties. By comparing the model with field-based RSL indicators from South America and the Caribbean, the best-fit scenario for all sites involves a reduced lithospheric thickness of 71 km. Concerning the RSL indicators from Curaçao (Klosowska, 2003) used by Milne et al. (2005) – and also the ones from Lagun –, reduced lithospheric thickness only represents the second best-fit scenario. A slightly steeper and lower curve was calculated by modifying upper mantle viscosity from 10^{20} to 10^{21} Pa s. While this local best-fit-scenario was considered to be unlikely by Milne et al. (2005) in the context of other local case studies, it is possible that small local differences in cumulative effects of GIA and related effects between the island of Curaçao (for which the reference model was calculated) and Bonaire apply. Using follow-up versions of the reference model applied by Milne et al. (2005), Toscano et al. (2011) explained the gap between the high trend of the model prediction and coral-based field evidence from St. Croix (NE Caribbean) through underestimation of the influence of "rotational feedback", i.e. the interrelation between the ice-water balance and the rotational state of the earth, in the calculation.

8.5.2.2 Saliña di Cai (Fig. 49B)

Further south, at Saliña di Cai near Lac Baai, the net uplift rate of c. 0-3 cm per 1000 years is almost negligible. Considering that sample LAC 7/3 ^{14}C is potentially root-contaminated, the difference between the sea level indicators (purely mangrove peat) and the reference model can be explained by compaction (up to 1 m in pure mangrove peat). However, additional karst-related subsidence cannot be excluded. Several adjacent karst features are visible. Even the initial formation of Lac Baai might be related to limestone solution. Within the range of existing uncertainties, the sea level index points of the last 2500 years from Saliña di Cai would support both the reference model and a marginally lower RSL curve.

8.5.2.3 Saliña Tam (Fig. 49C)

At Saliña Tam, on the northwestern leeward coast, net uplift is comparable to Lagun, but incision of the LT during the period of lower sea level continued as well. Sea level references of SAT lie very low. Compaction is likely to be significant in core SAT 9 (*Chapter 6*; Engel et al., in press), particularly regarding the oldest peat samples (Fig. 49C). Comparing the sediment traps of SAT and W of SAT and assuming that the peat of W of SAT (located right above an overwash deposit of *Acropora cervicornis* fragments [*Chapter 6*; Engel et al., in press]) is slightly affected by root contamination, the discrep-

ancy may point to two different patterns of Middle to Late Holocene vertical movement at both sites. This could be explained by subsidence related to micro-scale normal faulting at SAT.

8.5.2.4 Klein Bonaire (Fig. 49C)

Klein Bonaire is the only site where sea level index points are in full agreement with the reference model and do not support a lower RSL curve. The record includes two ^{14}C dates from a short core obtained in a shallow pond right behind a coral rubble beach. Since the LT is not as well developed as on the main island and no radiometric ages exists, the application of Eq. (22) in order to calculate tectonic uplift is not possible. However, we consider vertical uplift to having overcompensated compaction of the dated strata in the short core (Engel et al., in press), which is estimated to be around 20 cm.

8.5.2.5 Boka Bartol, Wayaka and Boka Funchi (Fig. 49D)

The uplift rate in the area of Wayaka and Boka Funchi is slightly higher compared to Lagun, calculateed to range between 5 and 9 cm per 1000 yrs, but generally, observations are similar. However, due to the longer sediment record, compaction losses are estimated to compensate for a large part of the vertical discrepancies regarding the reference model. RSL index points from the tributary basin of Boka Bartol ($BBA_{tributary}$) match these observations and, considering a moderate degree of compaction, also indicate that the reference model is located slightly above the RSL evolution on Bonaire.

Fig. 50: Oblique view of Boka Bartol (see Fig. 49) directed to the east. Coring sites of BBA 10 in the main basin (BBAmain), BBA 11 in the tributary basin (BBAtributary), and the cross section of Fig. 51 are indicated. The white solid lines show the inferred micro-graben structure which continues inland and is reflected by a gap in the batholith (Washikemba Formation [WF]). Subsidence of Boka Bartol results in water depths of up to 5.5 m b.l.l. (below lake level) measured at the seaward end of BBA_{main} during a bathymetric survey using a Lowrance LMS-522 C iGPS fish-finder. Please note that at the time of the photograph (A. Scheffers, December 2008) the water level is unusually high. Most of the year, the coring sites are not inundated. Regarding Quaternary deposits, only the Lower Terrace (LT), dated to MIS 5e (Herweijer and Focke, 1978), is preserved at Boka Bartol, whereas on the left (foreground) the living (Holocene) reef is visible.

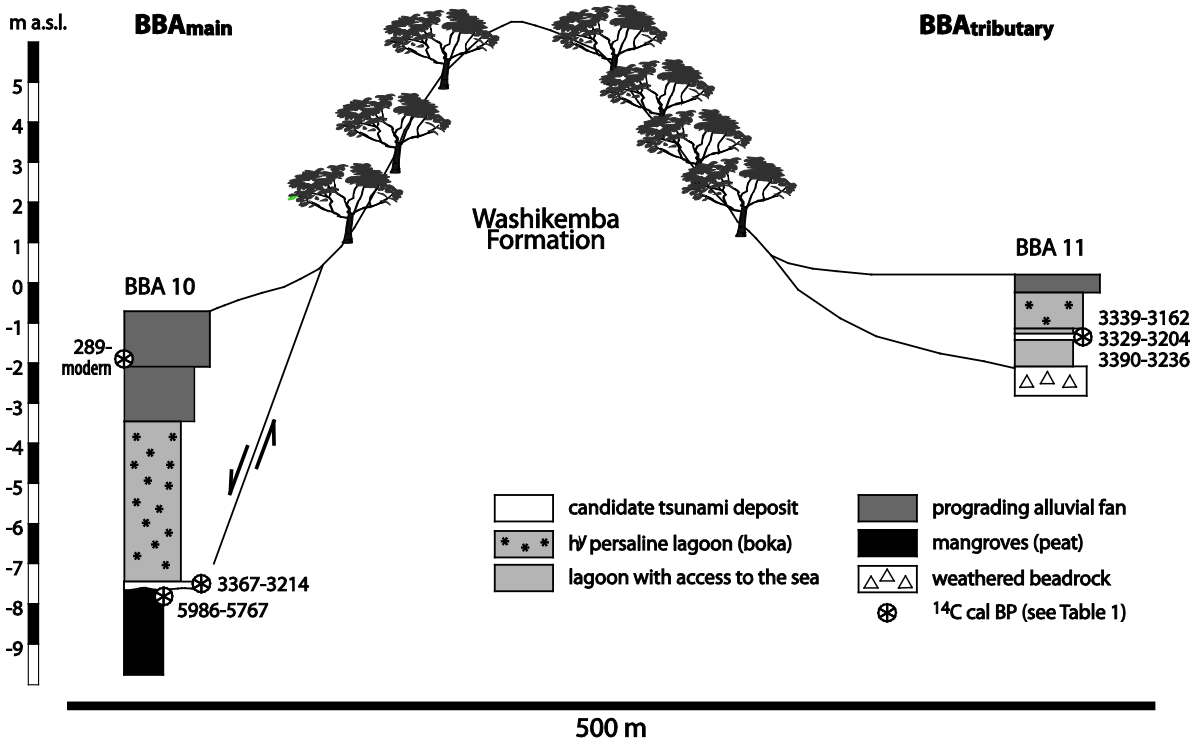

Fig. 51: Cross section between sediment cores BBA 10 and BBA 11 at Boka Bartol (see Fig. 50) illustrating normal faulting at the main basin of Boka Bartol (BBA_{main}). Both coring sites are situated at the shore of the water body and are usually not inundated. Lake water level approximately coincides with the surface of BBA 10. The scale on the left is adjusted to present mean sea level (0 m).

The most interesting findings from the northwest of Bonaire are the deeply buried sea level indicators of the main basin of Boka Bartol (BBA_{main}) (Figs. 49 and 50). Even samples with a maximum age of c. 280 years are buried by more than 1 m of sediment of the unvegetated, prograding proximal alluvial fan (fig. 51). High sediment loads were triggered abruptly when European land use practices were initiated in the 16th century AD. The northwest of Bonaire was intensely used as a plantation with high lifestock densities, especially goats (STINAPA, 2003/2009; De Freitas et al., 2005). Even though compaction of the 9 m-sediment column is expected to be quite substantial, post-depositional subsidence of BBA_{main} and its southeast extension is due to normal faulting, thereby providing accommodation space for the increased sediment loads of modern times.

$BBA_{tributary}$ is part of the slowly uplifted northwestern tip of the island, whereas BBA_{main} forms a micro-graben or halfgraben. The northwestern orientation of BBA_{main} conforms to the larger graben structures (East and West Curaçao Basins) separating the ABC islands. Normal faulting in this area is associated with Miocene to present extensional dynamics and NNE-SSW to NE-SW trending rifting within the Leeward Antilles ridge. However, NW-trending normal faults affecting the Cretaceous batholith have thus far only been systematically mapped on Aruba (Hippolyte and Mann, 2011). Unusual tectonic subsidence of BBA_{main} is also indicated by its water depth of up to 5 m. Bokas of comparable areal extent (e.g. Saliña Tam) have maximum depths of 1.5 m (*Chapter 6*; Engel et al., in press). Relative subsidence of BBA_{main} may be in the range of up to 1.5 mm yr^{-1} based on age and vertical displacement of correlating candidate tsunami deposits in BBA 10 and 11 (and subtraction of estimated compaction according to Bird et al., 2004), given that the deposit in BBA 10 formed near sea level ot slightly below as indicated by the underlying mangrove peat.

8.5.2.6 Playa Grandi (Fig. 49E)

RSL indicators at Playa Grandi derive from two cores. While samples from the stratigraphy right behind the present boulder beach (core PGR 3) lie c. 1.5 m below the reference model, the ones from the landward floodplain are located even 1 m further down. The influence of compaction at PGR 3 is considered to be very low since both dated objects are located just above a thick unit of sandy (sub-)littoral facies (*Chapter 4*; Engel et al., 2010b). In contrast, the landward stratigraphy exclusively comprises highly compressible strata within the uppermost 5 m or more (coring did not reach bedrock). Thus, PGR 3 contains more reliable RSL references than PGR 1.

8.6 Synthesis

A large number of Holocene RSL index points with varying degrees of accuracy are available on Bonaire (Fig. 49, Table S2). Vertical displacement of depositional RSL indicators ranges from zero to several meters of subsidence in Mid- to Late Holocene times. Calculated tectonic uplift (ΔU in Eq. (22)), though moderate, is reflected by the raised Eemian palaeo-reef (LT) surrounding the island and ranges from around zero (Saliña di Cai) to 50 cm in total (Lagun, Boka Bartol, Klein Bonaire) within the last 6000 years. Our results are congruent with the spatially undifferentiated value of 2-8 cm per 1000 years suggested by Herweijer and Focke (1978). More effective is sediment compaction, estimated to range from zero (dated samples close to bedrock or other incompressible strata) to more than 1.5 m (PGR 1, Saliña Tam, BBA_{main}). Several sediment archives are underlain by limestone (e.g. Saliña di Cai) and potentially biased by collapsed cavities. Local tectonic subsidence in terms of normal faulting and/or micro-graben formation is difficult to determine and can only be excluded at Klein Bonaire and Saliña di Cai. However, at Boka Bartol we showed that a micro-graben, formed by long-term extensional dynamics of the Leeward Antilles ridge, is highly active at present, implying a vertical slip rate of up to 1.5 mm yr^{-1}. This is particularly interesting due to the fact that to date faults have never been systematically mapped on Bonaire (Hippolyte and Mann, 2011). Small-scale normal faulting might also apply to Saliña Tam, though this has not yet been verified.

A construction of two local RSL curves for Bonaire which consider the differences of Holocene tectonic uplift on the N and S tips of the island is obstructed by local variations of other relevant parameters, such as different unpredictable degrees of compaction as well as subsidence, root contamination effects and uncertainties in palaeo-water depth (e.g. lagoonal deposits, candidate tsunami deposits). The discrepancy, however, would lie in the range of <50 cm. We evaluated the set of RSL indicators, rejected negative outliers, individually estimated compaction, and present in this paper the first Holocene RSL curve for Bonaire (Fig. 52). In general, it is higher than the reference model (Milne et al., 2005) until 7000 cal BP, followed by an underestimation of less than 1 m until 4000 cal BP, and an asymptotical approximation until today. Only on Klein Bonaire RSL index points potentially support an entirely stable sea level for the last 4000 years (= eustatic curve for the ice model of Tushingham and Peltier, 1991). The gap between the results from this study and the model prediction (Milne et al., 2005) may either result from underestimation of compaction in the core data, underestimation of the influence of sea-level history on the earth's rotational state in the model (Toscano et al., 2011) or possible discrepancies between the Curaçao reference model and a not yet existing reference model for Bonaire.

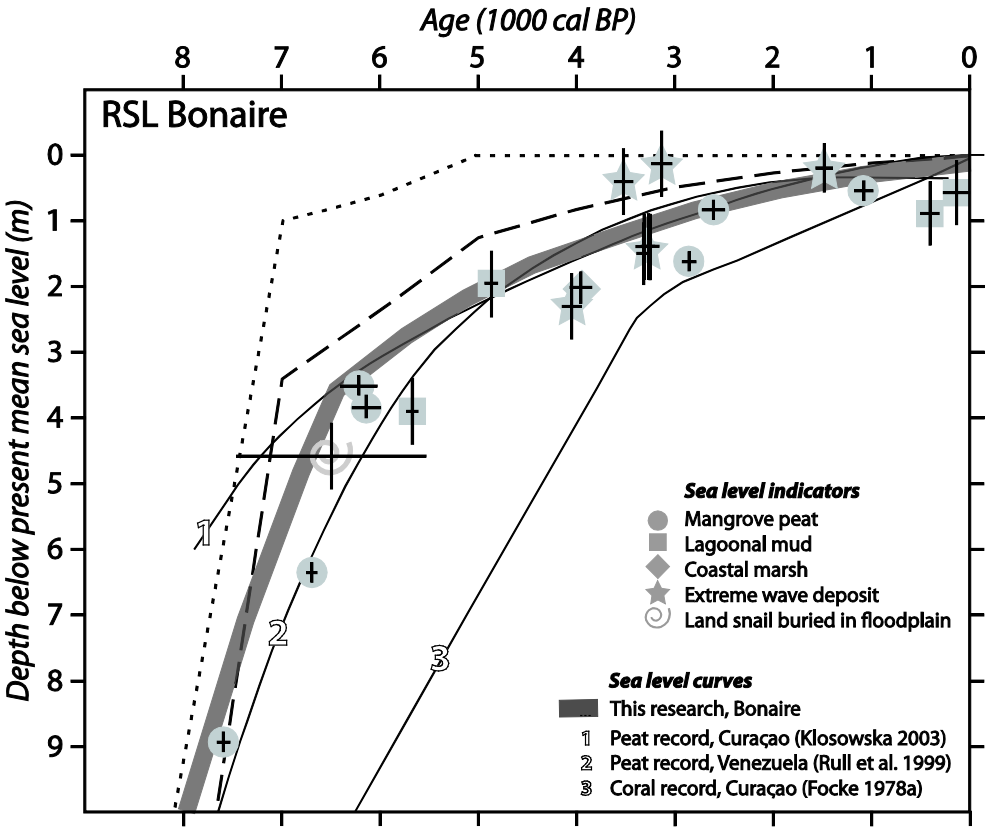

Fig. 52: Compilation of "reliable" relative sea level (RSL) indicators from Bonaire pointing to a Mid- to Late Holocene RSL evolution traced by the grey solid line. Comparable regional records of the southern Caribbean Sea are plotted as well. The vertical extent of the crosses specifies the range of the assumed sea level position associated with the sedimentary environment (indicated by grey symbols) of the sample. The lateral extent of the crosses indicates the 2σ range of calibrated radiocarbon ages. Instead of an envelope curve which spans the crosses of the index points and includes all regional and local uncertainties (cf. Vött, 2007; Brückner et al., 2010), we chose a depiction tentatively corrected for sediment compaction, thus providing the best possibility for comparison with other regional RSL curves. Eustatic sea level according to the global ICE-3G deglaciation model by Tushingham and Peltier (1991) (dotted line) is displayed as well as the reference model of Milne et al. (2005), which also involves correction for $\Delta\xi_{iso}$ (glacioisostatic rebound, gravitational effects) and is tuned to reduced lithospheric thickness (dashed line).

In contrast, the RSL curve from this study is quasi-congruent with the one established for St. Joris Bay on Curaçao (Klosowska, 2003), at least for the last 6500 years, and is also similar to the one inferred for Venezuela (Rull et al., 1999) with regard to the last 5000 years. This observation reflects a similar regional response to glacial isostasy as well as a comparable bias of compaction of the local geoarchives. The coral-based curve of Holocene RSL rise from Bullenbaai on Curaçao (Focke, 1978a) lies significantly below the one presented in this study and is discarded due to large uncertainties of palaeo-water depths linked to corals such as *Montastrea annularis* or *Acropora palmata*. These corals are particularly suitable for reconstructing sea level records of larger magnitude and time scales (Fairbanks, 1989, Schellmann et al., 2004), but lack vertical sensitivity during periods of decelerated RSL rise (Klosowska, 2003).

8.7 Supplementary Material

Table S2: ^{14}C-AMS dates used in this study. Sample series BON, LGU, BWA and PGR are published in Engel et al. (2010b), apart from LGU 5 (unpublished). KLB and SAT are published in Engel et al. (in press). BBA, WAY and BFU are presented in *Chapter 7*. Lab IDs: KN = Radiocarbon Lab Cologne, Institute of Prehistoric Archaeology, Universität zu Köln (conventional radiocarbon analysis); Erl = AMS C14-Labor Erlangen, Friedrich-Alexander-Universität Erlangen-Nürnberg; UGAMS = Center for Applied Isotope Studies, University of Georgia, Athens. Samples marked with an asterisk are considered to be too old and not adequately represent their stratum according to other dating results from the same depth or an adjacent core.

Location	Sample	Depth (m b.s.)	Elev. (m a.s.l.)	Lab ID	Material	δ^{13}C	^{14}C age	Age cal BP (2σ)	Palaeo-environment/ facies (water depth)
Lagun 12°10'50.9"N 68°13'13.7"W	BON 10/1-1	1.16-1.11	0.05	KN-5851	Wood	-27.0	130 ± 30	275-modern	Lagoonal deposit (0-1 m b.s.l.)
	BON 10/1-4	1.45-1.44	0.05	Erl 10610	Plant fragm. (peat)	-27.4	366 ± 46	503-314	Lagoonal deposit (0-1 m b.s.l.)
	BON 4/18 PF	3.60-3.53	0.05	Erl 10609	Plant fragm. (peat)	-22.7	5469 ± 61	6404-6029	Mangroves (±0.15 m a.s.l.)
	BON 10/4-1	3.96-3.85	0.05	Erl 10611	Plant fragment (peat)	-26.8	5369 ± 60	6282-5999	Mangroves (±0.15 m a.s.l.)
Lagun 12°10'49.1"N 68°13'15.8"W	LGU 2/10 G	2.80-2.70	0.15	UGAMS 3206	*Cerithium* sp. (marine snail)	-1.62	2330 ± 25	2100-1921	Uppermost part of a candidate tsunami deposit (0-1 m b.s.l.)
	LGU* 2/11 G	3.25-3.15	0.15	UGAMS 3207	*Bulla striata* (marine snail)	-2.09	2540 ± 25	2333-2168	Lowermost part of a candidate tsunami deposit (0.5-1.5 m b.s.l.)
Lagun 12°10'52.5"N 68°13'03.2"W	LGU 5/22	3.91-3.88	0.07	UGAMS 3208	Plant fragment (peat)	-18.3	2360 ± 25	2459-2383	Mangroves (±0.15 m a.s.l.)
	LGU 5/30 F*	6.82-6.75	0.07	UGAMS 3209	*Crassostrea rhizophorae* (marine bivalve)	-0.9	6300 ± 25	6901-6727	Mangroves (±0.15 m a.s.l.)
	LGU 5/30	6.82-6.75	0.07	UGAMS 3210	Plant fragment (peat)	-25.8	6380 ± 25	7415-7261	Mangroves (±0.15 m a.s.l.)
Lagun 12°10'52.9"N 68°13'11.7"W	LGU 7/8 ^{14}C	2.57-2.56	0.03	UGAMS 4199	Plant fragment (peat)	-26.2	300 ± 25	455-299	Lagoonal deposit (0-1 m b.s.l.)
	LGU 7/12 ^{14}C	2.74-2.71	0.03	UGAMS 4200	Plant fragment (peat)	-26.9	1730 ± 25	1705-1566	Lagoonal deposit (0-1 m b.s.l.)
Boka Washikemba 12°10'24.5"N 68°12'40.3"W	BWA 1/18	3.82-3.80	0.58	UGAMS 3204	Wood	-26.0	3520 ± 825	3870-3707	Coastal marsh (0-0.5 m a.s.l.)
	BWA 1/21 M	4.66	0.58	UGAMS 3205	*Cerion uva* (terr. snail)	-6.5	8480 ± 25	7455-5528	Floodplain (0-1 m a.s.l.)
Saliña di Cai 12°06'26.8"N 68°12'51.9"W	LAC 7/1 ^{14}C	0.24	c. -0.35	UGAMS 5991	Plant fragment (peat)	-24.9	1160 ± 25	1171-983	Mangroves (±0.15 m a.s.l.)
	LAC 7/2 ^{14}C	0.53	c. -0.35	UGAMS 5992	Plant fragment (peat)	-26.0	2500 ± 25	2723-2487	Mangroves (±0.15 m a.s.l.)
	LAC 7/3 ^{14}C	1.32	c. -0.35	UGAMS 5993	Plant fragment (peat)	-26.7	2760 ± 25	2925-2782	Mangroves (±0.15 m a.s.l.)
Klein Bonaire 12°09'05.2"N 68°18'54.0"W	KLB 1/a 43	0.43	c. -0.20	UGAMS 7588	*Cerithium* sp. (marine snail)	-4.1	3240 ± 25	3236-3028	Candidate tsunami deposit (0-1 m b.s.l.)
	KLB 1/a 70	0.70	c. -0.20	UGAMS 7589	*Cerithium* sp. (marine snail)	-5.3	3570 ± 30	3614-3426	Candidate tsunami deposit (0-1 m b.s.l.)
Saliña Tam 12°13'24.7"N 68°24'03.0"W	SAT 7/11*	2.73	-0.24	UGAMS 3212	*Cerithium* sp. (marine snail)	-3.74	2740± 25	2607-2462	Candidate tsunami deposit (0-1 m b.s.l.)

	SAT 8/7	2.43	-0.24	UGAMS 5996	*Cerithium* sp. (marine snail)	0.3	2280 ± 20	2021-1869	Candidate tsunami deposit (0-1 m b.s.l.)
	SAT 8/28	2.72	-0.24	UGAMS 7577	*Cerithium* sp. (marine snail)	2.8	3110 ± 20	3039-2857	Candidate tsunami deposit (0-1 m b.s.l.)
Saliña Tam 12°13'43.1"N 68°23'49.0"W	SAT 9/a	3.25	-0.40	UGAMS 7578	*Cerithium* sp. (marine snail)	-3.8	3360 ± 25	3359-3206	Restricted lagoon (0-0.5 m b.s.l.)
	SAT 9/1	3.55	-0.40	UGAMS 5999	Plant fragment (peat)	-24.4	4030 ± 25	4568-4424	Mangroves (±0.15 m a.s.l.)
	SAT 9/2	3.60	-0.40	UGAMS 6000	Plant fragment (peat)	-26.4	4160 ± 25	4826-4584	Mangroves (±0.15 m a.s.l.)
W of Saliña Tam 12°13'25.5"N 68°24'11.9"W	SAT 10/4 Ko	0.50	0.19	UGAMS 7579	*Acropora cervicornis* (coral)	-3.0	1890 ± 25	1563-1395	Overwash deposit in alluvial context (-0.50-0.25 m a.s.l.)
	SAT 10/10	2.10	0.19	UGAMS 7580	Plant fragment (peat)	-26.9	2080 ± 25	2295-2004	Mangroves (±0.15 m a.s.l.)
Boka Bartol 12°17'47.3"N 68°23'32.4"W	BBA 8/6 PF	2.43	-0.57	UGAMS 3201	Plant fragment	-25.0	840 ± 25	789-693	Distal alluvial fan/lagoonal deposit (0-1 m b.s.l.)
	BBA 8/22	5.78	-0.57	UGAMS 3202	Plant fragment	-24.6	5860 ± 25	6742-6636	Mangroves (±0.15 m a.s.l.)
	BBA 8/32	8.36	-0.57	UGAMS 3203	Plant fragment	-27.8	6730 ± 25	7657-7525	Mangroves (±0.15 m a.s.l.)
Boka Bartol 12°17'50.5"N 68°23'34.6"W	BBA 10-124	1.24	-0.72	UGAMS 6007	Plant fragment	-28.7	190 ± 20	289-modern	Distal alluvial fan/lagoonal deposit (0-1 m b.s.l.)
	BBA 10-680	6.80-6.64	-0.72	UGAMS 6009	Articul. *Corbula* sp.	1.0	3370 ± 25	3367-3214	Uppermost part of a candidate tsunami deposit (1-3 m b.s.l.)
	BBA 10-690	6.90-6.84	-0.72	UGAMS 6010	Wood	-25.7	5150 ± 25	5986-5767	Mangroves (± 0.15 m a.s.l.)
Boka Bartol 12°17'56.8"N 68°23'22.5"W	BBA 11/9 ^{14}C	1.47	0.18	UGAMS 6005	Plant fragment	-24.9	3030 ± 25	3339-3162	Candidate tsunami deposit, upper part (0-1 m b.s.l.)
	BBA 11/10 Venus	1.58	0.18	UGAMS 6006	*Chione cancellata*	-0.1	3320 ± 25	3329-3204	Candidate tsunami deposit (0.1-1.1 m b.s.l.)
	BBA 11/10	1.60-1.55	0.18	UGAMS 7584	*Corbula* sp.	-0.1	3390 ± 25	3390-3236	Candidate tsunami deposit (0.1-1.1 m b.s.l.)
Wayaka 12°16'04.9"N 68°24'42.2"W	WAY 1/20 ^{14}C	4.63	0.23	UGAMS 7585	Plant fragment	-24.2	4900 ± 25	5727-5608	Lagoonal deposit (0-1 m b.s.l.)
Wayaka 12°16'13.0"N 68°24'27.9"W	WAY 2/10 F	2.55-2.49	0.07	UGAMS 7586	Plant fragment	0.8	4580 ± 25	4932-4797	Lagoonal deposit (0-1 m b.s.l.)
Boka Funchi 12°16'51.1"N 68°24'37.8"W	BFU 1/17 ^{14}C	3.28-3.20	0.44	UGAMS 7587	*Chione cancellata*	-1.8	3980 ± 25	4143-3951	High-energy wave deposit? (0-1 m b.s.l.)
Playa Grandi 12°16'07.7"N 68°20'14.3"W	PGR 1/15 H	4.11	0.46	UGAMS 4202	Plant fragment	-24.6	3530 ± 25	3885-3720	Coastal marsh/lake (0-0.5 m b.s.l.)
	PGR 1/17 H	4.35-4.31	0.46	UGAMS 4203	Plant fragment	-23.0	3960 ± 25	4518-4299	Coastal marsh (0-1 m b.s.l.)
Playa Grandi 12°16'12.8"N 68°20'12.0"W	PGR 3/10 PR	2.58	0.62	UGAMS 4204	Plant fragment	-25.5	3100 ± 30	3384-3247	candidate tsunami deposit (0-0.5 m b.s.l.)
	PGR 3/13 ^{14}C	2.88	0.62	UGAMS 4205	Plant fragment	-25.8	3620 ± 30	4066-3843	Coastal marsh (0-0.5 m b.s.l.)

9 Summary and synopsis

This summary starts with a synthesis of sedimentary evidence for prehistoric tsunamis (*Chapter 9.1*). It is followed by direct reference to the two main research goals established in *Chapter 1*:

- ➔ **evaluating the long-term influence of extreme wave events on the coastal geo-ecosystems (***Chapter 9.2*), and
- ➔ **improving the chronology of major prehistoric tsunamis for Bonaire and the southern Caribbean** (*Chapter 9.3*).

The latter topic is enriched with a selection of new and unpublished chronological data from subaerial coral deposits. Finally, an outlook is provided, depicting possible implications for coastal management and hazard assessment on Bonaire (*Chapter 9.4*).

9.1 High-energy wave deposits on Bonaire

In search of evidence for prehistoric extreme wave events (EWE) on Bonaire, two main groups of geoarchives were investigated independently (see also outline of the research program in *Chapter 1*).

(i) The coarse-clast record comprises subaerial deposits and their landforms, mainly consisting of blocks (main axis >4.1 m, cf. Blair and McPherson, 1999), boulders (>0.25 m), and cobbles (>6.4 cm). Some landforms, such as ramparts, also exhibit a sand-dominated matrix.

(ii) Coastal morphological depressions store marine overwash deposits, mostly comprising carbonate mud and sand as well as shell material, which is often mixed with terrestrial sediments.

9.1.1 Blocks and boulders

Although this dissertation mainly focuses on group (ii), blocks and boulders were also investigated to tentatively rule out storm waves – which develop lower kinetic energy than tsunamis – for their dislocation. The tsunami hypothesis on Bonaire, an island without any account on tsunami occurrence in historical times, was established by Scheffers (2002, 2004, 2005), who linked a significant part of the supralittoral coarse-clast deposits to flooding by major prehistoric tsunamis. This conclusion was challenged by Morton et al. (2006, 2008) and Spiske et al. (2008).

In *Chapter 2*, the numerical approach of Nott (1997, 2003), which basically involves the balance of uplifting forces (cumulated wave force) and restraining forces (boulder weight, tensile force of the boulder attached to the limestone terrace), was slightly modified based on suggestions of Benner et al. (2010) and Nandasena et al. (2011), and own considerations. If the uplifting forces applied to the boulder – i.e. the intensity or height of the wave (Noormets et al., 2004) – exceed the restraining forces, the boulder is moved. By comparing calculated minimum storm wave heights necessary to quarry and move the largest blocks of Spelonk and Boka Olivia on northeastern Bonaire with maximum wave heights observed during recent high-category hurricanes and the those from the buoy record, little doubt remains that major tsunamis occurred in Mid- to Late Holocene times. This confirmation of the tsunami hypothesis of Scheffers (2002, 2004, 2005) provides a very important

framework condition for the interpretation of the subsurface overwash deposits in the coastal stratigraphical geoarchives.

9.1.2 Subsurface overwash deposits

The identification of palaeotsunami deposits in a trench or in a suite of sediment cores is difficult, as demonstrated by the extended literature review of *Chapter 3*. Besides the presence of sedimentary characteristics listed in Table 5, which were repeatedly documented in modern tsunami deposits, the following tasks may substantially support sedimentary interpretation:

(i) Inferences on tsunami occurrence from boulders or blocks, see *Chapter 9.1.1*;

(ii) thorough analysis of the marine and terrestrial sedimentary environment within the area of interest in order to clearly identify source areas, which may be out of reach for relatively short storm waves;

(iii) documentation of local reference deposits from either recent or historically well documented tsunami or severe storm events enhance interpretation of a palaeo-deposit;

(iv) evaluation of the "tsunami potential" (Peters and Jaffe, 2010a: p. 2) of a site, as well as the potential for other coastal flooding processes.

In order to study subsurface overwash deposits, the coast of Bonaire was divided into three areas: The windward coast (east), the leeward coast (west), and the northwestern part of the island. At the windward coast (*Chapter 4*), a detailed facies model was established based on geochemistry, grain size distribution, and mollusc shell and *Halimeda* taphonomy. This model was used to link every sedimentary unit encountered in the geoarchives of Playa Grandi, Lagun and Boka Washikemba with certain palaeoenvironments and marine overwash processes. The marine overwash processes inferred from the stratigraphy were interpreted to be tsunamis based on their similarity to modern tsunami deposits from other sites (Table 5) and, in particular due to the marginal sedimentary input of severe hurricane swells affecting the coasts of Bonaire during the last decade (Table 6).

At Saliña Tam (*Chapter 6*), both palaeotsunami and palaeostorm deposits were identified based on multi-proxy sediment analyses. Two *ex-situ* marine strata were considered to be tsunamigenic, since they contain planktonic foraminifers in addition to those of a broad spectrum of shelfal to brackish environments. The diversity of foraminifers indicates sediment source areas never reached by storm waves. Other deposits, stacked in a sequence of fining-upward sand layers and separated by thin mud strata, show significantly lower foraminiferal abundance and diversity and were linked with storm deposits. Both candidate tsunami deposits chronologically correlate with those from Playa Grandi and Lagun.

At Boka Bartol, northwestern Bonaire (*Chapter 7*), one allochthonous sediment unit was present in each core indicating a major marine flooding event. The following sedimentary signatures link the deposit with a palaeotsunami: It contains reefal bivalve shells including articulated specimen and shell fragments with predominantly angular breaks. Its geochemical signature is marine (high CO_3^{2-} values, low magnetic susceptibility). The lower contact is erosional indicated by a large hiatus according to ^{14}C ages. The layer has a fining-up pattern and reveals a significantly increased abundance and diversity of ostracods and foraminifers including brackish to open marine taxa. Foraminiferal taxa originating from the deeper shelf indicate a partial sediment source below the storm wave base. A proximal sediment source is indicated by shallow marine and lagoonal microfaunal taxa for the lower

part of the unit, whereas increased microfossil diversity in the upper part including deeper dwelling taxa reflects the final suspension stage, which is typical for tsunami sedimentation. ^{14}C ages obtained from the deposit at all coring sites match those from Playa Grandi and Saliña Tam. As evident for almost all other coring sites, no marine or littoral sediments were deposited during recent hurricanes.

The sedimentary composition of the overwash deposits is a matter of their source. On Bonaire, the major part of these deposits originates from the shallow sublittoral area adjacent to the beaches or boulder ridges. In case of the smaller bokas, they are dominated by *Halimeda* sand and, in smaller amounts, carbonate mud and shells, i.e. the finer sediment fraction of shallow reefs. Beneath the floodplain of Lagun, they mainly consist of heavy shells of *Chione cancellata* and *Crassostrea rhizophorae*, indicating that most of the materal stems from the shallow open embayment of Lagun.

However, the inferences that certain sediment layers result from tsunami flooding are based on individual lines of arguments touched on above and discussed in detail in *Chapters 4*, *6*, and *7*. A definite proof for these interpretations does not exist, due to the lack of a local reference deposit of a recent tsunami. Thus, a storm surge largely exceeding the energy of those accompanying modern hurricanes in the southern Caribbean cannot entirely be ruled out as a possible source for the candidate tsunami layers.

The deposits of ancient flooding events reveal a very disjunct spatial pattern. Their occurrence in geoarchives around the coast of Bonaire is unpredictable. The creation and preservation of a sedimentary record by an extreme wave event is influenced by the pre-impact topography, the approaching angle of wave trains, the availability of a sediment source, and post-depositional alteration. Post-depositional processes, such as bioturbation, may rapidly alter tsunami-laid sediments and hamper their interpretation, as demonstrated by Yawsangratt et al. (2011) and Szczuciński (2012).

9.2 The influence of extreme wave events on the Holocene evolution of bokas and saliñas on Bonaire

The facies models established for each sedimentary archive not only permit inferences on high-energy wave events, they also support the reconstruction of Holocene coastal change. A very important outcome of facies determination and radiocarbon datings from this study is the first relative sea-level curve for Bonaire spanning the last 8000 years (*Chapter 8*). Moreover, substantial and long-lasting environmental changes induced by the high-energy wave events were determined.

In (Early to) Mid-Holocene times, most of the investigated sites were mangrove-fringed embayments, which developed due to flooding of indentations along the coastline (drainage channels cutting the limestone terraces). This applies to Lagun, Boka Bartol, Saliña Tam, Klein Bonaire and Saliña di Cai. Lagun is the only site where mangroves are still established in present times. The stratigraphy of Lagun and Boka Bartol reflects impacts of high-energy wave events – potentially tsunamis – dated to post-2000 BP and post-3300 BP, respectively. The sediments overlying the *ex-situ* marine deposit remarkably differ from the strata below and indicate substantial shifts of both geo-ecosystems.

At Lagun, this is additionally confirmed by palynological investigations. Pollen spectra prior to the wave impact are dominated by mangrove types (*Rhizophora*), whereas a significantly lower percentage of *Rhizophora* pollen in the post-tsunami samples and a subsequent gradual increase in (sub-)recent sediments indicate that the tsunami induced long-lasting modification of the geomorphology

and ecology of Lagun. Mangroves seem to have only gradually recovered from the impact (*Chapter 5*).

In contrast to Lagun, the bokas and saliñas of Bonaire are cut off from the sea by a barrier of beachrock and coral rubble implying low permeability. The candidate tsunami deposit of Boka Bartol is vertically confined by mangrove peat (below) and evaporite-rich mud (above). This pattern is interpreted as the transformation of an open mangrove-fringed embayment (pre-tsunami) into a poly- to hypersaline lagoon (post-tsunami) due to the establishment or final closure of the barrier of coral material during the event. The high amount of gypsum and halite crystals and thin layers of inorganic carbonate are the result of high salinity in the top layer of the water body during the dry season and subsequent precipitation of evaporites in the order of their solubility. The absence of marine faunal remains also indicates lacking surface exchange with ocean water. In line with the findings from Boka Bartol, sediment cores from Wayaka and Boka Funchi also reflect a rather abrupt change from marginal marine conditions to a closed poly- to hypersaline lagoon.

Recent environmental change – as reflected by the stratigraphy of Lagun – is dominated by high terrestrial sedimentation rates and the extension of a vegetation-free floodplain. At Boka Bartol, high sediment loads feed a prograding alluvial fan, which drives silting up of Boka Bartol from its landward end.

9.3 The tsunami chronology of Bonaire

9.3.1 The stratigraphical record

A chronology of events based on the case studies of *Chapters 4*, *5*, and *7* is compiled in the "Caribbean synthesis" of Fig. 48. The oldest extreme wave deposit (EWE I) found in Bonaire's coastal stratigraphies is from Klein Bonaire (around 3600 BP). A well-preserved candidate tsunami deposit from Boka Bartol with a maximum age of 3300 BP (EWE II) has counterparts on the leeward coast (Klein Bonaire, Saliña Tam, possibly between Saliña Tam and Punt'i Wekua) and the windward coast (Playa Grandi, possibly Boka Washikemba). EWE II can be identified as the best-documented potential palaeotsunami on Bonaire. EWE XII, 2000 BP or later, left massive shell-dominated deposits at Lagun (windward side) and Saliña Tam, both of which were interpreted as tsunamigenic. Deposits of another younger unspecified EWE XVI (pre-500 BP) were found between Saliña Tam and Punt'i Wekua and Boka Washikemba. Based on these results, a preliminary estimation of the recurrence interval of high-energy wave events on Bonaire, which reveal magnitudes significantly exceeding those of waves during recent high-category hurricanes and which are therefore likely to be major tsunamis, is in the order of roughly 1000 years or less.

9.3.2 Preliminary correlation with the coarse-clast record

Physical age estimations of subaerial coarse-clast deposits were previously used to infer certain extreme wave events from clustering ages (Scheffers, 2002, 2004, 2005; Scheffers et al. 2006, 2009a). Discussions in *Chapters 4*, *6*, and *7* refer to these results. Morton et al. (2008) pointed out the broad distribution of ages from the coarse-clast landforms of Bonaire and attributed this to repeated impact of storm events or a combination of storm waves and a few tsunamis.

An additional set of ESR (Electron Spin Resonance) and ^{14}C data obtained on surface coral rubble within the framework of the research program outlined in Fig. 2 is currently being processed and

interpreted (Scheffers et al., in prep.). ESR samples were prepared and analyzed at the Geographical Institute of the Universität zu Köln (for details see Hänßler, 2009; Löhr, 2009) following the approach of Schellmann and Radtke (2001). ^{14}C data were generated by Beta Analytic Inc. and calibrated using Calib 6.0.1 (Reimer et al., 2009). Here, preliminary results for selected sites are presented in order to compare them with the stratigraphical record of the same site. The chronological data are presented as a relative probability plot, which shows "the normalised sum of the probability distributions of individual ages". Distinct peaks in the plot represent age groupings, whereas their height correlates with the number of ages in the group and their fractional error (Fitzsimmons et al., 2007: p. 2609). The class range is 300 years. The distance of each data point to the coast and its geomorphological context (in the form of separate units) is indicated as well. One possible way to interpret the relative probability plots is to link a major wave event with the younger end of a right-skewed peak by assuming that such an event destroyed and transported living corals as well as mobilized a large quantity of coral rubble which accumulated over many centuries.

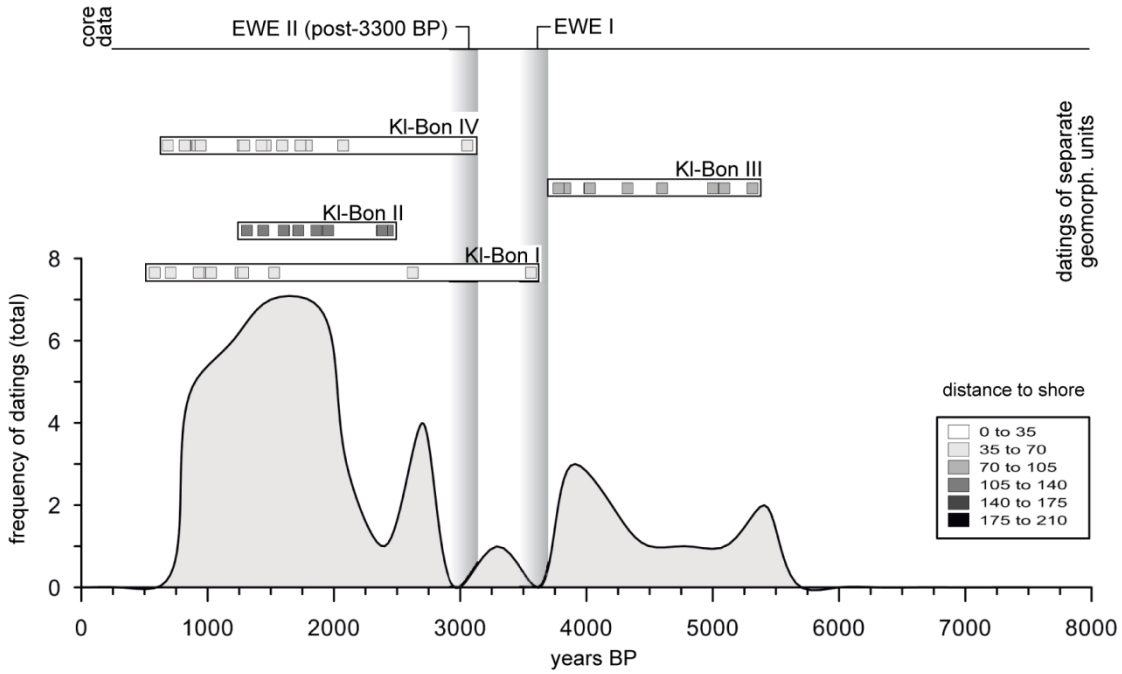

Fig. 53: Relative frequency plot of ESR and ^{14}C data from northern and western Klein Bonaire (Scheffers et al., in prep). Age ranges of EWE I and II were determined in Chapter 6 (design: R. Joannes-Boyau, S.M. May, M. Engel).

9.3.2.1 Klein Bonaire

At the northern and western coast of Klein Bonaire (Fig. 29), coral samples from distinct ridges (KL-Bon I-IV) were taken for dating (Fig. 53). These ridges of coral material are most likely the product of extraordinary wave events, such as high-category tropical cyclones or tsunamis (Scheffers et al., 2012). The landward ridge Kl-Bon III consists of surface ages between 5500 and 3700 BP supporting the timing of EWE I around 3600 BP, which was inferred from sediment core KLB 1. EWE II (post-3300 BP), though present in KLB 1 as well, is not directly supported by the age distribution of coarse-clast deposits. However, low amounts of chronologically correlating coral rubble might be explained by a lack of source material after EWE I and slow recovery of the rubble-producing coral reef (cf. Scheffers et al., 2006). Surface coral boulders of the ridges closer to the coast (Kl-Bon I, II, and IV) show significantly younger ages. No age younger than 500 years occurs, possibly indicating that the formation of ridges stopped since then. The last event significantly contributing to ridge formation might have been the tsunami of 1530 AD, which affected almost the entire north coast of Venezuela according to

historical accounts (Schubert, 1994; O'Loughlin and Lander, 2003) and which may be responsible for the formation of ridge Kl-Bon I and/or Kl-Bon IV, according to the youngest components of these ridges.

9.3.2.2 Saliña Tam

At Saliña Tam (Fig. 30), two shore-perpendicular transects crossing the broad ridge, dominated by fragments of *Acropora cervicornis*, were sampled for dating. Additionally, an older dataset is depicted (Fig. 54). The surface part of the broad ridge appears to be rather young. It is remarkable, how distance to the shore positively correlates with age. This may indicate that historical storms, such as Hurricane Lenny in 1999 or Tecla in 1877 continuously accumulated coral rubble at the seaward part of the ridge, as previously stated by Scheffers (2005). Stepwise growth or progradation of the ridge, respectively, during major wave events is assumed and might have been initiated by a rather old event not represented by the surface samples compiled in Fig. 54; e.g. EWE I (post-3600 BP). Based on core data from inside Saliña Tam (*Chapter 6*), the time between EWE II (post-3300 BP) and EWE XII (2000-1800 BP) was associated with poor protection of the saliña from washover events – most likely due to a rudimentary or partially destroyed ridge which was much lower and more narrow than it is at present. The peak in relative probability around 1000 BP and a possible event-induced supply of coral material is supported by a ^{14}C age obtained from the alluvial deposits at the landward side of the ridge, which was attributed to EWE XVI (post-1300 BP). These might challenge the uniqueness of EWE XVI and possibly rank it among other high-category storms of the last 1300 years, whereas a tsunami should be also excluded by no means.

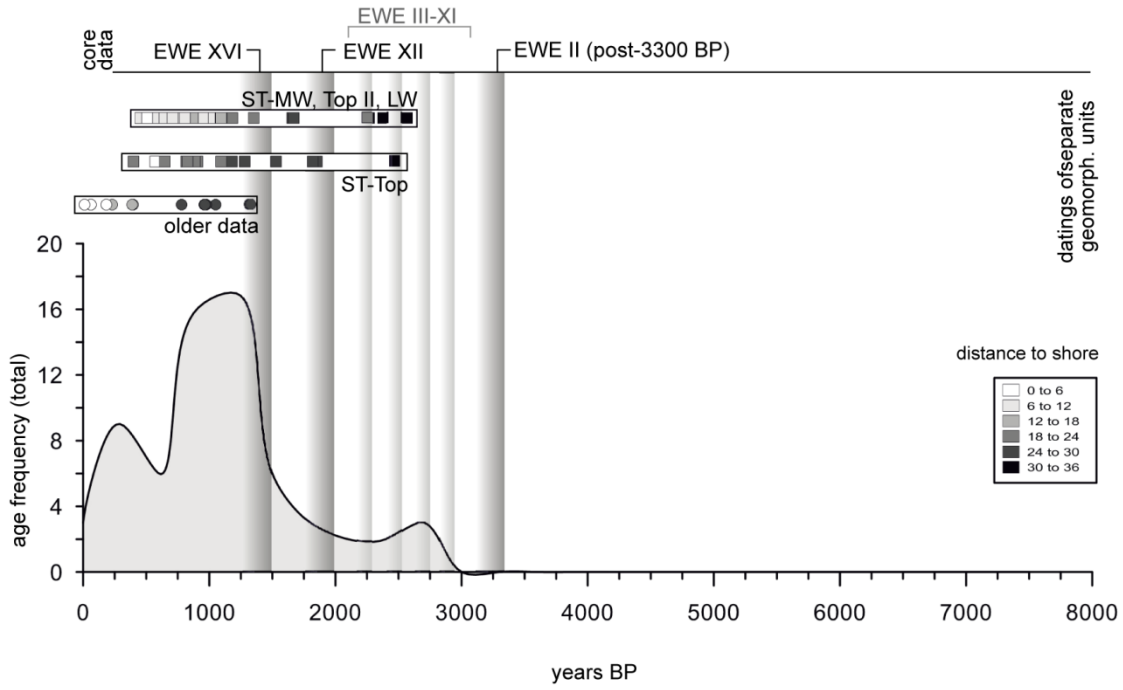

Fig. 54: Relative frequency plot of ESR and ^{14}C data from Saliña Tam (Scheffers et al., in prep). Age ranges of EWEs were determined in *Chapter 6* (design: R. Joannes-Boyau, S.M. May, M. Engel).

9.3.2.3 Boka Bartol

At Boka Bartol (Fig. 42), all subaerial coral samples collected from the barrier of coral rubble (Fig. 55) are younger than the prominent overwash deposit of EWE II (post-3300 BP) in the sediment cores. Based on the stratigraphical pattern in the sediment cores (*Chapter 7*), the establishment or at least

subaerial growth of the massive barrier of coral rubble separating Boka Bartol from the sea occurred during EWE II. Thus, there is no conflict in interpretation, if assuming that the samples taken from the surface represent post-EWE II storms or tsunamis which transported further coral material on top of the barrier. Correlation between age and distance to the shore at sampling sites Boka B I & II as well as several young ages indicate that the barrier still grows laterally towards the sea during recent tropical cyclones. The relevance of high-category tropical cyclonces in forming ridges of coral rubble on the northwestern tip of Bonaire has been demonstrated by Scheffers and Scheffers (2006) and Spiske and Jaffe (2009) for Hurricane Lenny in 1999 and Hurricane Ivan in 2004.

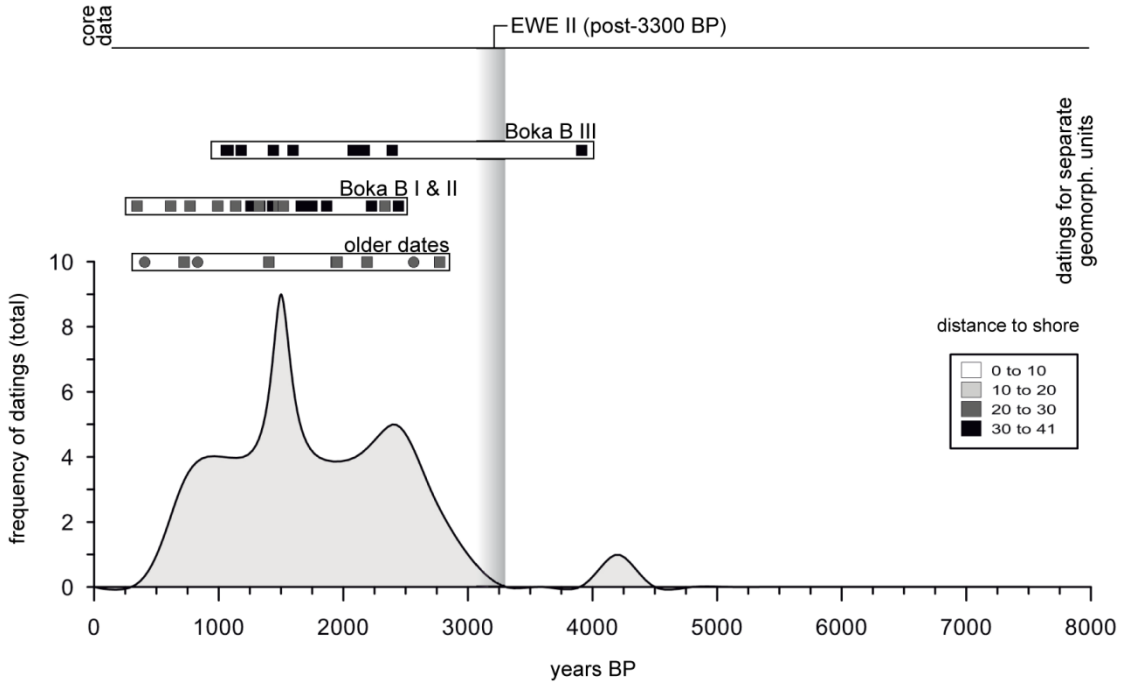

Fig. 55: Relative frequency plot of ESR and ^{14}C data from Boka Bartol (Scheffers et al., in prep). Age ranges of EWE II were determined in *Chapter 7* (design: R. Joannes-Boyau, S.M. May, M. Engel).

9.3.2.4 Correlation of the coarse-clast and stratigraphical record of EWEs – Discussion

Among these local examples none directly questions reconstructions of EWEs from the sediment cores. However, only few peaks of the relative frequency plots unambiguously support the interpretations of EWEs from the cores, such as ages from ridge Kl-Bon III on Klein Bonaire matching the age of the deposit of EWE I in core KLB 1 (*Chapter 6*). Uncertainties regarding analytical procedures, data calculation – e.g. a very small amplitude of the ESR dating signal in Late Holocene samples (Schellmann et al., 2011) –, or local reservoir effects in ^{14}C dating, reworking and incorporation of older material within an EWE deposit (Goff et al., 2012), and the fact that the chronological data only represents maximum ages for an event, hamper more precise chronological estimates. These uncertainties also obstruct more precise correlations between the fine and coarse deposits of the same EWE. For the final analysis of the entire coarse-clast dataset (Scheffers et al., in prep), it is suggested to interpret the ages from each site individually in the light of the local geomorphological setting and its Holocene evolution.

For future studies on sedimentary evidence of Holocene EWEs, U-Th dating might be preferred over ESR or ^{14}C for age estimates of corals (Schellmann et al., 2011). This method provides higher precision and better possibilities of correlating coarse and fine deposits, as for instance demonstrated by Yu et al. (2009) and Zhao and Yu (2010). In order to deduce distinct tsunami events from the largest

blocks, for which storm wave transport was ruled out (*Chapter 2*), efforts to avoid problems associated with ESR and ^{14}C dating of wave-transported living objects summarized above and to directly date the transport process are currently under way. In a pioneering project, exposure ages of surfaces of boulders overturned during the tsunami are being determined using *in situ*-produced cosmogenic nuclides (^{36}Cl) (Rixhon et al., 2012).

9.4 Perspectives for coastal management

As outlined in *Chapter 1*, this dissertation focuses on the identification, characterisation and dating of high-energy wave deposits, in order to improve the Mid- to Late Holocene tsunami chronology for the southern Caribbean. These data are valuable for subsequent tasks or analyses, such as probabilistic tsunami hazard assessment. Palaeotsunami deposits have the ability to extend short historical records and may provide reliable recurrence rates for major earthquake-generated tsunamis (Keating et al., 2008; Dunbar et al., 2009). In combination with models of tsunami inundation they supply crucial input into local flood hazard maps (González et al., 2009).

This study fostered the conclusion of Scheffers (2002, 2005), that the hazard of tsunami does exist on Bonaire, although historical accounts on tsunami ocurrence are lacking. Low-lying, densely populated areas, such as Kralendijk, are particularly threatened, as evidenced by nearby sediment archives such as Klein Bonaire (*Chapter 6*) or Noord Salina (unpublished) in the back of Harbour Village.

The Caribbean special municipalities of the Netherlands, including Bonaire, are organised within the "Tsunami and Other Coastal Hazards Warning System for the Caribbean and Adjacent Regions" (Caribe EWS), installed by the UNESCO Intergovernmental Oceanographic Commission (IOC), for which improvements, in particular regarding communication, are highly mandatory (IOC, 2011). The Meteorological Department of Curaçao, on the sister island of Bonaire, recently implemented a working group which developed a document communicating local tsunami hazard assessment (Meteorological Service Netherlands Antilles and Aruba, 2010a) and local risk analysis (Meteorological Service Netherlands Antilles and Aruba, 2010b) in order to raise public awareness and stimulate local tsunami education. Palaeotsunami research of Scheffers (2002) was considered for the evaluation of the local tsunami hazard (see bibliography in Meteorological Service Netherlands Antilles and Aruba, 2010a). The risk analysis provides a definition of areas of high risk for lives and infrastructure (Meteorological Service Netherlands Antilles and Aruba, 2010b).

A similar approach is highly recommended for Bonaire. It should be accompanied by a study of modelling tsunami inundation based on the spectrum of tsunami triggering mechanisms and previous inundation inferred from the overwash deposits identified in this study (see also González et al., 2009). These activities may include, amongst other measures, the design of evacuation routes and tsunami "safe" locations (see e.g. Jonientz-Trisler et al., 2005, for a comprehensive catalogue of possible countermeasures). Structures which may damp the effects of tsunami overland flow are the natural ridges and ramparts along the coast which originate from high-energy wave events events. At least, during Hurricane Ivan in 2004, waves did not cross these barriers. Unfortunately, these landforms are heavily being mined for construction purposes and only a fraction of their original extent is preserved (Scheffers, 2005).

References

Abbott, R.T., Dance, S.P., 2000. Compendium of Seashells. Odyssey Publications, El Cajon.

Ad-hoc-Arbeitsgruppe Boden der Staatlichen Geologischen Dienste und der Bundesanstalt für Geowissenschaften und Rohstoffe (ed.), 2005. Bodenkundliche Kartieranleitung. Schweizerbart, Stuttgart.

Alexander, C.S., 1961. The marine terraces of Aruba, Bonaire, and Curaçao, Netherlands Antilles. Annals of the Association of American Geographers 51, 102-123.

Andrade, C., Freitas, C., Miranda, J.M., Baptista, A.M., Cachao, M., Silva, P.G., Munha, J., 2003. Recognizing possible tsunami sediments in the ultradissipative environment of the Tagus estuary (Portugal). In: Davis, R.A., Sallenger, A., Howd, P. (eds.), Crossing Disciplinary Boundaries. Proceedings of the International Conference "Coastal Sediments '03" at Clearwater Beach, FL, USA, 18-23 May 2003 (CD-Rom). World Scientific Publishers.

Andrade, C., Freitas, M.C., Moreno, J., Craveiro, S.C., 2004. Stratigraphical evidence of Late Holocene barrier breaching and extreme storms in lagoonal sediments of Ria Formosa, Algarve, Portugal. Marine Geology 210, 339-362.

Anonymous (ed.), 1977. Guide to the Field Excursions on Curaçao, Bonaire and Aruba, Netherlands Antilles. 8th Caribbean Geological Conference Curaçao, 9-24 July 1977. GUA Paper of Geology 10.

Atwater, B.F., 1987. Evidence for great Holocene earthquakes along the outer coast of Washington State. Science 236, 942-944.

Atwater, B.F., Moore, A.L., 1992. A tsunami about 1000 years ago in Puget Sound, Washington. Science 258, 1614-1617.

Atwater, B.F., ten Brink, U.S., Buckley, M., Halley, R.S., Jaffe, B.E., López-Venegas, A.M., Reinhardt, E.G., Tuttle, M.P., Watt, S., Wei, Y., 2011. Geomorphic and stratigraphic evidence for an unusual tsunami or storm a few centuries ago at Anegada, British Virgin Islands. Natural Hazards, doi: 10.1007/s11069-010-9622-6.

Audemard, F.J., 2007. Revised seismic history of the Pilar fault, northeastern Venezuela, from the Cariaco 1997 earthquake and recent preliminary paleoseismic results. Journal of Seismology 11, 311-326.

Audemard, F.A., Romero, G., Rendon, H., Cano, V., 2005. Quaternary fault kinematics and stress tensors along the southern Caribbean from fault-slip data and focal mechanism solutions. Earth-Science Reviews 69, 181-233.

Babu, N., Suresh Babu, D.S., Mohan Das, P.N., 2007. Impact of tsunami on texture and mineralogy of a major placer deposit in southwest coast of India. Environmental Geology 52, 71-80.

Bahlburg, H., 2008. Storm and tsunami deposits in light of cyclone Nargis, Burma, May 2 and 3, 2008. In: Kunkel, C., Hahn, S., ten Veen, N., Rameil, N., Immenhauser, A. (eds.), Abstracts of the 26th IAS Meeting of Sedimentology, Bochum, Germany, 1-3 September 2008. Schriften der Deutschen Gesellschaft für Geowissenschaften 58, 42.

Bahlburg, H., Weiss, R., 2007. Sedimentology of the December 26, 2004, Sumatra tsunami deposits in eastern India (Tamil Nadu) and Kenya. International Journal of Earth Sciences 96, 1195-1209.

Bak, R.P.M., 1977. Coral reefs and their zonation in the Netherlands Antilles. In: Frost, S.H., Weiss, M.P., Saunders, J.B. (eds.), Reefs and related carbonates – Ecology and sedimentology. AAPG Studies in Geology 4, 3-16.

Bandoian, C.A., Murray, R.C., 1974. Pliocene-Pleistocene carbonate rocks of Bonaire, Netherlands Antilles. Geological Society of America Bulletin 85, 1243-1252.

Barbano, M.S., Pirrotta, C., Gerardi, F., 2010. Large boulders along the south-eastern Ionian coast of Sicily: Storm or tsunami deposits? Marine Geology 275, 140-154.

Barkan, R., ten Brink, U.S., Lin, J., 2009. Far field simulations of the 1755 Lisbon earthquake: implications for tsunami hazard to the U.S. East Coast and the Caribbean. Marine Geology 264, 109-122.

Beck, R., Burger, D., Pfeffer, K.-H., 1993. Laborskript. Kleinere Arbeiten aus dem Geographischen Institut der Universität Tübingen 11.

Beets, D.J., Mac Gillavry, H.J., Klaver, G., 1977. Geology of the Cretaceous and early Tertiary of Bonaire. In: Anonymous (ed.), Guide to the field excursions on Curacao, Bonaire and Aruba, Netherlands Antilles. 8th Caribbean Geological Conference on Curaçao, 9-24 July 1977. GUA Paper of Geology 10, 18-28.

Benner, R., Browne, T., Brückner, H., Kelletat, D., Scheffers, A., 2010. Boulder Transport by Waves: Progress in Physical Modeling. Zeitschrift für Geomorphologie N.F. 54(Suppl. 3), 127-146.

Benson, R.H., 1959. Ecology of recent ostracodes of the Todos Santos Bay region, Baja California. The University of Kansas Paleontological Contributions 23.

Bertran, P., Bonnissent, D., Imbert, D., Lozouet, P., Serrand, N., Stouvenot, C., 2004. Paléoclimat des Petit Antilles depuis 4000 ans BP: l'enregistrement de la lagune de Grand-Case à Saint-Martin. Comtes Rendues Geoscience 336, 1501-1510.

Beven, J.L., Landsea, C., 2009. Tropical Cyclone Report, Hurricane Omar (AL 152008), 13-18 October 2008. National Hurricane Center, URL: http://www.nhc.noaa.gov/pdf/TCR-AL152008_Omar.pdf, last access: 03-31-2009.

Biasutti, M., Sobel, A.H., Camargo, S.J., Cretys, T.T., 2011. Projected changes in the physical climate of the Gulf Coast and Caribbean. Climatic Change, doi: 10.1007/s10584-011-0254-y.

Bilham, R., 2010. Lessons from the Haiti earthquake. Nature 463, 878-879.

Bird, E. 2008. Coastal Geomorphology – An Introduction. Wiley & Sons, Chichester.

Bird, M.I., Fifield, L.K., Chua, S., Goh, B., 2004. Calculating sediment compaction for radiocarbon dating of intertidal sediments. Radiocarbon 46, 421-435.

Blair, T.C., McPherson, J.G., 1999. Grain-size and textural classification of coarse sedimentary particles. Journal of Sedimentary Research 69, 6-19.

Blott, S.J., Pye, K., 2001. GRADISTAT: a grain size distribution and statistics package for the analysis of unconsolidated sediments. Earth Surface Processes and Landforms 26, 1237-1248.

Blume, H., 1962. Beiträge zur Klimatologie Westindiens. Erdkunde 16, 271-289.

Bondevik, S., Svendsen, J.I., Mangerud, J., 1997. Tsunami sedimentary facies deposited by the Storegga tsunami in shallow marine basins and coastal lakes, western Norway. Sedimentology 44, 1115-1131.

Bondevik, S., Mangerud, J., Dawson, S., Dawson, A., Lohne, Ø., 2005. Evidence for three North Sea tsunamis at the Shetland Islands between 8000 and 1500 years ago. Quaternary Science Reviews 24, 1757-1775.

Bourgeois, J., 2009. Geologic effects and records of tsunamis. In: Robinson A.R., Bernard, E.N. (eds.), The Sea, Volume 15: Tsunamis. Harvard University Press, pp. 53-91.

Bourgeois, J., MacInnes, B., 2010. Tsunami boulder transport and other dramatic effects of the 15 November 2006 central Kuril Islands tsunami on the island of Matua. Zeitschrift für Geomorphologie N.F. 54(Suppl. 3), 175-195.

Boyajian, G.E., Thayer, C.W., 1995. Clam Calamity: A Recent Supratidal Storm-Deposit as an Analog for Fossil Shell Beds. Palaios 10, 494-489.

Bridge, J.S., 2008. Discussion of articles in "Sedimentary features of tsunami deposits". Sedimentary Geology 211, 94.

Bridge, J.S., Demicco, R.V., 2008. Earth Surface Processes, Landforms and Sediment Deposits. Cambridge University Press, New York.

Bries, J.M., Debrot, A.O., Meyer, D.L., 2004. Damage to the leeward reefs of Curaçao and Bonaire, Netherlands Antilles from a rare storm event: Hurricane Lenny, November 1999. Coral Reefs 23, 297-307.

Brill, D., Brückner, H., Jankaew, K., Kelletat, D., Scheffers, A., Scheffers, S., 2011. Potential predecessors of the 2004 Indian Ocean Tsunami – Sedimentary evidence of extreme wave events at Ban Bang Sak, SW Thailand. Sedimentary Geology 239, 146-161.

Brooks, W.W., 1973. Distribution of Recent Foraminifera from the Southern Coast of Puerto Rico. Micropaleontology 19, 385-416.

Brooks, G.R., Devine, B., Larson, R.A., Rood, B.P., 2007. Sedimentary development of Coral Bay, St. John, USVI: A shift from natural to anthropogenic influences. Caribbean Journal of Science 43, 226-243.

Brückner, H., 2000. Küsten – sensible Geo- und Ökosysteme unter zunehmendem Stress. Petermanns Geographische Mitteilungen 143, 6-19.

Brückner, H., Radtke, U., 1990. Küstenlinien – Indikatoren für Neotektonik und Eustasie. Geographische Rundschau 42, 654-661.

Brückner, H., Brill, D., Jankaew, K., Kelletat, D., Klasen, N., Vött A., 2010. Tsunami deposits from the west coast of Thailand: Predecessors of the Indian Ocean Tsunami – identification and dating. Abstract Volume of the 3rd International Tsunami Field Symposium, Sendai, Japan, 10-16 April 2010, pp. 53-54.

Brückner, H., Kelterbaum, D., Marunchak, O., Porotov, A. & Vött, A., 2010. The Holocene sea level story since 7500 BP – Lessons from the Mediterranean, the Black and the Azov Seas. Quaternary International 225, 160-179.

Bryant, E., 2008. Tsunami – The Underrated Hazard. Springer, Berlin.

Bucher, D.J., Harriot, V.J., Roberts, L.G., 1998. Skeletal micro-density, porosity and bulk density of acroporid corals. Journal of Experimental Marine Biology and Ecology 228, 117-136.

Buckley, M.L., Wei, Y., Jaffe, B.E., Watt, S.G., 2011. Inverse modeling of velocities and inferred cause of overwash that emplaced inland fields of boulders at Anegada, British Virgin Islands. Natural Hazards, doi: 10.1007/s11069-011-9725-8.

Buitrago, J., Capelo, J., Gutiérrez, J., Rada, M., Hernández, R., Grune, S., 2006. Living macromolluscs from a paleo-reef region on the northeastern Venezuelan continental shelf. Estuarine, Coastal and Shelf Science 66, 634-642.

Bungenstock, F., Schäfer, A., 2009. The Holocene relative sea-level curve for the tidal basin of the barrier island Langeoog, German Bight, Southern North Sea. Global and Planetary Change 66, 34-51.

Burr, G.S., Edwards, R.L., Donahue, D.J., Druffel, E.R.M., Taylor, F.W., 1992. Mass Spectrometric ^{14}C and U-Th measurements in coral. Radiocarbon 34, 611-618.

Cambers, G., 2008. Lesser Antilles. In: Bird, E.C.F. (ed.), Encyclopedia of the World's Coastal Landforms – Volume 1. Springer, Dordrecht, pp. 299-310.

Caron, V., 2011. Contrasted textural and taphonomic properties of high-energy wave deposits cemented in beachrocks (St. Bartholomew Island, French West Indies). Sedimentary Geology 237, 189-209.

Chagué-Goff, C., Dawson, S., Goff, J.R., Zachariasen, J., Berryman, K.R., Garnett, D.L., Waldron H.M., Mildenhall D.C., 2002. A tsunami (ca. 6300 years BP) and other Holocene environmental changes, northern Hawke's Bay, New Zealand. Sedimentary Geology 150, 89-102.

Chagué-Goff, C., 2010. Chemical signatures of palaeotsunamis: A forgotten proxy? Marine Geology 271, 67-71.

Choowong, M., Murakoshi, N., Hisada, K., Charoentitirat, T., Charusiri, P., Phantuwongraj, S., Wongkok, P., Choowong, A., Subsayjun, R., Chutakositkanon, V., Jankaew, K., Kanjanapayont, P., 2008. Flow conditions of the 2004 Indian Ocean tsunami in Thailand inferred from capping bedforms and sedimentary structures. Terra Nova 20, 141-149.

Choowong, M., Phantuwongraj, S., Charoentitirat, T., Chutakositkanon, V., Yumuang, S., Charusiri, P., 2009. Beach recovery after 2004 Indian Ocean tsunami from Phang-nga, Thailand. Geomorphology 104, 134-142.

Church, J.A., White, N.J., 2006. A 20th century acceleration in global sea-level rise. Geophysical Research Letters 33, L01602.

Church, J.A., White, N.J., Aarup, T., Wilson, W.S., Woodworth, P.L., Domingues, C.M., Hunter, J.R., Lambeck, K., 2008. Understanding global sea levels: past, present and future. Sustainable Science 3, 9-22.

Cisternas, M., Atwater, B.F., Torrejón, F., Sawai, Y., Machuca, G., Lagos, M., Eipert, A., Youlton, C., Salgado, I., Kamataki, T., Shishikura, M., Rajendran, C.P., Malik, J.K., Rizal, Y., Husni, M., 2005. Predecessors of the giant 1960 Chile earthquake. Nature 437, 404-407.

Clague, J.J., Bobrowsky, P.T., Hutchinson, I., 2000. A review of geological records of large tsunamis at Vancouver Island, British Columbia, and implications for hazard. Quaternary Science Reviews 19, 849-863.

Clark, S.K., 2010. A shift in scientific literacy: Earthquakes generate tsunamis. Eos 91, 316-317.

Corliss, B.H., 1991. Morphology and microhabitat preferences of benthic foraminifera from the northwest Atlantic Ocean. Marine Micropaleontology 17, 195-236.

Costa, P.J.M., Andrade, C., Freitas, M.C., Oliveira, M.A., Jouanneau, J.-M., 2009. Preliminary results of exoscopic analysis of quartz grains deposited by a palaeotsunami in Salgados lowland (Algarve, Portugal). Journal of Coastal Research, SI 56, 39-43.

Cotilla Rodríguez, M.O., Córdoba Barba, D., 2011. Comments about tsunami occurrences in the northern Caribbean. In: Mokhtari, M. (ed.), Tsunami – A growing disaster. InTech, Rijeka, pp. 133-160.

Cox, J.C., Machemehl, J., 1986. Overland bore propagation due to overtopping wave. Journal of Waterway, Port, Coastal, and Ocean Engineering 112, 161-163.

Croudace, I.W., Rindby, A., Rothwell, R.G., 2006. ITRAX: description and evaluation of a new multi-function X-ray core scanner. In: Rothwell, R.G. (ed.), New Techniques in Sediment Core Analysis. Geological Society, London, Special Publication 267, 51-63.

Culver, S.J., 1990. Benthic Foraminifera of Puerto Rican mangrove-lagoon systems: potential for palaeoenvironmental interpretations. Palaios 5, 34-51.

Cutter, S.L., 1996. Vulnerability to environmental hazards. Progress in Human Geography 20, 529-539.

Dahanayake, K., Kulasena, N., 2008. Recognition of diagnostic criteria for recent- and paleo-tsunami sediments from Sri Lanka. Marine Geology 254, 180-186.

Dawson, A., 1996. The geological significance of tsunamis. Zeitschrift für Geomorphologie N.F., Suppl. Vol. 102, 190-210.

Dawson, S., 2007. Diatom biostratigraphy of tsunami deposits: Examples from the 1998 Papua New Guinea tsunami. Sedimentary Geology 200, 328-335.

Dawson, A.G., Shi, S., 2000. Tsunami deposits. Pure and Applied Geophysics 157, 875-897.

Dawson, A., Long, D., Smith, D.E., 1988. The Storegga slides: evidence from eastern Scotland for a possible tsunami. Marine Geology 82, 271-276.

Dawson, A.G., Shi, S., Dawson, S., Takahashi, T., Shuto, N., 1996. Coastal sedimentation associated with the June 2nd and 3rd, 1994 tsunami in Rajegwesi, Java. Quaternary Science Reviews 15, 901-912.

De Buisonjé, P.H., 1974. Neogene and Quaternary geology of Aruba, Curaçao and Bonaire (Netherlands Antilles). PhD thesis, Rijksuniversiteit Utrecht, The Netherlands.

De Freitas, J.A., Nijhof, A.C., Rojer, A.C., Debrot, A.O., 2005. Landscape ecological vegetation map of the island of Bonaire (Southern Caribbean). Royal Netherlands Academy of Arts and Sciences, Amsterdam.

Deffeyes, K.S., Lucia, F.J., Weyl, P.K., 1965. Dolomitization of recent and Plio-Pleistocene sediments by marine evaporate waters on Bonaire, Netherlands Antilles. In: Pray, L.C., Murray, R.C. (eds.), Dolomitization and limestone diagenesis. SEPM Special Publications 13, 71-88.

Deicke, M., Karius, V., Jahnke, W., Kallweit, W., Rebens, M., Reyer, D., 2007. Charakterisierung von Sturmflutablagerungen auf Hallig Hooge – Quantifizierung des Sedimentwachstums seit 1914. Coastline Reports 9, 93-102.

Delaney, C., Devoy, R., 1995. Evidence from sites in Western Ireland of late Holocene changes in coastal environments. Marine Geology 124, 273-287.

Deplus, C., Le Friant, A., Boudon, C., Komorowski, J.-C., Villemant, B., Harford, C., Ségoufin, J., Cheminée, J.-L., 2001. Submarine evidence for large-scale debris avalanches in the Lesser Antilles Arc. Earth and Planetary Science Letters 192, 145-157.

Digerfeldt, G., Hendry, M.D., 1987. An 8000 year Holocene sea-level record from Jamaica: implications for interpretation of Caribbean reef and coastal history. Coral Reefs 5, 165-169.

Dix, G.R., Patterson, R.T., Park, L.E., 1999. Marine saline ponds as sedimentary archives of late Holocene climate and sea-level variation along a carbonate platform margin: Lee Stocking Island, Bahamas. Palaeogeography, Palaeoclimatology, Palaeoecology 150, 223-246.

Dominey-Howes, D.T.M., 1996. Sedimentary deposits associated with the July 9th 1956 Aegean Sea tsunami. Physics and Chemistry of the Earth 21, 51-55.

Dominey-Howes, D.T.M., Humphreys, G.S., Hesse, P.P., 2006. Tsunami and palaeotsunami depositional signatures and their potential value in understanding the late-Holocene tsunami record. The Holocene 16, 1095-1107.

Donato, S.V., Reinhardt, E.G., Boyce, J.I., Rothaus, R., Vosmer, T., 2008. Identifying tsunami deposits using bivalve shell taphonomy. Geology 36, 199-202.

Donnelly, J.P., 2005. Evidence of past intense tropical cyclones from backbarrier salt pond sediments: a case study from Isla de Culebrita, Puerto Rico, USA. Journal of Coastal Research, SI 42, 201-210.

Donnelly, J.P., Woodruff, J.D., 2007. Intense hurricane activity over the past 5,000 years controlled by El Niño and the West African monsoon. Nature 447, 465-468.

Dunbar, P.K., Stroker, K.J., Brocko, V.R., Varner, J.D., McLean, S.J., Taylor, L.A., Eakins, B.W., Carignan, K.S., Warnken, R.R., 2009. Long-term tsunami data archive supports tsunami forecast, warning, research, and mitigation. Pure and Applied Geophysics 165, 2275-2291.

Emanuel, K., 2005. Increasing destructiveness of tropical cyclones over the past 30 years. Nature 436, 686-688.

Engel, M., Brückner, H., 2011. The identification of palaeo-tsunami deposits – a major challenge in coastal sedimentary research. In: Karius, V., Hadler, H., Deicke, M., von Eynatten, H., Brückner, H., Vött, A. (eds.), Dynamische Küsten – Grundlagen, Zusammenhänge und Auswirkungen im Spiegel angewandter Küstenforschung. Coastline Reports 17, 65-80.

Engel, M., May, S.M., 2012. Bonaire's boulder fields revisited: Evidence for Holocene tsunami impact on the Leeward Antilles. Quaternary Science Reviews, doi: 10.1016/j.quascirev.2011.12.011.

Engel, M., Bolten, A., Brückner, H., Daut, G., Kelletat, D., Schäbitz, F., Scheffers, A., Scheffers, S.R., Vött, A., Wille, M., Willershäuser, T., 2009a. Reading the chapter of extreme wave events in nearshore geo-bioarchives of Bonaire (Netherlands Antilles) – initial results from Lagun and Boka Bartol. Marburger Geographische Schriften 145, 157-178.

Engel, M., Knipping, M., Brückner, H., Kiderlen, M., Kraft, J.C., 2009b. Reconstructing middle to late Holocene palaeogeographies of the lower Messenian plain (southwestern Peloponnese, Greece): Coastline migration, vegetation history and sea level change. Palaeogeography, Palaeoclimatology, Palaeoecology 284, 257-270.

Engel, M., Brückner, H., Messenzehl, K., Frenzel, P., Wennrich, V., May, S.M., Daut, G., Willershäuser, T., Scheffers, A., Scheffers, S., Vött, A., Kelletat, D., 2010a. Palaeotsunami in the southern Caribbean: clarity through new geological archives? Eos Transactions AGU, Fall Meeting Suppl., Abstract OS31D-1452.

Engel, M., Brückner, H., Wennrich, V., Scheffers, A., Kelletat, D., Vött, A., Schäbitz, F., Daut, G., Willershäuser, T., May, S.M., 2010b. Coastal stratigraphies of eastern Bonaire (Netherlands Antilles): new insights into the palaeotsunami history of the southern Caribbean. Sedimentary Geology 231, 14-30.

Engel, M., Brückner, H., Messenzehl, K., Frenzel, P., May, S.M., Scheffers, A., Scheffers, S., Wennrich, V., Kelletat, D., in press. Shoreline changes and high-energy wave impacts at the leeward coast of Bonaire (Netherlands Antilles). Earth, Planets and Space.

Etienne, S., Buckley, M., Paris, R., Nandasena, A.K., Clark, K., Strotz, L., Chagué-Goff, C., Goff, J., Richmond, B., 2011. The use of boulders for characterizing past tsunamis: Lessons from the 2004 Indian Ocean and 2009 South Pacific tsunamis. Earth-Science Reviews 107, 76-90.

Fairbanks, R.G., 1989. A 17,000-year glacio-eustatic sea level record: influence of glacial melting rates on the Younger Dryas event and deep-ocean circulation. Nature 342, 637-642.

Farrell, W.E., Clark, J.A., 1976. On postglacial sea level. Geophysical Journal of the Royal Astronomical Society 46, 647-667.

Farreras, S., Ortiz, M., Gonzalez, J.I., 2007. Steps towards the implementation of a tsunami detection, warning, mitigation and preparedness program for southwestern coastal areas of Mexico. Pure and Applied Geophysics 164, 605-616.

Felton, E.A., 2002. Sedimentology of rocky shorelines: 1. A review of the problem, with analytical methods, and insights gained from the Hulope Gravel and the modern rocky shoreline of Lanai, Hawaii. Sedimentary Geology 152, 221-245.

Fitzpatrick, S.M., 2012. On the shoals of giants: natural catastrophes and the overall destruction of the Caribbean's archaeological record. Journal of Coastal Conservation 16, 173-186.

Fitzsimmons, K.E., Rhodes, E.J., Magee, J.W., Barrows, T.T., 2007. The timing of linear dune activity in the Strzelecki and Tirari Deserts, Australia. Quaternary Science Reviews 26, 2598-2616.

Floth, U., Vött, A., May, S.M., Brückner, H., Brockmüller, S., 2009. Geo-scientific evidence versus computer models of tsunami landfalls in the Lefkada coastal zone (NW Greece). Marburger Geographische Schriften 145, 140-156.

Focke, J.W., 1978a. Holocene development of coral fringing reefs, Leeward off Curaçao and Bonaire (Netherlands Antilles). Marine Geology 28, M31-M41.

Focke, J.W., 1978b. Limestone cliff morphology on Curaçao (Netherlands Antilles), with special attention to the origin of notches and vermetid/coralline algal surf benches ("corniches", "trottoirs"). Zeitschrift für Geomorphologie N.F. 22, 329-349.

Folk, R.L., Ward, W.C., 1957, Brazos River Bar: a study in the significance of grain size parameters. Journal of Sedimentary Petrology 27, 3-26.

Font, E., Nascimento, C., Baptista, M.A., Silva, P.F., 2010. Identification of tsunami-induced deposits using numerical modelling and rock magnetism techniques: A study case of the 1755 Lisbon tsunami in Algarve, Portugal. Physics of the Earth and Planets Interiors 182, 187-198.

Frenzel, P., Boomer, I., 2005. The use of ostracods from marginal marine, brackish waters as bioindicators of modern and Quaternary environmental change. Palaeogeography, Palaeoclimatology, Palaeoecology 225, 68-92.

Fritz, H.M., Blount, C.D., Thwin, S., Kyaw Thu, M., Chan, N., 2009. Cyclone Nargis storm surge in Myanmar. Nature Geoscience 2, 448-449.

Fritz, H.M., Kalligeris, N., Borrero, J.C., Broncano, P., Ortega, E., 2008. The 15 August 2007 Peru tsunami runup observations and modeling. Geophysical Research Letters 35, L10604.

Frohlich, C., Hornbach, M.J., Taylor, F.W., Shen, C.-C., Moala, 'A., Morton, A.E., Kruger, J., 2009. Huge erratic boulders in Tonga deposited by a prehistoric tsunami. Geology 37, 131-134.

Fujiwara, O., Masuda, F., Sakai, T., Irizuki, T., Fuse, K., 2000. Tsunami deposits in Holocene bay mud in southern Kanto region, Pacific coast of central Japan. Sedimentary Geology 135, 219-230.

Fukui, Y., Nakamura, M., Shiraishi, H., Sasaki, Y., 1963. Hydraulic study on tsunami. Coastal Engineering in Japan 6, 67-82.

García-Cubas, A., Reguero, M., 1995. Moluscos de la laguna Sontecompan, Veracruz, México: sistemática y ecología. Hidrobiológica 5, 1-24.

Gehrels, W.R., 1999. Middle and late Holocene sea-level changes in eastern Maine reconstructed from foraminiferal saltmarsh stratigraphy and AMS ^{14}C dates on basal peat. Quaternary Research 52, 350-359.

Gehrels, W.R., Horton, B.P., Kemp, A.C., Sivan, D., 2011. Two millennia of sea level data: The key to predicting change. Eos 92, 289-290.

Gelfenbaum, G., Jaffe, B.E., 2003. Erosion and sedimentation from the 17 July, 1998 Papua New Guinea Tsunami. Pure and Applied Geophysics 160, 1969-1999.

Gischler, E., 2003. Holocene lagoonal development in the isolated carbonate platforms off Belize. Sedimentary Geology 159, 113-132.

Goff, J., Chagué-Goff, C., Nichol, S., 2001. Palaeotsunami deposits: a New Zealand perspective. Sedimentary Geology 143, 1-6.

Goff, J., McFadgen, B.G., Chagué-Goff, C., 2004. Sedimentary differences between the 2002 Easter storm and the 15th-century Okoropunga tsunami, southeastern North Island, New Zealand. Marine Geology 204, 235-250.

Goff, J., Pearce, S., Nichol, S.L., Chagué-Goff, C., Horrocks, M., Strotz, L., 2010. Multi-proxy records of regionally-sourced tsunamis, New Zealand. Geomorphology 118, 369-382.

Goff, J. Chagué-Goff, C., Nichol, S., Jaffe, B., Dominey-Howes, D., 2012. Progress in palaeotsunami research. Sedimentary Geology 243-244, 70-88.

Goldenberg, S.B., Shapiro, L.J., 1996. Physical mechanisms for the association of El Niño and West African Rainfall with Atlantic Major Hurricane Activity. Journal of Climate 9, 1169-1187.

González, F.I., Geist, E.L., Jaffe, B., Kanoglu, U., Mofjeld, H., Synolakis, C.E., Titov, V.V., Arcas, D., Bellomo, D., Carlton, D., Horning, T., Johnson, J. Newman, J., Parsons, T., Peters, R., Peterson, C., Priest, G., Venturato, A., Weber, J., Wong, F., Yalciner, A., 2009. Probabilistic tsunami hazard assessment at Seaside, Oregon, for near- and far-field seismic sources. Journal of Geophysical Research 114, C11023.

González, C., Urrego, L.E., Martínez, J.I., Polanía, J., Yokoyama, Y., 2010. Mangrove dynamics in the southwestern Caribbean since the 'Little Ice Age': A history of human and natural disturbances. The Holocene 20, 849-861.

Goodfriend, G.A., 1987. Radiocarbon age anomalies in shell carbonate of land snails from semi-arid areas. Radiocarbon 29, 159-167.

Goodfriend, G.A., Gould, S.J., 1996. Paleontology and chronology of two evolutionary transitions by hybridization in the Bahamian land snail *Cerion*. Science 274, 1894-1897.

Gornitz, V., 2005. Natural Hazards. In: Schwartz, M.L. (ed.), Encyclopedia of Coastal Science. Springer, Dordrecht, pp. 678-684.

Goto, K., Okada, K., Imamura., F., 2009. Characteristics and hydrodynamics of boulders transported by storm waves at Kudaka Island, Japan. Marine Geology 262, 14-24.

Goto, K., Kawana, T., Imamura, F., 2010. Historical and geological evidence of boulders deposited by tsunamis, southern Ryukyu Islands, Japan. Earth-Science Reviews 102, 77-99.

Goto, K., Chagué-Goff, C., Fujino, S., Goff, J., Jaffe, B., Nishimura, Y., Richmond, B., Sugawara, D., Szczuciński, W., Tappin, D.R., Witter, R.C., Yulianto, E., 2011. New insights of tsunami hazard from the 2011 Tohoku-oki event. Marine Geology 290, 46-50.

Grauert, M., Björck, S., Bondevik S., 2001. Storegga tsunami deposits in a coastal lake on Suðuroy, the Faroe Islands. Boreas 30, 263-271.

Grindlay, N.R., Hearne, M., Mann, P., 2005. High risk of tsunami in the Northern Caribbean. Eos 86, 121; 126.

Hammer, Ø., Harper, D.A., Ryan, P.D., 2001. PAST: paleontological statistics software package for education and data analysis. Palaeontologia Electronica 4, 1-9.

Hänßler, E., 2009. Ablagerungen holozäner Extremereignisse an der Ostküste Bonaires, Niederländische Antillen, und ihre Datierung mittels der Elektronen-Spin-Resonanz-Methode (ESR). Diploma thesis, Universität zu Köln, Germany.

Hansom, J.D., Barltrop, N.D.P., Hall, A.M., 2008. Modelling the process of cliff-top erosion and deposition under extreme waves. Marine Geology 253, 36-50.

Hart, A.M., Kaesler, R.L., 1986. Temporal changes in Holocene lagoonal assemblages of Foraminifera from northeastern Yucatán Peninsula, Mexiko. Journal of Foraminiferal Research 16, 98-109.

Hartog, J., 1978. A short history of Bonaire. De Wit, Aruba.

Haug, G.H., Günther, D., Peterson, L.C., Sigman, D.M., Hughen K., Aeschlimann B., 2003. Climate and the collapse of Maya civilization. Science 299, 1731-1735.

Havach, S.M., Collins, L.S., 1997. The distribution of recent benthic Foraminifera across habitats of Bocas del Toro, Caribbean Panama. Journal of Foraminiferal Research 27, 232-249.

Haviser, J.B., 1991. The first Bonaireans. Reports of the Archaeological-Anthropological Institute of the Netherlands Antilles 10.

Hawkes, A.D., Bird, M., Cowie, S., Grundy-Warr, C., Horton, B.P., Hwai, A.T.S., Law, L., Macgregor, C., Nott, J., Ong, J.E., Rigg, J., Robinson, R., Tan-Mullins, M., Sa, T.T., Yasin, Z., Aik, L.W., 2007. Sediments deposited by the 2004 Indian Ocean Tsunami along the Malaysia—Thailand Peninsula. Marine Geology 242, 169-190.

Hearty, P.J., 1997. Boulder deposits from Large Waves during the Last Interglaciation on North Eleuthera Island, Bahamas. Quaternary Research 48, 326-338.

Heinrich, P., Guibourg, S., Mangeney, A., Roche, R., 1999. Numerical modeling of a landslide generated tsunami following a potential explosion of the Montserrat Volcano. Physics and Chemistry of the Earth, Part A 24, 163-168.

Hemphill-Haley, E., 1995. Diatom evidence for earthquake-induced subsidence and tsunami 300 yr ago in southern coastal Washington. Bulletin of the Geological Society of America 107, 367-378.

Hendry, M.D., 1987. Tectonic and eustatic control on late Cenozoic sedimentation within an active plate boundary zone, west coast margin, Jamaica. Geological Society of America Bulletin 99, 718-728.

Herweijer, J.P., Focke, J.W., 1978. Late Pleistocene depositional and denudational history of Aruba, Bonaire and Curaçao (Netherlands Antilles). Geologie en Mijnbouw 57, 177-187.

Herweijer, J.P., de Buisonjé, P.H., Zonneveld, J.I.S., 1977. Neogene and Quaternary geology and geomorphology. In: Anonymous (ed.), Guide to the field excursions on Curacao, Bonaire and Aruba, Netherlands Antilles. 8th Caribbean Geological Conference on Curaçao, 9-24 July 1977. GUA Paper of Geology 10, 39-55.

Higuera-Gundy, A., Brenner, M., Hodell, D.A., Curtis, J.H., Leyden, B.W., Binford, M.W., 1999. A 10,300 ^{14}C yr record of climate and vegetation change from Haiti. Quaternary Research 52, 159-170.

Hills, J.G., Mader, C.L., 1997. Tsunami produced by the impacts of small asteroids. Annals of the New York Academy of Sciences 822, 381-394.

Hindson, R.A., Andrade, C., 1999. Sedimentation and hydrodynamic processes associated with the tsunami generated by the 1755 Lisbon earthquake. Quaternary International 56, 27-38.

Hippolyte, J.C., Mann, P., 2011. Neogene–Quaternary tectonic evolution of the Leeward Antilles islands (Aruba, Bonaire, Curaçao) from fault kinematic analysis. Marine and Petroleum Geology 28, 259-277.

Hobgood, J., 2005. Tropical cyclones. In: Oliver, J.E. (ed.), Encyclopedia of World Climatology. Dordrecht, Springer, pp. 750-755.

Hornbach, M.J., Mann, P., Wolf, S., King, W., Boon, R., 2008. Assessing slope stability at Seroe Mansinga and Caracas Bay, Curaçao. Final report for APNA, Willemstad, Curaçao. URL: http://www.apna.an/apna/library/files/VistaRoyal/APNAfinalreport.pdf, last access: 09-22-11.

Hornbach, M.J., Mann, P., Taylor, F.W., Bowen, S.W., 2010. Estimating the Age of Near-Shore Carbonate Slides Using Coral Reefs and Erosional Markers: A Case Study from Curaçao, Netherlands Antilles. The Sedimentary Record 8, 4-10.

Horton, B.P., Shennan, I., 2009. Compaction of Holocene strata and the implications for relative sea-level change on the east coast of England. Geology 37, 1083-1086.

Horton, B.P., Rossi, V., Hawkes, A.D., 2009. The sedimentary record of the 2005 hurricane season from the Mississippi and Alabama coastlines. Quaternary International 195, 15-30.

Hughen, K.A., Baillie, M.G.L., Bard, E., Bayliss, A., Beck, J.W., Bertrand, C., Blackwell, P.G., Buck, C.E., Burr, G., Cutler, K.B., Damon, P.E., Edwards, R.L., Fairbanks, R.G., Friedrich, M., Guilderson, T.P., Kromer, B., McCormac, F.G., Manning, S., Bronk Ramsey, C., Reimer, P.J., Reimer, R.W., Remmele, S., Southon, J.R., Stuiver, M., Talamo, S., Taylor, F.W., van der Plicht, J., Weyhenmeyer, C.E., 2004. Marine04 marine radiocarbon age calibration, 26-0 ka BP. Radiocarbon 46, 1059-1086.

Hughes, T.P., 1987. Skeletal density and growth form of corals. Marine Ecology – Progress Series 35, 259-266.

Hughes, J.F., Mathewes, R.W., Clague, J.J., 2002. Use of pollen and vascular plants to estimate coseismic subsidence at a tidal marsh near Tofino, British Columbia. Palaeogeography, Palaeoclimatology, Palaeoecology 185, 145-161.

Hussain, S. M., Krishnamurthy, R., Suresh Gandhi, M., Ilayaraja, K., Ganesan, P., Mohan, S.P., 2006. Micropalaeontological investigations on tsunamigenic sediments of Andaman Islands, Current Science 91(12), 1655-1667.

Imamura, F., Goto, K., Ohkubo, S., 2008. A numerical model for the transport of a boulder by tsunami. Journal of Geophysical Research 113, C01008.

IOC (Intergovernmental Oceanographic Commission), 1998. Post-tsunami survey field guide. IOC Manuals and Guides 37.

IOC (Intergovernmental Oceanographic Commission), 2008a. Caribe EWS Implementation Plan. Discussion Paper for the third session of the Intergovernmental Coordination Group for the tsunami and other coastal hazards warning system for the Caribbean and adjacent regions (ICG/CARIBE EWS-III). Panama, 12-14 March 2008. URL: http://www.ioc-tsunami.org/images/stories/documents/caribeipe.pdf, last access, 03-07-12.

IOC (Intergovernmental Oceanographic Commission), 2008b. Tsunami glossary, 2008. IOC Series 85. URL: http://ioc3.unesco.org/itic/contents.php?id=19, last access: 03-07-12.

IOC (Intergovernmental Oceanographic Commission), 2011. Intergovernmental Coordination Group for the Tsunami and Other Coastal Hazards Warning System for the Caribbean Sea and Adjacent Regions (ICG/CARIBE EWS) – Sixth Session. Santo Domingo, Dominican Republic, 26-29 April 2011. URL: http://www.ioc-cd.org/components/com_oe/oe.php?task=download&id=15436&version=1.0&lang=1&format=1, last access: 03-15-12.

Jackson, T.A., Robinson, E., 1994. The Netherlands and Venezuelan Antilles. In: Donovan, S.K., Jackson T.A. (eds.), Caribbean Geology: An Introduction. University of the West Indies Press, Kingston, pp. 249-263.

Jaffe, B.E., Gelfenbaum, G., 2007. A simple model for calculating tsunami flow speed from tsunami deposits. Sedimentary Geology 200, 347-361.

Jaffe, B.E., Gelfenbaum, G., Rubin, D.M., Peters, R., Anima, R., Swensson, M., Olcese, D., Anticona, L.B., Gomez, J.C., Riega, P.C., 2003. Identification and interpretation of tsunami deposits from the June 23, 2001 Perú tsunami. In: Davis, R.A., Sallenger, A., Howd, P. (eds.), Crossing Disciplinary Boundaries. Proceedings of the International Conference “Coastal Sediments '03” at Clearwater Beach, FL, USA, 18-23 May 2003 (CD-Rom). World Scientific Publishers.

Jaffe, B.E., Morton, R.A., Kortekaas, S., Dawson, A.G., Smith, D.E., Gelfenbaum, G., Foster, I.D.L., Long, D., Shi, S., 2008. Reply to Bridge (2008) Discussion of articles in “Sedimentary features of tsunami deposits”. Sedimentary Geology 211, 95-97.

Jagodziński, R., Sternal, B., Szczuciński, W., Lorenc, S., 2009. Heavy minerals in 2004 tsunami deposits on Kho Khao Island, Thailand. Polish Journal of Environmental Studies 18, 103-110.

Jankaew, K., Atwater, B.F., Sawai, Y., Choowong, M., Charoentitirat, T., Martin, M.E., Prendergast, A., 2008. Medieval forewarning of the 2004 Indian Ocean tsunami in Thailand. Nature 455, 1228-1231.

Jessen, C.A., Pedersen, J.B.T., Bartholdy, J., Seidenkrantz, M.-S., Kuijpers, A., 2008. A late Holocene palaeoenvironmental record from Altona Bay, St. Croix, US Virgin Islands. Danish Journal of Geography 108(2), 59-70.

Jones, B., Hunter, I.G., 1992. Very large boulders on the coast of Grand Cayman: the effects of giant waves on rocky coastlines. Journal of Coastal Research 8, 763-774.

Jonientz-Trisler, C., Simmons, R.S., Yanagi, B.S., Crawford, G.L., Darienzo, M., Eisner, R.K., Petty, E., Priest, G.R., 2005. Planning for tsunami-resilient communities. Natural Hazards 35, 121-139.

Kamthonkiat, D., Rodfai, C., Saiwaurungkul, Koshimura, S., Matsuoka, M., 2011. Geoinformatics in mangrove monitoring: damage and recovery after the 2004 Indian Ocean tsunami in Phang Nga, Thailand. Natural Hazards and Earth System Science 11, 1851-1862.

Keating, B.H., Wanink, M., Helsley, C.E., 2008. Introduction to a tsunami-deposits database. In: Shiki, T., Tsuji, Y., Yamazaki, T., Minoura, K. (eds.), Tsunamiites – Features and Implications. Elsevier, Amsterdam, Oxford, pp. 359-381.

Kelletat, D., 1988. Zonality of modern coastal processes and sea-level indicators. Palaeogeography, Palaeoclimatology, Palaeoecology 68, 219-230.

Kelletat, D., 2003. Tsunami durch Impacts von Meteoriten im Quartär? Essener Geographische Arbeiten 35, 27-38.

Kelletat, D., 2005. A Holocene sea level curve for the eastern Mediterranean from multiple indicators. Zeitschrift für Geomorphologie N.F., Suppl. Vol. 137, 1-9.

Kelletat, D., 2008. Comments to Dawson, A.G. and Stewart, I. (2007), Tsunami deposits in the geological record. Sedimentary Geology 211, 87-91.

Kelletat, D., Schellmann, G., 2002. Tsunamis on Cyprus: field evidences and ^{14}C dating results. Zeitschrift für Geomorphologie N.F. 46, 19-34.

Kelletat, D., Scheffers, A., Scheffers, S., 2004. Holocene tsunami deposits on the Bahaman Islands of Long Island and Eleuthera. Zeitschrift für Geomorphologie N.F. 48, 519-540.

Kelletat, D., Scheffers, S.R., Scheffers, A., 2007. Field signatures of the SE-Asian mega-tsunami along the west coast of Thailand compared to Holocene paleo-tsunami from the Atlantic region. Pure and Applied Geophysics 164, 413-431.

Keyser, D., 1977a. Brackwasser-Cytheracea aus Süd-Florida (Crust.: Ostracoda: Podocopa). Abhandlungen und Verhandlungen des naturwissenschaftlichen Vereins Hamburg 20: 43-85.

Keyser, D., 1977b. Ecology and zoogeography of recent brackish-water Ostracoda (Crustacea) from South-West Florida. In: Löffler, H. (eds.), Aspects of ecology and zoogeography of recent and fossil Ostracoda. Kluwer, The Hague, pp. 207-222.

Khan, S., Robinson, E., Rowe, D.-A., Coutou, R., 2010. Size and mass of shoreline boulders moved and emplaced by recent hurricanes, Jamaica. Zeitschrift für Geomorphologie N.F. 54(Suppl. 3), 281-299.

Kilfeather, A.A., Blackford, J.J., van der Meer, J.J.M., 2007. Micromorphological analysis of coastal sediments from Willapa Bay, Washington, USA: A technique for analysing inferred tsunami deposits. Pure and Applied Geophysics 164, 509-525.

Kim, K.H., Lee, D.-J., 1999. Distribution and depositional environments of corralline lithofacies in uplifted Pleistocene coral reefs of Bonaire, Netherlands Antilles. Journal of the Paleontological Society of Korea 15, 115-133.

Klosowska, B.B., 2003. Late Holocene embayment and salina record of Curaçao (Dutch Antilles): Criteria to monitor environmental change and biodiversity. PhD thesis, Vrije Universiteit Amsterdam, The Netherlands.

Klosowska, B.B., Troelstra, S.R., van Hinte, J.E., Beets, D., van der Borg, K., de Jong, A.F.M., 2004. Late Holocene environmental reconstruction of St. Michiel saline lagoon, Curaçao (Dutch Antilles). Radiocarbon 46, 765-774.

Kobluk, D.R., Crawford, D.R., 1990. A modern hypersaline organic mud- and gypsum-dominated basin and associated microbialites. Palaios 5, 134-148.

Kobluk, D.R., Lysenko, M.A., 1992. Storm features on a southern Caribbean fringing coral reef. Palaios 7, 213-221.

Köhn, M., 1928. Bemerkungen zur mechanischen Bodenanalyse. III. Ein neuer Pipettierapparat. Journal of Plant Nutrition and Soil Science 11, 50-54.

Komatsubara, J., Fujiwara, O., 2007. Overview of Holocene tsunami deposits along the Nankai, Suruga, and Sagami Troughs, southwest Japan. Pure and Applied Geophysics 164, 493-507.

Kortekaas, S., Dawson, A.G., 2007. Distinguishing tsunami and storm deposits: An example from Martinhal, SW Portugal. Sedimentary Geology 200, 208-221.

Kozak, L., Siepak, J., 2009. The chemical study of tsunami deposits in south Thailand – Review. Polish Journal of Environmental Studies 18, 137-139.

Kraft, J.C., 1978. Coastal stratigraphic sequences. In: Davis, R.A. (ed.), Coastal Sedimentary Environments. Springer, New York, pp. 361-383.

Kraus, N.C., 2005. Beach profile. In: Schwartz, M. (ed.), Encyclopedia of Coastal Science. Springer, Dordrecht, pp. 169-172.

Lambeck, K., 2002. Sea level change from mid Holocene to recent time: An Australian example with global implications. In: Mitrovica, J.X., Vermeersen, B.L.A. (eds.), Ice sheets, sea level and the dynamic earth. American Geophysical Union, Washington D.C., pp. 33-50.

Lampe, R., 2005. Lateglacial and Holocene water-level variations along the NE German Baltic Sea coast: review and new results. Quaternary International 133-134, 121-136.

Lario, J., Luque, L., Zazo, C., Goy, J.L., Spencer, C., Cabero, A., Bardají, T., Borja, F., Dabrio, C.J., Civis, J., González-Delgado, J.Á., Borja, C., Alonso-Azcárate, J., 2010. Tsunami vs. storm surge deposits: a review of the sedimentological records of extreme wave events (EWE) during the Holocene in the Gulf of Cadiz, Spain. Zeitschrift für Geomorphologie N.F. 54(Suppl. 3), 301-316.

Lauterjung, J., Münch, U., Rudloff, A., 2009. Geotechnik im Dienst der Menschheit. Geographische Rundschau 61(12), 36-41.

Lauterjung, J., Münch U. & Rudloff A., 2010. The challenge of installing a tsunami early warning system in the vicinity of the Sunda Arc, Indonesia. Natural Hazards and Earth System Science 10, 641-646.

Lavigne, F., Gomez, C., Giffo, M., Wassmer, P., Hoebreck, C., Mardiatno, D., Prioyono, J., Paris, R., 2007. Field observations of the 17 July 2006 Tsunami in Java. Natural Hazards and Earth System Science 7, 177-183.

Le Friant, A., Boudon, G., Arnulf, A., Robertson, R.E.A., 2009. Debris avalanche deposits offshore St. Vincent (West Indies): Impact of flank-collapse events on the morphological evolution of the island. Journal of Volcanology and Geothermal Research 179, 1-10.

Liew, S.C., Gupta, A., Wong, P.P., Kwoh, L.K., 2010. Recovery from a large tsunami mapped over time: the Aceh coast, Sumatra. Geomorphology 114, 520-529.

Liu, K.-b., 2004. Paleotempestology: Principles, methods and examples from Gulf Coast lake sediments. In: Murname, R.J., Liu, K.-b. (eds.), Hurricanes and typhoons: Past, present, and future. Columbia University Press, New York, pp. 13-57.

Löhr, N., 2009. Holozäne Extremereignisse an der Westküste Bonaires, Niederländische Antillen, und die Datierung korrelater Grobsedimente mittels der Elektronen-Spin-Resonanz-Methode (ESR). Diploma thesis, Universität zu Köln, Germany.

Long, D., Dawson, A.G., Smith, D.E., 1989. Tsunami risk in northwestern Europe: a Holocene example. Terra Nova 1, 532-537.

Lucia, F.J., 1968. Recent sediments and diagenesis of South Bonaire, Netherlands Antilles. Journal of Sedimentary Petrology 38, 845-858.

Luque, L., Lario, J., Civis, J., Silva, P.G., Zazo, C., Goy, J.L., Dabrio, C.J., 2002. Sedimentary record of a tsunami during Roman time, Bay of Cadiz, Spain. Journal of Quaternary Science 17, 623-631.

MacInnes, B.T., Bourgeois, J., Pinegina, T., Kravchunovskaya, E. A., 2009a. Tsunami geomorphology: Erosion and deposition from the 15 November 2006 Kuril Island tsunami, Geology, 37, 995-998.

MacInnes, B.T., Pinegina, T.K., Bourgeois, J., Razhigaeva, N.G., Kaistrenko, V.M., Kravchunovskaya, E.A., 2009b. Field survey and geological effects of the 15 November 2006 Kuril Tsunami in the Middle Kuril Islands. Pure and Applied Geophysics 166, 9-36.

Macintyre, I.G., Toscano, M.A., Lighty, R.G., Bond, G.B., 2004. Holocene history of the mangrove islands of Twin Cays, Belize, Central America. Atoll Research Bulletin 510.

Malaizé, B., Bertran, P., Carbonel, P., Bonnissent, D., Charlier, K., Galop, D., Imbert, D., Serrand, N., Stouvenot, C., Pujol, C., 2011. Hurricanes and climate in the Caribbean during the past 3700 years BP. The Holocene 21, 911-924.

Mamo, B., Strotz, L., Dominey-Howes, D., 2009. Tsunami sediments and their foraminiferal assemblages. Earth-Science Reviews 96, 263-278.

Martin, M.E., Weiss, R., Bourgeois, J., Pinegina, T.K., Houston, H., Titov, V.V., 2008. Combining constraints from tsunami modeling and sedimentology to untangle the 1969 Ozernoi and 1971 Kamchatskii tsunamis. Geophysical Research Letters 35, L01610.

Martis, A., van Oldenborgh, G.J., Burgers, G., 2002. Predicting rainfall in the Dutch Caribbean – more than El Niño? International Journal of Climatology 22, 1219-1234.

Mastronuzzi, G., Sansò, P., 2000. Boulders transport by catastrophic waves along the Ionian coast of Apulia (southern Italy). Marine Geology 170, 93-103.

Matsukura, Y., Maekado, A., Aoki, H., Kogure, T., Kitano, Y., 2007. Surface lowering rates of uplifted limestone terraces estimated from the height of pedestals on a subtropical island of Japan. Earth Surface Processes and Landforms 32, 1110-1115.

Matsumoto, D., Naruse, H., Fujino, S., Surphawajruksakul, A., Jarupongsakul, T., Sakakura, N., Murayama, M., 2008. Truncated flame structures within a deposit of the Indian Ocean Tsunami: evidence of syn-sedimentary deformation. Sedimentology 55, 1559-1570.

Mattioli, G.S., Voight, B., Linde, A.T., Sacks, I.S., Watts, P., Widiwijayanti, C., Young, S.R., Hidayat, D., Elsworth, D., Malin, P.E., Shalev, E., Van Boskirk, E., Johnston, W., Sparks, R.S.J., Neuberg, J., Bass, V., Dunkley, P., Herd, R., Syers, T., Williams, P., Williams, D., 2007. Unique and remarkable dilatometer measurements of pyroclastic flow-generated tsunamis. Geology 35, 25-28.

Mattox, N.T., 1949. Studies on the biology of the edible oyster, *Ostrea rhizophorae* Guilding, in Puerto Rico. Ecological Monographs 19, 339-356.

May, S.M., Vött, A., Brückner, H., Brockmüller, S., 2007. Evidence of tsunamigenic impact on Actio headland near Preveza, NW Greece. Coastline Reports 9, 115-125.

May, S.M., Willershäuser, T., Vött, A., 2010. Boulder transport by high-energy wave events at Cap Bon (NE Tunisia). Coastline Reports 16, 1-10.

May, S.M., Vött, A., Brückner, H., Grapmayer, R., Handl, M., Wennrich, V., 2012. The Lefkada barrier and beachrock system (NW Greece) – Controls on coastal evolution and the significance of extreme wave events. Geomorphology 139-140, 330-347.

McAdie, C.J., Landsea, C.W., Neumann, C.J., David, J.E., Blake, E.S., Hammer, G.R., 2009. Tropical cyclones of the North Atlantic Ocean, 1851–2006. Historical Climatology Series 6-2, 6th revision, URL: http://www.nhc.noaa.gov/pdf/TC_Book_Atl_1851-2006_lowres.pdf, last access: 05-11-2010.

McCloskey, T.A., Keller, G., 2009. 5000 year sedimentary record of hurricane strikes on the central coast of Belize. Quaternary International 195, 53-68.

McGregor, D.F.M., Potter, R.B., 1997. Environmental change and sustainability in the Caribbean: Terrestrial perspectives. Beiträge zur Geographischen Regionalforschung in Lateinamerika 10, 1-15.

McKee, K.L., Cahoon, D.R., Feller, I.C., 2007. Caribbean mangroves adjust to rising sea level through biotic controls on change in soil elevation. Global Ecology and Biogeography 16, 545-556.

Meschede, M., Frisch, W., 1998. A plate-tectonic model for the Mesozoic and Early Cenozoic history of the Caribbean plate. Tectonophysics 296, 269-291.

Meteorological Department Curaçao, n.d. Climate summary – the Dutch Leeward Antilles. URL: http://www.meteo.an/Climate_Sum.asp, last access: 03-15-12.

Meteorological Service Netherlands Antilles and Aruba, 2010a. Beoordeling Tsunami Gevaar voor het Eilandgebied Curaçao – Deel I: "Tsunami Hazard Assessment". URL: http://www.meteo.an/include/Pub/documents/TSU%20_final.pdf, last access: 03-15-12.

Meteorological Service Netherlands Antilles and Aruba, 2010b. Beoordeling Tsunami Gevaar voor het Eilandgebied Curaçao – Deel II: "Risicoanalyse". URL: http://www.meteo.an/include/Pub/documents/RA_final.pdf, last access: 03-15-12.

Meteorological Service Netherlands Antilles and Aruba, 2010c. Hurricanes and Tropical Storms in the Netherlands Antilles and Aruba. URL: http://www.meteo.an/include/HurricanesandTropicalStorms.pdf, last access: 03-08-11.

Milne, G.A., Long, A.J., Bassett, S.E., 2005. Modelling Holocene relative sea-level observations from the Caribbean and South America. Quaternary Science Reviews 25, 1183-1202.

Milne, G.A., Gehrels, W.R., Hughes, C.W., Tamisiea, M.E., 2009. Identifying the causes of sea level change. Nature Geoscience 2, 471-478.

Miller, D.J., 1960. The Alaska Earthquake of July 10, 1958: Giant wave in Lituya Bay. Bulletin of the Seismological Society of America 50, 253-266.

Minoura, K., Nakata, T., 1994. Discovery of an ancient tsunami deposit in coastal sequences of southwest Japan: Verification of a large historic tsunami. Island Arc 3, 66-72.

Minoura, K., Gusiakov, V.G., Kurbatov, A., Takeuti, S., Svendsen, J.I., Bondevik, S., Ota, T., 1996. Tsunami sedimentation associated with the 1923 Kamchatka earthquake. Sedimentary Geology 106, 145-154.

Mitrovica, J.X., Milne, G.A., 2002. On the origin of ocean siphoning. Quaternary Science Reviews 21, 2179-2190.

Monacci, N.M., Meier-Grünhagen, U., Finney, B.P., Behling, H., Wooller, M.J., 2009. Mangrove ecosystem changes during the Holocene at Spanish Lookout Cay, Belize. Palaeogeography, Palaeoclimatology, Palaeoecology 280, 37-46.

Moore, H.B., Lopez, N.N., 1969. The ecology of *Chione cancellata*. Bulletin of Marine Science 19, 131-148.

Moore, J.G., Moore, G.W., 1984. Deposit from a giant wave on the island of Lanai, Hawaii. Science 226, 1312-1315.

Morrison, J., Smith, D.E., Cullingford, R.A., Jones R.L., 1981, The culmination of the main postglacial transgression in the Firth of Tay area, Scotland. Proceedings of the Geologists' Association 92, 197-209.

Morton, R. A., 1978. Large-scale rhomboid bed forms and sedimentary structures associated with hurricane washover. Sedimentology 25, 183-204.

Morton, R.A., Richmond, B.M., Jaffe, B.E., Gelfenbaum, G., 2006. Reconnaissance investigation of Caribbean extreme wave deposits – preliminary observations, interpretations, and research directions. USGS Open-File Report 2006-1293.

Morton, R.A., Gelfenbaum G., Jaffe B.E., 2007. Physical criteria for distinguishing sandy tsunami and storm deposits using modern examples. Sedimentary Geology 200, 184-207.

Morton, R.A., Richmond, B.M., Jaffe, B.E., Gelfenbaum, G., 2008. Coarse-clast ridge complexes of the Caribbean: A preliminary basis for distinguishing tsunami and storm-wave origins. Journal of Sedimentary Research 78, 624-637.

Moscardelli, L., Hornbach, M., Wood, L., 2010. Tsunamigenic risks associated with mass transport complexes in offshore Trinidad and Venezuela. In: Mosher, D.C., Shipp, R.C., Moscardelli, L., Chaytor, J.D., Baxter, C.D.P., Lee, H.J., Urgeles, R. (eds.), Submarine Mass Movements and Their Consequences. Springer, Dordrecht, pp. 733-744.

Moya, J.C., Mercado, A., 2006. Geomorphologic and stratigraphic investigations on historic and pre-historic tsunami in northwestern Puerto Rico: implications for long term coastal evolution. In: Mercado-Irizarry, A., Liu, P. (Eds.), Caribbean tsunami hazard. World Scientific, Singapore, pp. 149-177.

Murray, J.W., 2006. Ecology and applications of benthic foraminifera. Cambridge University Press.

Nagendra, R., Kamalak Kannan, B.V., Sajith, C., Sen, G., Reddy, A.N., Srinivasalu, S., 2005. A record of foraminiferal assemblage in tsunami sediments along Nagappattinam coast. Current Science 89, 1947-1952.

Nair, R.R., Buynevich, I., Goble, R.J., Srinivasan, P., Murthy, S.G.N., Kandpal, S.C., Vijaya Lakshmi, C.S., Trivedi, D., 2010. Subsurface images shed light on past tsunamis in India. Eos 91, 489-490.

Nanayama, F., Shigeno, K., Satake, K., Shimokawa, K., Koitabashi, S., Miyasaka, S., Ishii, M., 2000. Sedimentary differences between the 1993 Hokkaido nansei-oki tsunami and the 1959 Miyakojima typhoon at Taisei, southwestern Hokkaido, northern Japan. Sedimentary Geology 135, 255–264.

Nanayama, F., Furukawa, R., Shigeno, K., Makino, A., Soeda, Y., Igarashi, Y., 2007. Nine unusually large tsunami deposits from the past 4000 years at Kiritappu marsh along the southern Kuril Trench. Sedimentary Geology 200, 275-294.

Nandasena, N.A.K., Paris, R., Tanaka, N., 2011. Reassessment of hydrodynamic equations: Minimum flow velocity to initiate boulder transport by high energy events (storms, tsunamis). Marine Geology 281, 70-84.

Naruse, H., Fujino, S., Suphawajruksakul, A., Jarupongsakul, T., 2010. Features and formation processes of multiple deposition layers from the 2004 Indian Ocean Tsunami at Ban Nam Kem, southern Thailand, Island Arc 19, 399-411.

NGDC (National Geophysical Data Center), 2011. NOAA/WDC Historical Tsunami Database at NGDC. URL: http://www.ngdc.noaa.gov/hazard/ tsu_db.shtml, last access: 03-24-11.

NGDC (National Geophysical Data Center), 2012. Significant Earthquake Database. URL: http://www.ngdc.noaa.gov/nndc/struts/form?t=101650&s =1&d=1, last access: 06-03-12.

Nichol, S.L., Chagué-Goff, C., Goff, J., Horrocks, M., McFadgen, B.G., Strotz, L.C., 2010. Geomorphology and accommodation space as limiting factors on tsunami deposition: Chatham Island, southwest Pacific Ocean. Sedimentary Geology 229, 41-52.

Nishimura, Y., Miyaji, N., 1995. Tsunami deposits from the 1993 Southwest Hokkaido earthquake and the 1640 Hokkaido Komagatake eruption, northern Japan. Pure and Applied Geophysics 114, 525-536.

Noormets, R., Crook, K.A.W., Felton, E.A., 2004. Sedimentology of rocky shorelines: 3. Hydrodynamics of megaclast emplacement and transport on a shore platform, Oahu, Hawaii. Sedimentary Geology 172, 41-65.

Nomanbhoy, N., Satake, K., 1995. Generation mechanism from the 1883 Karakatau eruption. Geophysical Research Letters 22, 509-512.

Nott, J., 1997. Extremely high-energy wave deposits inside Great Barrier Reef, Australia: determining the cause – tsunami or tropical cyclone. Marine Geology 141, 193-207.

Nott, J., 2003. Waves, coastal boulder deposits and the importance of the pre-transport setting. Earth and Planetary Science Letters 210, 269-276.

Nott, J., 2006. Tropical cyclones and the evolution of the sedimentary coast of northern Australia. Journal of Coastal Research 22, 49-62.

Ntageretzis, K., Hoffmeister, D., Vött, A., Brückner, H., Hadler, H., Willershäuser, T., 2011. High-resolution 3D laser scanning measurements of dislocated boulders on the coasts of the Lakonian Gulf and on Cefalonia Island (Greece). Abstract volume of the 29th annual meeting of the German working group on "Geography of Oceans and Coasts", Bremen, 28-30 Apr 2011, pp. 22-23.

Okal, E.A., Fritz, H.M., Synolakis, C.E., Borrero, J.C., Weiss, R., Lynett, P.J., Titov, V.V., Foteinis, S., Jaffe, B.E., Liu, P.L.-F., Chan, I., 2010. Field Survey of the Samoa Tsunami of 29 September 2009. Seismological Research Letters 81, 577-591.

O'Loughlin, K., Lander, J.F., 2003. Caribbean Tsunamis – A 500-Year History from 1498-1998. Kluwer, Dordrecht.

Palmer, S., Burn, M., 2011. A Late-Holocene record of marine washover events from a coastal lagoon in Jamaica, West Indies. XVIII. INQUA Bern 2011, Switzerland, Abstract ID 2098.

Pantosti, D., Barbano, M.S., Smedile, A., De Martini, P.M., Tigano, G., 2008. Geological evidence of paleotsunamis at Torre degli Inglesi (northeast Sicily). Geophysical Research Letters 35, L05311.

Pararas-Carayannis, G., 2004. Volcanic tsunami generating source mechanisms in the eastern Caribbean region. Science of Tsunami Hazards 22, 74-114.

Pareschi, M.T., Boschi, E., Favalli, M., 2007. Holocene tsunamis from Mount Etna and the fate of Israeli Neolithic communities. Geophysical Research Letters 34, L16317.

Paris, R., Lavigne, F., Wassmer, P., Sartohadi, J., 2007. Coastal sedimentation associated with the December 26, 2004 tsunami in Lhok Nga, west Banda Aceh (Sumatra, Indonesia). Marine Geology 238, 93-106.

Paris, R., Wassmer, P., Sartohadi, J., Lavigne, F., Barthomeuf, B., Desgages, E., Grancher, D., Baumert, P., Vautier, F., Brunstein, D., Gomez, C., 2009. Tsunamis as geomorphic crises: lessons from the December 26, 2004 tsunami in Lhok Nga, West Banda Aceh (Sumatra, Indonesia). Geomorphology 104, 59-72.

Paris, R., Fournier, J., Poizot, E., Etienne, S., Morin, J., Lavigne, F., Wassmer, P., 2010. Boulder and fine sediment transport and deposition by the 2004 tsunami in Lhok Nga (western Banda Aceh, Sumatra, Indonesia): A coupled offshore-onshore model. Marine Geology 268, 43-54.

Park, L.E., Siewers, F., Metzger, T., Sipahioglu, S., 2009. After the hurricane hits: Recovery and response to large storm events in a saline lake, San Salvador Island, Bahamas. Quaternary International 195, 98-105.

Parsons, M.L., 1998. Salt marsh sedimentary record of the landfall of Hurricane Andrew on the Louisiana coast: Diatoms and other paleoindicators. Journal of Coastal Research 14, 939-950.

Parsons, T., Geist, E.L., 2009. Tsunami probability in the Caribbean region. Pure and Applied Geophysics 165, 2089-2166.

Pérez, L., Bugja, R., Massaferro, J., Steeb, P., van Geldern, R., Frenzel, P., Brenner, M., Scharf, B., Schwalb, A., 2010a. Post-Columbian environmental history of Lago Petén Itzá, Guatemala. Revista Mexicana de Ciencas Geológicas 27, 490-507.

Pérez, L., Lorenschat, J., Bugja, R., Brenner, M., Scharf, B., Schwalb, A., 2010b. Distribution, diversity and ecology of modern freshwater ostracodes (Crustacea), and hydrochemical characteristics of Lago Petén Itzá, Guatemala. Journal of Limnology 69, 146-159.

Peros, M.C., Reinhardt, E.G., Davis, A.M., 2007. A 6000-year record of ecological and hydrological changes from Laguna de la Leche, north coastal Cuba. Quaternary Research 67, 69-82.

Peters, R., Jaffe, B.E., 2010a. Identification of tsunami deposits in the geologic record: developing criteria using recent examples. USGS Open-File Report 2010-1239.

Peters, R., Jaffe, B.E., 2010b. Recent tsunami deposit database. USGS Open-File Report 2010-1172.

Pignatelli, C., Sansò, P., Mastronuzzi, G., 2009. Evaluation of tsunami flooding using geomorphologic evidence. Marine Geology 260, 6-18.

Pignatelli, C., Scheffers, A., Scheffers, S., Mastronuzzi, G., 2010. Assessment of extreme wave flooding from geomorphologic evidence in Bonaire (Netherlands Antilles). Zeitschrift für Geomorphologie N.F. 54(Suppl. 3), 219-245.

Pijpers, P.J., 1933. Geology and paleontology of Bonaire (D.W.I.). Geographische en Geologische Mededeelingen, Physiographisch-Geologische reeks 8.

Pindell, J.L., Kennan, L., 2009. Tectonic evolution of the Gulf of Mexico, Caribbean and northern South America in the mantle reference frame: an update. In: James, K.H., Lorente, M.A., Pindell, J.L. (eds.), The origin and evolution of the Caribbean Plate. Geological Society, London, Special Publication 328, 1-55.

Pirazzoli, P.A., 2005. Sea-level indicators, geomorphic. In: Schwartz, M.L. (ed.), Encyclopedia of Coastal Science. Springer, Dordrecht, pp. 836-838.

Prendergast, A., 2006. Echoes of ancient tsunamis. AusGeo News 83, 1-5.

Radtke, U., Schellmann, G., Scheffers, A., Kelletat, D., Kromer, B., Kasper, H.U., 2003. Electron spin resonance and radiocarbon dating of coral deposited by Holocene tsunami events on Curaçao, Bonaire and Aruba (Netherlands Antilles). Quaternary Science Reviews 22, 1309-1315.

Ramcharan, E.K., 2004. Mid-to-late Holocene sea level influence on coastal wetland development in Trinidad. Quaternary International 120, 145-151.

Ramcharan, E.K., McAndrews, J.H., 2006. Holocene development of coastal wetland at Maracas Bay, Trinidad, West Indies. Journal of Coastal Research 22, 581-586.

Rappaport, E.N., Fernandez-Partagas, J., 1997. The deadliest Atlantic tropical cyclones, 1492-1996. NOAA Technical Memorandum NWS NHC 47, URL: http://www.nhc.noaa.gov/pastdeadly.shtml?, last access 03-06-12.

Reading, A.J., 1990. Caribbean tropical storm activity over the past four centuries. International Journal of Climatology 10, 365-376.

Regnauld, H., Oszwald, J., Planchon, O., Pignatelli, C., Piscitelli, A., Mastronuzzi, G., Audevard, A., 2010. Polygenetic (tsunami and storm) deposits? A case study from Ushant Island, western France. Zeitschrift für Geomorphologie N.F. 54(Suppl. 3), 197-217.

Reimer, P.J., Baillie, M.G.L., Bard, E., Bayliss, A., Beck, J.W., Bertrand, C., Blackwell, P.G., Buck, C.E., Burr, G., Cutler, K.B., Damon, P.E., Edwards, R.L., Fairbanks, R.G., Friedrich, M., Guilderson, R.P., Hughen, K.A., Kromer, B., McCormac, F.G., Manning, S., Ramsey, C.B., Reimer, R.W., Remmele, S., Southon, J.R., Stuiver, M., Talamo, S., Taylor, F.W., van der Plicht, J., Weyhenmeyer, C.E., 2004. IntCal04 terrestrial radiocarbon age calibration, 0-26 cal kyr BP. Radiocarbon 46, 1029-1058.

Reimer, P.J., Baillie, M.G.L., Bard, E., Bayliss, A., Beck, J.W., Blackwell, P.G., Bronk Ramsey, C., Buck, C.E., Burr, G.S., Edwards, R.L., Friedrich, M., Grootes, P.M., Guilderson, T.P., Hajdas, I., Heaton, T.J., Hogg, A.G., Hughen, K.A., Kaiser, K.F., Kromer, B., McCormac, F.G., Manning, S.W., Reimer, R.W., Richards, D.A., Southon, J.R., Talamo, S., Turney, C.S.M., van der Plicht, J., Weyhenmeyer, C.E., 2009. IntCal09 and Marine09 radiocarbon age calibration curves, 0-50,000 years cal BP. Radiocarbon 51, 1111-1150.

Reimnitz, E., Marshall N.F., 1965 Effects of the Alaska earthquake and tsunami on recent deltaic sediments. Journal of Geophysical Research 70: 2363-2376.

Rhodes, B., Tuttle, M., Horton, B., Doner, L., Kelsey, H., Nelson, A., Cisternas, M., 2006. Paleotsunami research. Eos 87, 205; 209.

Richmond, B.M., Buckley, M.L., Jaffe, B.E., Watt, S., Gelfenbaum, G., Apostos, A.A., Étienne, S., 2010. Boulder deposition in the Samoa Islands from September 29, 2009 South Pacific Tsunami. Abstract Vol. of the 3rd International Tsunami Field Symposium, Sendai, Japan, 10-16 April 2010, pp. 41-42.

Richmond, B.M., Jaffe, B.E., Gelfenbaum, G., Morton, R.A., 2006. Geologic Impacts of the 2004 Indian Ocean Tsunami on Indonesia, Sri Lanka, and the Maldives. Zeitschrift für Geomorphologie, Suppl. Vol. 146, 235-251.

Rixhon, G., Brückner, H., Engel, M., May, S.M., Dunai, T., 2012. Dating tsunami-induced transport of coral reef megaclasts on Bonaire (Leeward Antilles): a cosmogenic nuclide dating approach (^{36}Cl). Abstract for the International Geographical Congress, Cologne, 26-30 August 2012.

Robinson, E., Rowe, D.-A.C., Khan, S.A., 2006. Wave-emplaced boulders on Jamaica's rocky shorelines. Zeitschrift für Geomorphologie N.F., Suppl.-Vol. 146, 39-57.

Robinson, E., Khan, S., Rowe, D.A., Coutou, R., 2008. Size of boulders moved and emplaced by recent hurricanes, Jamaica. In: Mastronuzzi, G., Pignatelli, P., Sansó, P., Milella, M., Selleri, G. (eds.), Abstract volume of the 2nd International Tsunami Field Symposium, Ostuni (Italy) and Ionian Islands (Greece), 22-28 September 2008. GI²S Coast Research Publication 6, 135-138.

Robson, G.R., Canales, L., 1968. Venezuela – The Caracas Earthquake of 29 July 1967. UNESCO Report, Serial No. 571, URL: http://unesdoc.unesco.org/images/0001/000152/015201eb.pdf, last access 04-01-11.

Rowe, D.-A., Khan, S., Robinson, E., 2009. Hurricanes or tsunami? Comparative analysis of extensive boulder arrays along the southwest and north coasts of Jamaica: Lessons for coastal management. In: McGregor, D., Dodman, D., Barker, D. (eds.), Global change and Caribbean vulnerability. University of the West Indies Press, Kingston, pp. 49-73

Rubin, K.H., Fletcher III, C.H., Sherman, C., 2000. Fossiliferous Lana'i deposits formed by multiple events rather than a single tsunami. Nature 408, 675-681.

Ruiz, F., Rodríguez-Ramírez, A., Cáceres, L.M., Vidal, J.R., Carretero, M.I., Abad, M., Olías, M., Pozo, M., 2005. Evidence of high-energy events in the geological record: mid-Holocene evolution of the southwestern Doñana National Park (SW Spain). Palaeogeography, Palaeoclimatology, Palaeoecology 229, 212-229.

Rull, V., Vegas-Vilarrúbia, T., Espinoza de Pernía, N., 1999. Palynological record of an early-mid Holocene mangrove in eastern Venezuela. Implications for sea-level rise and disturbance history. Journal of Coastal Research 15, 496-504.

Sagar, A., Kademani, B.S., Garg, R.G., Kumar, V., 2010. Scientometric mapping of tsunami publications: a citation based study. Malaysian Journal of Library & Information Science 15, 23-40.

Sato, H., Shimamoto, T., Tsutsumi, A., Kawamoto, E., 1995. Onshore tsunami deposits caused by the 1993 southwest Hokkaido and 1983 Japan Sea Earthquake. Pure and Applied Geophysics 144, 693-717.

Sawai, Y., Jankaew, K., Martin, M.E., Prendergast, A., Choowong, M., Charoentitirat, T., 2009. Diatom assemblages in tsunami deposits associated with the 2004 Indian Ocean tsunami at Phra Thong Island, Thailand. Marine Micropaleontology 73, 70-79.

Sawall, Y., Phongsuwan, N., Richter, C., 2010. Coral recruitment and recovery after the 2004 Tsunami around the Phi Phi Islands (Krabi Province) and Phuket, Andaman Sea, Thailand. Helgoland Marine Research 64, 357-365.

Scicchitano, G., Monaco, C., Tortorici, L., 2007. Large boulder deposits by tsunami waves along the Ionian coast of south-eastern Sicily (Italy). Marine Geology 238, 75-91.

Scheffers, A., 2002. Paleotsunami in the Caribbean: field evidences and datings from Aruba, Curaçao and Bonaire. Essener Geographische Arbeiten 33.

Scheffers, A., 2004. Tsunami imprints on the Leeward Netherlands Antilles (Aruba, Curaçao, Bonaire) and their relation to other coastal problems. Quaternary International 120, 163-172.

Scheffers, A., 2005. Coastal response to extreme wave events – hurricanes and tsunamis on Bonaire. Essener Geographische Arbeiten 37.

Scheffers, A., 2006. Sedimentary impacts of Holocene tsunami events from the intra Americas seas asnd southern Europe: A review. Zeitschrift für Geomorphologie N.F., Suppl.-Vol. 146, 7-37.

Scheffers, A., Kelletat, D., 2003. Sedimentologic and geomorphologic tsunami imprints worldwide – a review. Earth-Science Reviews 63, 83-92.

Scheffers, A., Kelletat, D., 2006. New evidence and datings of Holocene paleo-tsunami events in the Caribbean (Barbados, St. Martin and Anguilla). In: Mercado-Irizarry, A., Liu, P. (eds.), Caribbean tsunami hazard. World Scientific, Singapore, pp. 178-202.

Scheffers, A., Scheffers, S., 2006. Documentation of Hurricane Ivan on the Coastline of Bonaire. Journal of Coastal Research 22, 1437-1450.

Scheffers, A., Scheffers, S., Kelletat, D., 2005. Paleo-tsunami relics on the southern and central Antillean Island Arc. Journal of Coastal Research 21, 263-273.

Scheffers, S., Scheffers, A., Radtke, U., Kelletat, D., Staben, K., Bak, R., 2006. Tsunamis trigger long-lasting phase-shift in a coral reef ecosystem. Zeitschrift für Geomorphologie N.F., Suppl.-Vol. 146, 59-79.

Scheffers, S.R., Haviser, J., Browne, T., Scheffers, A., 2009a. Tsunamis, hurricanes, the demise of coral reefs and shifts in prehistoric human populations in the Caribbean. Quaternary International 195, 69-87.

Scheffers, A., Kelletat D., Engel, M., 2009b. Die Entwicklung der Tsunamiforschung nach der Katastrophe vom 26. Dezember 2004. Geographische Rundschau 61(12), 12-18.

Scheffers, A., Engel, M., Squire, P., Kelletat, D., Scheffers, S., 2012. Beach ridge systems – archives for Holocene coastal events? Progress in Physical Geography 36, 5-37.

Scheffers, A., Brill, D., Kelletat, D., Brückner, H., Scheffers, S., Fox, K., accepted. Holocene sea levels along the Andaman Sea Coast of Thailand. The Holocene.

Scheffers, A.M., Engel, M., Scheffers, S.R., May, S.M., Hänßler, E., Löhr, K., Joannes-Boyau, R., Kelletat, D.H., Brückner, H., Vött, A., Schellmann, G., Schäbitz, F., Radtke, U., Sommer, B., in prep. Coastal landforms and event histories in a tropical carbonate environment. In: Martini, I.P. (ed.), Coastal Environments: from the Arctic to the Tropics. Geological Society, London, Special Publication.

Schellmann, G., Radtke, U., 2001. Progress in ESR dating of Pleistocene corals – a new approach for D_E determination. Quaternary Science Reviews 20, 1015-1020.

Schellmann, G., Radtke, U., Scheffers, A., Whelan, F., Kelletat, D., 2004. ESR Dating of coral reef terraces on Curaçao (Netherlands Antilles) with estimates of Younger Pleistocene sea level elevations. Journal of Coastal Research 20, 947-957.

Schellmann, G., Radtke, U., Brückner, H., 2011. Electron Spin Resonance Dating (ESR). In: Hopley, D. (ed.), Encyclopedia of Modern Coral Reefs – Structure, Form and Process, Part 5. Springer, Dordrecht, pp. 368-372.

Scheucher, L.E.A., Piller, W.E., Vortisch, W., 2011. Foraminiferal analysis of tsunami deposits: two examples from the northeastern and southwestern coast of the Dominican Republic. In: Bornemann, A., Brachert, T.C., Ehrmann, W. (eds.), SEDIMENT 2011 – Sediments: Archives of the Earth System, Leipzig, June 23-26, 2011, Abstracts, pp. 86-87.

Schleupner, C., 2008. Evaluation of coastal squeeze and its consequences for the Caribbean island Martinique. Ocean & Coastal Management 51, 383-390.

Scholl, D.W., Stuiver, M., 1967. Recent submergence of southern Florida: A comparison with adjacent coasts and other eustatic data. Geological Society of America Bulletin 78, 437-454.

Schubert, C., 1994. Tsunami in Venezuela: some observations on their occurrence. Journal of Coastal Research, SI 12, 189-195.

Schubert, C., Valastro, S., 1976. Quaternary geology of La Orchilla Island, central Venezuelan offshore, Caribbean Sea. Geological Society of America Bulletin 87, 1131-1142.

Shepard, F.P., Macdonald, G.A., Cox, D.C., 1949. The tsunami of April 1, 1946. Bulletin of the Scripps Institution of Oceanography 5, 391-528.

Shi, S., Dawson, A.G., Smith, D.E., 1995. Coastal sedimentation associated with the December 12th, 1992 Tsunami in Flores, Indonesia. Pure and Applied Geophysics 144, 525-536.

Smith, D.E., Cullingford, R.A., Brooks, C.L., 1983. Flandrian relative sea level changes in the Ythan Valley, northeast Scotland. Earth Surface Processes and Landforms 8, 423-438.

Smith, D.E., Cullingford, R.A., Haggart, B.A., 1985. A major coastal flood during the Holocene in Eastern Scotland. Eiszeitalter & Gegenwart (Quaternary Science Journal) 35, 109-118.

Smith, D.E., Shi, S., Cullingford, R.A., Dawson, A.G., Dawson, S., Firth, C.R., Foster, I.D.L., Fretwell, P.T., Haggart, B.A., Holloway, L.K., Long, D., 2004. The Holocene Storegga Slide tsunami in the United Kingdom. Quaternary Science Reviews 23, 2291-2321.

Sommer, B., Harrison, P.L., Brooks, L., Scheffers, S.R., 2011. Coral community decline at Bonaire, southern Caribbean. Bulletin of Marine Science 87, 541-565.

Soulsby, R.L., Smith, D.E., Ruffman, A., 2007. Reconstructing tsunami run-up from sedimentary characteristics – a simple mathematical model. In: Kraus, N.C., Rosati, J.D. (eds.), Proceedings of the Sixth International Symposium on Coastal Engineering and Science of Coastal Sediment Processes “Coastal Sediments '07”, 13-17 May 2007, New Orleans, Louisiana, pp. 1075–1088.

Spahn, H., Hoppe, M., Vidiarina, H.D., Usdianto, B., 2010. Experience from three years of local capacity development for tsunami early warning in Indonesia: challenges, lessons and the way ahead. Natural Hazards and Earth System Sciences 10, 1411-1429.

Spiske, M., Jaffe, B.E., 2009. Sedimentology and hydrodynamic implications of a coarse-grained hurricane sequence in a carbonate reef setting. Geology 37, 839-842.

Spiske, M., Böröcz, Z., Bahlburg, H., 2008. The role of porosity in discriminating between tsunami and hurricane emplacement of boulders – A case study from the Lesser Antilles, southern Caribbean. Earth and Planetary Science Letters 268, 384-396.

Spiske, M., Weiss, R., Bahlburg, H., Roskosch, J., Amijaya, H., 2010. The TsuSedMod inversion model applied to the deposits of the 2004 Sumatra and 2006 Java tsunami and implications for estimating flow parameters of palaeo-tsunami. Sedimentary Geology 224, 29-37.

Srinivasalu, S., Thangadurai, N., Switzer, A.D., Ram Mohan, V., Ayyamperumal, T., 2007. Erosion and sedimentation in Kalpakkam (N Tamil Nadu, India) from the 26th December 2004 tsunami. Marine Geology 240, 65-75.

Srinivasalu, S., Rajeshwara Rao, N., Thangadurai, N., Jonathan, M.P., Roy, P.D., Ram Mohan, V., Saravanan, P., 2009. Characteristics of 2004 tsunami deposits of the northern Tamil Nadu coast, southeastern India. Boletín de la Sociedad Geológica Mexicana 61, 111-118.

Srisutam, C., Wagner, J.-F., 2010. Tsunami sediment characteristics at the Thai Andaman coast. Pure and Applied Geophysics 167, 215-232.

Stanley, D.J., Warne, A.G., 1994. Worldwide initiation of Holocene marine deltas by deceleration of sea-level rise. Science 265, 228-231.

Stewart, S.R., 2004. Tropical Cyclone Report – Hurricane Ivan, 2-24 September 2004. URL: http://www.nhc.noaa.gov/2004ivan.shtml, last access: 03-08-11.

STINAPA, 2003/2009. Washington Slagbaai National Park – History. URL: http://www.washingtonparkbonaire.org/history.html, last access: 01-30-12.

Sugawara, D., Minoura, K., Imamura, F., 2008. Tsunamis and tsunami sedimentology. In: Shiki, T., Tsuji, Y., Yamazaki, T., Minoura, K. (eds.), Tsunamiites – Features and Implications. Elsevier, Amsterdam, Oxford, pp. 9-49.

Swain, F.M., Gilby, J.M., 1967. Recent Ostracoda from Corinto Bay, Western Nicaragua, and their relationship to some other assemblages of the Pacific Coast. Journal of Paleontology 41, 306-334.

Switzer, A.D., 2010. Distinguishing between storm and tsunami in the geological record; progress, perturbations and potential. Eos Transactions AGU, Fall Meeting Suppl., Abstract OS42B-04.

Switzer, A.D., Burston, J.M., 2010. Competing mechanisms for boulder deposition on the southeast Australian coast. Geomorphology 114, 42-54.

Switzer, A.D., Jones, B.G., 2008a. Large-scale washover sedimentation in a freshwater lagoon from the southeast Australian coast: sea-level change, tsunami or exceptionally large storm? The Holocene 18, 787-803.

Switzer, A.D., Jones, B.G., 2008b. Setup, deposition, and sedimentary characteristics of two storm overwash deposits, Abrahams Bosom Beach, Southeastern Australia. Journal of Coastal Research 24(1A), 189-200.

Switzer, A.D., Pucillo, K., Haredy, R.A., Jones, B.G., Bryant, E.A., 2005. Sea Level, Storm, or Tsunami: Enigmatic Sand Sheet Deposits in a Sheltered Coastal Embayment from Southeastern New South Wales, Australia. Journal of Coastal Research 21, 655-663.

Switzer, A.D., Bristow, C.S., Jones, B.G., 2006. Investigation of large-scale washover of a small barrier system on the southeast Australian coast using ground penetrating radar. Sedimentary Geology 183, 145-156.

Switzer, A.D., Sloss, C.R., Jones, B.G., Bristow, C.S., 2010. Geomorphic evidence for mid-late Holocene higher sea level from southeastern Australia. Quaternary International 221, 13-22.

Synolakis, C.E., Okal E.A., 2005. 1992-2002: Perspective on a decade of post-tsunami surveys. In: Satake, K. (ed.), Tsunamis – case studies and recent developments. Advances in Natural and Technological Hazards Research 23, 1-29.

Szczuciński, W., 2010. Post-depositional changes of sedimentological and geochemical monitoring. Abstract Volume of the 3rd International Tsunami Field Symposium, Sendai, Japan, 10-16 April 2010, pp. 189-190.

Szczuciński, W., 2012. The post-depositional changes of the onshore 2004 tsunami deposits on the Andaman Sea coast of Thailand. Natural Hazards 60, 115-133.

Szczuciński, W., Chaimanee, N., Niedzielski, P., Rachlewicz, G., Saisuttichai, D., Tepsuwan, T., Lorenc, S., Siepak, J., 2006. Environmental and geological impacts of the 26 December 2004 Tsunami in coastal zone of Thailand – Overview of short and long-term effects. Polish Journal of Environmental Studies 15, 793-810.

Szczuciński, W., Niedzielski, P., Kozak, L., Frankowski, M., Zioła, A., Lorenc, S., 2007. Effects of rainy season on mobilization of contaminants from tsunami deposits left in a coastal zone of Thailand by the 26 December 2004 tsunami. Environmental Geology 53, 253-264.

Tanguy, J.-C., 1994. The 1902-1905 eruptions of Montagne Pelée, Martinique: anatomy and retrospection. Journal of Volcanology and Geothermal Research 60, 87-107.

Tanioka, Y., Yudhicara, Kususose, T., Kathiroli, S., Nishimura, Y., Iwasaki, S.-I., Satake, K., 2006. Rupture process of the 2004 great Sumatra-Andaman earthquake estimated from tsunami waveforms. Earth, Planets and Space 58, 203-209.

Tappin, D.R., Watts, P., Grilli, S.T., 2008. The Papua New Guinea tsunami of 17 July 1998: Anatomy of a catastrophic event. Natural Hazards and Earth System Sciences 8, 243-266.

Tedesco, K., Thunell, R., 2003. High resolution tropical climate record for the last 6,000 years. Geophysical Research Letters 30(17), 1891.

Teeuw, R., Rust, D., Solana, C., Dewdney, C., 2009. Large coastal landslides and tsunami hazard in the Caribbean. Eos 90, 81-82.

ten Brink, U.S., Geist, E.L., Andrews, B.D., 2006. Size distribution of submarine landslides and its implication to tsunami hazard in Puerto Rico. Geophysical Research Letters 33, L11307.

Thom, B.G., 1967. Mangrove ecology and deltaic geomorphology: Tabasco, Mexico. Journal of Ecology 55, 301-346.

Thompson, P.M.E., Kempton, P.D., White, R.V., Saunders, A.D., Kerr, A.C., Tarney, J., Pringle, M.S., 2004. Elemental, Hf-Nd isotopic and geochronological constraints on an island arc sequence associated with the Cretaceous Caribbean plateau: Bonaire, Dutch Antilles. Lithos 74, 91-116.

Tinti, S., Manucci, A., Pagnoni, G., Armigliato, A., Zaniboni, F., 2005. The 30 December 2002 landslide induced tsunamis in Stromboli: sequence of the events reconstructed from eyewitness accounts. Natural Hazards and Earth System Sciences 5, 763-775.

Tobin, G.A., Montz, B.E., 2009. Risk: Geophysical processes in natural hazards. In: Clifford, N.J., Holloway, S.L., Rice, S.P., Valentine, G. (eds.), Key concepts in Geography. SAGE, London, pp. 405-424.

Tomblin, J., 1981. Earthquakes, volcanoes and hurricanes: A review of natural hazards and vulnerability in the West Indies. Ambio 10, 340-344.

Toscano, M.A., Macintyre, I.G., 2003. Corrected western Atlantic sea-level curve for the last 11,000 years based on calibrated ^{14}C dates from *Acropora palmata* framework and intertidal mangrove peat. Coral Reefs 22, 257-270.

Toscano, M.A., Peltier, W.R., Drummond, R., 2011. ICE-5G and ICE-6G models of postglacial relative sea-level history applied to the Holocene coral reef record of northeastern St Croix, U.S.V.I.: investigating the influence of rotational feedback on GIA processes at tropical latitudes. Quaternary Science Reviews 30, 3032-3042.

Treece, G.D., 1980. Bathymetric records of marine shelled Mollusca from the northeastern shelf and upper slope of Yucatan, Mexico. Bulletin of Marine Science 30, 552-570.

Tushingham, A.M., Peltier, W.R., 1991. ICE-3G: a new global model of late Pleistocene deglaciation based on geophysical predictions of post-glacial relative sea level change. Journal of Geophysical Research 96, 4497-4523.

Tuttle, M.P., Ruffman, A., Anderson, T., Jeter, H., 2004. Distinguishing tsunami from storm deposits in eastern North America: the 1929 Grand Banks Tsunami versus the 1991 Halloween Storm. Seismological Research Letters 75, 117-131.

Uchida, J.-I., Fujiwara, O., Hasegawa, S., Kamataki, T., 2010. Sources and depositional processes of tsunami deposits: analysis using foraminiferal tests and hydrodynamic verification. Island Arc 19, 427-442.

Urquhart, G.R., 2009. Palaeoecological record of hurricane disturbance and forest regeneration in Nicaragua. Quaternary International 195, 88-97.

Van Duyl, F.C., 1985. Atlas of the living reefs of Curaçao and Bonaire (Netherlands Antilles). Natuurwetenschappelijke Studiekring voor Suriname en de Nederlandse Antillen 117.

Vélez, A., 1991. Biology and culture of the Caribbean or mangrove oyster, *Crassostrea rhizophorae* Guilding, in the Caribbean and South America. In: Menzel, W. (ed.), Estuarine & Marine Bivalve Mollusc Culture. CRC Press Inc, Boca Raton, pp. 117-134.

Vilibić, I., Šepić, J., Ranguelov, B., Strelec Mahović, N., Tinti S., 2010. Possible atmospheric origin of the 7 May 2007 western Black Sea shelf tsunami event. Journal of Geophysical Research 115, C07006.

Vött, A., 2007. Relative sea level changes and regional tectonic evolution of seven coastal areas in NW Greece since the mid-Holocene. Quaternary Science Reviews 26, 894-919.

Vött, A., Brückner, H., May, M., Lang, F., Brockmüller, S., 2007. Late Holocene tsunami imprint at the entrance of the Ambrakian gulf (NW Greece). Méditerranée 108, 139-172.

Vött, A., Brückner, H., May, S.M., Lang, F., Herd, R., Brockmüller, S., 2008. Strong tsunami impact on the Bay of Aghios Nikolaos and its environs (NW Greece) during Classical-Hellenistic times. Quaternary International 181, 105-122.

Vött, A., Brückner, H., Brockmüller, S., Handl, M., May, S.M., Gaki-Papanastassiou, K., Herd, R., Lang, F., Maroukian, H., Nelle, O., Papanastassiou, D., 2009. Traces of Holocene tsunamis across the Sound of Lefkada, NW Greece. Global and Planetary Change 66, 112-128.

Vött, A., Bareth, G., Brückner, H., Curdt, C., Fountoulis, I., Grapmayer, R., Hadler, H., Hoffmeister, D., Klasen, N., Lang, F., Masberg, P., May, S.M., Ntageretzis, K., Sakellariou, D., Willershäuser, T., 2010. Beachrock-type calcarenitic tsunamites along the shores of the eastern Ionian Sea (western Greece) – case studies from Akarnania, the Ionian Islands and the western Peloponnese. In: Zeitschrift für Geomorphologie N.F. 54 (Suppl. 3), 1-50.

Vött, A., Lang, F., Brückner, H., Gaki-Papanastassiou, K., Maroukian, H., Papanastassiou, D., Giannikos, A., Hadler, H., Handl, M., Ntageretzis, K., Willershäuser, T., Zander, A., 2011. Sedimentological and geoarchaeological evidence of multiple tsunamigenic imprint on the Bay of Palairos-Pogonia (Akarnania, NW Greece). Quaternary International 242, 213-239.

Wagner, B., Bennike, O., Klug, M., Cremer, H., 2007. First indication of Storegga deposits from East Greenland. Journal of Quaternary Science 22, 321-325.

Wahr, J.M., Davis, J.L., 2002. Geodetic Constraints on Glacial Isostatic Adjustment. In: Mitrovica, J.X., Vermeersen, B.L.A. (eds.), Ice sheets, sea level and the dynamic earth. American Geophysical Union, pp. 3-32.

Wang, P., Horwitz, M.H., 2007. Erosional and depositional characteristics of regional overwash deposits caused by multiple hurricanes. Sedimentology 54, 545-564.

Wang, D.W., Mitchell, D.A., Teague, W.J., Jarosz, E., Hulbert, M.S., 2005. Extreme waves under Hurricane Ivan. Science 309, 896.

Ward, S.N., Day, S., 2001. Cumbre Vieja Volcano – potential collapse and tsunami at La Palma, Canary Islands. Geophysical Research Letters 28, 3397-4000.

Watt, S.G., Jaffe, B.E., Morton, R.A., Richmond, B.M., Gelfenbaum, G., 2010. Description of extreme-wave deposits on the northern coast of Bonaire, Netherlands Antilles. USGS Open-File Report 2010-1180.

Weiss, M.P., 1979. A saline lagoon on Cayo Sal, Western Venezuela. Atoll Research Bulletin 232.

Weiss, R., 2008. Sediment grains moved by passing tsunami waves: Tsunami deposits in deeper water. Marine Geology 250, 251-257.

Westermann, J.H., Zonneveld J.I.S., 1956. Photo-geological observations and land capability & land use survey of the Island of Bonaire (Netherlands Antilles). Koninklijk Institut voor de Tropen, Amsterdam.

Wille, M., Maidana, N.I., Schäbitz, F., Fey, M., Haberzettl, T., Janssen, S., Lücke, A., Mayr, C., Ohlendorf, C., Schleser, G.H., Zolitschka, B., 2007. Vegetation and climate dynamics in southern South America: The microfossil record of Laguna Potrok Aike, Santa Cruz, Argentina. Review of Palaeobotany and Palynology 146, 234-246.

Willershäuser, T., 2008. Holozäne Paläogeographie der Bucht von Lagun (Bonaire, Niederländische Antillen) – Untersuchungen zum Einfluss extremer Wellenereignisse auf die Küstenentwicklung. Diploma thesis, Philipps-Universität Marburg, Germany.

Williams, H.F.L., 2009. Stratigraphy, sedimentology, and microfossil content of Hurricane Rita storm surge deposits on southwest Louisiana. Journal of Coastal Research 25, 1041-1051.

Wilson, A.G., 1972. Theoretical Geography: Some Speculations. Transactions of the Institute of British Geographers 57, 31-44.

Wirth, E., 1979. Theoretische Geographie. Teubner, Stuttgart.

Wisner, B., Blaikie, P., Cannon, T., Davis, I., 2004. At risk: Natural hazards, people's vulnerability and disasters. Routledge, New York.

Woodruff, J.D., Donnelly, J.D., Mohrig, D., Geyer, W.R., 2008. Reconstructing relative flooding intensities responsible for hurricane induced deposits from Laguna Playa Grande, Vieques, Puerto Rico. Geology 36: 391-394.

Woodroffe, C.D., 1981. Mangrove swamp stratigraphy and Holocene transgression, Grand Cayman Island, West Indies. Marine Geology 41, 271-294.

Woodroffe, C.D., 2002. Coasts. Cambridge University Press.

Wright, C., Mella, A., 1963. Modifications to the soil pattern of South-Central Chile resulting from seismic and associated phenomena during the period May to August 1960. Bulletin of the Seismological Society of America 53, 1367-1402.

Yawsangratt, S., Szczuciński, W., Chaimanee, N., Chatprasert, S., Majewski, W., Lorenc, S., 2011. Evidence of probable paleotsunami deposits on Kho Khao Island, Phang Nga Province, Thailand. Natural Hazards, doi: 10.1007/s11069-011-9729-4.

Yu, K.-F., Zhao, J.-X., Shi, Q., Meng, Q.-S., 2009. Reconstruction of storm/tsunami records over the last 4000 years using transported coral blocks and lagoon sediments in the southern South China Sea. Quaternary International 195, 128-137.

Zahibo, N., Pelinovsky, E.N., 2001. Evaluation of tsunami risk in the Lesser Antilles. Natural Hazards and Earth System Sciences 1, 221-231.

Zahibo, N., Pelinovsky, E., Yalciner, A., Kurkin, A., Koselkov, A., Zaitsev, A., 2003. The 1867 Virgin Island tsunami: observations and modeling. Oceanologica Acta 26, 609-621.

Zhao, J.-X., Yu, K.-F., 2010. U-series dating of past extreme events. Abstract volume of the 1st IGCP 588 "Preparing for Coastal Change" conference in Hongkong, 30 Nov - 4 Dec 2010, p. 25.

Zong, Y. (2004): Mid-Holocene sea-level highstand along the Southeast Coast of China. Quaternary International 117, 55-67.

Zonneveld, J.I.S., de Buisonjé, P.H., Herweijer, J.P., 1977. Geomorphology and denudation processes. In: Anonymous (ed.), Guide to the field excursions on Curaçao, Bonaire and Aruba, Netherlands Antilles. 8th Caribbean Geological Conference on Curaçao, 9-24 July 1977. GUA Paper of Geology 10, 56-68.

Erklärung

Ich versichere, dass ich die von mir vorgelegte Dissertation selbständig angefertigt, die benutzten Quellen und Hilfsmittel vollständig angegeben und die Stellen der Arbeit – einschließlich Tabellen, Karten und Abbildungen –, die anderen Werken im Wortlaut oder dem Sinn nach entnommen sind, in jedem Einzelfall als Entlehnung kenntlich gemacht habe; dass diese Dissertation noch keiner anderen Fakultät oder Universität zur Prüfung vorgelegen hat; dass sie – abgesehen von unten angegebenen Teilpublikationen – noch nicht veröffentlicht worden ist sowie, dass ich eine solche Veröffentlichung vor Abschluss des Promotionsverfahrens nicht vornehmen werde. Die Bestimmungen dieser Promotionsordnung sind mir bekannt. Die von mir vorgelegte Dissertation ist von Univ.-Prof. Dr. Helmut Brückner betreut worden.

Nachfolgend genannte Teilpublikationen liegen vor

- Engel, M., Brückner, H., 2011. The identification of palaeo-tsunami deposits – a major challenge in coastal sedimentary research. In: Karius, V., Hadler, H., Deicke, M., von Eynatten, H., Brückner, H., Vött, A. (eds.), Dynamische Küsten - Grundlagen, Zusammenhänge und Auswirkungen im Spiegel angewandter Küstenforschung. Proceedings of the 28th Annual Meeting of the German Working Group on Geography of Oceans and Coasts, 22-25 Apr 2010, Hallig Hooge. Coastline Reports 17, 65-80.
- Engel, M., May, S.M., 2012. Bonaire's boulder fields revisited: Evidence for Holocene tsunami impact on the Leeward Antilles. Quaternary Science Reviews, doi: 10.1016/j.quascirev.2011.12.011.
- Engel, M., Bolten, A., Brückner, H., Daut, G., Kelletat, D., Schäbitz, F., Scheffers, A., Scheffers, S.R., Vött, A., Wille, M., Willershäuser, T., 2009. Reading the chapter of extreme wave events in nearshore geo-bio-archives of Bonaire (Netherlands Antilles) – initial results from Lagun and Boka Bartol. Marburger Geographische Schriften 145, 157-178.
- Engel, M., Brückner, H., Wennrich, V., Scheffers, A., Kelletat, D., Vött, A., Schäbitz, F., Daut, G., Willershäuser, T., May, S.M., 2010. Coastal stratigraphies of eastern Bonaire (Netherlands Antilles): new insights into the palaeotsunami history of the southern Caribbean. Sedimentary Geology 231, 14-30.
- Engel, M., Brückner, H., Messenzehl, K., Frenzel, P., May, S.M., Scheffers, A., Scheffers, S., Wennrich, V., Kelletat, D., in press. Shoreline changes and high-energy wave impacts at the leeward coast of Bonaire (Netherlands Antilles). Earth, Planets and Space.

_____

(Max Engel)